Experiments and 3D modelling of hydrodynamics, sediment transport, settling and resuspension under unsteady conditions in an urban stormwater detention basin

Hexiang Yan

N° d'ordre 2013ISAL0034
Année 2013

Thèse

Expérimentations et modélisations tridimensionnelles de l'hydrodynamique, du transport particulaire, de la décantation et de la remise en suspension en régime transitoire dans un bassin de retenue d'eaux pluviales urbaines

Experiments and 3D modelling of hydrodynamics, sediment transport, settling and resuspension under unsteady conditions in an urban stormwater detention basin

Présentée devant
L'Institut National des Sciences Appliquées de Lyon

Pour obtenir
Le grade de docteur

Formation doctorale : Génie Civil
École doctorale: Mécanique, Energétique, Génie Civil, Acoustique (MEGA)

Par
Hexiang YAN

Soutenue le 28 Mai 2013 devant la Commission d'examen

Jury

F. Anselmet	Professeur - ECM - Rapporteur
G. Chebbo	Directeur de recherche HDR – LEESU - Rapporteur
G. Lipeme Kouyi	Maître de conférences –INSA Lyon – Co-directeur de thèse
J.-L. Bertrand-Krajewski	Professeur – INSA Lyon - Directeur de thèse
R. Mohn	Professeur – IWARU - Examinateur
R. Mosé	Professeur – Université de Strasbourg - Président
V. R. Stovin	Senior Lecturer – Sheffield University - Rapporteur

Laboratoire de Génie Civil et d'Ingénierie Environnementale (LGCIE)

INSA Direction de la Recherche – Ecoles Doctorales-Quinquennal 2011-2015		
Sigle	**Ecole doctorale**	**Responsable**
CHIMIE	CHIMIE DE LYON INSA de Lyon : R.Gourdon	Jean Marc LANCELIN Université de Lyon – Collège Doctoral Bât ESCPE 43 bd du 11 novembre 1918 69622 VILLEURBANNE Cedex Tél : 04.72.43 13 95 directeur@edchimie-lyon.fr
E.E.A.	ELECTRONIQUE, ELECTROTECHNIQUE, AUTOMATIQUE Secrétariat : M.C. HAVGOUDOUKIAN eea@ec-lyon.fr	Gérard SCORLETTI Ecole Centrale de Lyon 36 avenue Guy de Collongue 69134 ECULLY Tél : 04.72.18 60 97 Fax : 04 78 43 37 17 Gerard.scorletti@ec-lyon.fr
E2M2	EVOLUTION, ECOSYSTEME, MICROBIOLOGIE, MODELISATION INSA de Lyon : H.Charles	Gundrun BORNETTE CNRS UMR 5023 LEHNA Université Claude Bernard Lyon 1 Bât Forel 43 bd du 11 novembre 1918 69622 VILLEURBANNE Cédex Tél : 04.72.43.12.94 e2m2@biomserv.univ-lyon1.fr
EDISS	INTERDISCIPLINAIRE SCIENCES-SANTE Sec : Safia AIT CHALAL INSA de Lyon : M. Lagarde	Didier REVEL Hôpital Louis Pradel Bâtiment Central 28, Avenue Doyen Lépine - 69500 BRON Tél : 04 72 68 49 09 - Fax : 04 72 35 49 16 Didier.revel@creatis.uni-lyon1.fr
INFOMATHS	INFORMATIQUE ET MATHEMATIQUES	M. Johannes KELLENDONK Université Claude Bernard Lyon 1 INFOMATHS Bâtiment Braconnier 43 bd du 11 novembre 1918 69622 VILLEURBANNE Cedex Tél : 04.72. 44.82.94 Fax 04 72 43 16 87 infomaths@univ-lyon1.fr

INSA Direction de la Recherche – Ecoles Doctorales-Quinquennal 2011-2015		
Sigle	**Ecole doctorale**	**Responsable**
Matériaux	MATERIAUX DE LYON	Pr. Jean-Yves BUFFIERE Secrétaire : Mériem LABOUNE INSA de Lyon École Doctorale Matériaux Mériem LABOUNE Bâtiment Antoine de Saint-Exupéry 25bis Avenue Jean Capelle 69621 VILLEURBANNE Tél : 04 72 43 71 70 Fax : 04 72 43 72 37 ed.materiaux@insa-lyon.fr
MEGA	MECANIQUE, ENERGETIQUE, GENIE CIVIL, ACOUSTIQUE	Pr. Philippe BOISSE Secrétaire : Mériem LABOUNE INSA de Lyon École Doctorale MEGA Mériem LABOUNE Bâtiment Antoine de Saint-Exupéry 25bis Avenue Jean Capelle 69621 VILLEURBANNE Tél : 04 72 43 71 70 Fax : 04 72 43 72 37 mega@insa-lyon.fr Site web : http://mega.ec-lyon.fr/
ScSo	ScSo* Sec : Viviane POLSINELLI INSA de Lyon : J.Y Toussaint	Lionel OBADIA Université Lyon 2 86 rue Pasteur 69365 LYON Cedex 07 Tél : 04.78.69.72.76 Fax : 04.37.28.04.48 Lionel.Obadia@univ-lyon2.fr

**ScSo : Histoire, Geographie, Aménagement, Urbanisme, Archéologie, Science politique, Sociologie, Anthropologie*

Expérimentations et modélisations tridimensionnelles de l'hydrodynamique, du transport particulaire, de la décantation et de la remise en suspension en régime transitoire dans un bassin de retenue d'eaux pluviales urbaines

Résumé

Les bassins de retenue des eaux pluviales sont des ouvrages qui contribuent à mettre en place une gestion durable des eaux pluviales urbaines. Ces ouvrages spéciaux ont deux fonctions principales: i) lutter contre les inondations en écrêtant les pics de débit ; ii) piéger les polluants particulaires par décantation en vue de préserver la qualité des milieux récepteurs. Concernant le contrôle des polluants particulaires, les géométries et les volumes des bassins de retenue (obtenus à l'issue de la phase de dimensionnement hydraulique), ainsi que les temps de séjour associés ne sont pas toujours appropriés pour avoir des efficacités de décantation satisfaisantes. On constate que les processus de sédimentation et de remise en suspension dans ces bassins de retenue ne sont pas bien compris et modélisés. Afin de mieux comprendre ces processus dans des ouvrages *in situ*, cette thèse porte à la fois sur des expérimentations *in situ* et sur les modélisations de l'hydrodynamique et du transport particulaire dans les bassins de retenue pilotes et *in situ*.

Cette recherche s'est appuyée en grande partie sur le bassin Django Reinhardt (BDR) à Chassieu (volume: 32000 m^3, surface: 11000 m^2) dans le cadre de l'OTHU (Observatoire de Terrain en Hydrologie Urbaine) et sur les données expérimentales obtenues par Dufresne (2008) et Vosswinkel *et al.* (2012).

Les échantillons de sédiments accumulés dans le bassin depuis 2006 ont été prélevés et leurs caractéristiques physiques ont été analysées en laboratoire dans le but de cerner leur distribution spatiale. Concernant la modélisation numérique, dans un premier temps, les simulations de l'hydrodynamique en régime permanent ont été réalisées à l'aide du logiciel CFD Ansys Fluent version 14 et ont été évaluées à partir de l'analyse de corrélation entre le comportement hydrodynamique du bassin et la distribution spatiale des caractéristiques physiques des sédiments accumulés dans le bassin depuis 2006. Les conditions limites sur le fond couramment utilisées et largement décrites dans la littérature (à partir d'études sur pilotes en laboratoire) ont été testées dans le but de représenter la distribution spatiale des sédiments et l'efficacité de décantation du BDR. Les conditions testées sont : i) contrainte de cisaillement critique ou bed shear stress – BSS et ii) énergie cinétique turbulente critique ou bed turbulent kinetic energy - BTKE. L'approche Euler-Lagrange dite « particle tracking » (suivi de particules) a été mise en œuvre. En raison de l'échec de prédiction des zones de dépôt à l'aide des conditions limites disponibles (BSS et BTKE), une nouvelle relation a été proposée pour estimer le seuil BTKE. La condition à la limite obtenue en utilisant cette nouvelle relation (qui prend en compte la distribution des vitesses de chute des particules) a été testée sur un bassin pilote (Dufresne, 2008) et sur le BDR à l'aide de l'approche Euler-Lagrange en régime permanent. Les résultats obtenus n'étaient pas très satisfaisants concernant la prédiction des zones de dépôt et l'efficacité de décantation dans le bassin BDR, même en considérant une distribution granulométrique non uniforme. En effet, les résultats des simulations montrent que les conditions BTKE et BSS jouent le même rôle et permettent surtout de représenter la distribution spatiale des particules artificielles dans les bassins pilotes. Afin de mieux prédire les zones de dépôt dans le BDR, une nouvelle méthode a été proposée en considérant le transport des particules, leur décantation et leur érosion en régime transitoire.

Sur la base de la méthode proposée pour le transport des particules, la décantation et l'érosion en régime transitoire, plusieurs modélisations avec différentes conditions limites ont été réalisées dans un bassin de retenue pilote rectangulaire (Vosswinkel *et al.*, 2012). Les prédictions des efficacités et des zones de dépôt en régime transitoire avec la méthode proposée sont satisfaisantes. Finalement, la prise

en compte des effets liés au régime transitoire améliore considérablement la simulation du transport, de la décantation et de l'érosion des polluants particulaires dans les bassins de retenue.

Mots-clés: décantation, remise en suspension, bassins de retenue des eaux pluviales, régime transitoire, modélisation 3D, énergie cinétique turbulente, contrainte de cisaillement, la distribution des sédiments, efficacité de décantation, approche Euler/Lagrange

Experiments and 3D modelling of hydrodynamics, sediment transport, settling and resuspension under unsteady conditions in an urban stormwater detention basin

Abstract

Stormwater detention basins are of great importance for the sustainable management of urban stormwater. Stormwater detention basins have two main functions: i) preventing flooding by mitigating peak flow and ii) trapping particulate pollutants by means of settling processes in order to preserve the quality of receiving waters. Geometries, basin volumes (obtained from hydraulic design) and particle residence times are not always appropriate measures for determining satisfactory settling efficiencies for the removal of particulate pollutants. The processes of sedimentation and resuspension in these facilities are not well-understood and well-modeled. In order to gain a better understanding of these processes in real facilities, this thesis therefore focuses on both *in situ* experiments and the modelling of hydrodynamic and sediment transport in field detention basins and in small-scale basins in the laboratory.

This research was mainly undertaken in the Django Reinhardt basin (DRB) in Chassieu (volume: 32000 m^3, surface: 11000 m^2), part of the OTHU (Field Observatory for Urban Hydrology) program and using experimental data derived from Dufresne (2008) and Vosswinkel *et al.* (2012).

Samples of sediment accumulated in the basin since 2006 were collected and their physical characteristics were analysed in the laboratory in order to determine their spatial distribution. To carry out the numerical modelling, hydrodynamic simulations in steady state conditions were first performed using Ansys Fluent CFD software version 14 and these were then evaluated by correlating the hydrodynamic behaviour of the DRB and the spatial distribution of the physical characteristics of sediment accumulated in the basin since 2006.

The bed boundary conditions of small scale basins that are described and widely-used in scientific literature (taken from laboratory pilot studies) were tested in order to find values for the spatial distribution of sediment and the settling efficiency of the DRB. The conditions tested were: i) critical bed shear stress - BSS and ii) critical bed turbulent kinetic energy - BTKE. The Euler-Lagrange "particle tracking" approach was used. Given that it is not possible to make accurate predictions in relation to DRB deposit zones using the available bed boundary conditions, a new relationship based on particle settling velocities was proposed in order to estimate the BTKE threshold for bed boundary condition. The newly proposed boundary condition was tested in a pilot basin (Dufresne, 2008) and in the DRB using the Euler-Lagrange approach under steady flow conditions. The results were not very satisfactory for the DRB deposit zones, even when taking non-uniform grain size distribution into account. In fact, the simulated results in steady state showed that BSS/BTKE conditions play the same role and they only enable predictions to be made for artificial particle deposit zones in pilot basins.

In order to make better predictions for deposit zones and for settling efficiency in field detention basins, a new method was therefore proposed for modelling sediment transport, settling and erosion under unsteady conditions. Various simulations with different bed boundary conditions were carried out in a rectangular pilot basin (Vosswinkel *et al.*, 2012) using this proposed method for representing particle transport, settling and erosion processes under unsteady conditions. The predictions for removal efficiencies and deposition zones were satisfactory. Hence, by taking transient effects on both hydrodynamics and sediment transport into account, drastic improvements were made in the modelling of the spatial and temporal distribution of sediment settling in detention basins.

Keywords: settling, resuspension, stormwater detention basin, unsteady conditions, 3D modelling, turbulent kinetic energy, bed shear stress, sediment distribution, removal efficiency, Euler/Lagrange approach

Expérimentations et modélisations tridimensionnelles de l'hydrodynamique, du transport particulaire, de la décantation et de la remise en suspension en régime transitoire dans un bassin de retenue d'eaux pluviales urbaines

Présentation des résultats majeurs de la thèse – Résumé étendu exigé pour une thèse rédigée en anglais

Les bassins de retenue des eaux pluviales sont des ouvrages importants du système d'assainissement pour la gestion durable des eaux pluviales urbaines. Les bassins de retenue des eaux pluviales ont deux fonctions principales: i) lutter contre les inondations en écrêtant les pics de débit; ii) piéger les polluants particulaires par décantation en vue de préserver la qualité des milieux récepteurs. Le dimensionnement hydraulique est aujourd'hui maitrisé (quantifier le volume à stocker pour éviter les inondations, connaissant le débit régulé de sortie). Concernant le contrôle des polluants particulaires, les géométries et les volumes des bassins de retenue (obtenus à l'issue de la phase de dimensionnement hydraulique), ainsi que les temps de séjour associés ne sont pas toujours appropriés pour avoir des efficacités de décantation satisfaisantes. En effet, de nombreux bassins de retenue existants ont été initialement conçus exclusivement pour atténuer le débit de pointe et ainsi protéger les zones situées à l'aval du bassin. Par conséquent, l'efficacité de dépollution est très variable et peu satisfaisante. On constate que les processus de sédimentation et de remise en suspension dans ces bassins de retenue ne sont pas bien compris et modélisés. Au cours des deux dernières décennies, les recherches sur ces ouvrages ont été réalisées dans le but d'améliorer les performances de ces derniers en matière de piégeage des polluants particulaires. Au cours de ces programmes de recherche, des ouvrages complexes ont été observés in situ et des bassins rectangulaires ont été étudiés en laboratoire. En outre, les simulations numériques ont été réalisées dans des conditions contrôlées avec des géométries simples en vue de reproduire la répartition spatiale des sédiments artificiels au fond des bassins étudiés et les efficacités de décantation. Cependant, les résultats obtenus à partir des bassins pilotes restent difficilement transposables aux cas des bassins in situ, principalement pour les raisons suivantes:

- Géométrie plus complexe,
- Variations temporelles des flux d'eau et polluants et de l'état de l'hydrodynamique,
- Variations temporelles et spatiales des caractéristiques des polluants particulaires,
- Effets d'échelle de similitude surtout en ce qui concerne les caractéristiques des particules.

Par conséquent, il est nécessaire de porter l'effort de recherche sur les bassins in situ avec un suivi en continu et d'y associer un travail de modélisation dans le but de mieux comprendre les processus de décantation et de remise en suspension dans des ouvrages réels, et de mieux qualifier les modèles développés à partir des études sur pilotes (application des résultats obtenus à partir d'études sur pilotes aux cas d'ouvrages in situ afin de cerner les limites et de permettre les améliorations nécessaires de ces modèles).

Cette thèse porte donc à la fois sur des expérimentations *in situ* (analyse des caractéristiques physiques des sédiments) et sur les modélisations de l'hydrodynamique et du transport particulaire dans les bassins de retenue pilotes et *in situ*. Les objectifs scientifiques sont les suivants: i) contribuer à améliorer la compréhension de l'hydrodynamique et des mécanismes de sédimentation dans les bassins de retenue des eaux pluviales; ii) établir, tester et vérifier la

modélisation numérique 3D de l'hydrodynamique et du transport particulaire dans les bassins de retenue des eaux pluviales; iii) contribuer à améliorer la modélisation de l'interaction entre les particules et le fond du bassin; iv) proposer une nouvelle méthode qui permet de représenter les dynamiques associées au transport des sédiments et à leur entraînement en régime transitoire avec l'approche Euler-Lagrange.

Deux critères de performance ont été choisis pour évaluer les modèles: la distribution spatiale des particules sur le fond du bassin et l'efficacité de décantation (qui représente la masse des particules décantées par rapport à la masse totale des particules entrantes).

Cette recherche s'est appuyée en grande partie sur le bassin Django Reinhardt – BDR – à Chassieu (volume maximal: 32000 m^3, surface au sol: 11000 m^2) dans le cadre de l'OTHU (Observatoire de Terrain en Hydrologie Urbaine) et sur les données expérimentales obtenues par Dufresne (2008) et Vosswinkel *et al.* (2012).

Les échantillons de sédiments accumulés dans le BDR ont été prélevés et leurs caractéristiques physiques ont été analysées en laboratoire dans le but de cerner leur distribution spatiale. Cette distribution spatiale a été utilisée pour vérifier la modélisation hydrodynamique en raison de l'insuffisance des données appropriées pour valider les résultats de la modélisation. En effet, compte tenu de la taille du bassin et des conditions opératoires qui auraient été très difficiles, il n'a pas été possible de disposer de données de champ de vitesses ou de contraintes, de mesures de la surface libre dans le bassin, de mesures de quantités turbulentes, etc.

Concernant la modélisation numérique, dans un premier temps, les simulations de l'hydrodynamique en régime permanent ont été réalisées à l'aide du logiciel CFD Ansys Fluent version 14 et ont été évaluées à partir de l'analyse de corrélation entre le comportement hydrodynamique du bassin et la distribution spatiale des caractéristiques physiques des sédiments accumulés dans le bassin depuis 2006. Le lien entre le champ de vitesses (mais aussi les champs d'énergie cinétique turbulente et de contraintes de cisaillement, les zones de faibles vitesse près du fond) et la distribution spatiale des caractéristiques physiques des sédiments (en particulier leurs tailles) a été clairement établi (Figure 1). Sur cette base, un modèle hydrodynamique 3D du bassin Django Reinhardt (BDR) a été établi et a été utilisé comme référence pour l'étude du transport particulaire. Les conditions limites sur le fond couramment utilisées et largement décrites dans la littérature (à partir d'études sur pilotes en laboratoire) ont été testées dans le but de représenter la distribution spatiale des sédiments et l'efficacité de décantation du BDR. Les conditions testées sont : i) contrainte de cisaillement critique ou bed shear stress – BSS et ii) énergie cinétique turbulente critique ou bed turbulent kinetic energy - BTKE. L'approche Euler-Lagrange dite « particle tracking » (suivi de particules) a été mise en œuvre. En raison de l'échec de prédiction des zones de dépôt avec ces conditions limites, une nouvelle relation a été proposée pour estimer le seuil BTKE, sachant que la turbulence près du fond influence la décantation et la remise en suspension des sédiments. La relation proposée est la suivante:

$$k_c = \xi v_s^2$$

Où k_c est le seuil BTKE, v_s est la vitesse de chute de la particule, ξ est un coefficient d'ajustement qui permet de prendre en compte les effets de concentration lors de la décantation, les incertitudes sur les vitesses de chute, l'aspect cohésif de certaines particules, etc.

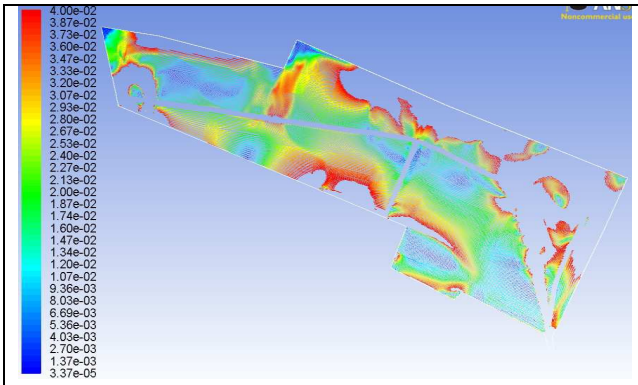

(a) champ de vitesse près du fond du BDR

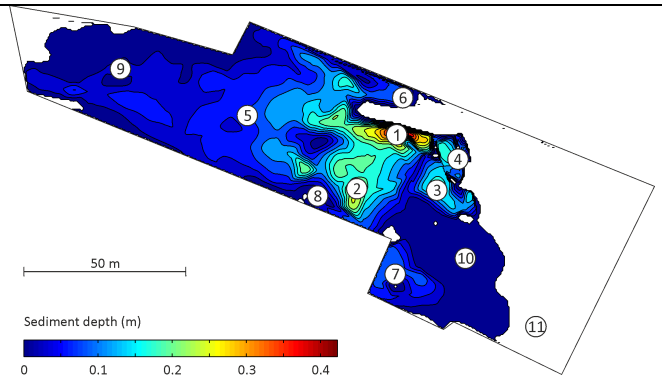

(b) emplacement des points de prélèvement des sédiments

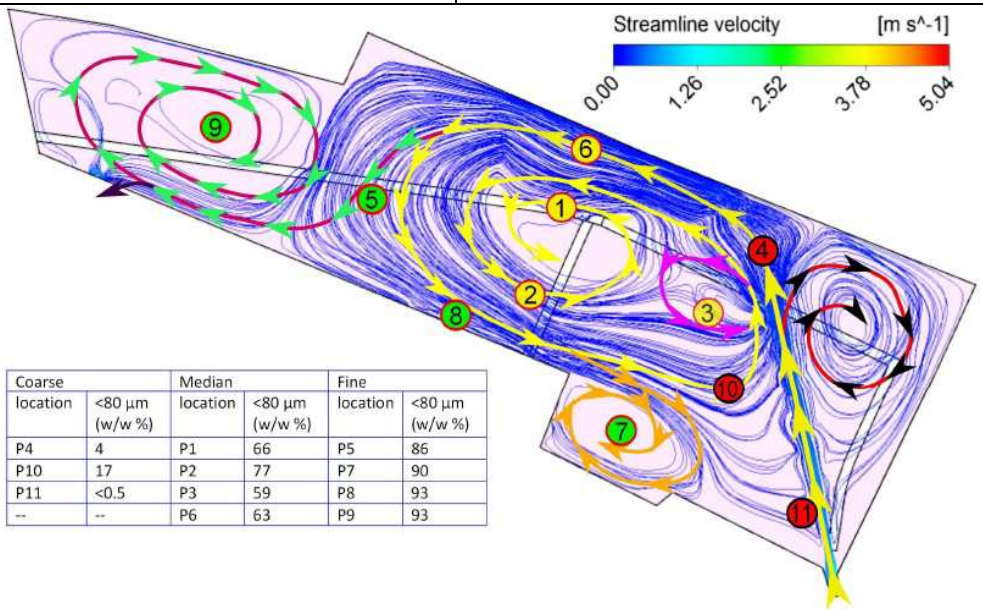

Coarse		Median		Fine	
location	<80 µm (w/w %)	location	<80 µm (w/w %)	location	<80 µm (w/w %)
P4	4	P1	66	P5	86
P10	17	P2	77	P7	90
P11	<0.5	P3	59	P8	93
--	--	P6	63	P9	93

(c) correspondance entre la distribution spatiale des caractéristiques physiques des sédiments et les lignes de courant probables dans le BDR – le tableau indique la fraction volumique des particules dont le diamètre est inférieur à 80 µm.

Figure 1 Mise en évidence du lien entre la distribution spatiale des caractéristiques physiques des sédiments (expérimentations) et le comportement hydrodynamique du BDR (résultats des simulations).

La condition limite sur le fond proposée a été testée sur un bassin pilote (Dufresne, 2008) et sur le BDR à l'aide de l'approche Euler-Lagrange en régime permanent. Les résultats obtenus n'étaient pas très satisfaisants, même en considérant une distribution granulométrique non uniforme.

Figure 2 Zones de dépôt simulées à l'aide la condition limite BTKE en fonction des vitesses de chute des particules (nouvelle condition limite proposée) – une distribution non uniforme des vitesses de chute des particules a été considérée à l'entrée du BDR

En effet, les résultats des simulations ont montré que les conditions BTKE et BSS jouaient le même rôle et permettaient de prédire les zones de dépôt des particules artificielles uniquement dans les bassins pilotes. Cependant, toutes les conditions limites testées ne permettent pas de prédire les zones de dépôt dans le BDR et elles entraînent une surestimation de l'efficacité de décantation. Néanmoins, les résultats de modélisation liés à la distribution spatiale des particules sur le fond du BDR sont améliorés en considérant une distribution non uniforme des vitesses de chute à l'entrée du bassin (voir Figure 2).
C'est pourquoi ces modèles ont été améliorés dans un deuxième temps, en considérant le transport des particules, leur décantation et leur érosion en régime transitoire. La figure 3 représente schématiquement la démarche employée pour mettre au point les nouvelles conditions limites sur le fond en régime transitoire:

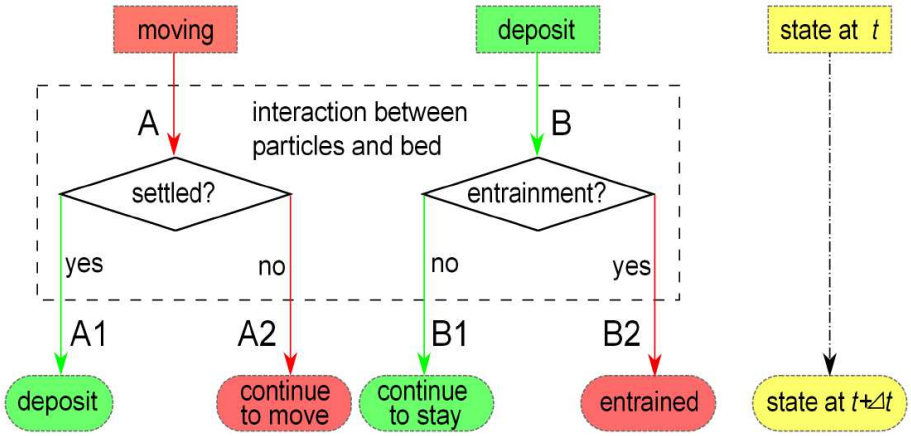

Figure 3 Traitement de la condition limite au fond en régime transitoire

Le traitement des particules en contact avec le fond dans le processus de suivi des particules en régime instationnaire est réalisé comme suit. On distingue deux états à l'instant t : soit la particule est en suspension, soit elle a sédimenté. En fonction de l'état à l'instant t, la méthode de traitement de la particule à l'instant $t+\Delta t$ est différente, comme décrit ci-après.

(**A**) : La particule qui était en mouvement peut soit entrer en contact avec le fond et sédimenter (état A1, Figure 3), soit continuer à se déplacer dans l'écoulement après une remise en suspension ou se déplacer par saltation après le contact avec le fond (état A2, Figure 3). La détermination de l'état de la particule après contact avec le fond est fondée sur le respect ou non d'un seuil de contrainte de cisaillement (Bed Shear Stress - BSS de l'ordre de 0.03 Pa selon Dufresne, 2008) ou d'un seuil d'énergie cinétique turbulente au fond (Bed Turbulent Kinetic Engergy – *BTKE* de l'ordre de $2x10^{-4}$ m^2/s^2 selon Dufresne, 2008). Si les valeurs locales de *BSS* ou *BTKE* sont inférieures aux seuils, la particule sédimente. Sinon elle est remise en suspension. On peut également utiliser les courbes de Shields (contrainte de cisaillement adimensionnelle) pour calculer un seuil de contrainte de cisaillement variable selon les caractéristiques des particules. Nous avons également proposé une nouvelle fonction permettant de calculer la valeur critique d'énergie cinétique turbulente. Cette fonction fait intervenir les vitesses de chute des particules.

(**A1**) Si la particule sédimente, on n'applique pas la condition « *trap* » (qui détruit l'historique de la trajectoire de la particule), mais on modifie la vitesse et les forces associées au mouvement de la particule de façon à faire rester sur place. Pour ce faire, nous avons développé des modules spécifiques ou *UDF* (user defined function) afin de modéliser cet état de la trajectoire.

(**A2**) Si la particule reste en mouvement, on applique la condition de type « *reflect* » (rebond de la particule dans une direction donnée avec une certaine vitesse et retour dans l'écoulement ou mouvement par saltation). Il est ainsi possible de prendre en compte les pertes d'énergie dues au frottement au fond à travers des coefficients de frottement suivant les directions normale et tangentielle. Par défaut, les coefficients suivant la normale au fond et la direction tangentielle valent 1. Le choix de l'orientation et l'intensité du vecteur vitesse lors du rebond ainsi que la prise en compte du frottement peuvent permettre de représenter la saltation. Nous avons développé une autre *UDF* pour modéliser ces mouvements possibles de la particule.

(**B**) La particule sédimentée à l'instant t peut être entraînée et se déplacer en suspension ou par charriage à l'instant $t+\Delta t$ si les caractéristiques de l'écoulement le permettent. La contrainte de cisaillement locale est comparée à une contrainte seuil obtenue à partir de la courbe de Shields. Si la contrainte locale est supérieure à la contrainte seuil, la particule est entraînée (état B2), sinon elle reste dans son état initial (situation B1).

(**B1**) La particule reste au même endroit.

(**B2**) Plusieurs recherches sont menées pour modéliser le charriage à l'échelle de la particule. La saltation est le mode dominant du mouvement par charriage. Plusieurs auteurs caractérisent la saltation par une hauteur et une longueur de saut et par la vitesse de démarrage du saut. Dans cette étude, on utilise la formule proposée par Hu et Hui (1996) pour estimer la vitesse initiale d'entraînement.

Si la particule est entraînée par le fluide, la vitesse tangentielle de la particule est considérée comme étant égale à la vitesse locale de l'écoulement près du fond projetée suivant la direction tangentielle.

Nous avons développé des programmes spécifiques (*UDF*) qui ont été implémentés dans le code FLUENT afin de réaliser les traitements des conditions aux limites sur le fond (conditions décrites précédemment, voir Figure 3).

La modélisation du transport des particules à l'aide de l'approche Euler/Lagrange avec les nouvelles conditions limites en régime transitoire a été menée dans le but de représenter les zones de dépôt et l'efficacité de décantation dans les deux bassins pilotes étudiés (Dufresne, 2008; Vosswinkel *et al*., 2012).
Sur la base de la méthode proposée pour le transport des particules, la décantation et l'érosion en régime transitoire, 12 modélisations avec différentes conditions limites (voir tableau 1) ont été réalisées dans un bassin pilote de retenue rectangulaire (Vosswinkel *et al.*, 2012). Toutes les conditions sont rappelées au tableau 1.

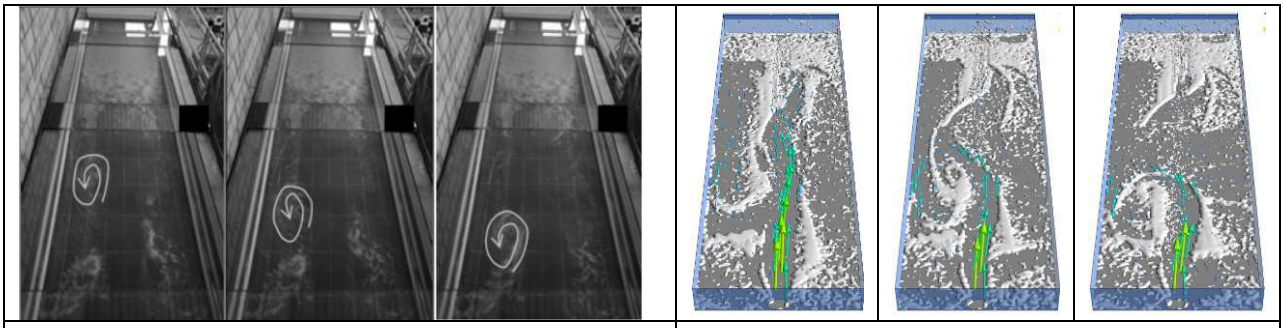

Expérience (Vosswinkel *et al.,* 2012)	Zones simulées

Figure 4 Comparaisons entre les zones de dépôt observées et simulées – la recirculation apparait sur le côté gauche - résultats du cas DPM 5, résultats obtenus après (de gauche à droite) 200,215 et 230s

La figure 4 montre la comparaison entre les zones de dépôt observées expérimentalement et simulées.
Le tableau 2 montre les efficacités de décantation simulées. En comparant les efficacités expérimentales (minimum = 83% -maximum = 87%, Vosswinkel *et al.*, 2012) et simulées, on constate que presque tous les cas, à l'exception du cas 7 (sans prise en compte du module de dispersion des particules noté DRWM pour *Discret Random Walk Model* ou modèle de dispersion particulaire), prédisent de façon satisfaisante cette efficacité. La prédiction des efficacités et des zones de dépôt en régime instationnaire avec la méthode proposée (Figure 3) sont sensibles au nombre de particules traitées, à la constante de Lagrange notée C_L , aux forces de résistance lors de la remise en suspension, à la vitesse initiale d'entrainement. Au final, les effets liés au régime instationnaire dans les bassins de retenue jouent un rôle prépondérant au regard du comportement des particules près du fond. Il est donc indispensable de les prendre en compte. En outre, la condition limite de type BTKE proposée est appropriée pour prédire les zones de dépôt alors que la condition de type BSS variable estimée à partir de la courbe de Shields reste appropriée pour représenter l'entrainement des particules dans les bassins pilotes lorsque ces particules sont considérées comme étant non cohésives.
Les perspectives de ce travail sont brièvement présentées ci-après. Concernant les expérimentations *in situ*: i) échantillonner les particules à l'entrée du BDR (un dispositif de type leaping weir sera installé à l'entrée du BDR et permettra de piéger les particules susceptibles de décanter dans le bassin), ii) collecter les sédiments dans des pièges (concevoir les pièges de façon à éviter toute perturbation des trajectoires des particules lors de la décantation ou de leur transport). Concernant la modélisation du transport solide avec les conditions aux limites proposées (Figure 3), il est envisagé d'améliorer la condition BTKE, en faisant en sorte que le coefficient d'ajustement soit fonction des caractéristiques des particules et des conditions hydrauliques près du fond. Une fonction mathématique pourrait être obtenue

à partir de mesures expérimentales en laboratoire. L'amélioration de cette condition BTKE (car elle engendre une surestimation de l'efficacité) pourrait également passer par le développement d'une relation mathématique permettant de relier les autres caractéristique physiques des particules décantées à la vitesse de chute. En effet, aucune formule mathématique viable n'existe aujourd'hui pour estimer correctement la vitesse de chute à partir des autres caractéristiques physiques des particules (taille, densité, forme, etc.).

Tableau 1 Conditions aux limites utilisées pour les 12 simulations – u* et τ* représentent respectivement la vitesse de frottement et la contrainte de cisaillement adimensionnelle

Cas traités	Processus A: conditions de décantation	Processus B: conditions d'entraînement	Nombre de particules injectées	Coefficients de résistance *e* (suivant la direction normale au fond) et *f* (suivant la direction tangentielle) lors du rebond des particules	Composantes de la vitesse initiale d'entraînement u_d (suivant la direction normale au fond) et v_d (suivant la direction tangentielle) – en m/s	Prise en compte du modèle de dispersion particulaire DRWM et Valeur de la constante de Lagrange C_L
1	BSS variable	BSS variable	22400	*e=1, f=1*	Hu and Hui (1996)	0.15
2	BSS variable	BSS variable	44800	*e=1, f= 1*	Hu and Hui (1996)	0.05
3	BSS variable	BSS variable	44800	*e=1, f=1*	Hu and Hui (1996)	0.25
4	BSS variable	BSS variable	44800	*e=1, f=1*	Hu and Hui (1996)	0.5
5	BSS variable	BSS variable	44800	$e=0.84-4.84\tau_*$ $f=0.73$	Hu and Hui (1996)	0.05
6	BSS variable	BSS variable	67200	$e=0.84-4.84\tau_*$ $f=0.73$	$u_d=2u_*$ $v_d=2u_*$	0.05
7	BSS variable	BSS variable	67200	$e=0.84-4.84\tau_*$ $f=0.73$	$u_d=2u_*$ $v_d=2u_*$	Sans DRWM
8	BTKE 1	BSS variable	22400	*e=1, f=1*	$u_d=2u_*$ $v_d=2u_*$	0.15
9	BTKE 2	BTKE 2	67200	$e=0.84-4.84\tau_*$ $f=0.73$	$u_d=2u_*$ $v_d=2u_*$	0.05
10	BTKE 1	BTKE 1	67200	$e=0.84-4.84\tau_*$ $f=0.73$	$u_d=2u_*$ $v_d=2u_*$	0.05
11	BTKE 2	BSS variable	67200	$e=0.84-4.84\tau_*$ $f=0.73$	$u_d=2u_*$ $v_d=2u_*$	0.05
12	BSS=0.03 Pa	BTKE 1	67200	$e=0.84-4.84\tau_*$ $f=0.73$	$u_d=2u_*$ $v_d=2u_*$	0.05

Tableau 2 Efficacités de décantation simulées pour les 12 cas avec la méthode proposée

Cas No.	1	2	3	4	5	6
Efficacité (%)	79.45	87.85	81.48	82.00	86.77	90.80
Cas No.	7	8	9	10	11	12
Efficacité (%)	98.41	73.02	85.02	85.19	86.06	85.83

Il est également prévu de réaliser les simulations de l'hydrodynamique et du transport solide en régime transitoire (en considérant des événements courts ou une partie d'un événement pluvieux long par exemple) dans le BDR. Dans ce cas, la dynamique liée aux concentrations de sortie sera également examinée par simulation (nous disposons de mesures de turbidité à l'entrée et à la sortie du BDR). La collision entre particules est un élément aussi à prendre en compte. Enfin, un dispositif innovant de mesure de la surface libre en 3D et du champ de vitesse de surface dans le BDR sera mis en place. Ce dispositif permettra enfin d'avoir des données hydrodynamiques pour la validation plus aboutie des modèles 3D développés.

Mots-clés: décantation, remise en suspension, bassins de retenue des eaux pluviales, régime transitoire, la modélisation 3D, énergie cinétique turbulente, contrainte de cisaillement, la distribution des sédiments, efficacité de décantation, approche Euler/Lagrange

Acknowledgements

First of all, I would like to express my gratitude to my supervisors, Jean-Luc Bertrand-Krajewski and Gislain Lipeme Kouyi for their exceptional supervision of my PhD research. Over the past three and half years, G. Lipeme Kouyi offered his valuable input during discussions and his support on the subject. I am particularly grateful for his extraordinary patience during our discussions, given my level of French. J.-L. Bertrand-Krajewski gave indispensable guidance for this research, in particular on experiments. His rigorous scientific attitude and extensive knowledge have deeply influenced me.

I am grateful to the members of the jury: Virginia Stovin for valuable discussions during UDM in Belgrade and seminars in INSA; Rainer Mohn for kindly receiving me in Münster, sharing experimental data and contributing pertinent suggestions on modelling; Ghassan Chebbo, Robert Mosé and Fabien Anselmet for being members of the jury for my thesis.

I would also like to thank all the members of the laboratory. Bernard Chocat for welcoming me at the LGCIE for this PhD. Sylvie Barraud, Pascal Le Gauffre, Fredieric Cherqui, Jean-Baptiste Aubin, Helene Castebrunet and the CANOE group: Herve Negro and Nicolas Invernon. I would also like to thank the great secretarial group: Valérie Orhon, Sabine Berton, Izabel Karabedian, Valérie Boiron, Christine Boyer, Nathalie Dangla, and Nadia Bensenouci. Etc.

I must thank the technical support group for their valuable assistance with the experimental work: Stephane, Serge, Nicolas, Nathalie, Dominique, Yvan, Sylvie, Christian.

I must appreciate the IWARU group (Rainer Mohn, Mathias Uhl, Nina Vosswinkel, Simon Ebbert…) from the Münster University of Applied Science and Matthieu Dufresne (ENGEES) for their kindness in sharing their experimental data and experience with me. I also thank Kristian for doing part of the experiments during his internship in LGCIE.

I also thank my colleagues who gave me valuable support during my thesis, friendly help in my daily life and so much more: Carolina, Siao, Mathieu, Christel, Céline, Adrien, Marjolaine, Tanguy, Abel, Farah, Enric, Nesrine, Hamouda, Abbas, Méhdi, Luis, Amélie, and Oras, etc.

I would like to acknowledge the scientific support given to me by the OTHU project and the financial support of the CSC (Chinese Scholarship Council) as well as the French National Research Agency for financial support given within the framework of the CABRRES (ANR 2011 CESA 012 01 - http://www.graie.org/cabrres) program, which made this research possible.

Finally, I am very grateful to my family, especially to my parents for their selfless support and love.

Table of contents

Résumé 5
Abstract 7
Acknowledgements 17
Table of contents 19
List of Figures 21
List of Tables 25
Notation 26
List of Abbreviation 31
Chapter 1 Introduction 33
1.1 Background 33
1.2 Motivation 34
1.3 Objectives 35
1.4 Structure of the Thesis 36
Chapter 2 Literatures review 37
2.1 Global view on stormwater detention basin 37
2.1.1 Definitions 38
2.1.2 General performances 38
2.1.3 Retrofit practices of detention basin for water quality 40
2.2 Mechanisms related to Sediment transport 42
2.2.1 Source of stormwater solids 42
2.2.2 Characteristics and quantities of Particulate pollutants in drainage systems 42
2.2.3 Mechanisms related to sediment transport 45
2.3 Modelling of experimental small scale stormwater basins 64
2.3.1 Empirical model of detention basins 64
2.3.2 Experimental investigation in small scale basins 66
2.4 Numerical modelling of flow and sediment transport in detention basin 69
2.4.1 Modelling of hydrodynamic behaviour of detention basins 70
2.4.2 Sediment transport modelling 75
2.5 Conclusions of Chapter 2 84
Chapter 3 Materials and methods 86
3.1 Methodology of the research 86
3.2 Experimental site 87
3.2.1 *In situ* site 87
3.2.2 Pilot basin 91
3.3 *In situ* experiments to characterize accumulated sediment 93
3.3.1 Introduction 93
3.3.2 Sampling of accumulated sediment 94
3.4 Numerical modelling strategy 101
3.4.1 Introduction 101
3.4.2 Fluid flow modelling 101
3.4.3 Sediment transport modelling 118
3.5 Conclusion of Chapter 3 135
Chapter 4 Sediment transport under steady state condition 136
4.1 Introduction 136
4.2 Accumulated sediment analysis 136

4.2.1 Sediment depth spatial distribution 138
4.2.2 Particle size distribution 140
4.2.3 Particles density and organic matter content 144
4.3 Preliminary 3D modelling of full scale detention basin Django Reinhardt 146
4.3.1 Modelling strategy 146
4.3.2 Correlation between hydrodynamic behaviours and spatial distribution of sediment physical characteristics 149
4.3.3 Bed roughness influence on vertical bed turbulence kinetic energy profile 160
4.3.4 Sediment transport modelling with DPM 164
4.4 Improvement of boundary condition for sedimentation modelling with DPM 169
4.4.1 Introduction 169
4.4.2 Test in small scale basin under steady state DPM 170
4.4.3 Test in full scale basin under steady state DPM 173
4.5 Conclusion of chapter 4 176
Chapter 5 Sediment transport under unsteady conditions 177
5.1 Preliminary test in a rectangular basin with permanent large recirculation 177
5.1.1 Model setup 177
5.1.2 Deposition zone in the bed of basin 178
5.1.3 Removal efficiency 180
5.2 Preliminary test in a basin with variable inflow jet and recirculation zones 181
5.2.1 Numerical model setup 181
5.2.2 Evolution of sediment transport and spatial distribution 183
5.2.3 Removal efficiency 196
5.3 Conclusion of chapter 5 197
Chapter 6 Conclusions and perspectives 198
6.1 General conclusions 198
6.2 Perspectives 200
References 202
Appendix 229

List of Figures

Figure 2-1 Main factors that influence the removal efficiency of basin 40
Figure 2-2 Sediment settling velocity measured with VICAS protocol..... 45
Figure 2-3 Processes of erosion, transport and sedimentation 45
Figure 2-4 Definition of bed load and suspended load 46
Figure 2-5 Sketch of representation of bed load movements..... 46
Figure 2-6 Dimensionless sediment discharge q_{bv*} versus Shields parameter τ_*. 52
Figure 2-7 Modified Shields diagram with power equations fitted by Van Rijn (note, $s=\rho_p/\rho$, from van Rijn, 1984b) 53
Figure 2-8 Hjulström curve (from http://en.wikipedia.org/wiki/Hjulstr%C3%B8m_curve , originates from Hjulström, 1935)..... 57
Figure 2-9 Saltation trajectory of sand measured by high speed camera..... 61
Figure 2-10 Definition diagram for collision-rebound with the bed..... 62
Figure 2-11 Settling conditions in an ideal rectangular settling basin 65
Figure 2-12 Inflow velocity/efficiency curve for a laboratory chamber..... 71
Figure 2-13 Comparison between the deposition zones and bed shear stress and bed turbulent kinetic energy in a rectangular detention basin..... 72
Figure 3-1 Location of OTHU experimental sites in the Lyon sewer system..... 87
Figure 3-2 Presentation of the Chassieu catchments..... 89
Figure 3-3 View of Django Reinhardt detention-settling and infiltration facility 90
Figure 3-4 Scheme of the Django Reinhardt detention- settling basin after its retrofit in 2004 90
Figure 3-5 Outlet of Django Reinhardt detention basin equipped with regulator gate with a maximum outflow rate of 350 L/s (Hydroslide® gate)..... 91
Figure 3-6 Bed elevation contour of the Django Reinhardt detention basin..... 91
Figure 3-7 Experimental tank and measurement devices..... 92
Figure 3-8 Experimental set-up (after Vosswinkel et al. 2012) 93
Figure 3-9 Sediment depth distributions in the Django Reinhardt detention basin. 95
Figure 3-10 A photo showing an example sediment zone in Chassieu (14/4/2011)..... 95
Figure 3-11 Layouts of the sediment sampling locations in the Django Reinhardt detention basin 96
Figure 3-12 Sampling process diagram..... 96
Figure 3-13 Laser Particle Sizer (LPS): Malvern Mastersizer 2000 equipped with the Hydro2000G sample dispersion accessory. 97
Figure 3-14 Sieves with selected sizes of 0.08 mm, 0.2 mm, 0.5 mm, 1.0mm, 2.0 mm and 5.0 mm..... 98
Figure 3-15 Pycnometer and accessories (experimental supports and a vacuum pump, etc.) . 99
Figure 3-16 Diagram of the measurement stations located at the inlet and outlet of the Django Reinhardt detention basin in Chassieu 100
Figure 3-17 Time averaging for a statistically steady flow (left) and an unsteady flow (right) 103
Figure 3-18 Velocity distribution near a solid wall..... 112
Figure 3-19 Scheme of near wall region treatment 113
Figure 3-20 Overview of pressure-based solution method 117
Figure 3-21 Cumulative size distributions of particles 124
Figure 3-22 Rosin-Rammler curve fit for the cumulative size distribution of particles 125

Figure 3-23 Diagram of the reflect boundary condition 126
Figure 3-24 Shields curve 128
Figure 3-25 Diagram of dynamic sedimentation and bed load entrainment under unsteady flow conditions 130
Figure 3-26 Scheme of uncoupled DPM 133
Figure 3-27 Diagram of the of two-way coupling DPM approach 134
Figure 3-28 Heat, mass, and momentum transfer between the discrete and continuous phase (Fluent, 2011b) 135
Figure 4-1 Accumulated sediment in the Django Reinhardt basin on 14/04/2011 137
Figure 4-2 Layout of the sediment thickness spatial measurements carried out on 14/4/2011 138
Figure 4-3 Overhead view of the Django Reinhardt basin (from Google Earth in 2012) and the contour of sediment depths measured on 14 April 2011 - Up until the time at which the measurements were taken, the sediment had been accumulating since 2006 139
Figure 4-4 Contour of sediment distribution in the Django Reinhardt basin 139
Figure 4-5 Layout of the sediment sampling locations in the basin, numbered according to sediment depth 140
Figure 4-6 Pictures of gravel-like sediment and of clayey/silty deposits accumulated in the Django Reinhardt basin. The picture of gravel sediment was taken in 2011 and the picture of clayey /silty deposits was taken in 2012. 141
Figure 4-7 Accumulated particle size distributions of the samples from the sieving analysis. The sample names refer to the locations shown in Figure 4-5 142
Figure 4-8 Particle size distributions of the sample P06 by Laser diffraction analysis 143
Figure 4-9 Density of each sieved fraction from sample points P03 and P04 145
Figure 4-10 Density of the fractions of sieving diameters of less than 0.08 mm and the organic matter content of the whole samples. 145
Figure 4-11 The geometric simplification of the Django Reinhardt detention basin 147
Figure 4-12 The simplified geometry of the Django Reinhardt basin and some of the mesh shown in detail 147
Figure 4-13 Changes in outflow rate against water depth h2 148
Figure 4-14 Inflow rate against the water depth h1 for the storm event 31/05/2007. 149
Figure 4-15 (a) Deposit spatial distribution, (b) BSS (<0.01 Pa) distribution and (c) Overhead view of sediment distribution of the basin 151
Figure 4-16 Velocity field of 5 cm under the free surface (top) and near bed low velocity field (<0.04 m/s) of Django Reinhardt basin (low) 152
Figure 4-17 Streamline of the fluid flow of DRB case two and the layout of the sample locations 153
Figure 4-18 Deduction of simulated flow pattern on the real basin with the sediment spatial distribution 154
Figure 4-19 Overhead view of sediment distribution on the bed of the Django Reinhardt basin from Google maps in 2007 and 2012. 155
Figure 4-20 Low bed turbulent kinetic energy (<4.5e-5) distribution of DRB case two in the basin 156
Figure 4-21 Bed shear stress in the Django Reinhardt basin in different inflow rates with an upper BSS limitation of 0.01Pa. 156
Figure 4-22 Streamline analysis of DRB case 1, 2 and 3 158
Figure 4-23 Superposition of streamlines of cases 1 and 2. 159
Figure 4-24 Superposition of streamlines of cases 2 and 3. 159

Figure 4-25 Similarity between observed deposition zones and simulated BTKE distribution (<4.4e-5= k_c) related to different surface roughnesses..... 161
Figure 4-26 Vertical TKE distribution of points checked..... 163
Figure 4-27 Experimental vertical TKE distribution profile adapted from Dey et al. (2011) and vertical TKE distribution for different roughness values (point 1, point 3 and point 4) 163
Figure 4-29 Simulated deposit zones using BTKE boundary conditions with different particle sizes and densities and using a time scale factor of C_L =0.15 and C_L = 2. 167
Figure 4-30 Simulated deposit zones using the Shield curve boundary condition with non-uniform particles sizes, the particle are shown as yellow dots..... 168
Figure 4-31 Computational tetrahedral mesh for small scale basin (Dufresne, 2008)..... 170
Figure 4-32 Rosin-Rammler curve fit showing the cumulative size distribution of particles 171
Figure 4-33 Comparison between (a) experimental sediment transport (Dufresne, 2008), and (b) simulated velocity field from k-ε model at the height of 9.5 cm from the bed with the inflow rate of 3L/s. 171
Figure 4-34 Comparison of sediment deposits zone between experimental observation and simulated deposit zones using bed boundary condition of fixed BTKE and using the proposed BTKE formula with different C_L values..... 172
Figure 4-35 Comparison between observed and simulated deposit zones using different boundary condition with non-uniform particles..... 175
Figure 5-1 Evolution of sediment transport with the varying BTKE boundary condition 178
Figure 5-2 Comparison between (a) experimental deposition zone (Dufresne, 2008), and (b) deposition zone simulated using fixed BTKE boundary condition under steady flow conditions (C_L=0.15) and (c) deposition zone simulated using the proposed dynamic sedimentation method with the varying BTKE boundary condition..... 179
Figure 5-3 Comparison between (a) experimental deposit zones, (b) ~ (e) simulated deposit zones using the proposed dynamic sedimentation method with different boundary conditions, and (f) simulated deposit zones with the trap boundary condition..... 179
Figure 5-4 Particle spatial concentration distributions in the basin by vertical cutting plane 180
Figure 5-5 The computational mesh..... 181
Figure 5-6 Comparison of the experimental (according to Vosswinkel et al., 2012) and simulated evolution of sediment transport after first injection at an interval of 5 seconds (results of case DPM 1, time 10s-15s-20s) 184
Figure 5-7 Evolution of experimental observations (according to Vosswinkel et al., 2012) and simulated recirculation at the left-hand side at a time interval of 15 s (results of case DPM 5, time-200s-215s-230s) 185
Figure 5-8 Evolution of experimental observations (according to Vosswinkel et al., 2012) and simulated recirculation at the right-hand side at a time interval of 15 s (results of case DPM 5, time-90s-105s-120s) 186
Figure 5-9 Comparison of (a) simulated deposit spatial distribution at the end ((results of case DPM 1)300s) and (b) experimental final deposit distribution (after Vosswinkel et al., 2012)..... 187
Figure 5-10 Monitoring sediment mass concentration at the basin outlet (simulation case DPM 11 from 0-300s) 188

Figure 5-11 (a) Simulated deposits in the basin (case DPM 5 at 105s), (b) simulated deposits + moving bed load (<0.002m) (case DPM 5 at 105s) and (c) top view picture of experimental sediment spatial distribution (after Vosswinkel et al., 2012) 189
Figure 5-12 (a) Simulated near bed particle concentration distribution, the contour shows the deposition zone, and (b) the deposition zone distribution rendering with concentration isosurface..... 190
Figure 5-13 Comparison of simulation particle distribution with DRWM (C_L=0.05) and without DRWM..... 191
Figure 5-14 Comparison of simulated particle bed concentration with different C_L: case DPM 5 at 230s with C_L=0.05 (above) and case DPM 1 at 230s with C_L=0.15 (below)..... 192
Figure 5-15 Comparison of simulated particle bed concentration with different C_L: case DPM 3 at 230s with C_L=0.25 (above) and case DPM 4 at 230s with C_L=0.5 (below)..... 193
Figure 5-16 Comparison of simulated particle bed concentration with different initial pickup velocity: case DPM 5 at 120s with Hu and Hui formula (left) and case DPM 6 at 120s with formula van Rijn (right) 194
Figure 5-17 Comparison of particle spatial distribution with different settling and entrainment boundary conditions 195
Figure 6-1 Sketch of dynamic sedimentation process treatment of interaction between particle and bed of basin under unsteady condition 199

List of Tables

Table 2-1 Efficiency of detention basin 38
Table 2-2 Efficiencies of detention basins 39
Table 2-3 Mean COD, metals and hydrocarbon concentrations observed in stormwater 43
Table 2-4 Percentage of the particulate fraction for different pollutants 43
Table 2-5 Grain size characteristics for suspended solids in urban wet weather discharges 44
Table 2-6 Fundamental dimensions of bed load 49
Table 2-7 Formulas for entrainment velocity 54
Table 2-8 formulas for critical Shields parameter τ_{*c} 55
Table 2-9 Saltation length L_S, saltation height h_s and averaged particle velocity V derived from experimental investigations 63
Table 3-1 Base elevation of inlet /outlet of Django Reinhardt detention basin 88
Table 3-2 Particle size distribution for pilot basin experiment 92
Table 3-3 Turbulence model available in commercial CFD codes 104
Table 3-4 Empirical constants α_1, α_2 and α_3 for different ranges of Re_p 120
Table 3-5 Particle size distribution by mass fraction 124
Table 3-6 Mass fractions Y_d with diameter larger than d % 124
Table 4-1 Particle size characteristics of the samples. 142
Table 4-2 Simulation flow condition for representative steady simulation cases 149
Table 4-3 Sediment depth of the sampling locations 154
Table 4-4 Strickler roughness coefficient K and equivalent sand grain roughness height k_s 160
Table 4-5 Mean particle sizes distribution (psd) of 15 trap samples from storm event 31/5/2007 165
Table 4-6 Simulated removal efficiencies with different bed boundary conditions (ρ=1700) 165
Table 4-7 Simulated removal efficiencies with different bed boundary conditions (ρ=2400) 166
Table 4-8 Comparison of experimental and simulated removal efficiency using bed boundary condition fixed BTKE and proposed BTKE formula with different C_L values. 173
Table 4-9 Measured settling velocities from storm event 31/5/2007 with 15 sediment trap sample 174
Table 5-1 Bed boundary conditions configuration for test 178
Table 5-2 Experimental and simulated removal efficiency in the basin 180
Table 5-3 Basic configurations for DPM model except bed boundary condition 182
Table 5-4 DPM setup and different bed boundary condition for proposed method 183
Table 5-5 Simulated removal efficiency of different case setup 196

Notation

A	Surface Area
A_c	Constant coefficient
a	Positive coefficient
B	Additive constant
ΔB	Roughness function
b	Positive coefficient
c	Local sediment concentration
C^*	Depth averaged suspended load concentration under equilibrium condition
C, $C(z)$	Averaged concentration of pollutant load, sediment concentration at a reference elevation z
C_b	Bed layer concentration of sediment
C_μ, $C_{\varepsilon 1}$, $C_{\varepsilon 2}$	Constants
C_{ijk}	Turbulent dissipation
C_D	Drag coefficient
C_L	Time scale constant
C_s	Roughness constant
c_b	Local sediment concentration near the interface of suspended load and bed load
c_{b*}	equilibrium concentration at the interface location
$\bar{c}_b$	Averaged concentration over the bed load layer thickness δ
d	Particle diameter
D^*	Dimensionless particle diameter
d_{50}， D_{50}	Median particle size
d_{90}	Sieve diameter for 90 percentage of mass
D_b	Deposition rate
D_m	Molecular diffusion coefficient
d_e	Effective diameter
$\overline{d_i}$	The i^{th} class particle mean size
$\bar{d}$	Size parameter for Rosin-Rammler distribution
E	Constant
E_b	Erosion rate
e	Restitution coefficient or Constants of nature
F_i	Body force
F_D	Coefficient
F_x	Additional force on particle
f	Friction coefficient

g	Gravity acceleration
g_x	Gravity acceleration along the x axis
h	Elevation or water depth
h_s	the max saltation height
I	Turbulence intensity
i	Subscribe of the Cartesian coordinates (i=1,2,3)
J	Slope of energy grade line
j	Subscribe of the Cartesian coordinates (j=1,2,3)
K	Strickler coefficient
K_s	physical roughness height
K_s^+	dimensionless roughness height
k	turbulent kinetic energy per unit mass
k_B	Ripple factor corresponding to the Manning – Strickler coefficient of the bed forms
k_p	turbulent kinetic energy at the near wall node p
k_r	Particle roughness corresponding to the Manning – Strickler coefficient of the particles
k_s	equivalent roughness height
k_c	Threshold of turbulent kinetic energy
l	Subscribe of the Cartesian coordinates (l=1,2,3) as suffix,
L_{bv}, L_{bm}, L_{bw}	Quantity of sediment moving in the bed layer by volume, or mass or weight
L_s	Saltation length
L_e	eddy length scale
L	Length scale of turbulence
l	Turbulent length reference scale
M	Empirical coefficient
M_{total}	Total mass of incoming particles
M_c	Mass transfer from particle phase to continuous phase
m	Mass of trap particles
m_{qp}	Mass transfer from phase q to phase p
m_{pq}	Mass transfer from phase p to phase q
Δm	Mass lost in the control cell
ΔM	Momentum exchange
$m_{p,0}$	Initial mass of the particle
$m_{\mathrm{p},0}$	initial mass flow rate of the particle injection
m_{p}	Current mass flow rate of the particles
P	Probability for deposition
P_k	Production of turbulent energy
p'	Porosity of the bed material
p_i	Percentage by mass of the i^{th} class of particles with mean size $\overline{d_i}$
p	Pressure
Q	Inflow/outflow discharge

Q_{bv}, Q_{bm}, Q_{bw}	Flux of sediment per unit width moving in the bed layer by volume, or mass or weight
q_{bv}, q_{bm}, q_{bw}	Flux of sediment per unit width moving in the bed layer by volume, or mass or weight
q_{bv*}	Dimensionless transport rate of sediment
q_s	Suspended load transport rate
R	Uniform random number
R_0	Rouse number
R_*	Hydraulic radius
R_b	Hydraulic radius related to the bed according to the side wall correction method of Einstein or Vanoni-Brooks
R_{ep}	Particle Reynolds number
R_{es}	Setting Reynolds number
Re	Reynolds number
R_h	Hydraulic radius for circular and rectangular section
r	Ratio of τ_* to τ_{*c}
S_L	Bed slope
S_{ij}	Rate of the strain tensor
s	Ratio of particle density to fluid density
T	Time that the inflow needs to flow through the pond
Δt	Time step
T_L	fluid Lagrangian integral time
c	Transport parameter
t	Time
t_{cross}	Particle eddy crossing time
U	Mean streamwise flow velocity for 1D/2D model (in x direction)
U_{ref}	Velocity at interface
U^*	Near wall flow dimensionless velocity
U_p	Velocity at the near wall node p
u	Flow velocity
u^+	Dimensionless velocity
u_d , v_d	Tangential and normal velocity component of particle
u_*	Shear velocity
u_p	Particle velocity
u_{*c}	Critical shear velocity
$u_*^{'}$	Effective bed shear velocity
u', v', w'	velocity fluctuation
V	Mean transverse flow velocity for 2D model (in y direction)

V_c	Critical flow velocity for incipient motion
v_c	Critical settling velocity
V_p	Averaged particle velocity
x	Position in the x direction
X_c	the fraction of particles having a settling velocity less than the critical settling velocity
ΔX_i	the fraction of fraction of particles having a settling velocity of v_{si}
Y	Distance from the wall
Y_d	Cumulative mass percentage
y	Position in the y direction
y^+, y^*	Dimensionless distance from the wall
y_p	Distance from the node p
Z	Parameter
z	Position in the z direction
z_b	Bed elevation
α	Non-equilibrium adaptation coefficient
α_{bx} , α_{by}	Direction cosines of bed load movement
α_k, α_ε	Constants
α_q	volume fraction of the q^{th} phase in multiphase flow
α_w	Water volume fraction in two phases mixture
α_1, α_2, α_3	Empirical constant
β	Parameter
β_s	Constant
β^*	Constant
γ	specific weight of fluid
γ_0	Constant
γ_p	specific weight of particle
δ_{ij}	Kronecker symbol
δ_k, δ_ε	Constant
ε_s	Diffusivity coefficient of sediment
ε_x, ε_y, ε_z	Turbulent dispersion coefficient
ε	Dissipation rate of turbulent kinetic energy
η	Parameter
η_0	Constant
κ	Von Kármán constant
ν	Kinematic viscosity of fluid
ρ	Fluid density
ρ_p	Particle density
ρ_q	volume fraction of the q^{th} phase in multiphase flow

σ	Parameter
σ_k	Constant
σ_ω	Constant
σ_c	Turbulent Schmidt number
τ	Particle relation time
τ_*	Dimensionless bed shear stress or Shields parameter
τ_{*c}, θ_{cr}	Critical dimensionless bed shear stress
τ_0	Local bed shear stress
τ_c	Critical bed shear stress
τ_{cd}	Critical bed shear stress for deposition
τ_{ce}	Critical bed shear stress for erosion
τ_{ij}	Viscous stress tensor
τ_w	Wall shear stress
τ_e	Lifetime of eddies
μ	Dynamic viscous coefficient
μ_t	Eddy viscosity
μ_{eff}	Total effective viscous coefficient
μ_w, μ_a	Dynamic water viscosity and air viscosity
φ	Repose angle
ϕ	Instantaneous flow properties such as velocity, density, and so on
$\overline{\phi}$, ϕ'	Time-averaged value and fluctuation component for flow component
ζ	a normal distributed random number
ξ	Coefficient
ψ	Simulated removal efficiency

List of Abbreviation

ADV	Acoustic Doppler Velocimeter
ASCE	American Society of Civil Engineers
BMPs	Best Management Practices
BOD_5	Biological Oxygen Demend in 5 days
BSS	Bed Shear Stress
BTKE	Bed Turbulent Kinetic Energy
CFD	Computational Fluid Dynamics
COD	Chemical Oxgyen Demand
DEM	Discrete Element Model
DNS	Direct Numerical Simulation
DPM	Discrete Phase Model
DRB/BDR	Django Reinhardt Basin/Bassin Django Reinhardt
DRWM	Discrete Random Walk Model
FDM	Finite Difference Method
FMG	Full MultiGrid initialization
FVM	Finite Volume Method
LBM	Lattice Boltzmann Method
LID	Low Impacts Development
LPS	Laser Particle Sizer
MDEP	Ma Department of Environment Protection
NS	Navier-Stokes
OTHU	Observatorie de Terrain en Hydrologie Urbaine
PCBs	Polychlorobyphenyls
PHAs	Polycyclic Aromatic Hydrocarbons
PISO	Pressure Implicit with Splitting of Operators
PVF	Particulate Volume Fractions
RANS	Reynolds time-Averaged Navier-Stokes
RE	Removal Efficiency
RNG	ReNormalized Group
RSM	Reynolds Stresses Model
SIMPLE	Semi-Implicit Method for Pressure Linked Equations
SIMPLEC	SIMPLE-Consistent
SPH	Smoothed Particle Hydrodynamics
SWMM	Storm Water Management Model
TKN	Total Kjeldahl Nitrogen
TSS	Total Suspended Solid
UDF	User Defined Function
USEPA	United States Environmental Protection Agency

VICAS	Vitesse de Chute en Assainissement
VOF	Volume of Fluid
WSUD	Water Sensitive Urban Design

Chapter 1 Introduction

1.1 Background

The process of urbanization has meant an increase in the proportion of impervious surfaces such as pavement and roofs in urbanized areas. These surfaces prevent precipitation from soaking into the ground naturally. Instead, a comparable volume of stormwater is discharged rapidly from the catchments. This overload of stormwater runoff runs quickly into storm drains, sewer systems, and drainage ditches and may cause:

- Downstream flooding
- Stream bank erosion
- Increased turbidity (muddiness created by stirred up sediment) from erosion
- Combined sewer overflow
- Infrastructure damage
- Contaminated streams, rivers, and coastal water

Stormwater runoff causes frequent flooding. and it also increases the load of pollutants conveyed by runoff, including nutrients, solids, metals, salt, pathogens, pesticides, hydrocarbons, etc. Generally, pollutants that have been deposited on land, streets, and motorways are scoured off and carried by runoff into nearby rivers, streams, lakes, ponds, wetlands, marine waters, groundwater, and the sewer system. This contaminated runoff significantly degrades water quality and aquatic habitats. For example, according to Massachusetts Department of Environment Protection (MDEP, 1997), stormwater runoff and the discharge from stormwater drain pipes were the largest contributors to water quality problems in the Commonwealth's rivers, streams, and marine waters.

Traditional stormwater management has focused on collecting stormwater in pipe networks and conveying it off site safely, economically, and as quickly as possible, either directly to streams or rivers, or to large stormwater management facilities (basins), or to combined sewer systems flowing to a wastewater treatment plant. With progressive urban development, natural waterways and drain and pipe systems in urbanized catchments have been increasingly taxed in their ability to convey the significantly increased quantities, and rate, of water flow (Wong *et al.*, 2006). This often results in urban flooding. Furthermore, there has been a growing global trend of flooding over recent years within the context of global climate change (Werritty *et al.*, 2002; Plate. 2002; Prudhomme *et al.*, 2003; Few *et al.*, 2004; Dore, 2005; Ryu and Butler, 2008).

Urbanization leads to changes in both the quantity and quality of stormwater runoff that is delivered to urban receiving waters. Growing public awareness of environmental issues in recent times has highlighted the importance of environmental management of urban stormwater. Traditional urban drainage systems were developed to meet the community's need to minimize the threat of flooding, rather than to preserve the quality of the environment. Therefore, in this field there is a clear need for additional design and assistance with implementation, as well as a need for greater information on managing the urban water cycle, especially the quality of stormwater (Alderson, 1999).

Sustainable urban development has been introduced into the management of stormwater. The main goals of stormwater management are to minimize stormwater runoff and to improve stormwater discharge quality in order to protect receiving water bodies. Stormwater management technologies and concepts (*e.g.* Water Sensitive Urban Design-WSUD, Low Impacts Development - LID, Best Management Practices - BMPs, etc.) have been developed to achieve these purposes. Stormwater Best Management Practices (BMPs) are recognized as one of the most effective and practical measures for reducing pollutants and for preventing pollutants from reaching the receiving water bodies, thus controlling the quality of runoff from a site.

Detention/retention systems are the first approach used in stormwater management, and involve large retention or detention basins or ponds. These basins can detain and retain stormwater discharge and allow sediment and trash to be removed or separated from the water before the stormwater is released into water receiving bodies. By reducing the flow velocity and controlling discharge rates, these facilities can decrease the likelihood of flooding and help to reduce the impact that impervious surfaces and urban development can have on water quality and aquatic habitats. They are still widely used in the U.S. (USEPA, 2011).

A detention basin is a dry pond or basin designed to hold storm water for at least 24 hours to reduce local and downstream flooding and to allow solids to settle. The detention basin should be able to regulate peak flow rates of large and infrequent storms (10, 25, or 100 years) and generally they remain dry. Unlike retention basins, detention basins have a limited ability for removing soluble pollutants due to the short time that stormwater runoff is detained.

1.2 Motivation

Nowadays stormwater detention basins have increasingly been used to control both stormwater quantity and quality. Originally, detention basins were designed solely to regulate the peak flow rate. However, monitoring studies have revealed that stormwater detention basins can also provide effective pollutant removal if they are of a sufficient size and if adequant settling time is available (Randall *et al.*, 1982; Grizzard *et al.*, 1986). The idea of using stormwater detention basins for the dual purpose of flood control and mitigation of pollutant runoff loads was put forward by several researchers in the 1970s (Ferrara *et al.*, 1983). Many existing stormwater detention basins fail to achieve the necessary levels of non-point source pollutant loading reduction. This includes those basins designed solely for stormwater runoff peak discharge magnitude mitigation as well as those detention basins designed both for quantity and quality control. Though improvements in the efficiency of detention basins have been extensively discussed in the literature over the past two decades (Ferrara *et al.*, 1983; Nix *et al.*, 1985; Loganathan *et al.*, 1994; Nix *et al.*, 1988; Marcoon and Guo, 2004; Akan, 2010; Takamatsu *et al.*, 2012) and some measurements have been applied to design, retrofitting and maintenance, not enough attention has been paid to improving understanding and representation. Due to the limited possibilities for the removal of soluble pollutants, usually the focus is on improving settlement efficiency for particulate pollutants within the basin. In the absence of a good understanding of the hydrodynamics of flow and the transportation of pollutant particles, many researchers consider the detention basin's water residence time to be the main way of evaluating the removal efficiency (noted as RE hereafter) of detention basins (Nix *et al.*, 1988; Persson, 2000; Marcoon and Guo, 2004;

Akan, 2010). Detention basins are generally designed assuming steady state and plug flow conditions, however, the behaviour of stormwater detention systems is very complex due to the dynamic nature of stormwater inflow, pollutant loads, and the state of the systems (*e.g.*, water depth, temperature, etc.). Nix *et al.* (1988) pointed out that steady state analyses were inappropriate for evaluating the performance of a stormwater detention basin system. In addition, the water residence time for existing detention basins is difficult to obtain. The removal rates of particulate pollutants are linked to sediments characteristic (in particular the settling velocity) and flow condition such as residence time. Over the past two decades, small-scale physical model experiments and corresponding numerical investigations have been carried out by researchers (*e.g.* Saul and Ellis, 1992; Stovin and Saul, 1994, 1996, 2000; Adamsson *et al.*, 2003; Dufresne, 2008; Dufresne *et al.*, 2009) to try to understand the sedimentation processes, but the results obtained remain difficult to apply to *in situ* basin (Torres, 2008), mainly due to:

- more complicated geometry
- temporal variation of flow and state of hydrodynamics
- variation of the pollutant loads and their properties
- Scale effect of similarity mainly regarding the particle characteristics

Therefore, it is necessary to carry out research in real full-scale basins via measurement and/or modelling, in order to further understand the sedimentation processes under *in situ* conditions, and to account for unsteady behaviour in order to represent the multiphase flow in both full and small-scale detention basins.

1.3 Objectives

This thesis aims i) to further improve the understanding of particulate pollutant sedimentation and resuspension processes in stormwater detention basins and ii) to provide effective ways for improvements to be made to the design and management of detention basins for stormwater quality.

The scientific objectives are:

- to contribute to further improving the understanding of the hydrodynamics and sedimentation characteristics in stormwater detention basins;
- to establish, test and verify the 3D numerical modelling of flow and particulate pollutants transport in stormwater detention basins;
- to contribute to improving the modelling of the interaction between particulate pollutants and the basin bottom;
- to develop a method which enables dynamic sediment transport, settling and entrainment under unsteady conditions to be represented using the Euler/Lagrange approach.

The investigations carried out in this thesis aim to provide ways of improving the pollutant removable performances of detention basins that may be applied in practice.

1.4 Structure of the Thesis

This thesis is organized in 6 chapters.

Chapter 1 gives a general introduction to the research undertaken.

Chapter 2 reviews relevant previous investigations on detention basins. These include research on the sediment sources, sediment characteristics, sediment transport mechanisms and investigations on detention basin performances with different methods such as scaled physical models, etc.

Chapter 3 introduces the experimental site and presents the methodology for experiments and numerical modelling.

Chapter 4 analyses the accumulated sediment's spatial distribution and its physical characteristics, such as density and particle size distribution, etc. It then presents the results of the flow modelling for the hydrodynamics in the Django Reinhardt detention basin, which are implicitly validated. The sediment transport modelling results under steady flow conditions are also analysed and discussed.

Chapter 5 mainly presents test cases for sediment transport under unsteady state conditions using the newly proposed method. The simulated results are explored and discussed.

Chapter 6 highlights general conclusions on the present work and outlines future perspectives.

Chapter 2 Literature review

This chapter begins with a general introduction to stormwater detention basins in urban drainage systems; this is followed by a presentation of experimental investigations on detention basins; finally, the numerical investigations are examined.

2.1 Global overview of stormwater detention basins

Stormwater is known to be one of the most important causes of water impairment in watercourses (German, 2005). The main objectives of stormwater management are to minimize stormwater runoff and to improve the quality of stormwater discharge in order to prevent the pollution of receiving water bodies. Sustainable urban development has been introduced into the management of stormwater. Stormwater management technologies and concepts (*e.g.* Water Sensitive Urban Design-WSUD, Low Impacts Development-LID, Best Management Practices -BMPs, etc.) have been developed for this purpose. Stormwater Best Management Practices (BMPs) are recognized as one of the most effective and practical measures for reducing and preventing pollutants from reaching water bodies and for controlling the quantity of runoff from a site (Lawrence *et al.*, 1996). For the last twenty to thirty years this has often been accomplished by constructing stormwater management ponds (or basins) on the site of new developments. Initially, the focus was on managing the runoff rate from a development in order to prevent flooding and erosion. In France, the use of detention basins dates back to the 1960s when '*Villes Nouvelles'*, or New Towns, were constructed. Such facilities have become much more widespread (Deutsch *et al.*, 1990). Meanwhile, it was realized that such basins could also play an important role in the reduction of urban rainfall runoff pollution (Valiron, 1985; Hall *et al.*, 1993). From that point on, stormwater basins were also used as settling basins to control stormwater quality. However, many existing stormwater basins have low removal efficiency for two main reasons: firstly, the majority of stormwater basins were designed solely for stormwater runoff peak discharge magnitude abatement and were enhanced later to improve pollutant removal performance through the addition of various retrofitting technologies; and, secondly, even if some stormwater basins were designed for both stormwater quantity and quality, they failed to achieve the necessary levels of pollutant load reduction due to an inadequate understanding of sedimentation processes (Guo *et al.*, 2000).

Detention basins are basins or reservoirs in which water is temporarily stored for the purpose of regulating a flood. Water can be released from the basin through its outlet which may be a weir, culvert or pipe. The storage volume may be recessed below natural ground level or above natural ground level with a road embankment acting as a dam wall. Detention basins can be classified according to both their location relative to the river channel or sewer (*e.g.* 'on-line' or 'off-line') and their content under dry weather flow conditions (*e.g.* 'dry' and 'wet') (Nascimento *et al.*, 1999). Dry and wet detention basins are often termed detention and retention facilities respectively, but for the purposes of this thesis the term 'detention basin' is used to encompass all flood storage basins in general. The general definitions are as follows:

2.1.1 Definitions

2.1.1.1 Dry basin (detention basin)

Detention basins are stormwater runoff containment areas that remain dry during dry weather except after rain storms when runoff is conveyed to them. The detention basins are designed initially to reduce and delay peak flow, to prevent local and downstream flooding and have subsequently been used to enhance the trapping of pollutants thanks to observations on their effective pollutant trap performance (Randall *et al.*1982; Grizzard *et al.*, 1986; Loganathan *et al.*, 1994). A detention basin often has a dry bed which is usually achieved with the use of a low – flow channel or pipe system. Thus, these basins may have multi-functional purposes and can be used for sporting activities and as open spaces. Detention basins generally provide only minimal water quality improvement (Department of Transport and Main Roads, 2013).

2.1.1.2 Wet basin (retention basin)

Retention basins are stormwater basins that incorporate a permanent pool and retain some water in the basin between storm events. These basins provide flood attenuation benefits during a range of flood events and provide water quality benefits during more frequent minor flood flow and regular storms. The permanent pool within a wet basin may consist of a lake, wetland, or water quality pond (Department of Transport and Main Roads, 2013). Retention basins are covered by the term detendtion basins for the purposes of discussion of sediment transport within this thesis.

2.1.2 General performances

As discussed above, the effective efficiency of detention basins has not been satisfactory to date due to the lack of consideration given to runoff quality control criteria and and the lack of appropriate design methods. Table 2-1 shows the annual potential and short-term removal efficiency of detention basin recorded by Adler (1993) in studies conducted by the French institution CEMAGREF in separate drainage systems, together with a synthesis carried out by Valiron and Tabuchi (1992).

Table 2-1 Efficiency of detention basin (Nascimento et al., 1999)

	Ulis Sud[a] detention basin			Pollutant reduction after 2 h of decantation (%)
	Annual inflow load (kg/ha imp.)	Annual outflow load (kg/ha imp.)	Annual removal efficiency (%)	
TSS	3902	387	90.1	88
BOD_5	829	107	87.1	76
COD	2598	521	79.9	-
TKN	189	91	51.8	-
P total	44	22	50.6	-
Pb	0.893	0.054	94.0	65
Zn	5.12	0.66	87.1	77

Cd	0.0310	0.0051	83.7	-
Cu	-	-	-	69
Hydrocarbons	65	4	94.2	-

[a] Watershed surface: 70ha; average runoff coefficient: 0.48
TSS: total suspended solid; BOD_5: biochemical oxygen demand for 5 days; COD: chemical oxygen demand; TKN: total Kjeldahl nitrogen

Table 2-2 shows the efficiency recorded in some UK detention basins, the overall range of trap efficiency reported in the literature and experimental settling rates (Nascimento *et al.*, 1999). The results from Table 2-1 indicate that detention basins may perform effectively at removing different pollutants from stormwater columns. However, the removal efficiency of detention basins is not variable. Table 2-2 indicates the pollutant removal efficiency recorded for some UK detention basins and compares those possessing inlet sediment control traps to the overall range of removal efficiencies reported in the literature and with experimental settling rates. From the Table 2-2, we can see that the removal efficiencies of different detention basins vary across a large range.

Table 2-2 Efficiencies of detention basins (Nascimento et al., 1999)

Pollutant	Imhoff settleablity(24h)	Detention basin 2h removal (%)	Detention basin 6h removal (%)	Range of observed removal efficiency (%)
TSS	68	34	84	49-91
BOD_5	32	13	48	14-53
P total	46	20	58	20-70
Pb	62	30	66	46-78
Oil/Hydrocarbons	69	18	62	20-78
Total coliforms	71	60	72	47-73

Gonzalez-Merchan (2012) estimated the annual removal efficiency of TSS in the Django Reinhardt detention basin located at Lyon in France using *in situ* monitoring data, and found it to be between 33% and 75% during the years 2004-2010. Pettersson *et al.* (1998) and Comings *et al.* (2000) also reported that the settleable solids' removal efficiencies were between 40% and 90%. In short, the removal efficiencies of the detention basin are not satisfactory or well-controlled.

Nix (1985) stated that detention basins are normally categorized as one of three types: plug flow, completely mixed flow and intermediate flow. Detention basins are often designed based on steady state conditions, which do not represent the situation in real basins. The discrepancies between theoretical and steady state values of mean residence time in unsteady conditions in real stormwater detention basins have resulted in poor pollutant control capabilities. In fact, detention basin's rate of efficiency in reducing solid pollutants is the result of the combination of a large number of variables, which include the physical, chemical and biological characteristics of the pollutants, as well as the precipitation regimes, resident time in the basin, geometric characteristics (*e.g.* depth, shape, volume, and outlet configuration), the quality of maintenance services, and so on. Zhang (2009) reported that sediment, flow and basin characteristics are the main factors which influence the RE of detention basins.

Given the many parameters that influence the settling processes in detention basins, it is very difficult to predict RE in a simple manner. The most accurate predictions will be those based

on theoretical relationships that incorporate all of the influencing factors (Verstraeten and Poesen, 2000). For example, factors such as pond shape, inlet/outlet configurations and physical environment should be included since they can significantly influence both hydraulic performances of these facilities and the sedimentation process. Such factors have led to different design recommendations for improving hydraulic performances and also ultimately for improving water quality. For dry or semi-dry ponds, the presence of a vegetation cover on the bottom of the pond can have major effects on the sedimentation process. However, traditional design methods do not address hydrodynamic features of flow, and these methods cannot evaluate sedimentation performances resulting from different measures such as baffles or different inlet/outlet positions in advance (Verstraeten and Poesen, 2000; Zhang, 2009). Figure 2-1summarizes the factors which impact the removal efficiency of basins.

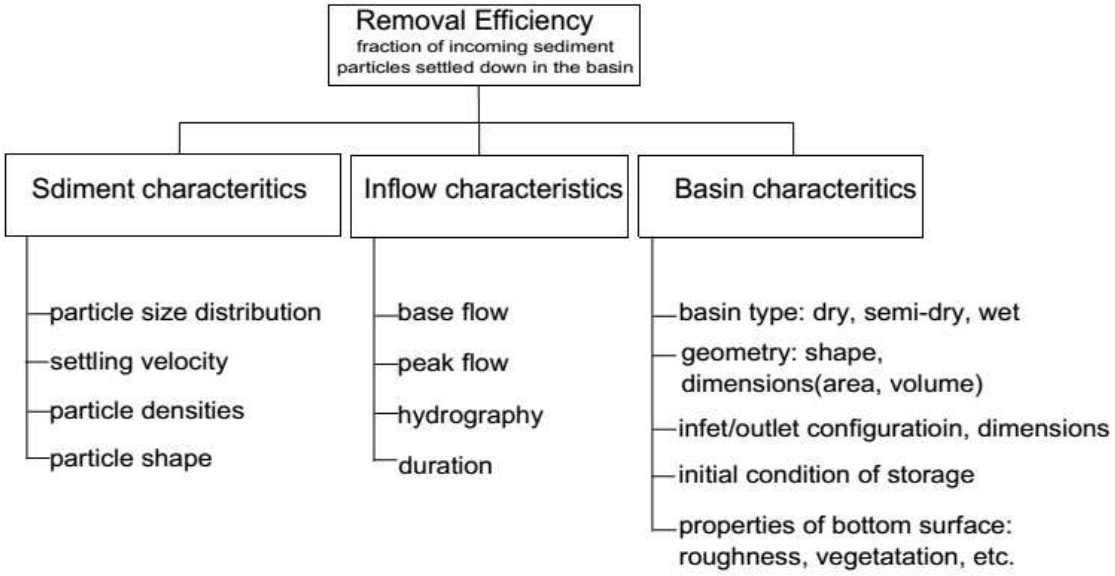

Figure 2-1 Main factors that influence the removal efficiency of basin (adapted from Verstraeten and Poesen, 2000)

2.1.3 Retrofit practices for improving water quality in detention basins

Retrofitting in existing stormwater detention facilities is of critical importance for restoring impaired watersheds. Many existing stormwater detention basins were designed solely for stormwater runoff peak discharge magnitude abatement or were designed for water quality control standards at the time of construction. With the purpose of improving the effectiveness of pollutant RE, many authors have investigated the impact factors on effectiveness, including basin geometry, inflow and outflow devices, and so on.

In order to extend detention time, Guo *et al.* (2000) tried retrofitting smaller outlet pipes and floating risers in the outlet of detention basins. By comparing monitoring data taken before and after retrofitting, it was found that both outlet modifications resulted in longer detention

times in the basin for the same volume of runoff inflow. However, contrary to what might have been expected it was found that the TSS (total suspended solids) removal efficiency did not correlate to the detention time. The extended residence time did not result in improved TSS removal efficiency. Marcoon *et al.* (2004) evaluated the different outlet structure designs for potential improvements in water quality using 2D modelling with PondPack^{TM} software. The analysis of hydraulic results enabled them to identify all possible design options, water quality benefits, and all potential negative impacts.

Vega *et al.* (2003) used MIKE21 to predict the effects of changes in sludge content, baffling, inlet-outlet positioning and basin geometry on the hydrodynamic performance of WSP. The results suggested that the provision of two baffles placed at 1/3L and 2/3L (L = length of basin) increases the pond retention factor and BOD_5 (Biological Oxygen Demand over 5 days) removal efficiency. Akan (2010) developed a set of procedures to be used when making a quick evaluation of existing retrofitted or trial designed dry detention basins. The methodology can also be employed in the preliminary sizing of a new extended dry detention basin and of its water quality outlets.

Guo (2009) illustrated how to retrofit existing detention basins with a perforated plate and micropool for water quality control. A designed outfall box with a slow release for micro events and a fast release for extreme events is recommended for new or existing basins.

Bennett *et al.* (1985) used dynamic programming methods to find the optimal minimum cost, location and the size of detention basins. Nix *et al.* (1988) demonstrated an approach for estimating the long-term performance of detention basin behaviour based on SWMM. The information generated can be used to provide guidance for the planning and design of a detention basin.

Ormsbee *et al.* (1987) proposed dynamic programming formulations for dual purpose detention systems. These proposed formulations can be used to determine the location and the dimensions of basins and associated outlet devices.

Akan (1992) presented a design aid for sizing detention basins and outlet facilities for the removal of particulate pollutants from runoff. With this design aid, one can determine the stage storage relationship for a basin, the size of outlet structure and storage volume.

The retrofit practices and methods mentioned above are mostly based on theoretical or empirical models which contribute to detention basin system design and management, either through positive practical experience or lessons from failures. Some retrofit measures can improve RE, while others have failed (Vega *et al.*, 2003). For example, common sense would suggest that a baffle would improve RE by decreasing the inflow velocity and increasing flow path length, but Nighman and Harhor (1997) reported that after modification using a baffle in the detention basin, the RE dramatically decreased from an average 68% to 2.7% for three storm events in four monitored cases. This shows that common sense is not always to be trusted and there is a need for further research for baffle design that will reliably increase RE for a range of flow conditions. Retrofit practices are sometimes ineffective and hard to quantify due to poor understanding of hydraulic performance and sedimentation processes. As mentioned above, many factors influence the removal efficiency of detention basins, but these

factors have not all been well-examined and the sedimentation processes are not well-understood.

2.2 Mechanisms related to Sediment transport

2.2.1 Source of stormwater solids

According to Ashley *et al.* (2004), the solids entering sewer systems originate from a variety of sources. Four principal sources are typically defined:

- The atmosphere, which contains fine dust and aerosols;
- Surfaces in catchments, where solids accumulate during dry weather periods and are washed off during storm events: roofs, streets, parkings, highways, etc.;
- The environment and processes taking place inside the drainage/sewer system: natural water body interactions, infiltration/exfiltration , decay and degradation of solids;
- Industrial and commercial effluents and solids from construction sites, which typically contributes very significantly to the solid loads entering sewers.

Ashley and Crabtree (1992) argued that it is not possible to draw up universal rules to identify which sources make the greatest contributions to sediment inputs for particular catchments. Localized effects can predominate; construction activities for example, have been shown (Broeker, 1984) to increase surface wash-off loadings by up to 300%.

Dembélé (2010) noted that the main pollutants in urban runoff primarily originate from two sources: the atmosphere and watersheds.

The sediment load is known to vary during a storm, and first flush flow rates in stormwater runoff are an example of this (Ashley *et al*., 2004). The finest particles and dissolved pollutants are washed off at the start of a storm and correspond to the majority of pollutants which are made up of the finest solids fractions, with particles smaller than 250 μm comprising some 75% of the total solids and chemical pollutant load washed in from road surfaces (Ashley *et al.*, 2004).

Deletic *et al.* (1997) monitored the solid and dissolved pollutants that washed off asphalt surfaces in Belgrade and Lund to show that a deterministic model for solid washoff was applicable and accounted for non-uniform sediment build-up over the contributing surface. The model was extended to estimate the transport of particles through grass filter strips (Deletic, 2001).

2.2.2 Characteristics and quantities of particulate pollutants in drainage systems

This section aims to give an overview of particulate pollutants characteristics in urban drainage systems.

Generally, the most common pollutant types that have attracted interest in sewer systems have been BOD_5 (biological oxygen demand in 5 day), COD (chemical oxygen demand), TKN (total Kjeldahl nitrogen), metals (*e.g.* Cd, Cr, Cu, Fe, Mn, Ni, Pb, Zn), hydrocarbon, PAHs (polycyclic aromatic hydrocarbons) and PCBs (polychlorobyphenyls) (Bertrand-Krajewski, 1993, cited in Ashley *et al.*, 2004). Table 2-3 shows general ranges for COD, heavy metals and hydrocarbon mean concentrations. More recently, microbial hazards have attracted more and more attention form researchers (Gourmelon *et al.*, 2010; Sebastian *et al.*, 2011). Some pollutants are attached to particles rather than being dissolved in the runoff, such as phosphorus, some heavy metals, and organic pollutants such as polynuclear aromatic hydrocarbons (Furumai *et al.*, 2002; Lee *et al.*, 2005; Vaze and Chiew, 2004). Hvitved-Jacobsen *et al.* (1994) also reported that 60-80% of phosphorus, 30-40% of Zn, 70-80% of Pb and 30-40% of Cu are associated with suspended solids charged in the stormwater runoff. Bertrand-Krajewski (1993), Chebbo (1992) and Bachoc *et al.* (1993) reported the percentage of pollutants attached to solids (in Table 2-4). It has been well-established that a diverse range of potential pollutants may attach themselves to solids and that the particulate fraction includes the largest proportion of potential pollution load (Ashley *et al.*, 2004). Absorption capacity depends on particle size. Generally, smaller particles have a higher absorption capacity per unit mass due to their larger specific surface area (Furumai *et al.*, 2002; Ashley *et al.*, 2004; Lee *et al.*, 2005). The finest particles and dissolved pollutants are washed off at the start of a storm and the strongest pollutants are associated with the finest solids fractions, with particulates smaller than 250 micron comprising some 75% of the total solids and chemical pollutant load washed from road surfaces (Ashley *et al.*, 2004). According to Ellis and Revitt (1982), about 70% of metals were attached to particles of less than 100 μm, which represent less than 15% by weight of settled solids at the sites monitored.

Table 2-3 Mean COD, metals and hydrocarbon concentrations observed in stormwater (Bertrand-Krajewski, 1993)

pollutant	Unit	Minimum	Maximum
COD	mg/L	20	160
Cd	μg/L	0.15	17
Cr	μg/L	0.16	14
Cu	μg/L	0.50	78
Fe	μg/L	0.10	300
Mn	μg/L	1	15
Ni	μg/L	1.5	50
Pb	μg/L	1.6	110
Zn	μg/L	5	800
Hydrocarbons	mg/L	0.02	0.07

Table 2-4 Percentage of the particulate fraction for different pollutants (Bertrand-Krajewski, 1993, in Ashley et al., 2004)

pollutant	COD	BOD_5	TKN	Cd	Pb	Zn	Hydrocarbons	PHAs	PCBs
Particulate fraction	83-90%	77-95%	57-82%	>95%	68-96%	>95%	80-90%	79-97%	90-93%

Chebbo and Bachoc (1993) reported that fine particles (<100 μm) with a median diameter (d_{50}) ranging from 25 μm to 44 μm were dominant in suspended solid during wet weather. As shown in

Table 2-5, the results of measurements taken showed about 68%-85% of TSS with a diameter of less than 100 μm. Becouze-Lareure (2010) measured the grain sizes for several storm events in a storm sewer network and the results indicated that grain size was heterogeneous, with values of d_{50} between 85 μm and 117 μm as opposed to the values of between 7 μm and 17 μm as reported in the literature for the same type of site (Marsalek *et al.*, 1998, Corsi *et al.*, 1999). Torres (2008) reported that the average d_{50} for two storm events ranged from 64 μm to 92 μm. These measured results may imply that fine particles are dominant in TSS and that grain size is heterogeneous in spatial and temporal ranges. Density is an important property of sediment. Typically, the largest particles have the lowest density in wastewater systems (Chocat, 1997; Ashley *et al*., 2004). However, lower density of finer fractions of particles in stormwater runoff has also been reported, as finer fractions of particles may contain more organic matter (Kayhanian *et al*., 2012). Hence, it seems that the density of sediment depends on the site. Generally, particle density is about 1700 kg/m^3 to 2200 kg/m^3 in a combined sewer network, lower than that (<2200 kg/m^3) in separate storm sewers (Chebbo and Bachoc, 1993; Ashley *et al*., 2004).

Table 2-5 Grain size characteristics for suspended solids in urban wet weather discharges (Chebbo, 1992)

Type of network	d_{10}(μm)	d_{50}(μm)	d_{90}(μm)	%< 100 μm
Storm sewer networks	6-9	29-38	265-1375	76%-85%
Combined networks	4-13	25-44	183-497	66%-82%

The settling velocity of particles is the most important property in sediment because it often depends on diameter, density, shape and surface roughness as well as the submerged fluid viscosity (Loch, 2001). Settling velocity has been used as a parameter in most transport models. Generally, the settling velocity of suspended solids is variable and it is difficult to obtain representative results for the settlement of sewage particulates (Ashley *et al.* 2004) due to the heterogeneity of suspended solids. However, the interval of settling velocity is relatively comparably similar. Torres (2008) reported average median settling velocity of between 0.2 m/h - 11 m/h in combined networks and 0.6 m/h - 9m/h in separated networks (Chocat *et al.*, 1997; Ashley *et al.*, 2004; Chocat *et al.*, 2007). Due to different measurement technologies and the complexity of sampling techniques, up to now there has been no common appropriate method agreed upon in the literature for giving the settling velocity for individual suspended solids in a drainage system. The settling velocity of suspended solids in drainage systems has often been measured in the laboratory using collected samples. The results have often been expressed as the possible maximum settling velocity for certain percentage mass with S-shaped curves as in Figure 2-2. Torres (2008) tried to find a relationship between the settling velocity (V_{50}) and other particles' properties such as the diameter (d_{50}) based on a series of storm sample measurement results with the VICAS protocol. Unfortunately, there no clear direct relationship was observed between the settling velocity and the particle sizes. Hence, it is difficult to perform a simulation to estimate the corresponding settling velocity for non-uniform particles.

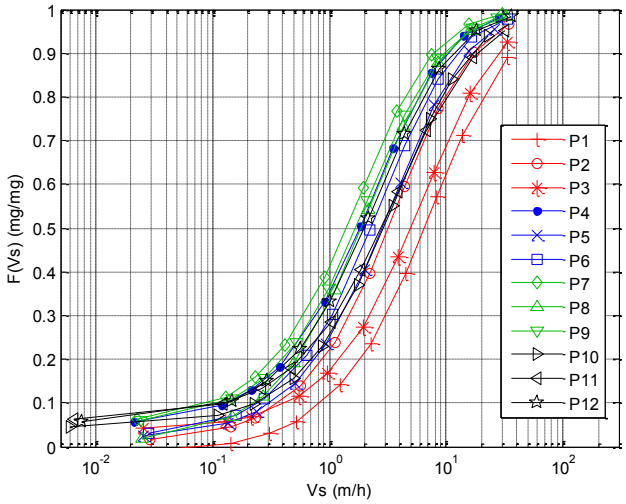

Figure 2-2 Sediment settling velocity measured with VICAS protocol (Torres, 2008)

2.2.3 Mechanisms related to sediment transport

2.2.3.1 Description of the key mechanisms

Sediment transport, where it refers to the motion of solid particles, usually consists of the natural processes of erosion, transportation and sedimentation. Figure 2-3 illustrates the general nature of a sediment transport process in flow (Julien, 2010). It is one of the most important and common processes or phenomenon encountered in the fields of hydraulics, hydrology and water resource engineering. Sediment transport occurs in rivers, reservoirs, channels, and marine environment, etc. It is a very complex multiphase phenomenon which involves complex physical, chemical and biological processes. It has been active throughout time and has shaped the present landscape of our world. Today, it can cause severe engineering and environmental problems. A lot of attention is paid to this field in order to to estimate, avoid or enhance engineering processes. For example, Kantoush *et al*. (2008c) investigated the sedimentation in shallow reservoirs with the aim of controlling the accumulation of sediment in reservoirs which leads to the reduction of the effective storage capacity.

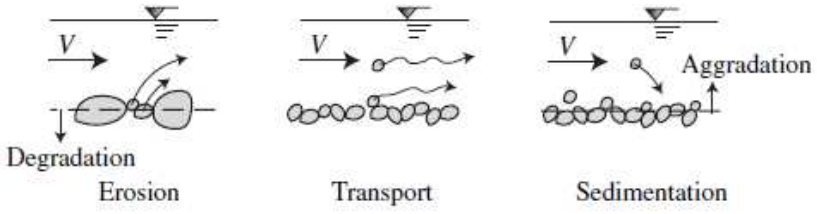

Figure 2-3 Processes of erosion, transport and sedimentation (Julien, 2010)

Sediment transport is usually divided into suspended load and bed load transport due to their different characteristics, as shown in Figure 2-4. The fraction of bed load and suspended load

varies dynamically due to the interaction between the erosion, transport and sedimentation processes.

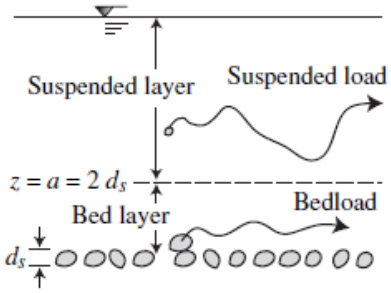

Figure 2-4 Definition of bed load and suspended load (Julien, 2010)

Generally, three types of sediment transport are identified: wash load, suspended load and bed load.

Wash load is the portion of sediment that is carried by fluid flow; it is in near-permanent suspension and is transported without deposition occuring, essentially passing straight through the stream. It consists of the finest particles and can be defined as having a Rouse number of <0.8, meaning that the turbulent mixing velocity is far greater than the settling velocity.

Suspended load is the portion of the sediment that is carried by fluid flow which settles so slowly that it hardly touches the bed. It is maintained in suspension by the turbulence in flowing water.

Bed load describes particles in a flowing fluid (usually water) that are transported along the bed. Bed load is complementary to suspended load and wash load. It often involves the motion of rolling, sliding, and/or saltating as shown in Figure 2-5.

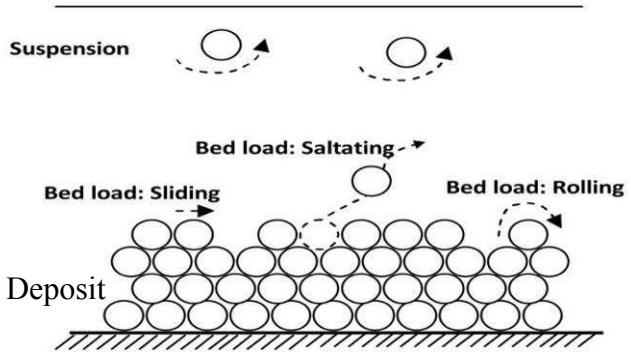

Figure 2-5 Sketch of representation of bed load movements

The total sediment load is the sum of the three types of load. Wash load is carried within the water column as part of the flow, and therefore moves with the mean flow velocity of the main stream. Because there is little or no interaction with the bed, the particles extract only negligible momentum from the flow. Many authors simply distinguish between bed load and

suspended load, assuming that the wash load is not really a mode of solid transport (Bertrand-Krajewski, 2012).

As the real sediment transport processes are interactive and dynamic, the interface of bed load and suspended load are partly arbitrary and hard to identify, however, making this distinction is useful for theoretical and experimental approaches and work. In practice it is commonly accepted that there is a thin bed load layer above the immobile bed. The top of the thin layer is considered to be the frontier between the suspended load and the bed load (Chanson, 1999).

2.2.3.2 Modelling of sediment transport mechanisms

Sediment transport mechanism is fundamental. In this section methods for predicting the suspended load and bed load transport rates are presented. Nowadays, CFD technology is becoming more and more popular, but empirical models for calculating sediment transport in rivers, reservoirs, basins, etc. are still dominant in engineering.

a. Suspended load transport

The suspended load is described by the concentration C in mass (kg/m^3) or in volume (m^3/m^3). The transport of suspended load material is controlled by a combination of advection, turbulent diffusion and convection. Diffusion characterizes the random motion and mixing of particles throughout the superimposed water depth along the longitudinal flow motion.

b. Advection-diffusion equation

The conservation of sediment mass in incompressible dilute suspension subject to diffusion, mixing, dispersion, and advection, is described by the advection-diffusion equation:

$$\underbrace{\frac{\partial C}{\partial t}}_{mass\ change} \underbrace{+u_x\frac{\partial C}{\partial x}+u_y\frac{\partial C}{\partial y}+u_w\frac{\partial C}{\partial z}}_{advective\ terms} = \underbrace{\left(D_m+\varepsilon_x\right)\frac{\partial C^2}{\partial x^2}+\left(D_m+\varepsilon_y\right)\frac{\partial C^2}{\partial y^2}+\left(D_m+\varepsilon_z\right)\frac{\partial C^2}{\partial z^2}}_{diffusive\ mixing\ terms}+\underbrace{S_c}_{sources\ term} \tag{2.1}$$

Where C is the concentration of suspended load, ε_x, ε_y and ε_z are the turbulent dispersion coefficients, D_m is the molecular diffusion coefficient and S_c is the term of phase change sources / sinks.

In laminar flow, the turbulent mixing and dispersive coefficients vanish ($\varepsilon_x = \varepsilon_y = \varepsilon_z = 0$). Conversely, in turbulent flow, the molecular diffusion coefficient D_m is negligible when compared to the turbulent mixing and dispersion coefficients ($D_m << \varepsilon$). The advection-diffusion equation has numerous applications in hydraulic modelling within the field of sediment and contaminant transport in open channels.

c. Vertical concentration profile

If the density of sediment is heavier than the continuous phase (normally water), the sediment concentration near the bottom is larger. Rouse (1937) established the following formula to describe the vertical concentration profile *C(z)*:

$$\frac{C(z)}{C(a)} = \left(\frac{h-z}{z} \frac{a}{h-a} \right)^{R_0} \tag{2.2}$$

$$R_0 = \frac{v_s}{\beta_s \kappa u_*} \tag{2.3}$$

Where $C(a)$ represents the reference sediment concentration at a reference elevation "a" above the bed elevation and h is water depth. The relative concentration $C(z)/C(a)$ depends on the elevation z above the reference elevation as derived by Rouse (1937). The exponent R_o refers to the Rouse number and reflects the ratio of sediment properties to the hydraulic characteristics of the flow. u_* is shear velocity, and v_s is particle settling velocity, with $\beta_s = 1$ and von Kármán constant $\kappa = 0.4$.

The suspended load transport rate q_s (in Kg/m^2/s) can be calculated using:

$$q_s = \int_a^h C(z) u(z) dz \tag{2.4}$$

Where *u(z)* is the logarithmic velocity profile along the vertical axis. For turbulent flow regime over a smooth bed, *u(z)* is given by:

$$u(z) = u_* \left(5.75 \log \left(\frac{z u_*}{\nu} \right) + 5.5 \right) \tag{2.5}$$

For a turbulent flow regime over a rough bed, *u(z)* is given by:

$$u(z) = u_* \left(5.75 \log \left(\frac{z}{k_s} \right) + 8.5 \right) \tag{2.6}$$

Where k_s is the bed sand equivalent roughness of Nikuradse: $k_s \approx 2d_{50}$ if the bed is flat, and k_s is equal to the height of the dunes if dunes are present on the bed.

Van Rijn (1984a) proposed a method for calculating the suspended load transport rate based on data from laboratory flume and river experiments. The computation method is complex and is not relevant in this case. Further information can be found in Van Rijn (1984a).

d. Bed load transport

It is widely accepted that bed load transport generally consists of sliding, rolling and saltating motion. Initially bed load transport was a problematic issue in sediment study due to the lack of advanced measuring instruments. Therefore, instead of investigating the sediment mechanism on a particle scale, early research on sediment transport mechanisms often looked at groups of particles on a macro scale. The concept of sediment transport rate (or bed load discharge) is often used to describe sediment transport. Bed load L_b refers to a quantity of sediment that is moving in the bed layer, which can be measured by volume, mass, or weight. In SI units, bed load is usually measured using mass in metric tons (1000 kg). Since some empirical formulas were not created using SI units, unit conversions are needed. Conversions from volume to mass involve the mass density of sediment ρ_p where $L_{bm} = \rho_p L_{bv}$. Similarly, conversions from mass to weight involve the gravitational acceleration g, i.e. $L_{bw} = gL_{bm} = \rho_p g L_{bv}$. The bed load discharge Q_b is the flux of sediment moving in the bed layer. The fundamental dimensions of Q_b by volume, mass, or weight are summarized in Table 2-6. The unit bed load discharge q_b is the flux of sediment per unit width and per unit time moving in the bed layer. The unit bed load discharge can be measured in weight (M/T^3), mass (M/LT) or volume (L^2/T)

Table 2-6 Fundamental dimensions of bed load (Julien, 2010)

	by volume	By mass	By weight
Bedload	$L_{bv}(L^3)$	$L_{bm}(M)$	$L_{bw}\ (ML/T^2)$
Bed load discharge	$Q_{bv}(L^3/T)$	$Q_{bm}(M/T)$	$Q_{bw}\ (ML/T^3)$
Unit bed load discharge	$q_{bv}(L^2/T)$	$q_{bm}\ (M/LT)$	$q_{bw}(M/T^3)$

Note: $L_{bw} = gL_{bm} = \gamma_p L_{bv}$, $L_{bm} = \rho_p L_{bv}$

$$Q_b = \int_0^w q_b dW \,, L_b = \int_0^T Q_b dT$$

Table 2-6 summarizes the relationships between bed load, bed load discharge, and unit bed load discharge. In terms of notation, the first subscript, *b,* refers to bed load and the second subscript refers to volume, mass, or weight.

A lot of research on bed load transport has been carried out and many models have been established over the past century. Usually, these models are based on equilibrium conditions. Bertrand-Krajewski (2012) classified these bed load transport formulas in four main categories, depending on their derivation:

- Formulas based on shear stress excess (τ_0- τ_c), where τ_0 is the local bed shear stress and τ_c is the critical bed shear stress for particle inception movement (*e.g.* Meyer-Peter Müller's formula);
- Formulas based on probability of movement(*e.g.* Einstein formulas);
- Formulas based on the stream power concept (*e.g.* Bagnold formula);
- Formulas based on dimensionless variables (*e.g.* van Rijn formula).

Another classification by Julien (2010) considered that bed load transport could be treated either as a deterministic or a probabilistic problem. Deterministic methods have been proposed by Du Boys (1879) and Meyer-Peter & Muller (1948); probabilistic methods were developed by Kalinske (1942) and Einstein (1950). Both approaches yield satisfactory estimates of bed load discharge.

e. Empirical Bedload transport formulas

Among these numerous bed load formulas, a few of them, which are widely used in engineering, are quoted below.

Duboys (1879) developed a bed load formula based on the concept that sediment moves in thin layers along the bed. The applied bed shear stress τ_0 must exceed the critical bed shear stress τ_c to initiate motion. The volume of gravel material in motion per unit width and time q_{bv} is calculated using (adapted into SI unit form by Julien, 2010):

$$q_{bv} = \frac{67.05655}{d^{3/4}} \tau_0 \tau_c \tag{2.7}$$

Where d is the particle size and τ_0 is the local shear stress. Note that in this formula the critical shear stress τ_c is calculated using (adapted into SI unit form Julien, 2010):

$$\tau_c = 0.00847 + 0.0000128693d \tag{2.8}$$

Meyer-Peter and Muller (1948) developed a complex bed load formula for sediment mixtures and various densities of the surface layer of the bed material.

$$\frac{\rho}{(\rho_s - \rho)d_e}\left(\frac{k_B}{k_r}\right)hJ = 0.047 + 0.25\frac{\rho^{1/3}}{g^{1/3}(\rho_p - \rho)^{1/3}\rho_p{}^{2/3}d_e}q_{bm}^{2/3} \tag{2.9}$$

Where q_{bm} is bed load discharge, h is the water depth, J is the energy gradient, d_e is effective diameter, calculated using the equation (2.10), k_B is ripple factor according to the Manning – Strickler coefficient of bed forms, k_r is particle roughness according to the Manning–Strickler coefficient of particles, given by Strickler (1923) in the equation (2.11).

$$d_e = \frac{\sum_i \overline{d}_i p_i}{\sum_i p_i} \tag{2.10}$$

Where p_i is the percentage by mass of the i^{th} class of particles whose mean size is $\overline{d}_i$.

$$k_r = \frac{21.1}{d_{50}^{1/6}} \tag{2.11}$$

Where d_{50} is the median particle size.

Chien (1956) demonstrated that the elaborate original formulation can be reduced to the following simple form if neither ripples nor other bed forms (dunes, anti-dunes) are present:

$$\frac{q_{bv}}{\sqrt{\left(\frac{\rho_{\mathrm{p}}-\rho}{\rho}\right)gd_e^3}} = 8\left(\tau_* - 0.047\right)^{3/2} = 8\left(\tau_* - \tau_{*_c}\right)^{3/2} \tag{2.12}$$

Where τ_* is the Shields parameter (or dimensionless shear stress, $\tau_* = \tau_0/(\gamma_p-\gamma)d$), and τ_{*c} is the critical dimensionless shear stress (here equal to 0.047).

Einstein (1942) introduced the idea that particles move in steps proportional to their sizes. He used probability concepts extensively to define a relationship of sediment discharge. Taking into account the correction proposed by Brown (1950), the formula can be expressed as:

$$q_{bv^*} = \frac{q_{bv}}{\sqrt{\left(\frac{\rho_p-\rho}{\rho}\right)gd^3}\left[\sqrt{\frac{2}{3}+\frac{36\nu^2}{\left(\frac{\rho_p-\rho}{\rho}\right)gd^3}}-\sqrt{\frac{36\nu^2}{\left(\frac{\rho_p-\rho}{\rho}\right)gd^3}}\right]} \tag{2.13}$$

Where ν is the kinematic viscous coefficient, q_{bv^*} is the dimensionless rate of sediment transport, this is shown in Figure 2-6 as a function of the Shields parameter τ_*, with the measurements from Gilbert (1914), Bogardi (1974) and Wilson (1966). For very coarse sand and gravel, q_{bv^*} can be estimated as:

$$q_{bv^*} \cong \frac{q_{bv}}{\sqrt{\left(\frac{\rho_p-\rho}{\rho}\right)gd^3}} \quad if\ d > 1\,mm \tag{2.14}$$

Brown (1950) suggested the following two relationships:

$$q_{bv^*} = 2.15\exp(-0.391/\tau_*) \quad if \quad \tau_* < 0.18 \tag{2.15}$$

$$q_{bv^*} = 40\,\tau_*^3 \quad if \quad 0.18 < \tau_* < 0.52 \tag{2.16}$$

For sediment transport at high shear rates, one obtains (Julien, 2010):

$$q_{bv^*} = 15\,\tau_*^{1.5} \quad if \quad \tau_* > 0.52 \tag{2.17}$$

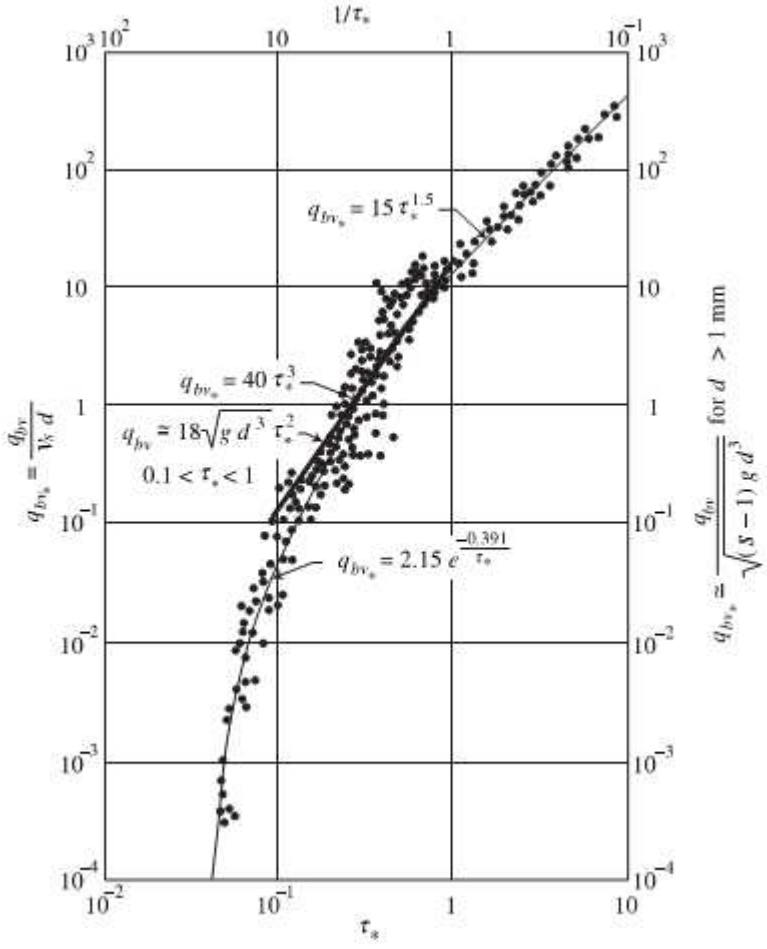

Figure 2-6 Dimensionless sediment discharge q_{bv*} versus Shields parameter τ_* (adapted from* Julien, 2010*).

Van Rijn (1984b) developed a formula for calculating the bed load discharge based on the empirical experimental data.

$$q_{bm} = 0.053 \frac{T'^{2.1}}{D*^{0.3}} \rho_p \sqrt{\left(\frac{\rho_p - \rho}{\rho}\right) g d_{50}^3} \tag{2.18}$$

Where $D*$ is the dimensionless particle diameter:

$$D* = d_{50}\left(\frac{\rho_p - \rho}{\rho \nu^2} g\right)^{1/3} \tag{2.19}$$

And T' is the transport parameter, calculated using:

$$T' = \frac{(u_*')^2 - (u_{*c})^2}{(u_*')^2} \tag{2.20}$$

$$u_*' = \frac{\sqrt{g}U}{18\log\left(\frac{12R_b}{3d_{90}}\right)} \tag{2.21}$$

Where U is the mean flow velocity, u_{*c} is the critical shear velocity according to the Shields diagram (shown in Figure 2-7), u_* is the effective bed shear velocity, R_b is the hydraulic radius which has a relationship with the bed according to Einstein (1942) or Vanoni-Brooks's (1957) side wall correction method.

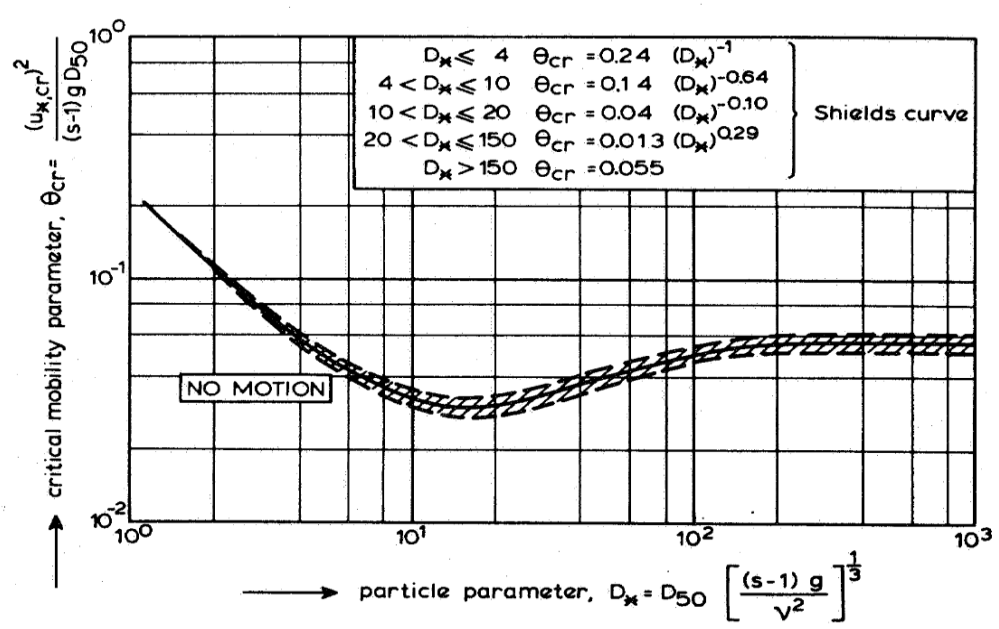

Figure 2-7 Modified Shields diagram with power equations fitted by Van Rijn (note, $s=\rho_p/\rho$, from van Rijn, 1984b)

Yalin (1963) proposed the following formula for bed load transport:

$$\frac{q_{bm}}{\sqrt{(s-1)gd^3}} = 0.635r\sqrt{\tau_*}\left[1 - \frac{1}{\sigma r}\ln(1+\sigma r)\right] \tag{2.22}$$

Where (2.23)

$$r = \frac{\tau_*}{\tau_{*c}} \tag{2.24}$$

$$\sigma = 2.45\frac{\sqrt{\tau_{*c}}}{s^{0.4}} \tag{2.25}$$

Nielsen (1992) proposed the following formula for bed load transport:

$$\frac{q_{bm}}{\sqrt{(s-1)gd^3}} = 12(\tau_* - \tau_{*_c})\sqrt{\tau_*} \tag{2.26}$$

Generally, the empirical bed load transport models were established under conditions of equilibrium. They are not suitable to for non-equilibrium conditions. These models are often used in species modelling. These models have not been used here, because the DPM (discrete phase model) approach has been selected instead to model the sediment transport.

f. Incipient motion (entrainment)

Fluid flow around sediment particles exerts forces which tend to initiate particle motion. The resisting force of non-cohesive material is made up of particle weight and frictional resistance from the boundary. Particles tend to incipient motion when the forces from the flow exceed the resistance forces. Many authors have investigated the criteria required to represent this condition's threshold. Such criteria are typically critical values of velocity or of bed shear stress.

Table 2-7 quotes some formulas for calculating the critical velocity, V_c, for incipient motion of bed load. However, in this study, these formulas were not suitable for the 3D modelling because the critical velocity was generally an integrated average velocity in the whole water depth.

Table 2-7 Formulas for entrainment velocity

Reference	Formula	Remarks
Bogardi(1968)	$V_c = 0.000044\, u_* \left(\frac{d\, g^{2/3}}{\nu^{2/3}}\right)^{1.8} \left(\frac{h}{d}\right)^{1.6}$	d is particle diameter in m
Novak and Nalluri (1972)	$V_c = 0.20\sqrt{s-1}\ \ d^{0.38}$	d is particle diameter in mm, for open channel with loose boundary, $s=\rho_p/\rho$.
Novak and Nalluri (1975)	$\frac{V_c}{\sqrt{g(s-1)d}} = 0.61\left(\frac{d}{R_h}\right)^{-0.27}$	R_h is hydraulic radius of flow, applicable for circular and rectangular sections on smooth fixed bed, d is particle diameter in m
Novak and Nalluri (1984)	$\frac{V_c}{\sqrt{g(s-1)d}} = 0.54\left(\frac{d}{R_b}\right)^{-0.38}$	R_b is hydraulic radius of related the bed (m) according to Einstein (1950) procedure; suitable for rough fixed bed, d is particle diameter in m

The most widely used approach is based on the critical shear stress τ_c. When local τ_0 exceeds the critical shear stress τ_c, incipient motion occurs. Due to the relationship of shear stress to the Shields parameter ($\tau_* = \tau_0/(\gamma_s-\gamma)d$), one often uses the critical Shields parameter τ_{*c} to determine the incipient motion based on initial work using the Shields curve (see Figure), which enables τ_c to be estimated in relation to the dimensionless particle diameter D^*. Many authors have dedicated work to establishing a formula for the relationship that fits the Shields curve. Table 2-8 summarizes some formulas for critical Shields parameter τ_{*c} estimation.

Table 2-8 formulas for critical Shields parameter τ_{*c}

Reference	Formula	Remarks
Vanoni (1975)	$\tau_{*_c} = 0.22\beta + 0.06\times 10^{-7.7\beta}$ $\beta = \left[\frac{\rho}{\mu}\sqrt{(s-1)gd^3}\right]^{-0.6}$	
Van Rijn (1984b)	$\tau_{*_c} = \begin{cases} 0.24D_*^{-1} & D_* \le 4 \\ 0.14D_*^{-0.64} & 4 < D_* \le 10 \\ 0.04D_*^{-0.1} & 10 < D_* \le 20 \\ 0.13D_*^{-0.29} & 20 < D_* \le 150 \\ 0.055 & D_* > 150 \end{cases}$	D_* is dimensionless diameter, defined as $D_* = d\left(\frac{(s-1)g}{\nu^2}\right)^{1/3}$ $s=\rho_p/\rho$
Soulsby (1997)	$\tau_{*_c} = \frac{0.30}{1+1.2D_*} + 0.055\left(1-\exp\left(-0.020D_*\right)\right)$	
Julien (2010)	$\tau_{*_c} = 0.3\exp\left(-D_*/3\right) + 0.06\tan\varphi\left[1-\exp\left(-0.05D_*\right)\right]$	φ is the repose angle

Based on non-cohesive uniform spherical sediment in a steady flow, Ling (1995) derived two threshold functions as criteria for incipient motion in spherical sediment particles: the rolling threshold function and lifting threshold function. The rolling threshold gives the minimum dimensionless shear stress required to start bed load movement in the form of rolling and the lifting threshold gives the minimum stress for suspension. The Shields curve, along with some classical representative data, lies mostly between the two thresholds.

Besides shear stress, many authors have argued that particle motion near the bottom has been found to be in close association with turbulent bursting in experiments (Sumer and Oguz 1978; Sumer and Deigaard 1981; Grass 1982). It has been recognized that the intermittent bursting process plays a central role in sediment transport (Sutherland 1967; Jackson 1976; Ikeda and Asaeda 1983; Dyer 1986; Kawanisi and Yokosi 1993). Based on bursting processes (such as ejection and sweep event), Cao (1997) proposed a sediment entrainment function using the averaged bursting period scaled on inner variables and the spatial scale of bursts.

The probabilistic approach to modelling sediment transport has shown some promise. Many authors have developed models that describe the entrainment of sediment (Wu and Chou, 2003). Sun and Donahue (2000) employed rolling probability in their fractional bed load equation, whereas Paintal (1971) used sliding probability in his bed load model. Cheng and Chiew (1998) provided a theoretical formula to describe lifting probability for sediment entrainment, which was later modified by Wu and Lin (2002). Both of these studies incorporated the probability distribution of instantaneous velocity in order to explore the relationship between lifting probability and flow condition. The Gaussian and log-normal distributions of instantaneous velocity were adopted in their analyses, respectively. Papanicolaou *et al.* (2002) provided a quantitative model for predicting sediment entrainment under three representative bed packing densities corresponding to the isolated, wake interference, and skimming flow regimes. However, further studies incorporating more

general considerations are needed in order to modify the formulation of entrainment probability. Wu and Chou (2003) developed theoretical components for evaluating the rolling and lifting entrainment probability in hydraulically smooth-bed and transitional open-channel flow. However, the sediment particle was assumed to be lying on a bed of closely packed particles and such a configuration represents only one of many possible situations.

Transition from bed load to suspended load is more complex than entrainment of bed load motion, and there is no simple criterion equivalent to the Shields criterion for bed load (Bertrand-Krajewski, 2012). Many authors focus on the ratio of shear velocity and settling velocity. Chanson (1999) said: "considering a particle in suspension, the particle motion in the direction normal to the bed is related to the balance between the particle settling velocity component and the turbulent velocity fluctuation in the direction normal to the bed." Turbulence studies have suggested that turbulent velocity fluctuation is of the same order of magnitude as shear velocity. Using this assumption, a simple criterion for the initiation of suspension is:

$$\frac{u_*}{v_s} > threshold \tag{2.27}$$

Bagnold (1966) suggested that $u_*/v_s=1$. Engelund (1965a, 1965b, 1967) stated that the threshold is equal to 0.25. Julien suggested suspension began at a value of 0.5-2. Van Rijn (1984a) developed a formula for calculating the threshold taking into consideration particle properties:

$$\begin{aligned} &\frac{u_*}{v_s} > \frac{4}{D^*} \qquad if \quad 1 < D^* < 10 \\ &\frac{u_*}{v_s} > 0.4 \qquad if \quad D^* > 10 \end{aligned} \tag{2.28}$$

Where D* is dimensionless diameter defined in equation (2.19).

Niño *et al*. (2003) modified Van Rijn's formula to better fit experimental data:

$$\frac{u_*}{v_s} = \begin{cases} 21.2D^{*-1.2} & if \quad 1 \le D^* \le 27.3 \\ 0.4 & if \quad D^* \ge 27.3 \end{cases} \tag{2.29}$$

g. Deposition

Deposition is one of the important topics for sediment transport. But when does deposition occur? A superficial answer is: when conditions are such that flow becomes overloaded, sediment is deposited. But this does not describe conditions under which flow becomes overloaded. Furthermore, this definition is based on equilibrium conditions in sediment transport. The most straightforward process involved in deposition is settling: the downward fall of sediment particles through the surrounding fluid acted on by the pull of gravity.

Observation shows that some particles reach the bottom and keep moving as bed load rather than settling out as deposition. This is absolutely critical for a true fundamental understanding of sediment deposition. Unfortunately, not nearly enough attention has been given to such matters in the literature on sedimentation, either by hydraulic engineers or by sedimentary geologists (Southard, 2006; Maa *et al.*, 2008).

Hjulström (1935) may be the first author who used velocity to determine the deposition of particles. He published a graph called **Hjulström curve** (shown in Figure 2-8) to determine whether a river will erode, transport, or deposit sediment. The graph takes sediment particle size and water velocity into account.

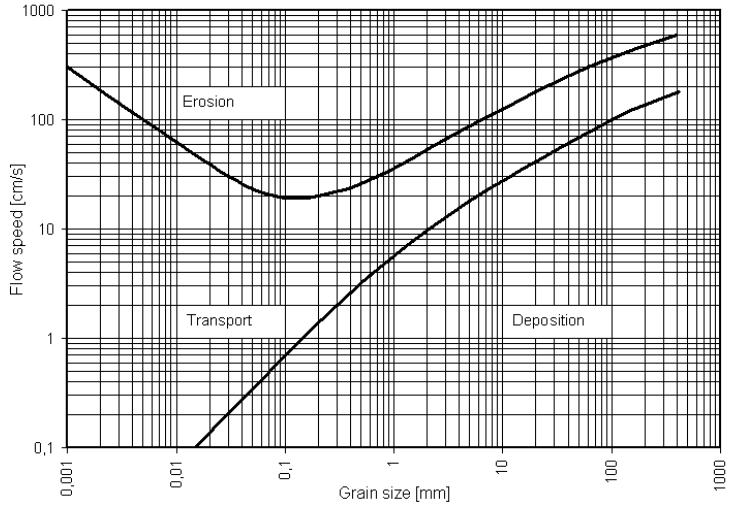

Figure 2-8 Hjulström curve (from http://en.wikipedia.org/wiki/Hjulstr%C3%B8m_curve , originates from Hjulström, 1935)

Figure 2-8 illustrates several key concepts in the relationships between erosion, transport, and deposition. However, for cohesive sediment, mostly clay but also silt, the *erosion* velocity increases with decreasing particle size, and the cohesive forces are relatively greater when the particles get smaller. The critical velocity for deposition, on the other hand, depends on the settling velocity which decreases with decreasing particle size. The curve was added to by Hjulström's disciple Sundborg (1956). He significantly improved the level of detail in the cohesive part of the diagram, and added lines for different modes of transport. However, an exact model showing the relationship can not be found in the literature.

Critical shear stress is also often used as a parameter for determining the deposition of sediment. Krone (1962) suggested the following widely used formula for deposition rate, D_b:

$$D_b = 0, \quad if \quad \tau_0 \geq \tau_{cd} \tag{2.30}$$

$$D_b = -Pv_s C_b, \quad if \quad \tau_0 < \tau_{cd} \tag{2.31}$$

$$P = 1 - \tau_0/\tau_{cd} \tag{2.32}$$

Where τ_0 and τ_{cd} are the local bed shear stress and the critical bed shear stress for deposition respectively, v_s is the particle settling velocity, C_b is the near bed concentration, and P represents the probability for deposition.

Stovin and Saul (1994) carried out sediment transport experiments in a small rectangular tank and they found that the distribution of deposited sediment may be predicted from the known velocity distribution in the tank and the values of the critical bed shear stresses τ_{cd} (0.03~0.04 Pa). It may be argued, therefore, that mathematically computed velocity distribution values may be used to predict sediment deposition in prototype storage tank designs. Based on the measurements for critical bed shear stress τ_{cd}, Adamsson and Stovin (2003) performed CFD modelling of hydrodynamics and particle tracking (Euler/Lagrange approach) to predict basin efficiency and the deposition zone.

Maa *et al.* (2008) reported results of laboratory experiments on cohesive sediment deposition behaviour. Direct observations of where and when deposition was formed suggested that deposition only occurs when the local bed shear stress τ_0 is less than a critical value, and this value, $\tau_{cd,}$ was close to 0.042 Pa. Gardner and Southard (1975) suggested that initial deposition of oceanic sediment occurs at 0.046 Pa. Mantz (1980) reported values of deposition shear stresses of around 0.033 Pa and 0.063 Pa for particle size distribution with median diameters of 18 μm (range 6-60 μm) and 42 μm (10-80 μm). Self *et al.* (1986) suggested that the typical values of τ_{cd}, are 0.05-0.1 Pa. There is no a single value for general conditions. The value seems to be dependent on the sediment characteristics and site.

However, using a probability function to represent the bed-shear stress distribution and excluding $\tau_{cd,}$ Winterwerp (2006) was able to simulate successfully deposition experiments carried out by Krone (1962) in a straight flume and sediment transport experiments in an annular flume performed by Mehta and Partheniades (1975). He deduced from this that there was no τ_{cd} at all.

Mahta and Partheniades (1975) suggested that the process of deposition of flocs appears to be controlled by stochastic turbulence in the zone near the bed. Dufresne (2008) introduced the threshold of bed turbulent kinetic energy as a criterion for determining the deposition of sediment through CFD modelling of hydrodynamics and sediment transport. The criteria for sediment deposition are still being debated.

h. Exchange of bed load and suspended load

The exchange of sediment in the interface of bed load and suspended load is often described using the concepts of sedimentation rate and erosion rate. The net exchange is calculated as the difference between them.

The sedimentation rate D_b can be estimated by (Krone, 1962) the equations (2.30-2.32). To calculate the erosion rate E_b, there are several equations provided in scientific literature. Cemagref (2004) uses the following equations:

$$E_b = 0, \qquad if \quad \tau_0 < \tau_{ce} \tag{2.33}$$

$$E_b = M\left(\frac{\tau_0}{\tau_{ce}} - 1\right), \quad if \quad \tau_0 < \tau_{ce} \tag{2.34}$$

Where M is the empirical coefficient, τ_0 is the local shear stress, and τ_{ce} is the critical shear stress calculated often using the Shields parameter. However, critical erosion bed shear stress values from experiments are also often used. For example, Stovin and Saul (1998) found that the erosion threshold was 0.06 Pa when using a small basin in the laboratory. El Ganaoui *et al.* (2004, 2007) observed that the critical shear stresses of erosion were in the range of 0.025 Pa - 0.05 Pa depending on the layer of the cohesive sediment.

Smith and McLean (1977) used the following equation for erosion rate:

$$E_b = \frac{0.65\gamma_0\left(\frac{\tau_0}{\tau_{ce}} - 1\right)}{1 + \gamma_0\left(\frac{\tau_0}{\tau_{ce}} - 1\right)} \tag{2.35}$$

Where γ_0 is a coefficient equal to 0.0024.

Garcia and Parker (1991) also use another equation:

$$E_b = \frac{AZ^5}{1 + \frac{AZ^5}{0.3}} \tag{2.36}$$

Where A is a parameter equal to 1.3e-7, and Z is calculated by Abad *et al.* (2007) as follows:

$$Z = \frac{u_*}{v_s}\left(\frac{v_s d}{\nu}\right)^{0.6} \tag{2.37}$$

2.2.3.3 Particle behaviour on a particle scale

In recent years, the development of advanced experimental equipment and methods (such as the high speed photographic techniques) have lead to a better understanding sedimentation phenomena, and many researchers have focused on the mechanical characteristics of sediment transport on a particle scale, which means observing individual particle motion mechanisms in fluids. The basic principle behind this equipment and these methods is the measurement of particle transport processes in order to analyse the balance of forces according to Newton's second law of motion. The bed load movement is the most popular area of investigation since it is not well-understood and is important for sediment transport investigation. The results obtained from experiments demonstrate that saltation is the main form of bed load movement under ordinary flow conditions (Hu and Hui, 1996). In fact, authors had already investigated the saltation phenomenon with experimental and theoretical analysis (Gilbert, 1914; Bagnold, 1941; Einstein, 1950; Gordon *et al.*, 1972; Francis, 1973; Luque and van Beek, 1976; Abbott

and Francis, 1977; White and Shulz, 1977) and obtained some interesting results, although the precision of these results was not high enough due to the limitation of measuring instruments available at that time. Van Rijn (1984a, 1984b), Bridge and Dominic (1984), Murphy and Aguirre (1985), Wiberg and Smith (1985), Anderson and Hallet (1986), Sekine and Kikkawa (1992), Lee and Hsu (1994), Hu *et al.* (1993) developed theories on saltation dynamics further. More recently, Hu and Hui (1996), Lee *et al.* (2002), Niño and Garcia (1994a, 1994b, 1998a, 1998b), Lajeunesse *et al.* (2010) measured the saltation trajectories of particles in flow and analysed the data using methods that combined mechanical and statistical theories for a better understanding of saltation mechanisms (*e.g.* the force acting on particle, jump height and length, etc.).

a. Forces acting on particle

Up to now, several kinds of forces that act on the particle near bed during the transport processes have been identified (Hu and Hui, 1996):

- Submerged weight due to the gravity and buoyancy forces
- Drag force due to the relative velocity
- Lift force (consisting of Magnus force due to particle rotation and Saffman force due to shear effect)
- The force due to the added mass effect
- The force due to the effect of fluid accelerating around a static particle
- The basset force due to the effect of duration of particle accelerating
- The bed impact force

It is generally accepted that submerged weight and drag force are the greatest forces. Many authors only examine drag force in experiments. The importance of the other forces still remains unclear. Van Rijn (1984b) suggested that the Magnus force could be neglected due to its low order of magnitude compared to Saffman force, while White and Shulz (1977) argued that the Magnus lift force was very important. Murphy and Aguirre (1985) suggested that the Basset force and Magnus force could be neglected. Reizes (1978) thought that the lift force could be omitted. Hu and Hui (1996) stated that the forces acting on a particle vary along the saltation trajectory, *e.g.* the drag and lift force in the rising and descending stages were different. They also pointed out that the impact force was bigger than the other forces.

b. Kinematic characteristics of saltation trajectories

A typical measured saltation trajectory is shown in Figure 2-9. Saltation is often described as having the following characteristics: a maximum saltation height h_s and saltation length L_s, average particle velocity V, lift angle and impact angle, and saltation step duration in time. Some previous results for saltation characteristics are summarized in Table 2.10. In Table 2-9, h_s and L_s are very different from each other, perhaps as a result of differing experimental conditions, but they were both found to be similarly dependent on average particle velocity V_p (Lajeunesse *et al.*, 2010):

$$V_p = a\left(u_* - bu_{*c}\right) \tag{2.38}$$

Where *a* and *b* are positive coefficients related to the effective friction coefficient and the effective fluid velocity at the height of the particles.

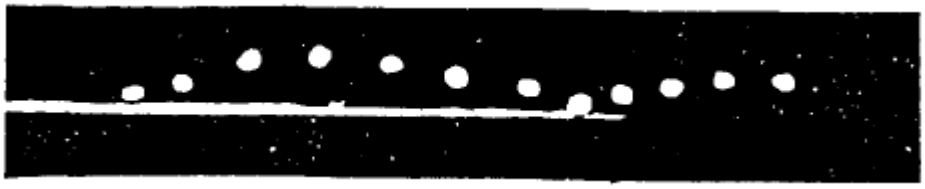

Figure 2-9 Saltation trajectory of sand measured by high speed camera (Hu and Hui, 1996)

Lajeunesse *et al.* (2010) also developed probability density functions (refered to as PDFs hereafter) for the transverse and longitudinal velocity components of particle saltation. They found the most probable flight duration time formula that fitted the experimental data. Hu and Hui (1996) reported the measured lift off angle varies from 10 to 40 degrees, and the impact angle varies from 5 to 12 degrees, and they pointed out that saltation parameters vary with flow intensity and specific particle conditions. Niño and Garcia (1994) also reported the lift off angle varies between 0 - 60 and the impact angle is in the range of 5 -30. They found that the mean value of lift off and impact angles decreases with the increase of τ_*.

In terms of the saltation process, initially, the particle on the bed begins to move when a threshold condition (often the flow intensity, or turbulent burst events) is met. The mode of particle transport (rolling, sliding and saltation) depends on flow intensity and specific particle characteristics. Hu and Hui (1996) illustrated that the proportion of rolling, sliding and saltation depended upon Shields parameter τ_*. The experimental results of Lajeunesse *et al.* (2010) and Hu and Hui (1996) indicated that saltation is the dominate mode of bed load transport. Successive saltation processes have been observed in experimental investigations. In relation to the initial velocity of saltation, Francis (1973) suggested that tangential and normal velocity components are approximately equal to $2u_*$. White and Shulz (1977) stated that the value for initial saltation velocity is between u_* and $2.5u_*$. Van Rijn (1984a) gave a value of saltation velocity as $2u_*$ in his analysis. Hu and Hui (1996) developed formulas for the initial velocity of saltation based on the shear velocity and Shields parameter. The formulas are expressed as tangential and normal component velocities for smooth bed and rough bed configurations respectively.

Some authors favour the concept of collision and rebound, whereas the others have put forward the idea that a particle does not actually rebound after collision but instead reestablishes saltation in an unsteady rolling motion. Niño and Garcia (1994a) maintained that the occurrence of modes of collision depends mainly on the local configuration of bed particles at the point of collision. Niño and Garcia (1994a) tested the collision-rebound type process, as shown in Figure 2-10, where a saltating particle approaching the bed strikes the bed. The striking particle velocity is resolved into tangential and normal components with respect to the collision surface $U_T|_{in}$ and $U_N|_{in}$. it is assumed that these components are reduced after the collision:

$$U_T\big|_{out} = fU_T\big|_{in} \tag{2.39}$$

$$U_N\big|_{out} = -eU_N\big|_{in} \tag{2.40}$$

Where e and f are restitution and friction coefficients respectively.

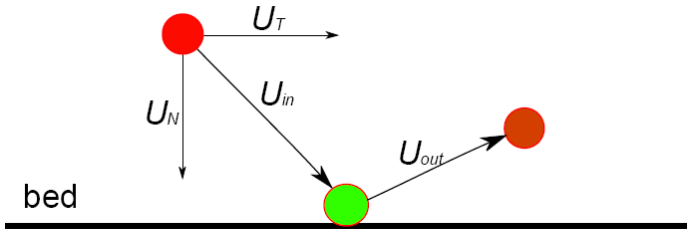

Figure 2-10 Definition diagram for collision-rebound with the bed

The calculated value of the coefficient f appears to be almost independent of flow intensity and dimensionless particle size, with a constant value of between 0.73 and 0.89 (Niño and Garcia, 1998). However, the coefficient e appears to be linearly related to τ_*, and can be described as (Niño and Garcia, 1994a):

$$e = 0.84 - 4.84\tau_* \tag{2.41}$$

If friction resistance is negligible, both e and f are equal to 1.

Table 2-9 Saltation length L_S, saltation height h_s and average particle velocity V derived from experimental investigations (using formulas adapted from Lajeunesse et al., 2010)

Reference	L_s	h_s	V_p	τ_*	S_L	R_{es}	R_{ep}	h/d
Fernandez-Luque and Van Beek (1976)	$\frac{L_s}{d}=16$	Dependency with τ_* and d	$V_p=11.5(u_*-u_{*c})$ $V_p=a(u_*-u_{*c})$ $a=13.4-14.3$	0.03-0.64 0.0076-1.556	0.21-0.4 0-0.0184	106-760 717-3538	18-608 62-4413	36-133 3-14
Sekine and Kikkawa(1992)	$\frac{L_s}{d}=3000\tau_*^{1/4}\left(\sqrt{\tau_*}-\sqrt{\tau_{*c}}\right)$	———	$V_p=8\sqrt{(u_*^2-u_{*c}^2)}$	0.043-0.233	———	120-3836	25-1825	———
Nino and Garcia (1994a)		Dependency with τ_*/τ_{*c} and d	$V_p=a(u_*-u_{*c})$ $a=6.8-8.5$	0.09-0.14	0.03-0.07	7400-21900	2220-8200	2.6-4.7
Lee and Hus (1994)	$\frac{L_s}{d}=196.3(\tau_*-\tau_{*c})^{0.788}$	$\frac{h_s}{d}=14.3(\tau_*-\tau_{*c})^{0.575}$	$V_p=11.53\,u_*(\tau_*-\tau_{*c})^{0.174}$	0.06-0.5	0.002-0.023	200-493	50-75	20-90
Hu and Hui (1996)	$\frac{L_s}{d}=27.54\left(\frac{\rho_p}{\rho}\right)^{0.94}\tau_*^{0.9}$ (for rough bed) $\frac{L_s}{d}=76.74\left(\frac{\rho_p}{\rho}\right)^{0.7}\tau_*^{0.86}$	$\frac{h_s}{d}=1.78\left(\frac{\rho_p}{\rho}\right)^{0.86}\tau_*^{0.69}$ (rough bed) $\frac{h_s}{d}=3.67\left(\frac{\rho_p}{\rho}\right)^{1.05}\tau_*^{0.82}$ (smooth bed)	$V_p=11.9(u_*-0.44u_{*c})$	0.07-1.67	0.001-0.014	58-1018	15-1315	21-60
Lajeunesse *et al.* (2010)	$\frac{L_s}{d}=(70\pm2)\frac{u_*-u_{*c}}{V_s}$ $V_s=\sqrt{\frac{\rho_p-\rho}{\rho}gd}$	———	$\frac{V_p-V_c}{V_s}=a(u_*-u_{*c})$ $a=4.4\pm0.2,$ $V_c=(0.11\pm0.03)V_s$	0.006-0.24	0.0017-0.12	156.9-1646	12-510	1.5-10

Note that the range of Shields parameter τ_*, bed slope S_L, setting Reynolds number R_{es}, particle Reynolds number R_{ep} and ration of water depth and particle size h/d explored in these experiments are also indicated in the table.

2.3 Modelling of experimental small scale stormwater basins

2.3.1 Empirical model of detention basins

Since detention basins can trap sediment through the settling of particulate pollutants, RE has become the most important parameter for evaluating the effectiveness of a detention basin. RE is thus one of the most significant criteria in the design and retrofit of stormwater detention basins. *Removal efficiency* is the property of a basin or reservoir. The basin's RE depends on the characteristics of the entering sediment and the retention time in the basin, which is controlled by the basin's geometry and flow characteristics (Verstraeten and Poesen, 2000; Zhang, 2009; Akan, 2010).

In order to reduce pollutants in stormwater runoff as much as possible so as to protect the receiving water body, efforts have been made to improve the RE of basins through observation, experimentation and modelling. In the past, two types of models were developed to predict RE: empirical models for predicting average RE based on a mid to long term observations and theoretical models for predicting the RE of an individual storm event for small ponds (Verstraeten and poesen, 2000). Heinemann (1984) gave an overview of the many empirical models that could be used to predict RE. Amongst them, the models proposed by Brune (1953) and Churchill (1948) were two of the most widely used. Brown (1943) linked empirical data on RE to reservoir characteristics and developed a curve relating RE to a capacity-watershed area ratio C/W (C/W: reservoir storage capacity/catchments area) based on the data from 15 reservoirs. Brune (1953) examined the model based on capacity-watershed area ratio (C/W) and found that of the predicted RE for the same C/W could be of completely different values if their catchments produced different runoff volumes due to the other hydrological characteristics. To overcome this problem, Brune (1953) used a capacity-annual inflow ratio C/I (C/I: reservoir storage capacity/ annual inflow rate) to predict RE. Churchill (1948) proposed that the amounts of sediment passing through the reservoir could be related to a sedimentation index (SI: period of retention divided by mean velocity through the reservoir). This model provided more detail on the hydraulic behaviour of a reservoir and could be more suitable for predicting RE. It was able to give more accurate RE values when compared to Brune's model, but it is difficult to obtain the input data for calculating the sedimentation index (Verstraeten and poesen, 2000). The empirical models were developed based on large ponds and they seem to be less applicable to small ponds and are not able to make predictions for event-based RE. To overcome these limitations, different theoretical models have been developed based on sedimentation principles. An overview of the theoretical RE models was provided by Haan *et al.* (1994). Camp's model, DEPOSITS, CSTRS, BASIN, STEP and SWMM are six of the theoretical models for predicting RE. Camp (1945) studied sedimentation in an ideal rectangular continuous flow basin (shown in Figure 2-11).This model assumes a quiescent, steady flow, complete mixing of the water and sediment, and no re-suspension. When sediment is flowing into the tank, discrete particles settle with a settling velocity of v_s, which is dependent on particle size. For an ideal pond one could also define a critical settling velocity (v_c) that will allow particles (for which v_s equals v_c) to settle in the pond. This critical settling velocity depends on the water depth (h) and the time that the inflow needs to flow through the pond (T):

$$v_c = \frac{h}{T} = \frac{Q}{A} \tag{2.42}$$

Where A is the surface area of the basin, and Q is the inflow or outflow discharge.

The critical settling velocity is equal to the *overflow rate* of the basin. Given in an ideal rectangular basin with a discrete particle size distribution, the RE can be calculated as follows:

$$RE = 100\left[\left(1 - X_c\right) + \sum_{i=1}^{n} \frac{v_{si}}{v_c} \Delta X_i\right] \tag{2.43}$$

Where X_c equals the fraction of particles with a settling velocity less than the critical settling velocity and ΔX_i equals the fraction of particles with a settling velocity of v_{si}.

Chen (1975) modified Camp's (1945) model to take turbulent flow into account:

$$RE = 100\left[1 - \exp\left(-\frac{v_s}{v_c}\right)\right] \tag{2.44}$$

Chen (1975) also compared his model with Brune and Churchill's models. He concluded that these empirical models overpredict RE for fine sediment but underpredict it for coarse sediment. It could, therefore, be misleading if one uses the empirical models for specific cases without the original data.

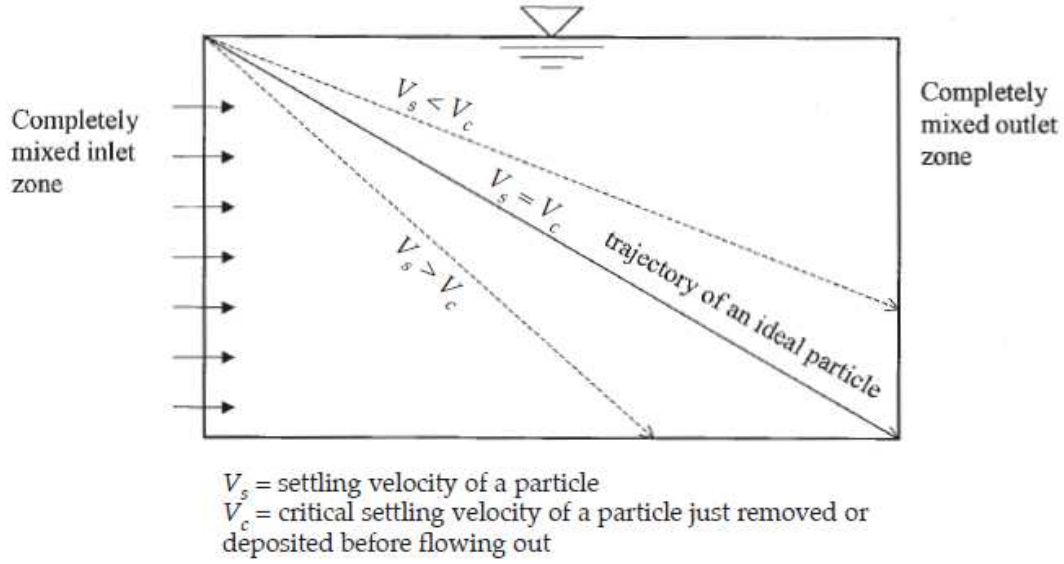

Figure 2-11 Settling conditions in an ideal rectangular settling basin (Verstraeten and poesen, 2000, from Camp, 1945)

The DEPOSITS model (Ward *et al.*, 1977 cited in Verstraeten and poesen, 2000) uses plug-flow approximation for pollutant routing. The CSTRS model (Wilson and Barfield, 1984) used simple reactor theory concepts. The BASIN model (Wilson and Barfield, 1985) combines the reactor theory concepts with advection–diffusion processes. In both the CSTRS and BASIN models, a pond is divided into a series of chambers of equal volume (Akan, 2010). Although the BASIN model is more sophisticated, Wilson and Barfield (1985) found that the two models produced similar results. The STEP model developed by Verstraeten and Poesen (2001) divides a pond into a series of chambers of equal surface area. A complete mixing formulation is used within each chamber. The widely known SWMM (Huber and Dickinson, 1988) also has a component to evaluate pollutant removal efficiencies of detention basins using the plug-flow concept. Nix and Heaney (1988) used the SWMM for a continuous simulation of flow and pollutant routing in a detention basin. Loganathan *et al.* (1994) used the simple physical-based equations together with probabilistic concepts to study the long-term efficiency of detention basins. Loganathan *et al.* (1994) developed a model to estimate overall efficiency using a probability concept. They considered pollutant removal to be dependent on settling time, and assumed retention time to be a measure of settling time. They provided a close-form, explicit equation for expected detention time, which is an effective parameter in assessing pollutant settling efficiency within a detention pond. However, Guo *et al.* (2000) plotted RE against the detention time for TSS and found that the RE did not correlate to detention time. Akan (2010) developed a model for dry detention basins based on the hydrologic storage equation and a concept of complete pollutant mixing in order to provide research findings in a format that could be of benefit to engineering in practice. Takamatsu et al (2010) developed a conceptual model for simulating the particle RE and outflow rate for rectangular stormwater detention basins based on ideal horizontal flow reactor theory.

These theoretical models or empirical models, however,are all limited because they are based either on plug flow or on complete mixing, both of which seldom occur in reality, and only some aspects of sediment transport processes were considered in each model (Zhang, 2009). Verstraeten and Poesen (2001) modeled the long-term sediment RE of small pond with the empirical model STEP, DEPOSITS and CSTRS. It was found that these models were ineffective for predicting long-term efficiency, with the exception of the STEP model in small ponds. These models treated the basin like a black box, so they were unable to take into account key basin features such as its geometry, inflow and outlet patterns, flow patterns, etc.

2.3.2 Experimental investigations in small scale basins

Field measurement and observation may be the best and most direct way to obtain data and knowledge about detention basins, for example, Leclaire (1997), Letondu (1997), Torres (2008), etc. As discussed in the preceeding section, these investigations in the field have led to the creation of empirical models and to retrofitting. But investigations based on field sites have their limitations (Adamsson *et al.*, 2005):

- The research results are specific to existing detention basins
- The high cost and difficulty in using them for measuring performance. It is also not possible to carry them out prior to basin creation;

- Real flow conditions during the storm events are unpredicted and uncontrollable, which implies that it is difficult to influence flow conditions.

For this reason, a number of researchers have studied basin hydraulics in the laboratory using scale models. Compared to field measurements, the scale models in laboratories have certain advantages for researchers: i) Low construction costs; ii) Easier to control and adjust; iii) More convenient for taking measurements for some specific purpose, such as PIV (particle image velocimetry) for field velocity measurement.

The work undertaken by Mangelson and Watters in the 1970s at the Utah Water Research Laboratory was one of the earliest and most extensive research projects on basin hydraulics (Zhang, 2009). Aimed at improving treatment effectiveness, the investigations were carried out on various factors such as the layout of basins, baffle installation, length to width ratio and the positioning of inlets and outlets. They found that the treatment effectiveness was greatly affected by these hydraulic characteristics (Mangelson and Watters, 1972; Watters *et al.*, 1973).

Kadlec (1990) and Moshiri (1993) investigated the influence of vegetation on hydraulic performance. Kadlec and Knight (1996) and Shaw *et al.* (1997) reported on the influence of wind on hydraulic performance. The influence of temperature has also been studied (Marecos de Monte and Mara 1987). Saul and Ellis (1992) developed a laboratory computer-controlled monitoring system for the purpose of visualizing flow and making a comparative assessment of sediment deposition and removal performance for different geometric configurations of storage tanks. It was found that flow patterns governed sediment settlement, and re-entrainment. It has been suggested that the length to width ratio, the longitudinal and benching gradients and the dry weather flow channel are the most significant geometrical properties for sedimentation.

Stovin and Saul (1994) described a series of laboratory experiments in which the sedimentation efficiency of a scale model storage chamber was measured. The scale model comprised of a chamber that was 2m long, 0.972 m wide and 0.45 m deep. The base of the chamber was horizontal and the inlet (pipe diameter = 0.19 m) and outlet (pipe diameter=0.15 m) were positioned centrally along the chamber width with the invert in each positioned level with the chamber base. The sediment used was 150 μm crushed olive stone with the D_{50} =47 μm. It was found that the velocity distribution in the storage tank was the primary factor in sedimentation and it was possible to predict the distribution of deposited sediment from knowledge of velocity distribution in the tank and the values of the critical bed shear stress (0.03~0.04 Pa). It was also concluded that in order to provide a realistic assessment of the sediment retention performance of a storage tank, it is essential to carry out the tests with time as a variable and using time series flow conditions, together with inflow suspended sediment concentrations representative of full scale conditions.

Stovin and Saul (1996) established a relationship between the inlet velocity and sedimentation efficiency for this scale model tank. Stovin (1996) tested different parameters for sediment transport in a scale model tank: the length to breadth ratio *(L/B)* the benching gradient *(S_b)*, the longitudinal gradient *(S_b)*, the dry weather flow channel *(D_{DWF})* and also the level of surcharge *(H/D)*. Both techniques suggested that the length to breadth ratio was the most important geometric parameter, although different conclusions were reached depending on the

predictive technique employed. However, the mean inlet velocity was found to have a significant impact in both cases. Regression relationships were derived from the measurements.

Garde *et al.* (1990) carried out a series of experiments in a 16 m long, 0.75 m wide and 0.5 m deep rectangular flume that could be adjusted to lengths of 10~15 m. A 0.30 m wide channel was constructed in the flume. A tailgate enabled the depth of flow in the flume to be adjusted. Two kinds of sand were used for experiments: 0.082 mm and 0.106 mm. 162 experiments were conducted with different inflow rates, sand sizes, concentration and flume length. The RE was found to be greatly influenced by the length to water depth ratio and the settling velocity to shear velocity ratio.

Saul *et al.* (1992) investigated sedimentation in a circular basin. The results were used to develop a simple theoretical model of settling.

Kowalski *et al.* (1999) carried out sediment transport experiments in a long cylindrical basin (length 9.3 m, diameter 0.441 m) with one input pipe (0.15 m) and two outputs (a circular overflow weir of 0.15 m and a throttle pipe of 0.05 m diameter). Based on the experimental results, a simple formula was proposed for predicting cleaning efficiency in CSDTs.

Frey *et al.* (1993) performed sediment transport experiments in a settling tank consisting of a sloping backward facing step and an outlet weir. Experiments were carried out with different sand samples, different discharges, length, depth, and slope. The experiment results were used to access the RE and to validate simulation results.

Luyckx *et al.* (1999) conducted efficiency experiments in overflow chambers with 20 different geometries. The length of the plenum, discharge and storage were adjustable. Four kinds of model particles were used for this test: three sizes of bakelite particles (0.4-0.5mm, 0.5-0.63mm, 0.63-2mm) and one size of nylon particle (2mm). A formula for efficiency was established based on the experiment results. By using sediment with different grain sizes and densities, efficiency curves were found for a high side weir overflow. The efficiency for a certain sediment fractions was found to be determined by its settling velocity only.

Kantoush *et al.* (2006, 2008a, 2008b, 2008c, 2010) and Dewals *et al.* (2008) conducted a series of experiments on sediment transport and deposition in a rectangular shallow basin, whose inner dimensions were 6.0 m long and 4.0 m in wide, with rectangular inlet and outlet channels, 0.25 m wide and 1.0 m long, and with a flap gate, 0.25 m wide and 0.30 m high, at the end of the outlet. To model suspended currents, crushed walnut shells with a median grain size weight of D_{50}=50μm and density=1500kg/m^3 were used. The water depth, inflow and outflow rate, concentration and flow velocity field were measured during the experiment. Different layouts within the shallow basin were tested. It was found that flow patterns are sensitive to boundary conditions and initial conditions. The basin's geometry influences the behaviour of large turbulence structures, and flow is sensitive to the geometric shape. Although the basin was symmetric, the flow pattern was asymmetric under certain conditions. This has also been observed by other authors (Stovin and Saul, 1994, 1996; Dufresne, 2008; Vosswinkel *et al.*, 2012).

Dufresne (2008), Dufresne *et al.* (2009) carried out a series of sediment transport experiments in a rectangular pilot basin, 1.80 m long, 0.76 m wide, and 0.40 m deep, limited by an overflow weir. It was equipped with an inlet (diameter = 0.08 m) and outlet pipe (diameter = 0.08 m). Non-uniform size polystyrol particles, from 350 μm to 1400 μm, with a density of 1030 kg/m^3 were used in the model as sediment. Two other kinds of particles of 1500 μm with density of 1060 Kg/m^3 and 2500 μm with the density of 1080 kg/m^3 were also used. 55 tests were carried out under various configurations: variants of inflow rate (2.0-5.0L/s), variants of outlet configuration (pipe or overflow weir), different particle types, without or with obstacles (vertical baffle or columns). It was found that the flow pattern changed with water depth. With a water depth lower than 15cm, the flow was quasi-steady and asymmetric with a single large horizontal recirculation pattern; for a water depth higher than 30 cm the flow pattern was also quasi-steady and resulted in two horizontal symmetrical recirculation patterns. For a water depth of between 15cm and 30cm, the flow patterns were unsteady with oscillation although the inflow rate was constant. The removal efficiencies were also measured.

Vosswinkel *et al.* (2012) performed sediment transport tests in a rectangular stormwater tank (L/W/H=3125/800/200mm) to evaluate the unsteady flow influence on sedimentation. The tank was equipped with a pipe (diameter =100 mm) as an inlet and overflow weir (discharge coefficient = 0.62) located 200 mm from the bottom of the tank. Non-uniform sized particles (300 μm ~700 μm, density =1020kg/m$^{3)}$ were used as sediment in the model. 10 tests were carried out with a constant inflow rate. It was found that the flow patterns within the tank were highly unsteady and asymmetrical even though the inflow was constant in a fully symmetrical tank. The tracer studies of the particles showed that unsteady effects were evident due to flow patterns.

It is easier to control flow conditions in a scale model in a laboratory, but results suffer from scale effects because most of the scaled-down models cannot completely satisfy all mechanical similarities, which include geometric, kinematic and dynamic similarities. For example, ensuring similarity of the Froude number in scale models may preclude the possibility of ensuring similarity for the Reynolds number. Consequently, laboratory models may over-emphasize viscous effects (Zhang, 2009). Basins' real geometries, the variability of hydrodynamic features, and the heterogeneity of sediment characteristics are much more complicated than those that scale models are able to replicate. Therefore the results obtained from scale models in laboratory conditions remain difficult to transpose to a real system, not only because of the effects of scale, but also due to the much more complex features in real conditions (Torres, 2008).

2.4 Numerical modelling of flow and sediment transport in detention basins

More recently, due to the limitation of field observations and the development of laboratory scale models, the potential application of Computational Fluid Dynamics (CFD) technology in storm basins has been identified as an alternative way of studying detention basins. Zhang (2009) summarizes the features of CFD that may be of benefit to the study of detention basins:

- CFD modelling makes it possible to numerically solve flow, mass and energy balances in complicated flow geometries. The results show specific flow or heat transfer patterns that are hard to obtain experimentally or with conventional modelling methods.
- CFD offers an alternative way to study and evaluate the performance of existing detention ponds based upon their hydrodynamic features.
- CFD is a powerful tool to help in the design of new pond systems. Unlike traditional design methods, which do not address the hydrodynamic features or problems, the CFD tool can predict flow patterns and short-circuiting problems before the pond is built, and can also predict the effects of measures such as baffles or inlet/outlet reposition in advance to improve performance, thus greatly aiding engineers during the design process.

CFD technology provides a way of taking more detailed flow and sediment characteristics into account. These features of CFD make it a very promising tool for the evaluation of existing basins and in the conception of new ones (Wood *et al.* 1998). Jarman *et al.* (2008) presented a review of CFD studies carried out on urban drainage system analysis. They concluded that CFD can be applied to gain insights into most fluid processes and associated phenomena and that they have the potential to provide values for the analysis of urban drainage systems, such as flow field performance, particle behaviours, water free surface and residence time distribution, etc. Once validated with measured data, these models can be used as tools to aid management and design processes.

2.4.1 Modelling the hydrodynamic behaviour of detention basins

Vertical integrated 2D and 3D modelling techniques have been used to analyse hydraulic characteristics of basins. Wood *et al.* (1995) used a CFD model to qualitatively investigate the hydrodynamics of four pond systems. Pettersson *et al.* (1997, 1998) simulated flow patterns in an open stormwater detention basin with FIDAP, commercial CFD software which is limited to 2D and steady flow in a laminar flow regime. Walker (1998) developed the depth-average *f* low equations model HYDRA to evaluate the characteristics of incoming flow for different configurations of a stormwater detention basin. Persson *et al.* (1999) and Persson (2000) used the model Mike21 to evaluate the hydraulic performance with different basin shapes and configurations. The authors tested the hydraulic efficiency (*e.g.* residence time distribution, short-circuiting, effective volume, etc.) in order to simulate results with which to analyse hydraulic performance. It was found that the length to width ratio and the location of inlets and outlets have a considerable impact on hydraulic performance and a submerged baffle or manifold inlet configuration made the flow less mixed and short-circuiting was reduced. Vega *et al.* (2003) used Mike21 to simulate the hydrodynamics and advection-dispersion process in a full-scale anaerobic basin with 12 different configurations including different basin shapes, baffling and inlet and outlet positions.

Stovin and Saul (1996, 1998, 2000) and Stovin *et al.* (1999) used Fluent to create 3D numerical models of the flow field and sediment transport in storage chambers in order to investigate the RE and the influence of different length to width ratios, dry channels on chambers performance. Stovin and Saul (1994) demonstrated that rectangular chamber

efficiency varied as a function of mean inflow velocity, thus they showed that the efficiency of any particular chamber could be found with the mean inflow velocity value using a mean velocity/efficiency curve (as shown in Figure 2-12). It was also found that chamber efficiency was directly related to the percentage of deposition coverage of the bed surface. For the deposition zones, Stovin and Saul (1994) found that the location of sediment depositions on the bed of a storage chamber could be predicted from the distribution of shear stress in the bed. A similar result was also found by Dufresne (2008). Dufresne (2008) found that the coverage of bed turbulent kinetic energy was lower than a threshold corresponding to the preferential sediment deposition zones. Chamber efficiency could therefore be obtained by making an estimation of the percentage of deposition coverage on the bed surface using a flow field simulation for bed shear stress lower than a certain threshold. However, this method is limited because it cannot predict efficiency greater than 60% because of the accumulation of sediment in the same locations (Stovin and Saul, 1996).The method is evidently also difficult to apply to real events because storm events are generally in an unsteady state, while this method was developed based on steady state laboratory experiments.

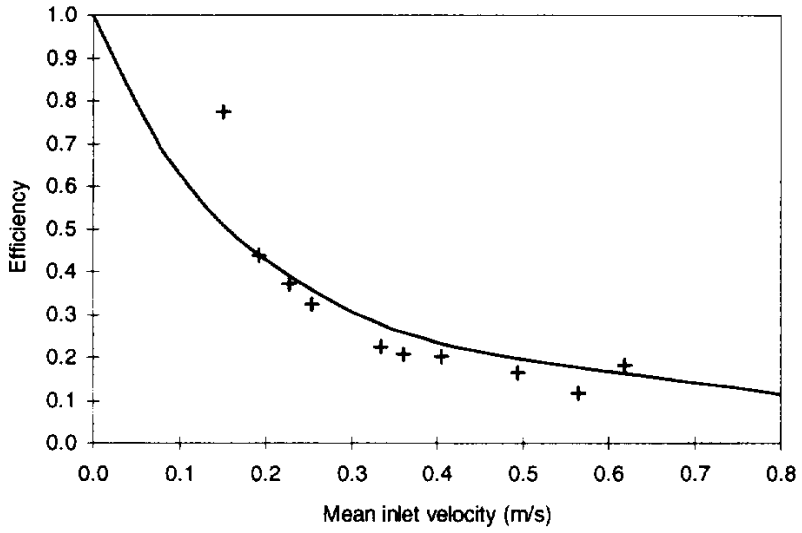

Figure 2-12 Inflow velocity/efficiency curve for a laboratory chamber (Stovin and Saul, 1996)

Kantoush *et al.* (2006, 2008a, 2008b, 2008c, 2010) and Dewals *et al.* (2008) used CCHE2D and FLOW-3D to simulate the flow patterns and sediment transport for a rectangular shallow basin. These simulations were validated with a series of measurements from experiements. It was concluded that numerical simulation can reproduce experimental flow features. The flow patterns could be simulated numerically using a parabolic eddy viscosity model. It was found that flow patterns are quite sensitive to the boundary and initial conditions.

Torres (2008) established 2D flow with and without sediment simulations modelling a full scale stormwater detention basin using Rubar 20 based on chosen storm events. Simulated results were validated with water depth measurements. It was found that Rubar 20 could be used to study the flow behaviour (field velocity and water depth) of basins for isolated storm events or a series of storm events. The sediment transport simulation based on a storm event s able to predict overall efficiency but does not reproduce the sediment zone within the

detention basin well. A 3D model for the same basin was also established using Fluent and simulations were performed for flow and sediment transport. Both simulation results for sediment deposition zones were unable to reproduce field observations well with the "*trap*" bed boundary conditions under steady flow conditions.

Dufresne (2008) created 3D models for pilot basins using Fluent and reproduced asymmetric flow patterns with simulations. It was found that the experimental sediment zones correspond to simulated bed shear stress or bed turbulent kinetic energy values lower than a defined threshold. However, according to Dusfresne's results (2008), it seems that predicting sediment deposition zones only using hydraulic simulation results is sometimes inadquate. As shown in Figure 2-13, there is no sediment deposited in the some low bed shear stress zones. This may imply that the sediment deposition zone is a process which deals with the interaction between flow and sediment, and that bed shear stress highlighted in the hydraulic simulation just demonstrated a deposited opportunity for sediment.

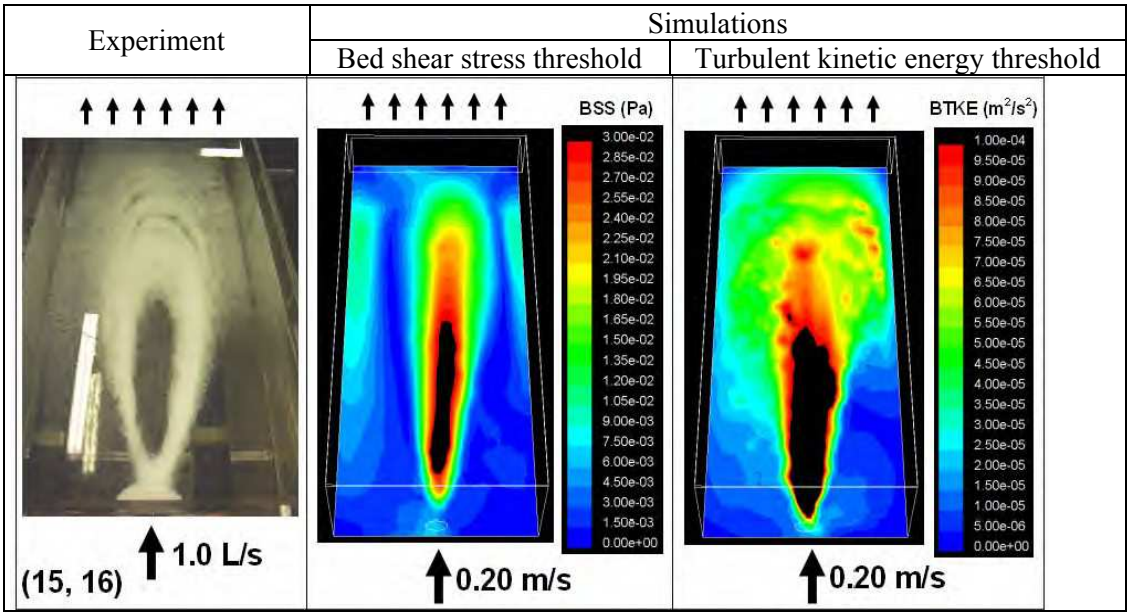

Figure 2-13 Comparison between the deposition zones and bed shear stress and bed turbulent kinetic energy in a rectangular detention basin (Dufresne, 2008)

Lipeme Kouyi *et al.* (2010) performed flow simulations in a large stormwater detention and settling basin. It was found that the main sediment zone observed was close to a bed turbulent kinetic energy zone below a critical value. The critical values differed according to the turbulent model (RSM and k-epsilon) and whether there was or was not free surface tracking.

Vosswinkel *et al.* (2012) investigated the influence of unsteady flow on sediment transport behaviour with a 3D simulation of a scale detention tank. It was observed that the flow patterns were highly variable even for a constant inflow in a symmetric rectangular tank. Obviously, the steady state flow simulation cannot reproduce the unsteady flow pattern. Unsteady flow simulation was needed in order to represent time-dependent flow performance.

Bentzen (2008a) investigated the effect of wind on retention time in a highway pond. Results showed that wind shear stress should be taken into account for the modeling retention time or flow patterns in shallow detention ponds i.

Zhang (2009) carried out flow pattern sediment transport simulation with different inlet and outlet configurations in a scale basin in order to predict the position of the sediment deposition zone and efficiency.

Stamou (2008) used CFD models to evaluate the guiding wall effects on hydraulic efficiency of main tanks in water networks in Greater Athens. It was found that the added guiding wall created flow fields in the tanks with significant volumes of plug flow and reduced short circuiting, creating a smaller recirculation region and thus less mixing.

Schimitt *et al.* (2002) and Stovin *et al.* (2002) carried out dynamic simulation of storage chambers. These investigations indicated that it is necessary to take the characteristically time-dependent nature of inflow and outflow into account.

2.4.1.1 Mesh sensitivity

Predictions made in the flow domain are sensitive to mesh density and mesh quality if one uses mesh-based methods (*e.g.* finite volume method - FVM, finite element method - FEM, and finite difference method - FDM). Meshing plays an important role in CFD techniques. It has a significant impact on solution accuracy, convergence features and computational time requirements (Ferziger and Peric, 2002; Knupp, 2007).

There are two kinds of basic mesh element types: structured and unstructured mesh. Generally, a structured mesh has more effective computational efficiency because of the lower quantity of storage memory required, but an unstructured mesh has more flexible features when recreating complex geometry conditions. The choice of an unstructured, structured or hybrid mesh depends on the individual conditions of each case.

No matter what kind of mesh type is chosen, mesh density and mesh quality are the key basic considerations to take into account. There are no finite rules governing ideal mesh resolution. Usually several meshes of different sizes are tested to see at which point the computational results become independent of mesh resolution (Jarman *et al.*, 2008). The simulators always try to find the small scale mesh possible that corresponds to the level of accuracy required in order to reduce computational time.

The appropriate mesh resolution is also dependent on the specific conditions and flow features the user requires, for example, solution accuracy. Sometimes it is also affected by the numerical solution method chosen, for instance, the treatment of the boundary layer or the discretization schemes. It should be noted that a finer mesh resolution does not necessarily deliver better results. This is due to the propagation and accumulation of numerical solution errors within the mesh. The more mesh cells there are, the larger the number of errors that may be accumulated and propagated in the computational domain.

Special attention should also be paid to the wall bound mesh for dealing with wall-bound turbulent flow. Salim and cheah (2009) concluded that the wall y^+ strategy is an accepted critia for wall boundary meshing.

Ta and Brignal (1998) modeled a full scale storage reservoir in three dimensions using approximately 7000 hexahedral cells, and stated that a finer mesh did not provide additional information in this case. Conversely, in the analysis by Lau *et al.* (2007), which focussed on a manhole several orders of magnitude smaller than the reservoir, the mesh sensitivity limit was found to be between 55 000 and 130 000 cells. It seems that the mesh density depends upon accuracy required. Momplot *et al.* (2012) tested 11 different density meshes for modelling the flow in an open channel junction. By validating the model using measured data, it was found that a median refined mesh was best able to simulate hydrodynamics across a subcritical open channel junction. These results confirm that mesh resolution is largely dependent on the phenomena the modeler wishes to resolve.

In addition to mesh density, it is important to consider mesh quality when aiming to create an accurate simulation on a computer. Good quality mesh helps modelers to obtain better solutions and to speed up the computation. Low quality mesh may lead to convergence issues. The criteria used to evaluate the mesh quality include smoothness, aspect ratio, and skewness. For example, Ip (2009) investigated the influence of smoothness on CFD solutions. He found that smoother meshes are better than rough meshes. Errors associated with rough meshes were far greater than expected. Furthermore, suitable mesh resolution also depends on the hydraulic conditions and the flow features the user is aiming to resolve. It is also affected by numerical solution parameters, such as discretization schemes. For instance, Ip (2009) found that higher order methods are more susceptible to mesh smoothness.

2.4.1.2 Turbulence models

In practice, many, if not most, significant engineering projects involve turbulent flow, so the turbulent flow regime is not merely of theoretical interest. Fluid engineers need access to viable tools capable of representing the effects of turbulence (Versteeg and Malalasakra, 2007). The most accurate approach to turbulence simulation aims to solve the Navier-Stokes equations directly. It is called direct numerical simulation (DNS) and is done without the use of any averaging or approximation other than numerical discretization for which errors can be estimated and controlled (Ferziger, 2002). DNS is not often used due to its very high computational cost. In engineering practice and normal academic research, the Reynolds Averaged Navier-Stokes (RANS) equations are often used to characterize turbulence features.

The RANS system is often closed using a 'turbulence model'. Among possible turbulence models, the k - ε model and its variant models, such as the Re normalized group (RNG) $k - \varepsilon$ model, are often used in urban drainage system for hydraulics modelling (Jarman *et al.*, 2008). The standard $k - \varepsilon$ model is an isotropic model and is widely used and has been validated in practice by engineering (Dufresne, 2008). The Reynolds Stress Model (RSM) is an anisotropic model and is considered by many authors to be better at representing turbulence when compared to these two other equation turbulence models, but it requires much higher computational time and is less stable. Within a review of CFD technique applications and best practice by Jarman *et al.* (2008), of the twenty-two selected studies on urban drainage systems, six used the RSM model and sixteen used the standard $k - \varepsilon$ or RNG $k - \varepsilon$ variant turbulence model. Dufresne (2008) employed the standard k- ε turbulent model for flow field and sediment transport modelling in a stormwater detention basin. The standard $k - \varepsilon$ model enabled the vertical recirculation in a circular basin (Quarini *et al.*, 1996; Jayanti,

2004) and horizontal recirculation in rectangular tanks (Stovin and Saul, 1994, 1996; Adamsson *et al*., 2005; Dufresne, 2008; Dufresne *et al.*, 2009) to be reproduced. Dufresne argues that the standard $k - \varepsilon$ model was sufficiently good to reproduce the flow in a detention basin. Vosswinkel *et al.* (2012) used the RNG $k - \varepsilon$ model to simulate flow field and tracer transport rather than a standard $k - \varepsilon$ model because the RNG $k - \varepsilon$ model enables the user to make a number of refinements. The results showed that the RNG $k - \varepsilon$ model reproduced the flow and observed unsteady features well. Hunze (2008) pointed out that the RNG $k - \varepsilon$ model is more suitable than the standard $k - \varepsilon$ model for the simulation of flow regimes with a low Reynolds number. Stovin *et al.* (2002) studied different turbulence models with the aim of exploring the extent to which turbulence models may affect the predicted flow field for sewerage structures. It was found that an RSM with quadratic pressure strain was better than the $k - \varepsilon$ and its variant models when results were compared with laboratory observations. Stovin *et al.* (2008) modeled solute transport in a storage tank using a species model and a discrete phase model (DPM) based on both the RSM and RNG $k - \varepsilon$ models. The authors found that for predicting flow fields, the RSM was better than the RNG $k - \varepsilon$ model, although both of them under-predicted the first arrival time and gave almost identical results for predictions for cumulative residence time distributions with particle tracking method. However, Dufresne *et al.* (2009) and Mignot *et al.* (2012) tested the standard k- ε model, the RNG k- ε model and the RSM in various urban drainage structures (three combined sewer overflow chambers for solid separation and open channel junctions) and found that the RSM model did not give significantly better results when compared to the RNG k- ε model.

Hence, while there is no doubt that Reynolds stress models have better potential for representing turbulent flow phenomena more accurately than the two equation turbulent models (Hadzic, 1999), in some cases the difference is so small as to be insignificant (Ferziger and Peric, 2002). It is not yet entirely clear which model is best for which kind of flow, partly due to the fact that in many of the attempts made to answer this question, the numerical errors have been too great to allow decisive conclusions to be drawn (Bradshaw *et al.*, 1994).

2.4.2 Sediment transport modelling

Sediment transport phenomena are encountered in many processes in industrial operations and engineering practice. Numerous examples can be found in coast, estuary, river, agricultural, reservoir and environment engineering, etc. Due to the inherent complexity of sediment transport flow, from a physical as well a numerical point of view, “general purpose” computational fluid dynamic (CFD) codes are non-existent. Sediment transport can be of many types (gas–solid, gas–liquid, liquid–liquid, etc.). In this thesis, the focus is on sediment transport in storm water discharge in a detention basin. It is therefore relevant to discuss, the different methods that can be used to model sediment transport in water here. In addition to flow fields, it can often be necessary to model additional physical characteristics at the same time. Three kinds of methods are generally used to model material transport in water flow: the species transport (scalar transport or single phase model) method, the Euler-Euler method (multiphase flow modelling) and the Euler-Lagrange method (discrete phase model). Some authors also distinguish two further categories: concentration tracking and particle tracking (Dufresne, 2008).

2.4.2.1 Species transport model approach

The species transport method is widely applied when examining river, estuary, reservoir and coastal problems (Zhang, 2009; Wu, 2004), and discussions on sediment transport often refer to the species transport method. Sediment transport modelling started in the 1950s and has been extensively developed and widely applied in practice in engineering since the 1970s (Wu, 2004). Sediment transport modelling is usually represented by spatial formulations varying from 1D and 2D depth average models to full 3D sediment flow models. This type of modelling can also be classified according to time dependent characteristics (steady or unsteady) or sediment transport characteristics (deposition & erosion, bed load & suspended load, cohesive & noncohesive, etc.). Papanicolaou *et al.* (2008) revised the current state of the art versions and future developments in sediment transport modelling. The common procedure is to split the model into a flow model and a sediment transport model (Zhang, 2009). Sediment transport is then calculated from the results of the flow field simulation in a decoupled way (or with one way coupling), which means the flow movement influences the sediment transport model but sediment movement does not affect flow behaviours.

Most of the 1D models are formulated in a rectilinear coordinate system and solve the differential conservation equations of mass and momentum of flow (the Saint Venant equations) along with the sediment mass continuity equation (Papanicolaou, 2008). Han, (1980), Chang (1982), Karim and Kennedy (1982), Thomas (1982), Holly and Rahuel (1990), Holly *et al.* (1990), Wu and Vieira (2002) used 1D models to calculate the long-term channel deposition and erosion under quasi-steady and unsteady flow conditions (Wu, 2004).

Since the early 1990s, many 2D and 3D sediment transport models (Shimizu *et al.,* 1990; Spasojevic and Holly, 1990; Lafond, 1995; Olsen, 1999; Cancio and Neves, 1999; Wu *et al.*, 2000; Wu, 2004; Bentzen *et al.,* 2008; Torres *et al.*, 2008) have also been created to simulate channel evolution in complex situations, such as estuarine systems and detention basins, in more detail. Usually many of them assume local equilibrium when simulating bed-load transport. Recent studies on the spatial and temporal lag of bed load transport show that a non-equilibrium transport model for bed load is also needed in many cases. For example, it is required where there is strong erosion and strong deposition, and especially under unsteady flow conditions. Furthermore, the hiding and exposure phenomena that exist in non-uniform sediment transport play an important role in bed material sorting and channel bed armouring. 2D models are depth-averaged models (2D St. Venant equations or shallow water equations) that can provide spatially varied information about water depth and bed elevation within rivers, lakes, and estuaries, as well as depth-averaged velocities. The 3D models solve the Navier-Stokes equations. Both the 2D and 3D flow models solve the sediment mass balance equations. If both the suspended load and bed load are taken into account, the sediment transport is generally subdivided into suspended load and bed load models. The suspended load transport is governed by the advection-diffusion equations incorporating sink/sources terms. For 2D model, the advection- diffusion equation is as follows (Wu, 2004):

$$\frac{\partial hC}{\partial t}+\frac{\partial UhC}{\partial x}+\frac{\partial VhC}{\partial y}=\frac{\partial}{\partial x}\left(\varepsilon_s h\frac{\partial C}{\partial x}\right)+\frac{\partial}{\partial y}\left(\varepsilon_s h\frac{\partial C}{\partial y}\right)+\alpha v_s\left(C_*-C\right) \tag{2.45}$$

Where h is water depth; U and V are depth-averaged flow velocities components in x and y directions; C is the depth-averaged suspended concentration of suspended load; C_* is the depth-averaged suspended load concentration under equilibrium conditions or the suspended load transport capacity; ε_s is diffusivity coefficient of sediment; α is nonequilibrium adaptation coefficient of suspended load if necessary; and v_s is settling velocity of sediment particles.

The mass balance equation in bed load for 2D model is (Wu, 2004):

$$(1-p')\frac{\partial z_b}{\partial t}+\frac{\partial \delta C_b}{\partial t}+\frac{\partial \alpha_{bx} q_b}{\partial x}+\frac{\partial \alpha_{by} q_b}{\partial y}+\omega v_s (C_*-C)=0 \tag{2.46}$$

Where δ is thickness of bed load zone; C_b is the averaged concentration of bed load in bed load zone, z_b is the bed elevation; α_{bx} and α_{by} are direction cosines of bed load movement, which are usually assumed to act along the direction of bed shear stress. q_b is the actual transport rate of bed material; p' is the porosity of bed material.

For 3D models, the advection- diffusion equation is as follows (Wu *et al.*, 2000):

$$\frac{\partial c}{\partial t}+\frac{\partial}{\partial x_j}\left[\left(u_j-v_s\delta_{j3}\right)c\right]=\frac{\partial}{\partial x_j}\left(\frac{\nu_t}{\sigma_c}\frac{\partial c}{\partial x_j}\right) \tag{2.47}$$

Where c is the local sediment concentration; v_s is settling velocity of sediment particles; δ_{j3} is Kronecker delta with $j=3$ indicating the vertical direction; σ_c the turbulent Schmidt number relating the turbulent diffusivity of the sediment to the eddy viscosity ν_t. If the sediment settling effect is not considered, the term ($v_s\delta_{j3}$) can be omitted. At a free surface, the vertical sediment flux is zero and hence the boundary condition is:

$$\frac{\nu_t}{\sigma_c}\frac{\partial c}{\partial z}+v_s c=0 \tag{2.48}$$

At the lower boundary of the suspended sediment layer, which is the interface with the bed load layer, the sediment net rate across the interface is introduced as a boundary condition, normally, the exchange of deposition rate D_b and Erosion rate E_b, and therefore the lower boundary condition is:

$$D_b-E_b=v_s\left(c_b-c_{b*}\right) \tag{2.49}$$

Where c_b is the local suspended load concentration near the interface of suspended load and bed load; c_{b*} is equilibrium concentration at the interface location.

The mass balance equation in bed load for 3D models is (Wu *et al.*, 2000):

$$(1-p')\frac{\partial z_b}{\partial t}+\frac{\partial \delta \overline{c_b}}{\partial t}+\frac{\partial \alpha_{bx} q_b}{\partial x}+\frac{\partial \alpha_{by} q_b}{\partial y}+\left(D_b-E_b\right)=0 \tag{2.50}$$

Where $\overline{c_b}$ is the averaged concentration over the bed load layer thickness δ.

Species models incorporate a certain degree of simplification in order to be computationally feasible. However, simplified models run the risk of not arriving at a reliable solution, whereas increasing the model complexity can complicate problem formulation and therefore, mean incurring more input data preparation, calibration and verification costs (Papanicolaou, 2008).

The species models developed to date have not been as universal as hydraulic engineers would like them to be. Species models are limited.

Most sediment entrainment is assumed to be triggered by the excess shear stress rather than by near bed turbulence characteristics. An increasing number of researches have shown that turbulent bursts (*e.g.* turbulent sweeps, ejections) are the primary triggering mechanisms of sediment entrainment (Nelson *et al.*, 1995; Papanicolaou, 1997, 2000; Papanicolaou *et al.*, 2001; Zanke, 2003; Dey *et al.*, 2011).

Traditionally, species models have often calculated the transport rate for a single characteristic grain size, for example, the median (Raudkivi, 1998). This type of model's weakness is its inability to account for the transport of sediment particles of different sizes (or densities). It is likely to underpredict or overpredict the transport rate of individual fractions when bimodal or multimodal distributions are present atop the bed surface (Papanicolaou *et al.*, 2008). In fact, a sediment particle of a certain size or density can be carried at different transport rates.

In the advection-diffusion equation, the treatment of the dispersion and diffusion coefficients as functions of the inner and outer variables, respectively, namely, the shear velocity, depth-averaged velocity, width of channel and mean flow depth is limited. It has been shown that the spatially averaged inner and outer quantities may not be good approximations of the dispersion process in channel constrictions or expansions and of flow near submerged or unsubmerged obstacles (Papanicolaou *et al.*, 2008).

Most species transport models have been based on equilibrium assumptions which do not often represent realistic conditions. Some researchers have considered non-equilibrium conditions with a non-equilibrium adaptation coefficient, but the results really depend on the modelling of non-equilibrium terms and hence on the value of the non-equilibrium adaptation length (Wu *et al.*, 2000; Wu, 2004). For the purposes of evaluating bed load transport, most of the available 3D models use empirical expressions for bed load transport modelling. However, the details of the processes that control sediment transport are not fully understood.

Furthermore, when it comes to modelling high sediment concentrations in fluids, the species model approach does not seem appropriate because it neglects the momentum exchanges between the fluid flow and particles. The solid volume fraction and relative velocity between fluid and solid phase is not considered (Zhang, 2009). In terms of species models which examine deposition and erosion, Torres (2008) performed 2D modelling of flow and sediment transport using Rubar20 for a large stormwater detention basin based on several measured storm events. The results showed the abilty of species models to model the global efficiency of a system, but failed to reproduce the preferential sediment deposition zones.

2.4.2.2 Euler-Euler approach

Sediment transport is made up of two phases: a liquid phase and a solid phase. There are two different modelling approaches that both take a multiphase view and use the grid-based CFD method to simulate the solid transport phase: Euler-Euler and Euler-Lagrange. However, in more recent years, new particle-based methods (such as Smoothed Particle Hydrodynamics-SPH, or Lattice Boltzmann Method-LBM) have been developed to simulate the solid transport phase (Krištof *et al.*, 2009;Vetsch, 2012; Ladd and Verberg, 2001; Joshi and Sun, 2009). With the SPH method, both the liquid and solid phases were treated with a particle-based approach within the Lagrange framework, and with a multiphase method. This method may be classified as a Lagrange-Lagrange approach. As these new methods (SPH and LBM) are still being developed, they will not be discussed further here and for the purposes of this thesis, we will observe the traditional classification of the two different approaches outlined above.

In the Euler-Euler approach, both the continuous and dispersed phases are described by Eulerian models. In these models, the dispersed phase, like the continuous phase, is treated as a continuous phase with appropriate closures, hence one calculates only the average local volume fraction, velocity, etc. but not the properties of each individual dispersed particle. Owing to the continuum description of the particulate suspension, Eulerian models require additional closure laws to describe the momentum transfer between the fluid phase and particle phase, which is described as viscous drag force, and to describe the momentum transfer between particle and particle phase, which is described as collision interaction.

For fluid-solid flow model based on the Euler-Euler approach, the interphase momentum transfer needs to be accounted for. Closure of the solid-phase momentum equation requires a description of the solid-phase stresses. Constitutive equations for the solid-phase stresses based on the kinetic theory can be used to describe the effective stresses in the solid phase resulting from particle streaming (kinetic contribution) and direct collisions (collision contribution)(van Wachem and Almstedt, 2003). This theory is basically an extension of the classical kinetic theory of gases for dense particulate flow. The closure models consist of a series of theoretical and empirical expressions, further description can be found in Lun *et al*.(1984) and van Wachem and Almstedt (2003).

Cao *et al.* (1995) carried out analysis of the flow field and sediment concentration profiles in an open channel. Hsu *et al.* (2001) introduced a sediment transport model based on the two-phase mass and momentum equations with appropriate closures on the near bed boundary conditions and fluid turbulence. The two-phase model is able to predict the time-averaged concentration under various combinations of maximum free-stream velocity and oscillatory period adequately. However, some discrepancies have been observed when comparing the time history of concentration profiles. Hsu *et al.* (2003) presented a two phase model that simulates fluid and sediment motion in the sheet flow region under oscillatory conditions. This model is able to provide accurate estimations of sediment concentrations because it uses constant equivalent sand roughness. Wanker and Gockler *et al.* (2001) used a Euler-Euler two-phase model to simulate the sedimentation effects and sediment transport. The model is valid for regions of high and low concentration. Bed changes are also accounted for directly without any adaptation of the grid. Bakhtyar *et al.* (2009) created a Eulerian two-phase flow model for fluid- sediment sheet flow simulation, that includes all the important forces such as

the fluid/particle and particle/particle interactions as well as the turbulent stresses. Zhao and Fernando (2007) successfully used a Eulerian two-phase model, which implemented Euler-Euler coupled governing equations for flow and sediment phase, to simulate the scour around a long fixed pipeline placed just above a non-cohesive sandy bed. Zhang and Chen (2007) used the Eulerian model to predict particle transport in an enclosed space. In comparison to experimental data, the numerical results showed that the Eulerian model is able to predict particle concentration under steady conditions.

In Eulerian models, the interactive forces between the sediment and fluid or the intergranular stress due to particle-particle collision are often simulated using single particle characteristics, such as the median size or density (Hsu *et al.*, 2003), hence the models is less appropriate for modelling particle size distribution and variable particle density.

2.4.2.3 Euler-Lagrange approach

The Euler-Lagrange approach is another approach used to describe the two phases of flow (fluid and sediment). In the Euler-Lagrange approach, the fluid phase flow is treated as a continuum and solid phase flow is treated as individual particles. This is called the Discrete Element Method (DEM). The DEM was introduced by Cundall and Strack in 1979. Withing the framework of the DEM, all particles are tracked using the Lagrangian approach that is based on Newton's second law of motion during computation. Further details are available in the literature (*e.g.* Campbell, 1990; Zhou *et al.*, 1999; Mattutis *et al.*, 2000; van Wachem and Almstedt, 2003; Bertrand *et al.*, 2005).

When a DEM is coupled with the Eulerian model to simulate sediment transport in fluid flow, this is known as the Euler-Lagrange approach. This approach considers the interphase momentum transfer as well as particle-particle interaction. In order to describe particle collisions, two types of approach are possible: the hard-sphere approach and the soft–sphere approach. In the hard-sphere approach, collisions between particles are assumed to be binary and instantaneous. During collision, energy is stored in the elastic deformation associated with both the normal and the tangential displacements of the contact point relative to the centre of the sphere. In the soft–sphere approach, particle interactions are modeled using potential forces. The soft-sphere approach is based on the concept that when two particles collide they deform. This deformation is described by an overlap displacement, and the particles lose kinetic energy. The normal force and frictional force are composed of a spring, a dashpot, and a friction slider. The time step in hard- sphere collision dynamics is governed by successive measures of the time between collisions. In dense systems this time step may be very small, which results in a very long computational time. The time step in soft-sphere collision dynamics is governed by the stiffness of the normal and tangential forces. The Hertzian contact theory predicts such high stiffness that in practical cases this also leads to very small possible time steps in dense suspensions (van Wachem and Almstedt, 2003; Apostolou and Hrymak，2008). Kloss *et al.* (2009) and Mezhericher *et al.* (2011) reported that the time step used in their sediment transport modelling has an order of magnitude of 10^{-6} s. Due to the huge computation time, the amount of discrete element models which can be used is, today and in the near future, limited (van Wachem and Almstedt, 2003) and it is difficult to perform large scale simulation with a DEM without advanced computer power.

For overcoming the disadvantages of creating a complete DEM, a compromise method called a discrete phase model (DPM) has been devised. It can be considered to be a simplified DEM. In DPM each "particle" represents a parcel of particles rather than an individual particle as in standard DEM. Like the DEM, the DPM tracks each particle trajectory based on the Newton's second law of motion, but without taking the collision between particles into consideration. Hence, it is only suitable for dilute suspension systems with a particulate phase volume fraction of less than 10%. Interphase moment transfer can also be added using one-way coupling or two-way coupling depending on what is needed. For dilute systems, the momentum involved in moving from solid phase flow to fluid phase flow has often been neglected in research (Stovin, 1996; Dufresne, 2008; Vosswinkel *et al.* 2012). DPM is able to use larger time steps than DEM because they do not take particle collision into consideration and since they track less particles, instead using the concept of parcels, which represent a number of particles. Hence DPM needs less computational time. Nevertheless, DPM are also less accurate because they do not take collisions between particles into consideration. Kloss *et al.* (2009) coupled DEMs and DPM for two phase flow simulation depending on the solid phase concentration. Particle transport was sped up by switching from DEM to DPM in dilute regions where interparticle collision could be neglected. But for this method to be applied, the DPM must use single particle rather than a parcel of particles.

In recent years, a growing number of research has used DPM to investigate sediment transport problems, such as research on stormwater basins (Lafond, 1995; Harwood and Saul, 1996; Cheebo *et al.*,1998; Dufresne, 2008; Torres, 2008; Dufresne *et al.*, 2009; Zhang, 2009; Yan *et al.*, 2011; Vosswinkel *et al.*, 2012), storage chambers (Stovin, 1996; Stovin and Saul, 1996, 1998, 2000; Stovin *et al.*, 1999), hydrodynamic separators for stormwater (Pathapati *et al.*, 2008; Pathapati and Sansalone, 2009; Sansalone and Pathapati, 2009), meandering river (Shams *et al.*, 2002) or Combined Sewer Overflow structures (Lipeme Kouyi, 2004; Dufresne *et al.*, 2009).

There has been considerable recent progress in computational modelling of particle transport, deposition, and resuspension processes in fields related to DPM. For stormwater basins, the RE and deposition zones are the most important applications. Stovin and Saul (1996, 1998) applied the DPM approach to storage chambers in order to predict RE. Shams *et al.* (2002) performed a computational modelling analysis of flow and sediment transport and deposition in a meandering river. Adamsson *et al.* (2003) used particle tracking with the Lagrange approach to model the sediment transport in rectangular chamber. Dufresne (2008) and Dufresne *et al.* (2009) also used the DPM approach to predict the efficiency and deposition zone in a detention tank. Zhang (2009) tested the influence of different inlet and outlet positions in a tank to determine the efficiency and deposition zone. Vosswinkel *et al.* (2012) used a DPM to evaluate the influence of unsteady behaviour on sediment transport and deposition in a detention basin. For this study, predictions of efficiency and deposition zones were found to be sensitive to particle properties and boundary conditions (it can be assumed that flow field simulation was satisfactory). Stovin and Saul (1998) found that efficiency was sensitive to physical properties (*e.g.* injection location, particle sizes and particle density) and boundary conditions in their test cases. The simulation results from a DPM showed that efficiency is more sensitive to the particle injection location and less sensitive to particle size. It should be noted that bed boundary conditions did not distinguish between different particles, which means that the particles were the same for bed boundary interaction treatment. They used a density of 2500 kg/m^3 in simulation instead of a real density of 1500

kg/m^3 because the former was the closest fit to the laboratory data. Efficiency was shown to be insensitive to the parameter of step length. According to the simulation results, turbulent dispersion was also a factor which had an impact on the prediction of efficiency and sediment deposition zones.

Simulated efficiency was highly sensitive to boundary condition configurations (Stovin and Saul, 1998). Stovin and Saul stated that the selection of boundary conditions should reflect an understanding of the physical processes. To describe the overall efficiency of the settling processes in storage tanks, Lafond (1995) demonstrated that complex 2D/3D CFD models did not necessarily lead to significantly better results than simple models based on modified Hazen or Camp theories. This is mainly due to critical hypotheses (especially the bottom boundary condition treatment applied to particles which reach the tank bottom), which are needed for CFD models but are difficult to verify or to prove in a field site, because of their complexity (Ashley *et al.*, 2004).

The basic boundary conditions of DPM, which are often used in urban drainage systems, are: trap, reflect and escape. Escape is often the inlet and outlet of a system. Reflect is often the vertical or side wall. Both trap and reflect are often used as the boundary conditions for the bottom of basin, representing particle behaviour when it reaches the bottom. The pure trap boundary condition for the bed often overestimates the efficiency and sediment deposition zone, while a pure reflect boundary condition often underestimates efficiency and deposition zones due to a bad reflection of particle transport processes such as dynamic saltation and erosion (Adamsson *et al.*, 2003). Stovin and Saul (1998) used finite reflect times (e.g. 25) for each bottom cell in an attempt to reflect particle saltation. However, this assumption cannot represent real physical processes. Chebbo *et al.* (1998) used a stochastic approach by linking the convection–diffusion equation to Fokker-Planck's equation to determine particle bed boundary condition treatment (the particle bounces on the bottom a random number of times then stops) for solid transport in a settling tank. This approach obtained a better efficiency prediction for a settling tank, and therefore offered an alternative method, but it did still not reflect the real dynamic physical transport processes. Bed boundary conditions were improved using a combination of trap and reflects with a bed shear stress threshold (Adamsson *et al.*, 2003). The particle was trapped if local bed shear stresses were lower than the threshold and, therefore, ended its trajectory; otherwise the particle rebounded and continued its trajectory. A similar approach was developed using a bed turbulent kinetic energy threshold to model sediment transport in a pilot detention basin (Dufresne, 2008).

Generally, a bed shear stress threshold or a bed turbulent kinetic energy threshold was measured in the laboratory or verified by comparing the flow simulation results with observed experimental sediment deposition zones. 0.03 - 0.04 Pa was found to be the critical bed shear stress for deposition (Stovin and Saul, 1994; Dufresne, 2008) and 0.06 Pa for erosion critical bed shear stress in a laboratory scale tank (Stovin and Saul, 1994). However, Stovin and Saul (1994) stressed that deposition and erosion of critical bed shear stress depend on the properties of the sediment, and of the rough bed conditions. Further work is required to derive appropriate values for full scale detention basins. Vosswinkel *et al.* (2012) used the Shields curve to calculate the critical deposition bed shear stress which depends on the particle properties used for modelling sediment transport in a detention basin. Lipeme Kouyi *et al.* (2010) performed a 3D flow simulation in a full stormwater detention basin, and found that the critical bed turbulent kinetic energy was of a much lower value than that observed by

Dufresne (2008) in small scale tank in a laboratory. To better estimate the critical bed turbulent kinetic energy and to account for particle properties, Yan *et al.* (2011b) proposed a formula for calculating the threshold based on the settling velocity of particles.

It should be noted that almost all the modelling research on detention basins for predicting efficiency and deposition zones have been based on steady state conditions with one way coupling. Vosswinkel *et al.* (2012) evaluated the unsteady flow influence on the particle settling processes. They performed unsteady flow modelling and saved each time step simulation result. Then they used the time step flow modelling results to performed steady state particle tracking under one way coupling. To a certain extent, this method accounts for the unsteady flow effect on sedimentation processes. In unsteady flow conditions, a particle that has been deposited at one moment may be entrained due to a change of local flow conditions in the next moment. However, dynamic erosion could not be taken into consideration when using this method because the modelling was disconnected. Thus it was a real unsteady particle tracking approach. However, it was an improvement on predictions made using only steady state modelling.

Over the past decade, progress has been with the use of DPM approaches for sediment transport modelling, but a lack of understanding of complex sedimentation processes is still an obstacle to adequate predictions of the efficiency and sediment deposition zones of stormwater detention basins. Many phenomena involved in sedimentation processes such as dynamic entrainment, aggregation, consolidation, particle collision due to dense concentration and so on still require further investigation.

2.4.2.4 Comparison of species model, Euler-Euler and Euler-Lagrange approaches

As mentioned above, the species model has its limitations in the modelling of sediment transport because of simplification and the usage of many empirical sediment transport formulas which were developed for very specific applications.

Without invoking a series of purely empirical sediment transport formulas, the two-phase models (the Euler-Euler and Euler-Lagrange approaches) were developed based on more fundamental dynamic principles. These two-phase models were expected to be more generally applicable to a range of problems. In Eulerian models, no empirical sediment transport formulas are required (Zhang, 2009). Thanks to the inclusion of flow-particle and particle-particle interactions, a two-phase model is also capable of modelling dense flow, which is difficult for species models. Stovin *et al.* (2008) modeled the residence time distribution in a storage chamber taking a DPM approach and using a species model. The results showed that the DPM approach was much faster (about 100 times faster) than the species model. Moreover, the DPM approach could more easily represent the particle size distribution of sediment.

The Euler-Euler and Euler-Lagrange approaches both have their own advantages and drawbacks. The Euler-Euler approach is less able to recover the characteristics of particles, such as particle size distribution and rotation of particle. However, the Euler-Euler approach has no a strict time step constraints like those found in a DEM collision model. DEM and

DPM enable more physical particle properties to be taken into account, such as non-uniform sediment sizes, densities etc. The Euler-Lagrange approach is better at representing physical and chemical treatments such as aggregation formation during the transport processes (Lu et al., 2007; Apostolou and Hrgmak, 2008). Zhang and Chen (2007) performed particle sediment transport and distribution in enclosed spaces with Eulerian and Lagrangian approaches respectively. For steady conditions, both the approaches were able to predict particle concentration distribution in an enclosed space reasonably. The Eulerian model needs less computing time than the Lagrangian approach, because the latter needs to track large number of particles to ensure statistical stability. Under unsteady conditions, the Eulerian model requires small time steps and needs more iteration per step to ensure the convergence. It turned out that the Eulerian model required more computational time and the particle tracking (DPM) approach was actually more computationally efficient. The particle tracking process did not significantly increase the computing time compared with that under steady state conditions. It was suggested that the DPM approach was more capable of modelling particle transport under unsteady conditions.

Multiphase flow has been modeled using a Eulerian-Eulerian approach or a Eulerian-Lagrangian approach (van Wachem and Almstedt, 2003) depending on the extent of coupling between phases, with the delimiter that a Eulerian-Eulerian approach is used for flow with particulate volume fractions (PVF) greater than 10% (Sansalone and Pathapati, 2009). Elghobashi (1991) proposed a regime map for appropriating the degree of interphase coupling, by analyzing length and time scales.

2.5 Conclusions of Chapter 2

The general performance of detention basins has been examined in order to give an overview of the background for this research. This research is focused on sediment transport in a detention basin and an intial review of the scientific context of the study highlighted the importance and necessity of the removal of particulate pollutants during wet weather conditions in detention basins in order to protect the receiving water bodies, as the majority of pollutants attach themselves to solid particles in stormwater runoff. Secondly, mechanisms related to sediment transport were introduced. Traditional sediment transport mechanisms were based on the concentration concept and relied on many empirical expressions. It has proved difficult to improve understanding of sedimentation phenomena further. Some researchers have used advanced equipment to examine this subject on a particle scale with the aim of further improving understanding of sediment transport.

Storm water detention basins are widely used in urban storm water management for both storm discharges quantity and quality control. However, the hydraulic and RE performance of basins are heterogeneous for historical reasons, the complexity of flow conditions and limited understanding of sediment transport phenomena.

During the development of detention basins, different methods (field observation and measurements, scaled models experiments and CFD modelling) have been performed to investigate potential improvements in hydraulic performance and removal efficiency. Each method has its own advantages and disadvantages, however, CFD modelling seems to be used more and more for research and engineering applications thanks to its low cost and the higher

level of information obtained. According to previous work on CFD modelling of fluid flow and sediment transport, the Euler-Lagrange approach seems to provide more information and have a higher potential for improving the understanding of sediment transport.

Progress has been made in the field of sediment transport modelling, but the lack of understanding of complex sedimentation processes is still an obstacle to accurately predicting the efficiency and sediment deposition zone of stormwater detention basins. Many phenomena involved in sedimentation processes such as dynamic entrainment, aggregation, consolidation, particle collision due to dense concentration and so on are not clearly defined.

In fact, the DPM method is not a new technique for modelling sedimentation phenomena in stormwater basins. As discussed above, the main problem is that no satisfactory bed boundary conditions have been established that clearly represent complex sedimentation phenomena such as dynamic settling and erosion. Furthermore, most research on efficiency and the prediction of sediment deposition zones has been based on laboratory scale models and it is difficult to apply this research to real full scale systems due to the effect of scale and the more complex conditions in real systems (geometry, surface conditions, variable inflow and outflow conditions, etc.). However, some research on full scale detention basins is available in scientific studies. In order to improve the design and management of full scale detention basins, more appropriate bed boundary conditions need to be developed and dynamic bed boundary treatment for unsteady particle tracking should be considered as a method for representing the dynamic deposition and erosion processes in real conditions.

Chapter 3 Materials and methods

3.1 Methodology of the research

As noted in chapter one, this PhD aims to contribute to the understanding of the mechanisms involved in the sedimentation processes in detention basins and to modelling sediment transport in detention basins. The results of the modelling can be used to improve the design and management of stormwater detention basins. Few researchers have directly investigated full-scale detention basin numerical modelling with DPM approach mainly due to difficulties regarding control and measurement in complex real-life conditions (complex geometry, surface condition, variable inflow/outflow and pollutant loads), and the high cost and huge requirements in terms of computational resources. Instead, most research has been carried out on scale models in laboratory conditions. However, it remains difficult to apply the results obtained from scale models to real-life systems. Therefore, this research focuses directly on a full-scale detention basin, in order to test the methods available in a full-scale basin and develop a new approach to model dynamic sedimentation processes. However, we also used the scale basins to test the newly-developed methods as they require less computational time and provide experimental data for validation.

The research strategy is as follows:

- In order to characterise the sediment accumulated in the basin, sediment samples were collected and analysed in laboratory in order to determine their physical properties; then analyses were performed to obtain the sedimentation characteristics spatial distribution in the basin.
- Preliminary flow field simulation tests were carried out based on a simplified geometry of a full-scale basin. Due to the lack of available flow field data measurements (such as velocity field, flow free surface, etc.) for full-scale basins against which the flow simulation results could be checked, we instead used the accumulated sediment spatial distribution characteristics to roughly and indirectly check flow pattern. This may constitute a promising approach to model verification given the difficulties in collecting appropriate hydrodynamic data from real basins.
- Based on the flow simulation results, we tested the available models (mainly the bed boundary conditions to represent the sedimentation processes) with a DPM approach in the full-scale basin in order to verify the capability of those bed boundary conditions in a real basin system.
- A new formula has been proposed to calculate the threshold of bed turbulent kinetic energy (BTKE) by taking into account the particle properties in order to determine the suitable thresholds for specific pollutants. When predicting the efficiency and sediment deposition zones in a new basin design, the threshold cannot be determined by comparing simulation results with an inbuilt basin as this is unfeasible. Therefore the new method was first tested on a small-scale basin to verify its feasibility.
- Then the new method was tested in the full-scale basin for sediment transport modelling.
- Another novel approach has been developed to model dynamic sediment transport, settling and entrainment in detention basin. Grain scale sediment transport

mechanisms were represented and tested in a small-scale detention basin. The newly developed method's potential capability for predicting efficiency and sediment deposition zone was explored.

In this chapter, the field experimental site is first briefly introduced, including the structure configurations and *in situ* monitoring equipment. Then the approaches used for the sampling and analysis of the sediment's physical properties are described. Finally, the numerical methods used in this research are described and discussed in detail mainly focusing on the fluid flow modelling and sediment transport modelling.

3.2 Experimental site

3.2.1 *In situ* site

Our research was carried out under the framework of OTHU (Observatoire de Terrain en Hydrologie Urbaine - Field Observatory for Urban Hydrology - http://www.graie.org/othu/). This outdoor field observatory was set up to acquire reliable data on urban effluents during wet weather, with the aim of monitoring both the quality and quantity of stormwater from urban catchments and providing methodologies in order to assess the sustainability of the urban water system and offer support for operational decision making (OTHU - http://www.graie.org/othu/).

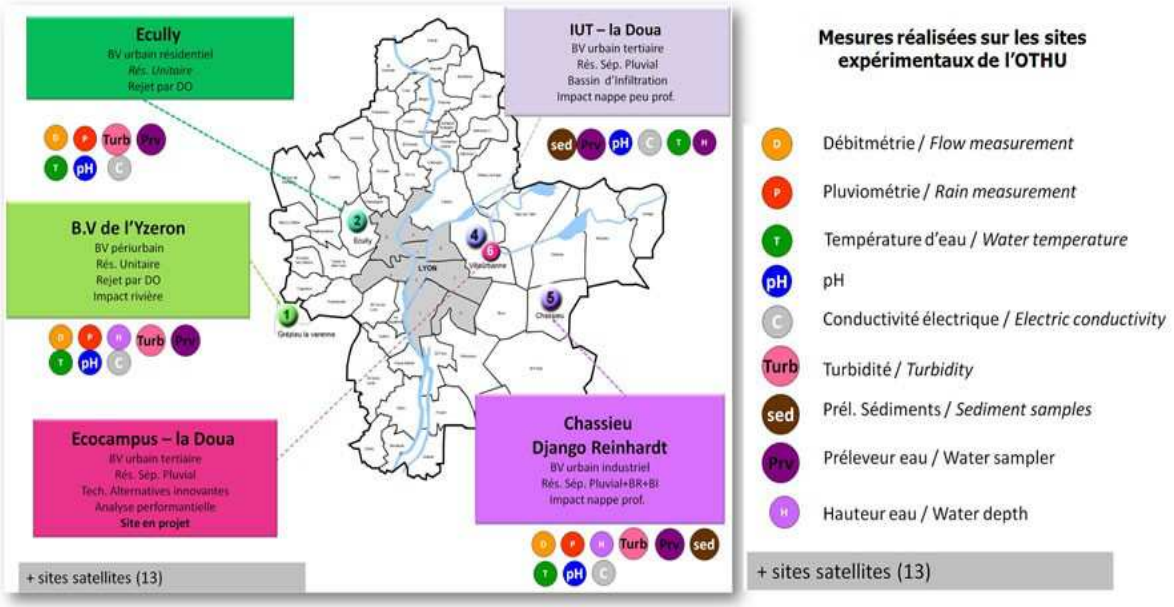

Figure 3-1 Location of OTHU experimental sites in the Lyon sewer system (OTHU, 2012)

Five experimental field sites come under the OTHU project (shown in Figure 3-1) which distributed in the drainage system of Grade Lyon.. One of these experimental sites is in Chassieu, located in the east of Lyon. As part of the OTHU's research, experimental and modelling investigations have been carried out in the Django Reinhardt large stormwater

detention basin in Chassieu (Lyon, France). These investigations aimed to contribute to improving the design and management of large stormwater detention basins. The Chassieu catchments are an industrial zone of 185 ha (dotted line polygon shown in Figure 3-2). The mean slope of the catchments is about 0.4%, with 75% impervious area. They consist of two sewer network systems, one for wastewater, and the other for stormwater, which is monitored by OTHU. Stormwater is conveyed through a separated sewer system towards the Django Reinhardt detention-infiltration basins. The Django Reinhardt detention-infiltration system facility was built in 1975 in Chassieu in order to collect stormwater from the industrial catchments of Chassieu (shown in Figure 3-3). It was renovated in 1985, in 2002 and then further retrofitted in 2004. The facility is composed of two sub-basins connected with a 60 cm diameter pipe. The first is a detention and settling basin (Figure 3-3) with an area of 11300 m² and a volume of 32200 m^3, where the stormwater is stored before being released downstream into the infiltration sub-basin. During dry weather, the detention basin drains a small amount of water from the surrounding industries, which are theoretically only authorised to discharge unpolluted cooling water. The bottom of the settling basin is sealed with bitumen and is equipped with a low-flow trapezoidal channel (depth = 20 cm, width = 2 m) which collects and guides the dry weather flow towards three orifices. The sides of the detention basin are covered with a plastic liner. The second basin is the infiltration basin with a surface of 10 000 m² and volume of about 61 000 m^3. The infiltration basin also receives (for extraordinary floods) water from a weir located 50 m upstream relative to the entrance (inlet 1) of the detention basin (Figure 3-3 View of Django Reinhardt detention-settling and infiltration facility (photo of 15/03/2012 from Google map)). The infiltration basin covers a layer located at a depth of about 13m.

A simplified sketch of the detention basin is shown in Figure 3-4. Stormwater enters the settling basin via two 1.6 m circular pipes (labeled as inlet 1 and inlet 2 in Figure 3-4). In order to enhance the detention process, a 1m high detention wall was built in 2004. In front of the outlet, there are three 19cm diameter outlet orifices (labeled o1, o2 and o3 in Figure 3-4) through the detention wall. When the water level is higher than the detention wall, an overflow weir is used as an additional outlet. The stormwater outflow towards the infiltration sub-basin is limited to 350 L/s by a regulator (see Figure 3-5). The contour of the basin bottom elevation and the outline dimensions are shown in Figure 3-6. The inlet and outlet base elevations are listed in Table 3-1.

Table 3-1 Base elevation of inlet /outlet of Django Reinhardt detention basin

Location of inlet / outlet (shown in Figure 3-4)	Original base elevation (m)	Base elevation relative to the lowest point (m)
Inlet 1	196.64	2.76
Inlet 2	196.25	2.37
Orifice 1	196.10	2.22
Orifice 2	195.43	1.55
Orifice 3	196.10	2.22
Central settling pit	193.88	0
Overflow weir	196.40±0.3	2.52±0.3
outlet	195.93	2.05

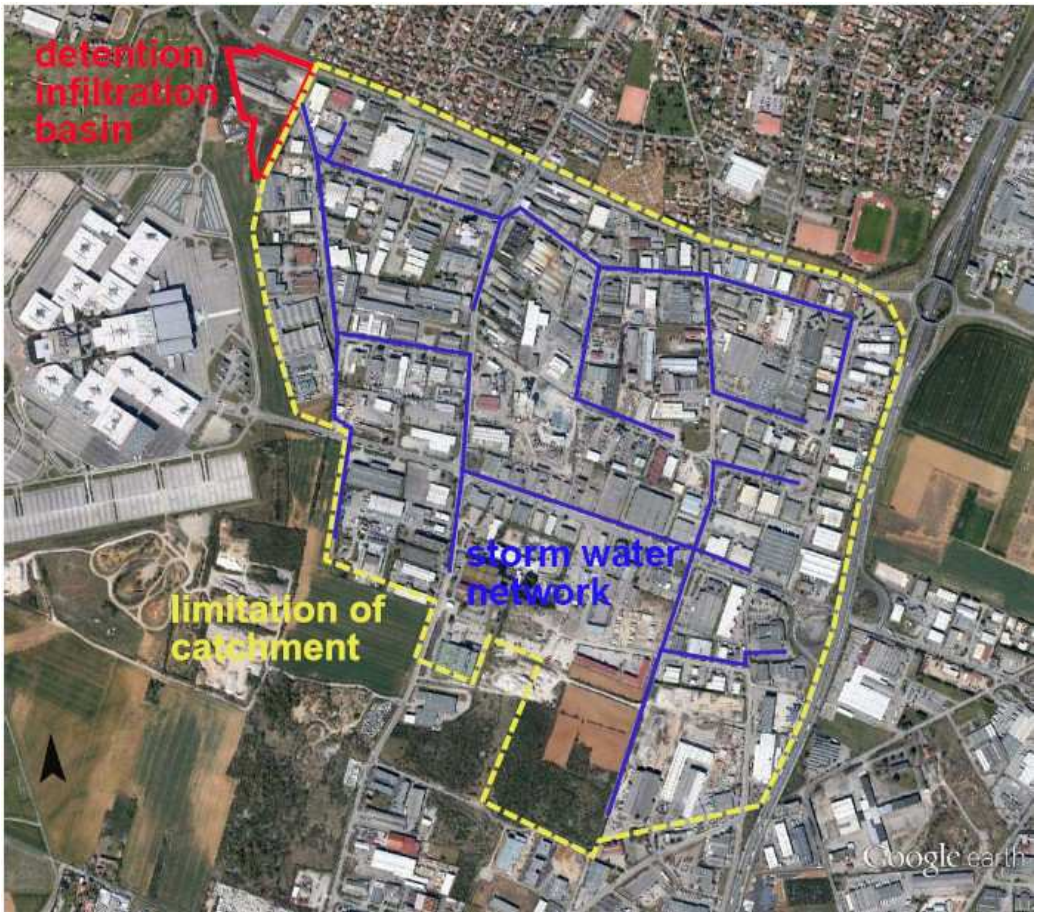

Figure 3-2 Presentation of the Chassieu catchments

Turbidity was measured using an infra-red 880 nm nephelometric sensor Endress+Hauser CUS 1 according to the NF EN 27027 standard (1994). Its use as a surrogate to estimate TSS equivalent concentrations is described by Bertrand-Krajewski (2004). The inlet and outlet discharges are calculated from simultaneous measurements of water depth and velocity in the pipes. Three water height sensors are located on the bottom of the basin (labeled as h1, h2 and h3 in Figure 3-4). All variables are recorded with a 2 minute time step in a S50 Sofrel data logger.

Figure 3-3 View of Django Reinhardt detention-settling and infiltration facility (photo of 15/03/2012 from Google map)

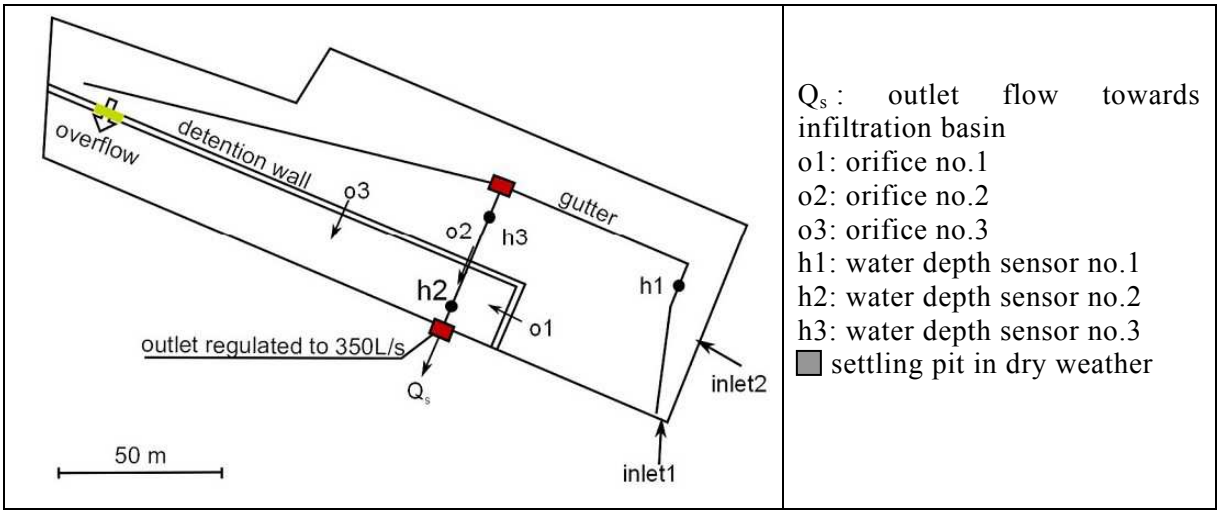

Figure 3-4 Scheme of the Django Reinhardt detention- settling basin after its retrofit in 2004

Figure 3-5 Outlet of Django Reinhardt detention basin equipped with regulator gate with a maximum outflow rate of 350 L/s (Hydroslide® gate)

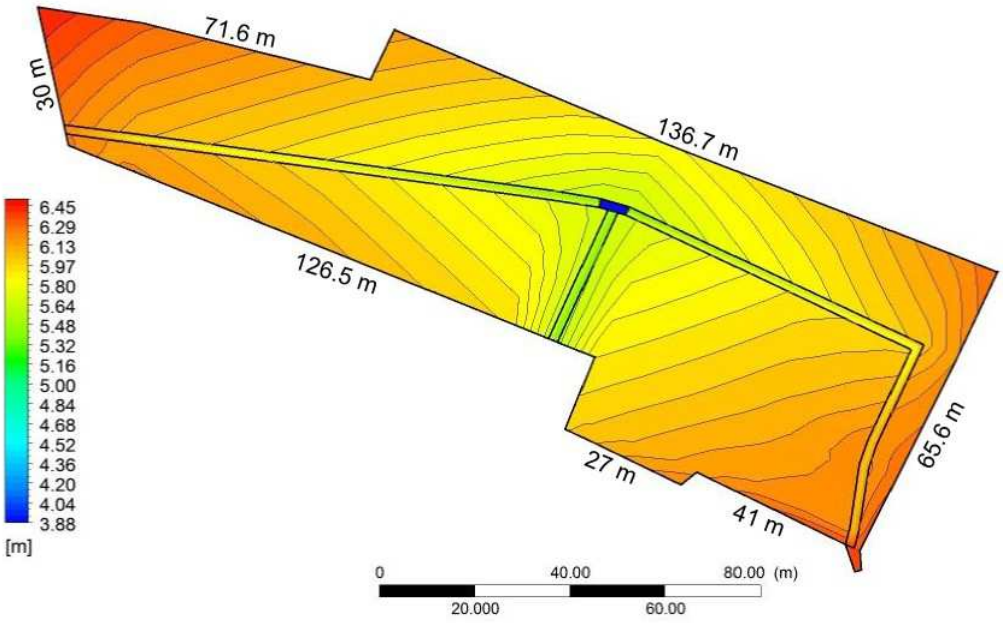

Figure 3-6 Bed elevation contour of the Django Reinhardt detention basin

3.2.2 Pilot basin

As we know, it is difficult to acquire detailed hydrodynamic data in a real large detention basin. Hence we used the pilot basin experiments to test the proposed methods, since pilot basin experiments can provide much more flow and sediment information. Two pilot basins from the literature (Dufresne, 2008; Vosswinkel *et al.*, 2012) were chosen for this research for their simplicity and the availability of experimental data.

Dufresne (2008) carried out a series of sediment transport experiments and performed simulations of hydrodynamics and sediment transport modelling.

The brief introduction from Dufresne *et al.* (2009) is summarized below in order to better understand the simulation set-up: The experimental pilot was a rectangular basin 1.80 m long and 0.76 m wide. It is equipped with an inlet pipe (diameter 80 mm), an outlet pipe (80 mm), and an overflow limiting the water depth to 0.40 m. A pump outputting between 1 and 10 L/s replenishes the tank. A valve regulates discharge in the outlet pipe and water depth in the tank. A flowmeter measures the inflow rate while two ultrasonic sensors measure water depth in settling tanks 1 and 2 (shown in Figure 3-7). The flow rates were then calculated using a weir law. An Acoustic Doppler Velocimeter (ADV) is used to measure the instantaneous velocities of liquid flow at different points in the tank. Each acquisition lasted for 120s, which corresponds to 6000 measurements (frequency: 50 Hz). A peristaltic pump injected white polystyrol particles over a period of 25 min. The particles were placed in the water for at least one day before each experiment. Their size is non-uniform, as shown inTable 3-2. The mean value equals 1034 kg/m^3, the standard deviation is 20 kg/m^3. The particles were recovered in two settling tanks. In this way it was possible to calculate the mass balance between the particles that are injected, and those which settled in the tank, overflow, and outflow. The experimental devices are shown in Figure 3-7.

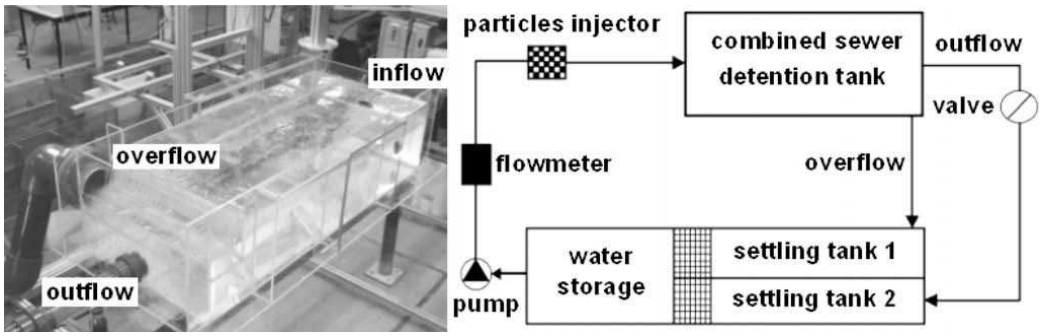

Figure 3-7 Experimental tank and measurement devices adapted from Dufresne et al. (2009)

Table 3-2 Particle size distribution for the pilot basin experiment, according to Dufresne (2008)

d_{min}	d_{10}*	d_{20}	d_{30}	d_{40}	d_{50}	d_{60}	d_{70}	d_{80}	d_{90}	d_{max}
350	535	593	642	689	738	790	851	931	1056	1400

*: d_{10} means sieving size with 10 percent of particle mass passing through.

In this section, we will further test the proposed method for dynamic sedimentation modelling. The simulation is based on the previous work conducted by Vosswinkel *et al.* (2012).

The experimental set-up (see Figure 3-8) consisted of a rectangular sedimentation tank made of glass (Length/Width/Depth = 3125/ 800/ 200 mm) plus an inlet tank to dissipate the energy in the water flow. The inflow was directed through a 100 mm diameter pipe located at the bottom of the tank. The particulate and dissolved tracers were also added to the flow. Discharge from the tank passed through a weir (discharge coefficient μ=0.62) with an upstream scum board. The inflow rate at the inlet was 2.19 L/s.

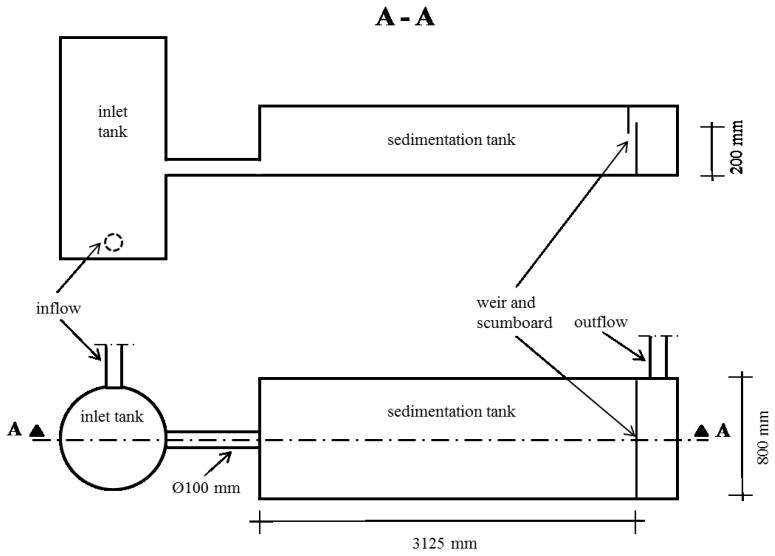

Figure 3-8 Experimental set-up (after Vosswinkel et al. 2012)

Polystyrene particles (P 426, manufacturer BASF) were added as the sediment in order to determine settling efficiency within the tank. The density of 1020 kg/m^3 was measured using a water pycnometer. The main particle sizes fell within the range of 300 to 700 μm with a median and maximum size of 500 μm and 800 μm respectively. The suspended particles were added by impulses through the injection mechanism in 10 steps with a volume of 100 ml injected at five-minute intervals. The volume of particles retained within the tank, as well as the volume of particles from the discharge, was determined using an Imhoff cone to calculate removal efficiency.

3.3 *In situ* experiments to characterise accumulated sediment

3.3.1 Introduction

Samples had to be collected from the inlet, outlet and inside of the basin, in order to characterise particulate pollutants from storm runoff. Previous work on sampling by Torres (2008) showed that when using a conventional sampler, it was difficult to collect samples from the inlet and outlet which were representative of the whole storm event. He analysed the limitations with the conventional sampler at inlet and outlet: i) spot sampling at specific intervals with the difficulty of integrating the entire rainfall event, ii) the limited storage capability of the automatic sampler, iii) the difficulty of ensuring representative sampling of an entrained solid (bed load) and/or a solid with high settling velocity, because the sampler is designed to collect total suspended solids. Considering all these difficulties, in this present reserch, we mainly focus on the sediment settled out at the bottom of the basin.

3.3.2 Sampling of accumulated sediment

Information on the characteristics of accumulated sediment are a fundamental requirement for improving our understanding of sedimentation processes in stormwater detention–settling basins. On the one hand, by analysing the properties of accumulated sediment, we can gain insights into some of the characteristics of the sedimentation process. On the other hand, the sediment characteristics (grain size distribution, density, settling velocity) constitute the input parameters required to simulate solid transport. In addition, using plastic sediment traps at the bottom of the basin may disturb settling processes due to the changes in key hydrodynamic quantities close to the bottom (turbulence kinetic energy, shear stresses, velocity distribution, etc.). Hence, sampling the accumulated sediment can also be considered as a complementary way of characterising this sediment which moves near the bottom.

3.3.2.1 Layout of sampling locations

We selected representative dispersion points for sediment sampling based on previous observations (Torres, 2008) and the first simulation results (Yan *et al.*, 2011a). Several key aspects concerning the physical properties of both particles and flow related to sedimentation were taken into account:

- Thickness of cumulated sediment
- Density
- Diameter
- Near bed flow conditions and flow pattern (*e.g.*, bed shear stress, turbulent kinetic energy, etc.).

In order to obtain the geometric data on the detention basin required for modelling mesh, topographic measurements were taken. About 500 points inside the basin were measured using the GPS technique and the details of some specific structures were also measured, for example, the inlet, outlet, orifices, etc. The spatial interval for themeasurement points was a 5m by 5 m square. Closer spacing of the measurement points was used in the centre of the basin and wider spacing close to the basin inlet.

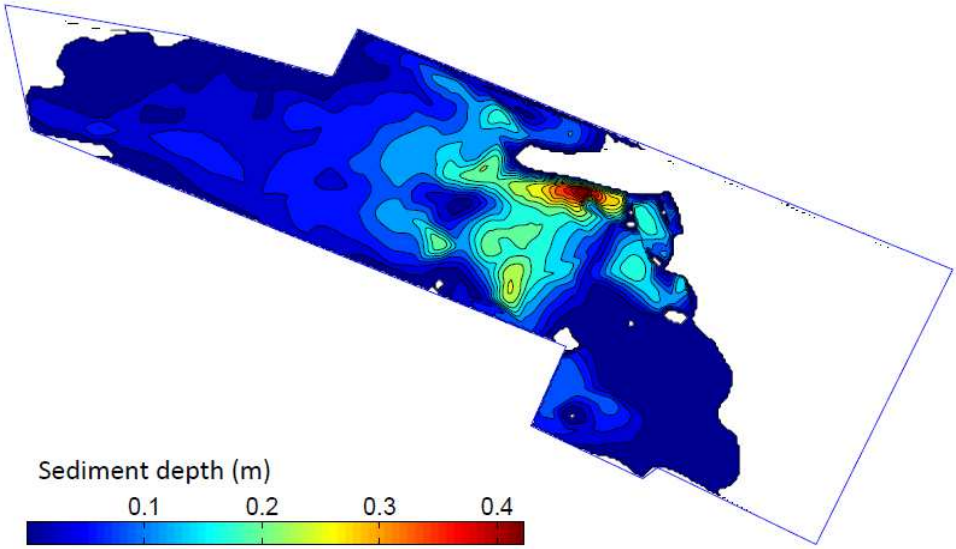

Figure 3-9 Sediment depth distributions in the Django Reinhardt detention basin.

Figure 3-10 A photo showing an example sediment zone in Chassieu (14/4/2011)

Figure 3-9 shows the cumulated sediment thickness spatial distribution. The sediment had been accumulating since 2006. The sediment thickness measurement was carried out in April 2011. According to previous observations from this site (see Figure 3-10), it is estimated that sediment in the polygon zone shown in yellow is different from the other zones in terms of density and diameter. Meanwhile, considering that the near bed turbulent kinetic energy distribution and bed shear stress from the preliminary 3D hydrodynamic simulation results in an inflow rate of 0.35 m^3/s, the layout of the sediment sampling points is shown in Figure 3-11. Elven different locations were chosen for sediment sampling, numbered roughly according to the thickness of the accumulated sediment measured in the year 2011.

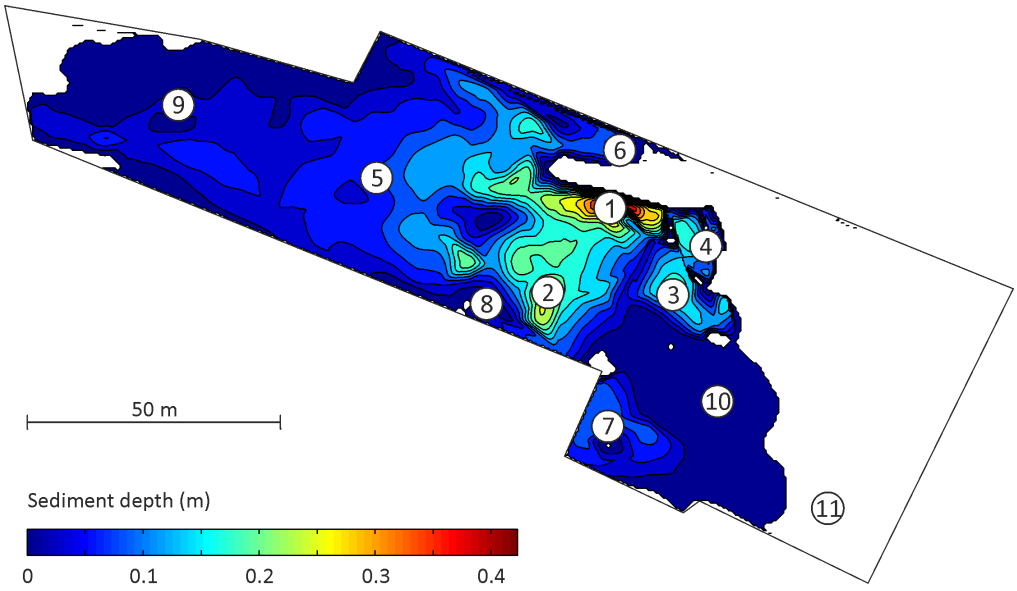

Figure 3-11 Layouts of the sediment sampling locations in the Django Reinhardt detention basin

3.3.2.2 Sediment sampling processes

The sediment sampling processes is summarised as follows:

- Measure the thickness of the sediment at each location indicated on Figure 3-11 (thickness of the sampling area)
- Mark off a square area of 0.5 m in length and mix all the sediment in the square, then divide it between four equal sub-squares as shown in Figure 3-12, dislodge two sub-squares of sediment at the diagonal, and then mix the left-hand sediment and repeat four times; finally collect about 1500 g from the left-hand homogenous sediment and put them into a plastic bag (NF P 18-533)
- The sediment samples are taken to laboratory and kept in the refrigerator.

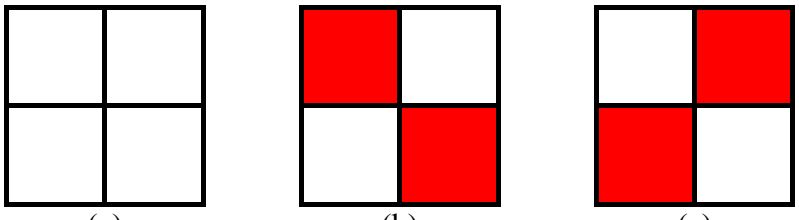

Figure 3-12 Sampling process diagram

3.3.2.3 Sediment analyses

The sediment analyses consist of: a) determining grain size distribution; b) particle density; c) organic material content of the accumulated sediment.

a. Determining grain size distribution

We analysed the particle size distribution between 0.1 μm and 1600 μm with the Laser Particle Sizer (LPS) using the Malvern Mastersizer 2000 equipped with the Hydro2000G sample dispersion accessory (shown in Figure 3-13). Due to the limited range of particle sizes processed by the Mastersizer 2000, we also used sieving technology to analyse particle size distribution, because preliminary measurements of certain sediment samples showed that a fraction of the particles were larger than 1600 μm.

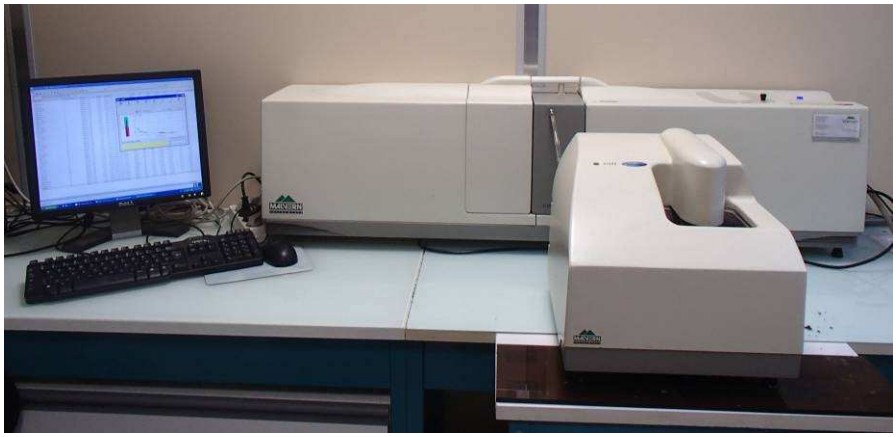

Figure 3-13 Laser Particle Sizer (LPS): Malvern Mastersizer 2000 equipped with the Hydro2000G sample dispersion accessory.

As regards the sieving technology, we carried out the experiments according to the XP P 94-041 standard for wet method sieving. Standard wet method sieving usually consists of the following main steps:

- Dry the sample
- Weigh the dry sample
- Wash the sample
- Sieving analysis with water
- Dry the sample
- Weigh the sample

Considering the cohesive properties of storm pollutants, drying the sample before sieving may enhance the sediment consolidation process through coagulation. This may induce some uncertainty concerning the measurement of particle size distribution. A preliminary comparative experiment was performed to evaluate the influence of the drying operation before sieving analysis. The results of the comparison showed that the drying operation before sieving enhances the size ofthe finer particles. We therefore eliminated this step to try to preserve the sediment in its original condition. Furthermore, in order to reproduce conditions similar to those in the detention basin, we used the stormwater collected from the Django Reinhardt detention basin filtrated with a 0.45 μm filter for the wet sieving analysis.

The present experiment used 0.08 mm, 0.2 mm, 0.5 mm, 1.0 mm, 2.0 mm and 5.0 mm sized sieves. These sieves are shown in Figure 3-14. The choice of sieve sizes was based on the

preliminary tests. It should be noted that the LPS analysis is quantified in volume fractions, while the sieving analysis is quantified in weight fractions. It is therefore difficult to combine the results obtained using these two different methods even with particle size.

Figure 3-14 Sieves with selected sizes of 0.08 mm, 0.2 mm, 0.5 mm, 1.0mm, 2.0 mm and 5.0 mm

b. Determining density

Particle density is one of the most important physical properties of sediment. Particle density was determined according to the French standard NF P 94-054, entitled "Determination of particle density- pycnometer method". The equipment used is shown in Figure 3-15.

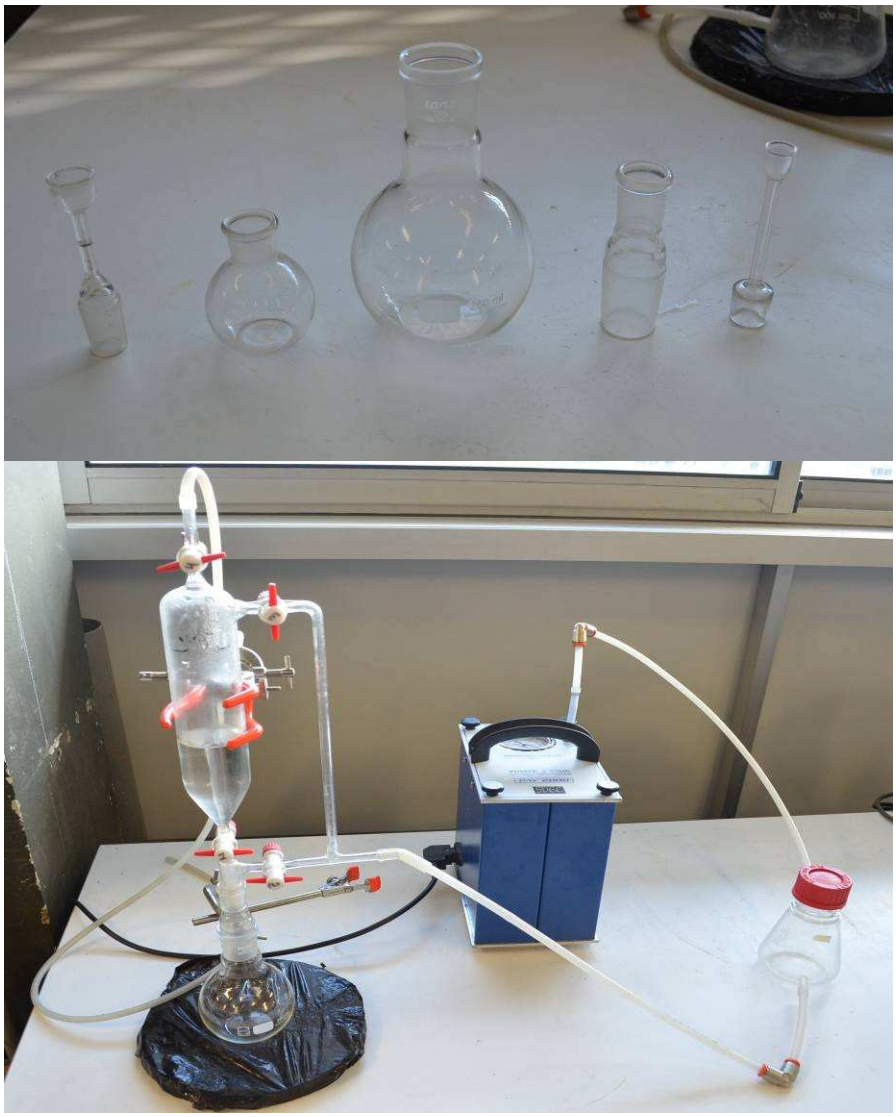

Figure 3-15 Pycnometer and accessories (experimental supports and a vacuum pump, etc.)

3.3.2.4 *In situ* Monitoring

In order to acquire reliable data on urban effluent during wet weather, stormwater quantity and quality are measured by monitoring stations. There are two monitoring stations located at the inlet and the outlet of the Django Reinhardt detention basin. The stormwater flow quantity was often determined by measuring velocity and water depth. With the sensors available in the station, the stormwater quality parameters measured are: turbidity, conductivity, temperature, PH (hydrogen ion concentration), UV-visible spectra. The specific equipment used to provide data for this thesis was as follows:

- Turbidity was measured by nephelometry using a 880 nm infrared sensor Endress + Hauser CUS-31 according to the NF EN 27027 standard. The sensors were installed in an experimental channel (length 2m, width 0.2m, invert and semicircular) inside the stations. Urban effluent is supplied by a peristaltic pump (flow rate of 1 L/s and suction velocity of 1 m/s) from the inlet or outlet pipe. The continuous turbidity

measurements are used to obtain TSS concentrations which are used to assess the RE of the basin.

- An ultrasound air sensor NIVUS Nivubar Plus II and a Doppler sensor NIVUS CMO / EM were installed in the inlet pipe (circular pipe with a diameter of 1.6 m) to measure the simultaneous water depth and flow velocity respectively, in order to estimate the inflow rate. Meanwhile, a Mace Flo-Pro ultrasound air sensor and Mace Flo-Pro Doppler sensor were also installed in the outlet pipe (circular pipe with a diameter of 0.6 m) to measure the simultaneous water depth and flow velocity respectively, in order to estimate the outflow rate.
- Two piezoresistive membrane sensors (NIVUS Nivubar Plus II) were installed at the bottom of basin to measure the water depth; the locations of two sensor were shown in Figure 3-4 labeled as h_1 and h_2.

All the sensors work with a time step of two minutes, and the measured data were saved in a S50 Sofrel data logger, except for the UV-visible spectra sensor data which were saved with a time step of two minutes on a dedicated PC.

In addition, a refrigerated automatic sampler (Sigma 900R) equipped with 24 1L bottles was installed in the stations to automatically collect effluent samples in the inlet and outlet pipe. These samples are used for analyses conducted at a later stage in the laboratory. The schematic configuration of sensors is shown in Figure 3-16.

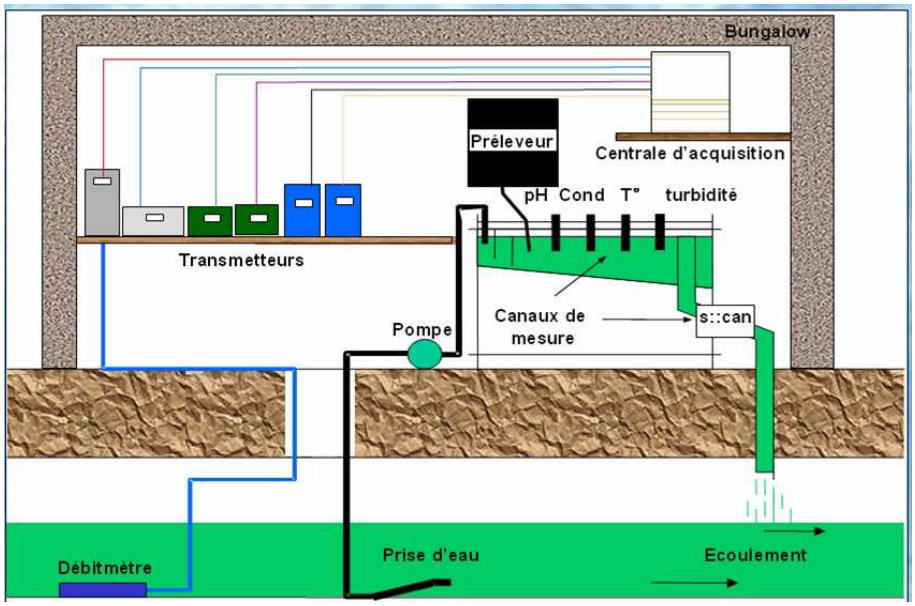

Figure 3-16 Diagram of the measurement stations located at the inlet and outlet of the Django Reinhardt detention basin in Chassieu (Mourad, 2000)

3.4 Numerical modelling strategy

3.4.1 Introduction

The objective of this section is to present in detail the mathematical model for single phase fluid flow / multiphase flow used in this thesis.

We choose the commercial CFD solver Anasys Fluent as the modelling tool for all the simulations. It is one of the most widely used commercial CFD solvers in industrial engineering and academic research. The RANS/URANS-based approaches integrated in Fluent CFD code have been widely tested for various hydraulic flow conditions in sewer systems (Stovin, 1996; Lipeme Kouyi, 2004; Lipeme Kouyi *et al.*, 2005; Lipeme Kouyi *et al.*, 2010, Bonakdari, 2006; Benett, 2012; etc). It provides a UDF (user defined function) interface, into which specific modules can be integrated to adapt to different requirements

3.4.2 Fluid flow modelling

3.4.2.1 Fluid flow

Fluids are substances whose molecular structure offers no resistance to external shear forces: even the smallest force causes *deformation* of a fluid particle (Ferziger and Peric, 2002). In most cases of interest, a fluid can be regarded as *continuum*, which can be treated as being differentiable from a mathematical point of view. Based on this hypothesis, the basic equations governing fluid flow, the Navier-Stokes equations, can be derived according to the basic conservation laws:

- Mass conservation
- Momentum conservation (Newton's second law of motion)
- Energy conservation (if required)

It is convenient to deal with the flow within a certain spatial region, so called the *control volume,* rather than in a parcel of matter which quickly passes through the region of interest. This method of analysis is called the *control volume approach*. Here we write the continuity equation (3.1) and momentum equation (3.2) directly in a partial differential form. More detailed derivations can be found in a number of standard texts on fluid mechanics (*e.g.* White, 1986; Versteeg and Malalasekera, 2007). Throughout this thesis, we shall adopt the Einstein convention that whenever the same index appears twice in any term, summation over the range of the range of that index is implied.

$$\frac{\partial \rho}{\partial t} + \frac{\partial (\rho u_i)}{\partial x_i} = 0, \tag{3.1}$$

$$\frac{\partial (\rho u_i)}{\partial t} + \frac{\partial (\rho u_j u_i)}{\partial x_j} = \frac{\partial \tau_{ij}}{\partial x_j} - \frac{\partial p}{\partial x_i} + F_i, \tag{3.2}$$

Where x_i (i=1, 2, 3) is the Cartesian coordinates and u_i is the Cartesian components of the velocity vector, ρ is the fluid density, p is the pressure, and F_i is the body force (*e.g.* gravity, Coriolis forces, centrifugal, etc). For Newton fluid, τ_{ij} is the viscous stress tensor. It can be described by equation (3.3). S_{ij} is the rate of strain (deformation) tensor, as written in equation (3.4).

$$\tau_{ij} = 2\mu S_{ij} - \frac{2}{3}\mu\delta_{ij}\frac{\partial u_l}{\partial x_l}, \tag{3.3}$$

$$S_{ij} = \frac{1}{2}\left(\frac{\partial u_i}{\partial x_j} + \frac{\partial u_j}{\partial x_i}\right), \tag{3.4}$$

Where δ_{ij} is Kronecker symbol (δ_{ij} =1 if i=j and δ_{ij} =0 otherwise), μ is the dynamic viscosity coefficient.

3.4.2.2 Turbulent flow

Most flow encountered in engineering practice is turbulent and therefore requires different treatment. The most accurate approach to turbulence simulation is to solve the Navier-Stokes equations without averaging or approximation other than numerical discretization where errors can be estimated and controlled (Ferziger and Peric, 2002). This approach is called *direct numerical simulation (DNS)*. DNS results provide very detailed information about the flow. However, it also requires high restrict grid resolution mainly depending on the Reynolds number (Tennekes and Lumley, 1976). The size of grid must be no larger than a viscously determined scale, called the Kolmogoroff scale. The DNS is limited by the processing speed and memory of the machine on which it is carried out. In engineering practice, an approach called *one –point* closure based on averaging the equations of motion over time and which leads to a set of partial differential equation called the *Reynolds-averaged-Navier-Stokes* equations (*RANS*) is widely used (Ferziger and Peric, 2002)., These equations do not form a closed set so this method requires the introduction of approximations which is called the *turbulence model*.

c. Reynolds-Averaged-Navier-Stokes equations

The RANS is based on the ideas proposed by Osborne Reynolds. In statistically steady flow, every variable can be written as the sum of a time-averaged value and a fluctuation around that value:

$$\phi(x_i,t) = \bar{\phi}(x_i) + \phi'(x_i), \tag{3.5}$$

where

$$\bar{\phi}(x_i) = \lim_{T\to\infty}\frac{1}{T}\int_0^T \phi(x_i,t)\mathrm{d}t, \tag{3.6}$$

Here t is the time and T is the averaging time interval. This interval must be large compared to the typical time scale of the fluctuations. If T is large enough, $\bar{\phi}$ does not depend on the time at which averaging is started.

For unsteady flow, this concept is described as equation (3.7).

$$\bar{\phi}(x_i) = \lim_{T \to N} \frac{1}{N} \sum_{n=1}^{N} \phi(x_i, t), \tag{3.7}$$

Where N is the number of members of the set, it must be large enough to eliminate the effect of the fluctuation. The concept is illustrated in Figure 3-17.

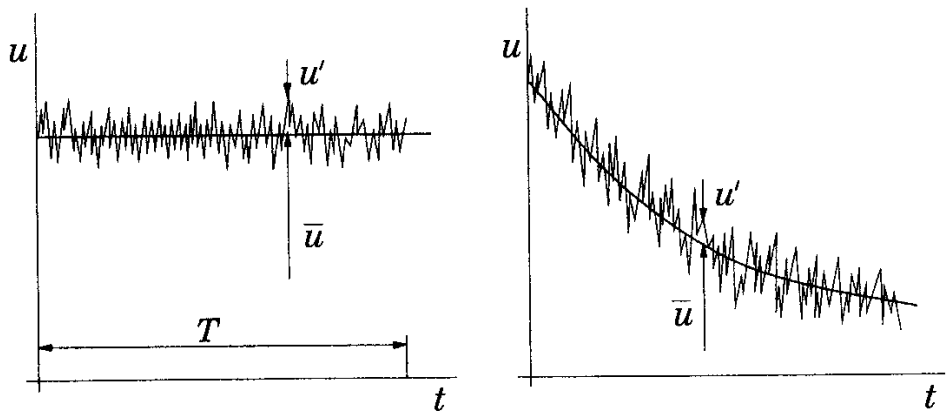

Figure 3-17 Time averaging for a statistically steady flow (left) and an unsteady flow (right) (Ferziger and Peric, 2002)

From equation (3.6), it follows that $\overline{\phi'} = 0$, thus averaging any linear term in the conversation equations simply gives the identical term for the averaged quantity.

$$\overline{u_i \phi} = \overline{\left(\overline{u_i} + u'\right)\left(\bar{\phi} + \phi'\right)} = \overline{u_i}\,\bar{\phi} + \overline{u_i' \phi'}, \tag{3.8}$$

Applying this rule to NS equations, for incompressible flow, the continuity and momentum equations so-called RANS can be written with tensor notation and Cartesian coordinates as:

$$\frac{\partial\left(\rho \overline{u_i}\right)}{\partial x_i} = 0, \tag{3.9}$$

$$\frac{\partial\left(\rho \overline{u_i}\right)}{\partial t} + \frac{\partial}{\partial x_j}\left(\rho \overline{u_j}\,\overline{u_i}\right) = \frac{\partial \bar{\tau}_{ij}}{\partial x_j} - \frac{\partial \bar{p}}{\partial x_i} + \frac{\partial}{\partial x_j}\left(-\rho \overline{u_j' u_i'}\right) + F_i, \tag{3.10}$$

Where the $\bar{\tau}_{ij}$ is the mean viscous tress tensor component:

$$\overline{\tau_{ij}} = \mu\left(\frac{\partial \overline{u_i}}{\partial x_j} + \frac{\partial \overline{u_j}}{\partial x_i}\right) - \frac{2}{3}\delta_{ij}\frac{\partial \overline{u_l}}{\partial x_l}, \tag{3.11}$$

The term contained in equation 3.10 as $-\rho \overline{u_j' u_i'}$, called the Reynolds stresses cannot be presented solely in terms of the mean quantities. The equation system is not closed because

the number of unknown variables is more than the number of independent equations. Closure requires the use of some approximations, which usually take the form of prescribing the Reynolds stress tensor and turbulent scalar fluxes in terms of the mean quantities. In engineering the approximations introduced are called turbulence model.

d. Turbulence models

Table 3-3 Turbulence models available in commercial CFD codes (Versteeg and Malalasakra, 2007)

Number of extra transport equation	name
Zero	Mixing length model
One	Spalart – Allmaras model
Two	k - ε model k – ω model Algebraic stress model
Seven	Reynolds stress model

Table 3-3 shows some of the turbulence models available in CFD codes. Here we describe briefly the *k-ε, k-ω,* Reynolds stress models, which are used in drainage structure modelling.

Standard *k-ε* model

It is based on an assumption that the effect of turbulence can be represented as increased viscosity. This leads to the eddy-viscosity model for Reynolds stress:

$$-\rho\overline{u_i'u_j'} = \mu_t\left(\frac{\partial\overline{u_i}}{\partial x_j}+\frac{\partial\overline{u_j}}{\partial x_i}\right)-\frac{2}{3}\rho\delta_{ij}k \tag{3.12}$$

Where μ_t is the eddy viscosity, k is the turbulent kinetic energy per unit mass:

$$k=\frac{1}{2}\overline{u_i'u_i'}=\frac{1}{2}\left(\overline{u_x'u_x'}+\overline{u_y'u_y'}+\overline{u_z'u_z'}\right) \tag{3.13}$$

In this simplest description, turbulence can be characterised by two parameters: its kinetic energy, k, and a length scale L. The dissipation rate of turbulence energy, ε, is also defined. The descriptions of k and ε are written as equations (3.13) and (3.14), more detailed information can be found in Wilcox (1993b).

$$\frac{\partial(\rho k)}{\partial t}+\frac{\partial\left(\rho\overline{u}_j k\right)}{\partial x_j}=\frac{\partial}{\partial x_j}\left[\left(\mu+\frac{\mu_t}{\delta_k}\right)\frac{\partial k}{\partial x_j}\right]+P_k-\rho\varepsilon, \tag{3.14}$$

$$\frac{\partial(\rho\varepsilon)}{\partial t}+\frac{\partial\left(\rho\overline{u}_j\varepsilon\right)}{\partial x_j}=\frac{\partial}{\partial x_j}\left(\mu+\frac{\mu_t}{\delta_\varepsilon}\frac{\partial\varepsilon}{\partial x_j}\right)+C_{\varepsilon 1}P_k\frac{\varepsilon}{k}-C_{\varepsilon 2}\rho\frac{\varepsilon^2}{k}, \tag{3.15}$$

Where

$$\mu_t=\rho C_\mu\sqrt{k}L=\rho C_\mu\frac{k^2}{\varepsilon}, \tag{3.16}$$

$$P_k = \mu_t \left(\frac{\partial \bar{u}_i}{\partial x_j} + \frac{\partial \bar{u}_j}{\partial x_i} \right) \frac{\partial \bar{u}_i}{\partial x_j}, \tag{3.17}$$

The model based on equations (3.13) and (3.14) is called the standard *k*- *ε* model and has been widely used. There are five parameters in the standard *k*- *ε,* the most commonly used values arrived at by comprehensive data fitting for a wide range of turbulent flow are (Launder and Spalding, 1972):

$$C_\mu = 0.09; \quad C_{\varepsilon 1} = 1.44; \quad C_{\varepsilon 2} = 19.2; \quad \delta_k = 1.0; \quad \delta_\varepsilon = 1.3; \tag{3.18}$$

Generally, the *k*- *ε* model is suitable for fully developed turbulent flow.

RNG *k*-*ε* model

The Renormalization Group (RNG) was devised by Yakhot and Orszag (1986) for hydrodynamic turbulence. They represented the effects of small-scale turbulence by means of a random forcing function in the Navier-Stokes equations (Versteeg and Malalasakra, 2007). Yakhot *et al.* (1992) expressed the RNG *k*- *ε* model as:

$$\frac{\partial(\rho k)}{\partial t} + \frac{\partial\left(\rho \bar{u}_j k\right)}{\partial x_j} = \frac{\partial}{\partial x_j}\left[\left(\alpha_k \mu_{eff}\right) \frac{\partial k}{\partial x_j} \right] + \bar{\tau}_{ij} \cdot \overline{S_{ij}} - \rho\varepsilon, \tag{3.19}$$

$$\frac{\partial(\rho\varepsilon)}{\partial t} + \frac{\partial\left(\rho \bar{u}_j \varepsilon\right)}{\partial x_j} = \frac{\partial}{\partial x_j}\left(\alpha_\varepsilon \mu_{eff} \frac{\partial \varepsilon}{\partial x_j} \right) + C_{\varepsilon 1} \frac{\varepsilon}{k} \bar{\tau}_{ij} \cdot \bar{S}_{ij} - C_{\varepsilon 2}^* \rho \frac{\varepsilon^2}{k}, \tag{3.20}$$

Where

$$\bar{\tau}_{ij} = 2\mu_t \bar{S}_{ij}, \tag{3.21}$$

$$\bar{S}_{ij} = \frac{1}{2}\left(\frac{\partial \bar{u}_i}{\partial x_j} + \frac{\partial \bar{u}_j}{\partial x_i} \right), \tag{3.22}$$

$$C_{\varepsilon 2}^* = C_{\varepsilon 2} + \frac{C_\mu \eta^3 \left(1 - \eta / \eta_0\right)}{1 + \beta \eta^3} \tag{3.23}$$

$$\eta = \frac{k}{\varepsilon} \sqrt{2 \bar{S}_{ij} \cdot \bar{S}_{ij}} \tag{3.24}$$

$$\mu_{eff} = \mu + \mu_t \tag{3.25}$$

The constants in the RNG *k*-*ε* model are:

α_k	α_ε	$C_{\varepsilon 1}$	$C_{\varepsilon 2}$	η_0	β	C_μ
1.39	1.39	1.42	1.68	4.38	0.012	0.085

Wilcox *k-ω* model

The second most commonly used model is the *k-ω* model, originally introduced by Saffmen but popularised by Wilcox (Ferziger and Peric, 2002). The *k-ω* model uses turbulence frequency $\omega=\varepsilon/k$ as the second variable. Then the eddy viscosity is given by:

$$\mu_t = \rho\frac{k}{\omega} \tag{3.26}$$

The transport equations for k and ω for turbulent flow are as follows (Wilcox, 1988, 1993a, b, 1994):

$$\frac{\partial(\rho k)}{\partial t}+\frac{\partial\left(\rho\bar{u}_j k\right)}{\partial x_j}=\frac{\partial}{\partial x_j}\left[\left(\mu+\frac{\mu_t}{\sigma_k}\right)\frac{\partial k}{\partial x_j}\right]+P_k-\beta^*\rho k\omega, \tag{3.27}$$

$$\frac{\partial(\rho\omega)}{\partial t}+\frac{\partial\left(\rho\bar{u}_j\omega\right)}{\partial x_j}=\frac{\partial}{\partial x_j}\left[\left(\mu+\frac{\mu_t}{\sigma_\varpi}\right)\frac{\partial\omega}{\partial x_j}\right]+\alpha P_k\frac{\omega}{k}-\beta\rho\omega^2, \tag{3.28}$$

The constants in the k- ω model are:

α	β	β^*	σ_k	σ_ϖ	ε
5/9	0.075	0.09	2.0	2.0	$\beta^*\omega k$

Reynolds Stress Model

The most complex classic turbulence model is the *Reynolds stress model (RSM)*, also called the second-order or second-moment closure model. Several major drawbacks of the *k*–ε model emerge when it is used in attempts to predict flow with complex strain fields or significant body forces. Under such conditions the individual Reynolds stresses are poorly represented by eddy-viscosity assumption, equation (3.11), even if the turbulent kinetic energy is computed with reasonable accuracy (Ferziger and Peric, 2002). The exact Reynolds stress transport equation on the other hand can account for the directional effects of the Reynolds stress field. The most complex model commonly used today is the *RSM* which is based on dynamic equations for the Reynolds stress tensor - $\rho\overline{u_i'u_j'}$ itself. These equations can be derived from the Navier-Stokes equations. The Reynolds stress transport equation is as follows:

$$\frac{\partial\left(\rho\overline{u_i'u_j'}\right)}{\partial t}+\frac{\partial\left(\rho\overline{u_i'u_j'}\bar{u}_j\right)}{\partial x_j}=\underbrace{-\left(\rho\overline{u_i'u_k'}\frac{\partial\bar{u}_j}{\partial x_k}+\rho\overline{u_j'u_k'}\frac{\partial\bar{u}_i}{\partial x_k}\right)}+\rho\varepsilon_{ij}-\prod_{ij}+$$

$$\frac{\partial}{\partial x_k}\left(\nu\frac{\partial\rho\overline{u_i'u_j'}}{\partial x_k}+C_{ijk}\right) \tag{3.29}$$

Where

$$\prod_{ij} = \overline{p'\left(\frac{\partial u_i'}{\partial x_j} + \frac{\partial u_j'}{\partial x_i}\right)} \tag{3.30}$$

$$\rho\varepsilon_{ij} = 2\mu\overline{\frac{\partial u_i'}{\partial x_k}\frac{\partial u_j'}{\partial x_k}} \tag{3.31}$$

$$C_{ijk} = \rho\overline{u_i'u_j'u_k'} + \overline{p'u_i'}\delta_{jk} + \overline{p'u_j'}\delta_{ik} \tag{3.32}$$

In equation (3.29), the first two terms of the right-hand side are the production terms and require no approximation. The term $\prod_{ij}$ is often called the pressure-strain term, which redistributes turbulent kinetic energy amongst the components of the Reynolds stress tensor but does not change the total kinetic energy. The next term $\rho\varepsilon_{ij}$ is the dissipation tensor. The last one C_{ijk} is often called turbulent diffusion. The dissipation, pressure–strain, and turbulent diffusion terms cannot be computed exactly in terms of the other terms in the equations and therefore must be modelled. The simplest and most common model for the dissipation term treats it as isotropic:

$$\varepsilon_{ij} = \frac{2}{3}\varepsilon\delta_{ij} \tag{3.33}$$

This means that a dissipation equation is needed in the RSM model. The pressure-strain term and turbulent diffusion term also need to be modelled. The simplest model for pressure-strain term is that one assumes that the function of this term is to make the turbulence more isotropic. However, it has met with great success and a number of suggestions for improvement have been made. More details can be found in the literature (Launder, 1990, Hanjalić, 1994, Versteeg and Malalasekera, 2007). The turbulent diffusion terms are usually modelled using the gradient diffusion type of approximation. Isotropic, anisotropic and nonlinear models have also been suggested (Ferizger, 2002).

Generally, the RSM model has the potential to more accurately represent the characteristics of turbulence flow compared to the one-equation and two-equation models. However, in some flows, there is very little difference in terms of performance. Indeed, none of the models can be expected to produce robust results for all flows. Furthermore, it is not yet clear which model is best for which kind of flow, perhaps due to numerical errors in modelling?

For three dimensions model, the *RSM* needs to solve seven partial differential equations excluding mean flow. More scalar equations may also need to be solved if required. Thus compared to two-equation model such as *k-ε*, model, the *RSM* requires far more computation time and memory, and the calculations usually converge more slowly.

e. Free surface modelling

The free surface (i.e. the interface between the water and air) is a key parameter when modelling hydrodynamics in stormwater detention basins. In general, researchers often use a VOF model to track the free surface, which will be a result of the simulation. Also, in some specific cases or conditions (such as when the level of flow is flat and horizontal) the free surface can be represented as symmetric surface or slip wall with zero shear stress. Both the VOF model and symmetric boundary condition are used in our work as briefly presented below..

Volume of fluid (VOF)

The VOF model can model two or more immiscible fluids by solving a single set of momentum equations and tracking the volume fraction of each of the fluids throughout the domain. Typical applications include the prediction of jet breakup, the motion of large bubbles in a liquid, and the motion of liquid after a dam break, and the steady or unsteady tracking of any liquid-gas interface. In our work, we tried to use the VOF model to track the free surface in the detention basin. Early in 1975, Nichols and Hirt proposed the VOF method and presented it as beingflexible and efficient for treating complicated free boundaries. To illustrate the method, a description of an incompressible hydrodynamics code SOLA-VOF, which uses the VOF technique to track the free fluid surface (Hirt and Nichols, 1981) is provided. In the VOF method, a variable, volume fraction of each phase, α_q is introduced into the computational cell.

In a cell the following three conditions are possible:

- $\alpha_q = 0$: the cell is empty(of the qth fluid)
- $\alpha_q = 1$: the cell is full (of the qth fluid)
- $0 < \alpha_q < 1$: The cell contains the interface between the qth fluid and one or more other fluid.

Based on the local value of α_q, the appropriate properties and variables will be assigned to each control volume within the domain. The tracking interface(s) between the phases is accomplished by the solution of a continuity equation for the volume fraction of one or more of the phases. For the qth phase, the volume fraction equation for each phase is written as equation (3.35) (Ansys, 2011). In each control volume, the volume fractions of all phases sum to unity, as written in equation (3.36).

$$\frac{1}{\rho_p}\left[\frac{\partial}{\partial t}\left(\alpha_q \rho_q\right) + \nabla \cdot \left(\alpha_q \rho_q \vec{v}_q\right) = \sum_{p=1}^{n}\left(m_{pq} - m_{qp}\right)\right] \tag{3.34}$$

$$\sum_{q=1}^{n} \alpha_q = 1 \tag{3.35}$$

Where m_{qp} is the mass transfer from phase q to phase p and m_{pq} is the mass transfer from p phase to phase q.

The properties featured in the transport equations are determined by the presence of the component phases in each control volume. In general, for an *n-phase* system, the volume-fraction-averaged density takes on the following form:

$$\rho = \sum \alpha_q \rho_q \tag{3.36}$$

All other properties (*e.g.*, viscosity) are computed in this manner. For example, in a two phase air and water system, the averaged dynamic viscosity, μ is calculated by the water fraction α_w and water dynamic viscosity μ_w and air viscosity μ_a:

$$\mu = \alpha_w \mu_w + (1 - \alpha_w)\mu_a \tag{3.37}$$

3.4.2.3 Initial condition and boundary condition

All CFD problems are defined in terms of initial and boundary conditions. It is important that the user specifies these correctly and understands their role in the numerical algorithm. In unsteady problems the initial values of all the flow variables need to be specified at all solution points in the flow domain (Versteeg and Malalasekera, 2007). Here we will briefly introduce some of the boundary conditions used in this investigation:

- Inlet
- Outlet
- Wall
- Symmetry

Inlet boundary condition

In hydraulics modelling, the *velocity inlet* or inflow rate is often used as the boundary condition at the inlets (Dufresne, 2008; Vosswinkel *et al.* 2012; Adamsson and Stovin, 2003). The *pressure inlet* boundary condition is recommended for channel simulation with free surface if VOF is involved. When using the *velocity inlet* as the inlet boundary condition, generally, a homogeneous velocity profile is often set due to the lack of a velocity profile. However, usually the homogeneous velocity profile for a cross section does not reflect reality thus an extended inlet (such as a pipe inlet) often is required to ensure a developed velocity profile in the domain of interest (Dufresne, 2008). For the reference pressure, it is common practice to fix the absolute pressure at one inlet node and set the pressure correction to zero at that node by specifying a reference pressure value (Versteeg and Malalasekera, 2007).

An estimation of turbulent kinetic energy k and dissipation rate ε at the inlet boundary is often required if a turbulent model is used. The most accurate simulations can only be achieved by supplying measured inlet values for turbulent kinetic energy k and dissipation rate ε. However, such data are often not available and in practicek and ε are often estimated using the approximate formula. It is possible to obtain k and ε from the turbulence intensity I

(typically turbulence intensity of between 1% and 6% is used) and the characteristic length L of the equipment (equivalent pipe diameter) using the following simple assumed forms:

$$k = \frac{2}{3}\left(U_{ref} I\right)^2 \tag{3.38}$$

$$\varepsilon = C_\mu^{3/4} \frac{k^{3/2}}{l_{ref}} \tag{3.39}$$

$$l_{ref} = 0.07L \tag{3.40}$$

$$I = 0.16\,\mathrm{Re}^{-1/8} \tag{3.41}$$

Where U_{ref} is the velocity in the inlet face, Re is the Reynolds number.

In some specific cases, the UDF is also used to specify the velocity distribution as needed, such as the velocity profile if available or inlet velocity changes with time in unsteady condition.

Outlet boundary condition

The outlet boundary condition may be used in conjunction with the inlet boundary condition. Two kinds of outlet boundary conditions are often used in hydraulic modelling: pressure-outlet and outflow. Pressure outlet boundary conditions require static (gauge) pressure at the outlet boundary to be specified. With the pressure outlet boundary condition, all other flow quantities are extrapolated from the interior domain.

Outflow boundary conditions in Ansys Fluent are used to model flow at certain points where details of the flow velocity and pressure are not known prior to solving the flow problem. No conditions are defined at the outflow boundaries (unless you are modelling radiative heat transfer, a discrete phase of particles, or split mass flow): Ansys Fluent extrapolates the required information from the interior. Note that outflow boundaries cannot be used in the following cases (Ansys, 2011b):

- When a problem includes pressure inlet boundaries; use pressure outlet boundary conditions instead
- When modelling compressible flow
- When modelling unsteady flow with varying density, even if the flow is incompressible
- With the multiphase models (Eulerian, mixture, and VOF).

Wall boundary conditions

The wall is the most common boundary encountered in confined fluid flow problems. With a solid wall parallel to the x–direction, the no-slip condition (tangential velocity component equals to zero, $u=v=0$) is usually the appropriate condition for the velocity components at solid walls. The normal velocity component can simply be set to zero at the boundary. For all other variables, specific source terms are constructed, according to the type of flow (laminar or turbulent flow). Obviously, the mean velocity field is affected through the no-slip condition that has to be satisfied at the wall. Due to the presence of the solid boundary, the flow behaviour and turbulence structure are considerably different from free turbulent flow. The turbulent models such as k-ε are valid only at the fully developed domain. So the near wall region needs to be treated using additional complementary models.

Very close to the wall the flow is influenced by viscous effects and does not depend on free stream parameters. The mean flow velocity only depends on the distance y from the wall, fluid density ρ and viscosity μ and the wall shear stress τ_w, dimensional analysis shows that

$$u^+ = \frac{U}{u_*} = f\left(\frac{\rho u_* Y}{\mu}\right) = f\left(y^+\right) \tag{3.42}$$

Formula (3.42) is the so called law of the wall and contains the definitions of two important dimensionless groups, u^+ and y^+, $u_*= (\tau_w/\rho)^{0.5}$ is friction velocity.

The turbulent boundary layer adjacent to a solid surface is composed of two regions: the inner region and the outer region. The outer region is free from direct viscous effects (Versteeg and Malalasekera, 2007). Within the inner region there are three zones:

- The viscous sublayer: viscous stresses dominate the flow adjacent to surface
- The buffer layer : viscous and turbulent stresses are of similar magnitude
- The log-law layer: turbulent stresses dominate

In the viscous sublayer, the shear stress is approximately constant and equal to the wall shear stress τ_w,

$$\tau(y) = \mu \frac{\partial U}{\partial y} \cong \tau_w \tag{3.43}$$

After integration with respect to y and application of boundary condition $U=0$ if y=0, we obtain:

$$U = \frac{\tau_w Y}{\mu} \tag{3.44}$$

Using the definition of u^+ and y^+, we get:

$$u^+ = y^+ \tag{3.45}$$

In the log law layer, the shear stress varies slowly with the distance from the wall. Schilichting (1979) derived a functional relationship between u^+ and y^+ for this layer.

$$u^+ = \frac{1}{\kappa}\ln\left(y^+\right) + B = \frac{1}{\kappa}\ln\left(Ey^+\right) \tag{3.46}$$

Where κ is the von Karman's constant $\kappa \approx 0.4$ and B is the additive constant $B \approx 5.5$ (or $E \approx 9.8$). This relationship is valid for u^+ between 30 and 500. Figure 3-18 shows the close agreement between theoretical equations (3.45) and (3.46) in their respective area of validity and experimental data.

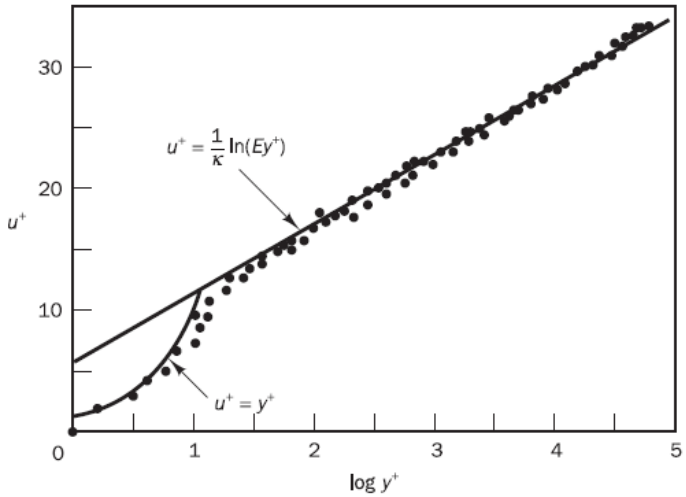

Figure 3-18 Velocity distribution near a solid wall (Versteeg and Malalasekera, 2007 adapted from Schilichting, 1979)

Traditionally, there are two approaches to modelling the near-wall region: the near-wall model approach and the wall function approach. For the near-wall model, the turbulence models are modified to enable the viscosity-affected region to be resolved with a mesh all the way to the wall, including the viscous sublayer. For the purposes of discussion, this will be termed the "near-wall modelling" approach. As shown in Figure 3-19 (left side), this approach requires refined meshes near the wall region to ensure the first mesh node is in the viscous sublayer (Salim and cheah, 2009), which are generally difficult to achieve.

For the wall function approach, the viscosity affected inner region (viscous sub layer and buffer layer) is not resolved. Instead, semi-empirical formulas called 'wall functions' are used to bridge the viscosity-affected region between the wall and the fully turbulent region (shown schematically in Figure 3-19 (right side)).

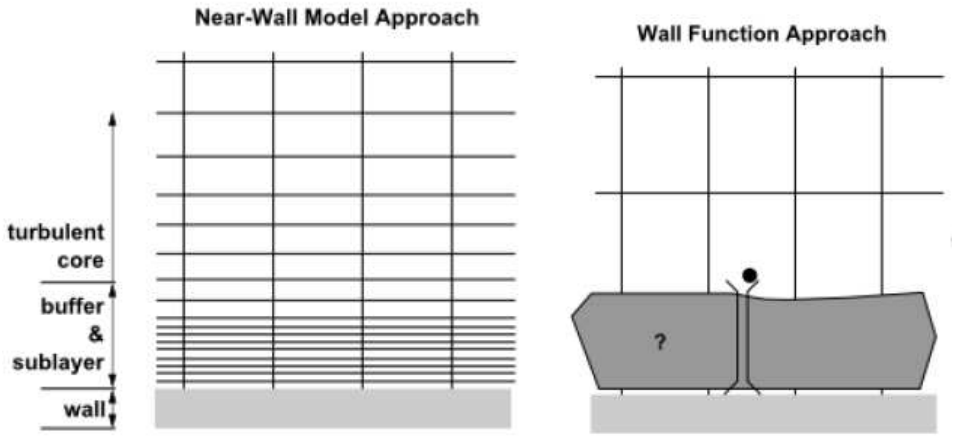

Figure 3-19 Scheme of near wall region treatment (Ansys, 2011b)

The use of wall functions obviates the need to modify the turbulence models to account for the presence of the wall. In Ansys Fluent, the wall function approach is employed by adapting equations (3.45) and (3.46). The near wall flow dimensionless velocity is defined as:

$$U^* = \frac{U_p C_\mu^{1/4} k_p^{1/2}}{\tau_w / \rho} \tag{3.47}$$

$$y^* = \frac{\rho C_\mu^{1/4} k_p^{1/2} y_p}{\mu} \tag{3.48}$$

And calculated by:

$$U^* = \begin{cases} y^* & (if\ y^* < 11.225) \\ \frac{1}{\kappa}\ln(Ey^*) & (if\ y^* > 11.225) \end{cases} \tag{3.49}$$

$$y^* = \frac{\rho C_\mu^{1/4} k_p^{1/2} y_p}{\mu} \tag{3.50}$$

Roughness effects

The surface roughness effects on turbulence quantities and bed shear stress are considered through the modified law-of-the-wall for roughness. The standard wall functions in Ansys Fluent are based on the work by Launder and Spalding (1974) and have been most widely used for industrial flow (Ansys, 2011a; Souders and Hirt, 2002). Experiments in rough pipes and channels indicate that the mean velocity distribution is influenced by the near rough walls and in the usual semi-logarithmic scale, has the same slope ($1/\kappa$) but a different intercept

(Tachie *et al.*, 2004; Akinlade *et al.*, 2004). Thus, the law-of-the-wall for mean velocity impacted by rough wall has the form (Ansys, 2011b):

$$\frac{U_p u_*}{\tau_w/\rho} = \frac{1}{\kappa}\ln(E\frac{\rho u_* y_p}{\mu}) - \Delta B \tag{3.51}$$

where

$u_* = C_\mu^{1/4} k_p^{1/2}$

κ= Von Kármán constant (= 0.4187)

E= empirical constant (= 9.793)

U_p= mean velocity of the fluid at the near-wall node P

k_p= turbulent kinetic energy at the near-wall node P

y_p= distance from point to the wall

μ= dynamic viscosity of the fluid

ΔB is a roughness function that quantifies the shift of the intercept due to roughness effects. ΔB depends on the type (uniform sand, rivets, threads, ribs, mesh-wire, etc.) and size of the roughness. There is no universal roughness function valid for all types of roughness. However, for sand-grain roughness and similar types of uniform roughness elements ΔB has been found to be well-correlated with the non-dimensional roughness height, $K_s^+ = \rho K_s u_* / \mu$, where K_s is the physical roughness height.

The turbulent flow regime is subdivided into three regimes, and the formulas proposed by Cebeci and Bradshaw (1977) based on Nikuradse's data were adopted to compute the roughness function, ΔB, for each regime (Ansys, 2011b).

For the smooth regime ($K_s^+ < 2.25$):

$$\Delta B = 0 \tag{3.52}$$

For the transitional regime ($2.25 < K_s^+ < 90$):

$$\Delta B = \frac{1}{\kappa}\ln\left[\frac{K_s^+ - 2.25}{87.75} + C_s K_s^+\right] \times \sin\left\{0.4258\left(\ln K_s^+ - 0.811\right)\right\} \tag{3.53}$$

where C_s is a roughness constant, and depends on the type of the roughness.

In the fully rough regime ($K_s^+ > 90$):

$$\Delta B = \frac{1}{\kappa}\ln\left(1 + C_s K_s^+\right) \tag{3.54}$$

In the present investigation of the Django Reinhardt detention basin, the bottom was considered to be covered in concrete and the equivalent sand grain roughness height was estimated using the following formula proposed by Hager (2010):

$$K \times k_s^{\frac{1}{6}} = 6.5 \times \sqrt{g} \tag{3.55}$$

Where K is Strickler coefficient and k_s is equivalent grain roughness heights, g is the gravity acceleration.

Symmetric boundary condition

The symmetry boundary condition means that there is no flow through the interface. The variables of the outside domain (virtual variables) are equal to the variables (actual variables) of the inside domain. In mathematical terms, this second condition results in gradients normal to the plane of symmetry of zero for all variables (Dufresne, 2008). The symmetry boundary condition is often used for free surface for some specific horizontal flat surface cases (Dufresne, 2008; Dufresne *et al.*, 2009; Stovin and Saul, 1994, 1996; Adamsson *et al.*, 2003; Vosswinkel *et al.*, 2012).

Initial conditions

The initial conditions play a very important role in CFD simulations, not only in terms of computational time, but also the convergence to the physical solution and accuracy. Providing an initial data field that is close to the final solution for steady–state cases means the solver has to do less work to reach the converged result. This therefore reduces simulation time. On the contrary, poor initial conditions mean more computational time is required. Typically, many users employ standard initialisation in Ansys Fluent; some use patching for localised control, especially for moving domains or multiphase analyses (Keating, 2011).

Within Ansys Fluent, thealternative full multigrid initialization (FMG) method or the Hybrid solution initialization method can be used to obtain better initial conditions (Keating, 2011). FMG can provide the initial and approximate solution at a minimum cost to the overall computational expense. Although the overall initialization time is longer than that using standard initialization by zone, it allows a much quicker solve. FMG solves Euler equations and provides the best guess initial solution. FMG is currently available for single phase.

Hybrid solution initialization uses a collection of recipes and boundary interpolation methods to efficiently initialize the solution based purely on simulation setup. This means the user does not need to provide any additional input for initialization. This method may improve convergence robustness many cases. Unlike FMG, this initialization method can be used for multiphase flow.

3.4.2.4 Numerical procedure

The NS or RANS equations are a group of partial differential equations for flow. Ansys Fluent uses the Finite Volume Method (FVM (Ansys, 2011b)) to convert the differential conservation equations into algebraic equations that can be solved numerically. We used the

pressure-based solver. The pressure-based solver makes it possible to solve flow problems in either a segregated or coupled manner. With the segregated algorithm, each iteration consists of the steps illustrated in Figure 3-20 and outlined below:

1. Update fluid properties (*e.g.*, density, viscosity, specific heat) including turbulent viscosity (diffusivity) based on the current solution.
2. Solve the momentum equations, one after another, using the recently updated values for pressure and face mass fluxes.
3. Solve the pressure correction equation using the recently obtained velocity field and the mass-flux.
4. Correct face mass fluxes, pressure, and the velocity field using the pressure correction obtained from step 3.
5. Solve the equations for additional scalars, if any, such as turbulent quantities, energy, species, and radiation intensity using the current values of the solution variables.
6. Update the source terms arising from the interactions among different phases (*e.g.*, source term for the carrier phase due to discrete particles).
7. Check for the convergence of the equations.

These steps are to be repeated until the convergence criteria are met.

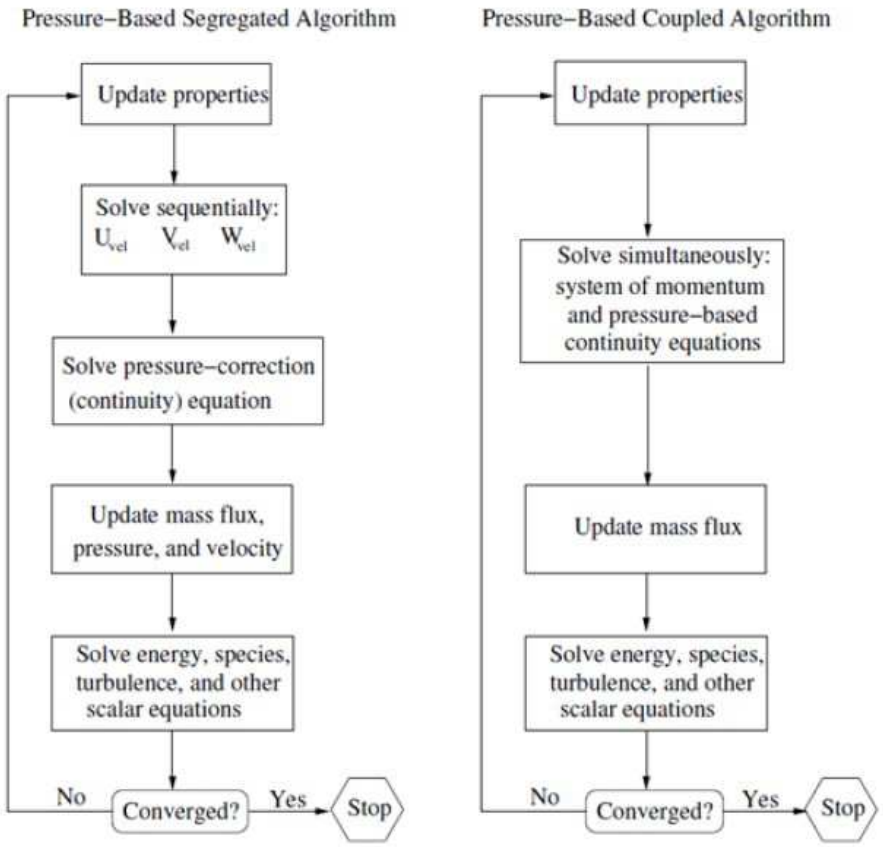

Figure 3-20 Overview of pressure-based solution method (Ansys, 2011b)

Fluent provides three methods for pressure-velocity coupling in the segregated solver: SIMPLE, SIMPLEC, and PISO. The SIMPLE (Semi-Implicit Method for Pressure Linked Equations) algorithm was proposed by Patankar and Spalding (1972, cited in Versteeg and Malalasekera, 2007) to ensure the correct linkage between pressure and velocity using staggered grid arrangement. Van Doormal and Rithby (1984) proposed the SIMPLEC (SIMPLE-consistent) algorithm, which omits terms in the velocity correction equations that are less significant than those in SIMPLE, in order to both simplify implementation and reduce solution costs. The PISO (Pressure Implicit with Splitting of Operators) algorithm proposed by Issa (1986, cited in Versteeg and Malalasekera, 2007) is a pressure–velocity calculation procedure originally developed for the non-iterative computation of unsteady compressible flow. It has been successfully adapted for the iterative solution of steady state problems (Versteeg and Malalasekera, 2007). Steady-state calculations will generally use SIMPLE or SIMPLEC, while PISO is recommended for unsteady calculations. PISO is recommended for unsteady calculations on highly skewed meshes (Ansys, 2011a).

Both the standard SIMPLE algorithm and the SIMPLEC (SIMPLE-Consistent) algorithm can be used in Fluent. SIMPLE is the default, but many problems will benefit from the use of SIMPLEC, particularly because of the increased under-relaxation that can be applied, which would make the calculation converge faster.

Convergence control

All the simulated cases in the present work are based on the second upwind discretization scheme for flow and turbulent variables. The convergence criterion within each time step will strongly affect solution costs, as a low criterion will result in an increased number of iterations. It is not possible to make general recommendations, as the required residual depends on the application. Furthermore, monitoring the residual is not the only way ofto adjusting the convergence. Flux conservation also needs to be checked. Generally speaking, the simulation is considered to be converged if the residuals reach the specified threshold (criteria). In some cases, the simulation cases are judged to be converged if the iterative variables are stable for steady state simulation. For unsteady simulations, the residual should be converged by approximately four orders of magnitude per time step.

3.4.3 Sediment transport modelling

3.4.3.1 Introduction

Obviously, sediment transport involves two phases: the liquid phase and the solid phase. Based on the two-phase concept, there are two different modelling approaches to simulate the sediment transport phenomenon: Euler-Euler and Euler-Lagrange (Van Wachem and Almstedt, 2003).

In the Euler-Euler approach, different phases (fluid and sediment) are modelled as a continuum using Navier-Stokes equations. In the past, the most common procedure for modelling sedimentation involved splitting the problem into a flow model and into a sediment transport model (Olsen 1999; Wu *et al.* 2000), namely the modelling the fluid phase and the solid phase in an uncoupled way. The flow model provides the hydrodynamics (local velocities) for sediment simulation. The sediment model only affects flow in terms of the changes in bed topography and in local bed friction (Zeng, 2006). The suspended load model and bed load models are coupled using more or less empirical formulas describing the mass exchange between suspended load, bed load and the deposited sediment itself (Zhang, 2009).

Up till the early 1980s, most computational models for multiphase flow at application level describe both the continuous phase and the dispersed phase as a continuum in coupled way, the so-called Eulerian model. Owing to the continuum description of the dispersed phase, Eulerian models require additional closure laws to describe particle-particle interactions. Most recent continuum models incorporate constitutive relations according to the kinetic theory of granular flow. This theory basically extends the classical kinetic theory of gases to dense particulate flow, which considers non-ideal particle-particle collisions and particle-particle drag. In these models the dispersed phase is described as a continuous phase fluid with appropriate closures. Therefore, only the average local volume fraction (mostly concentration), velocity, etc. are calculated and it cannot represent the properties of each individual dispersed particle. For example, the solid particle size is generally defined as a unique value for the whole domain (Cao *et al.*, 1995).

With the increases in the computational power available, the Lagrangian approach has

become a very useful and versatile tool for studying the particulate flow. In these models, the Newtonian equations of motion are solved for each individual particle, and a collision model is applied to handle particle encounters. Recently, such particle models have been combined with an Eulerian model for the continuous phase simulation, the so-called Euler-Lagrange approach. In the Euler-Lagrange approach, the solid phase is represented by tracking discrete particles, taking into account momentum, heat and mass transfer between the two phases. The Lagrange approach does not require additional closure equations for the particulate phase since it tracks the motion of each individual particle, taking into consideration collisions and external forces acting on the particles. This makes it a very convenient way of taking into account individual properties such as particle size distribution, density, settling velocity, etc. However, the amount of dispersed particles that can be tracked is, even today limited (Van Wachem and Almstedt, 2003) and is likely to remain so in the near future.

Multiphase flows are modelled using an Eulerian-Eulerian approach or a Eulerian-Lagrangian approach (van Wachem and Almstedt, 2003) depending on the extent of coupling between phases, with the delimiter that an Eulerian-Eulerian approach is used for flow with particulate volume fractions (PVF) greater than 10%. Elghobashi (1991) proposed a regime map for appropriating the degree of interphase coupling, by analysing length and time scales.

Preliminary studies focusing on the comparison between multiphase models integrated in Ansys Fluent package were carried out in order to identify the best approach. Eulerian-Granular, Mixture and uncoupled DPM models were tested for dissolved tracer transport in a rectangular channel (Laïly, 2012). Compared to the experimental observation derived from a review of the literature, the results showed that the uncoupled DPM model is better atrepresenting dispersion and mixing processes in rectangular channels. Moreover, Chocat *et al.* (2007) pointed out that fluid flow and solid transport in sewer systems can be modelled in an uncoupled way due to the low pollutant concentration. Subsequently, it was determined that a Lagrangian approach to tracking the solid phase is appropriate for flow with low PVF influent in stormwater detention basins.

3.4.3.2 DPM approach

The Lagrangian DPM is derived from force balances based on Newton's law describing particle trajectory. The force balance in the x-direction (in Cartesian coordinates) can be written as (Ansys, 2011b):

$$\frac{du_p}{dt} = F_D\left(u - u_p\right) + \frac{g_x\left(\rho_p - \rho\right)}{\rho_p} + F_x \tag{3.56}$$

Where u_p is the velocity of the particle, u is the instantaneous velocity of the fluid, g_x is the acceleration of gravity along the x axis, ρ_p is the density of the particle, ρ is the fluid density, and F_x is the additional forces. The left term in equation (3.56) corresponds to the x direction acceleration of the particle per unit particle mass. The first term on the right-hand side corresponds to the mass force of drag per unit particle mass. The coefficient F_D is expressed by equation (3.57).

$$F_D = \frac{18\mu}{\rho_p d^2}\frac{C_D \,\mathrm{Re}_p}{24} \tag{3.57}$$

Where μ is the dynamic viscosity of the fluid, d is the diameter of the particle; C_D is drag coefficient, and $\mathrm{Re_p}$ is the Reynolds number of the particle. The second term comprises of forces due to gravity per unit particle mass (competition between weight and buoyancy of the particle). The third term corresponds to additional forces per unit particle mass, including the added mass force and the force due to pressure gradient. It is a dimensionless number characterising the relative velocity between fluid and particle, defined in equation (3.58):

$$\mathrm{Re}_p \equiv \frac{\rho d\,\left|u - u_p\right|}{\mu} \tag{3.58}$$

The drag coefficient C_D depends on the flow regime. For the Reynolds number of small particles ($\mathrm{Re_p}$<0.1), the total drag coefficient is expressed by Stokes' law, as expressed in equation (3.59). With an increasing particle Reynolds number, Stokes' law underestimates the drag force. Schiller and Nauman proposed an expression for the drag coefficient (Clift *et al.* 1978) as written in equation (3.60).

Within Fluent, one can chose the drag coefficient expression proposed by Morsi and Alexander (1972) for spherical particles, which provides the most complete range of $\mathrm{Re_p}$, as written in equation (3.61).

$$C_D = \frac{24}{\mathrm{Re}_p} \tag{3.59}$$

$$C_D = \begin{cases} \dfrac{24}{\mathrm{Re}_p}\left(1 + 0.15\,\mathrm{Re}_p^{0.687}\right), \left(\mathrm{Re}_p < 1000\right) \\ 0.44 \qquad\qquad\qquad \left(\mathrm{Re}_p \geq 1000\right) \end{cases} \tag{3.60}$$

$$C_D = \alpha_1 + \frac{\alpha_2}{\mathrm{Re}_p} + \frac{\alpha_3}{\mathrm{Re}_p^2} \tag{3.61}$$

The empirical constants α_1, α_2 and α_3 depend on the particle's Reynolds number (Morsi and Alexander, 1972) and are shown in Table 3-4.

Table 3-4 Empirical constants α_1, α_2 and α_3 for different ranges of $\mathrm{Re_p}$ (Morsi and Alexander, 1972)

$\mathrm{Re_p}$	α_1	α_2	α_3
$\mathrm{Re_p}$<0.1	0	24.0	0
0.1<$\mathrm{Re_p}$<1	3.69	22.73	0.0903
1<$\mathrm{Re_p}$<10	1.222	29.1667	-3.8889
10<$\mathrm{Re_p}$<100	0.6167	46.5	-116.67
100<$\mathrm{Re_p}$<1000	0.3644	98.33	-2778
1000<$\mathrm{Re_p}$<5000	0.357	148.62	-4.75e+4
5000<$\mathrm{Re_p}$<10000	0.46	-490.546	5.787e+5
$\mathrm{Re_p}$>10000	0.5191	-1662.5	5.4167e+6

3.4.3.3 Simulation of the effect of fluctuating velocity on sedimentation processes

Sediment transport phenomena in turbulent flow are more striking than in laminar flow. Some researchers (Wilkinson and Waldie, 1994; Pettersson, 1997) assumed that particle trajectory can be calculated with the mean flow without taking into consideration the influence of flow turbulence. Others (Thomson, 1984, 1987; Stovin and Saul, 2000; Shams *et al.* 2002; Adamsson *et al.* 2003; Jayanti and Narayanan, 2004; Dufresne, 2008, Dufresne *et al.*, 2009; Vosswinkel *et al.,* 2012; Yan *et al.*, 2011a) argued that the dispersion of small particles is severely affected by turbulent flow. Dufresne (2008), Vosswinkel *et al.* (2012) tested the parameter concerned, the time scale constant value, using a discrete random walk model (DRWM) in a stormwater detention basin. The authors found that the RE and sediment deposit zone were sensitive to this parameter. Since most flow in nature is in a turbulent state and turbulent flow can be characterised by fluctuating velocity fieldsthe effect of turbulent flow field on the dispersion of particles should be taken into account to obtain more accurate results. The dispersion of particles due to turbulence in the fluid phase can be predicted using the stochastic tracking model DRWM. The stochastic tracking model in Fluent is based on the eddy interaction model and the discrete particle is assumed to interact with a succession of eddies. The DRWM includes the effect of instantaneous turbulent velocity fluctuations on particle trajectories by using stochastic methods by eddies. Each eddy is characterised by a Gaussian distributed random velocity fluctuation *u', v'*, and *w'*, a time scale (eddy lifetime), τ_e, and a length scale (eddy size), L_e. Velocity fluctuation *u', v',* and *w'* are expressed in equations (3.60) - (3.63), where ζ is a normal distributed random number, and k is the turbulent kinetic energy.

$$u' = \sqrt{\overline{u'^2}} \tag{3.60}$$

$$v' = \sqrt{\overline{v'^2}} \tag{3.61}$$

$$\mathrm{w}' = \sqrt{\overline{w'^2}} \tag{3.62}$$

$$\sqrt{u'^2} = \sqrt{v'^2} = \sqrt{w'^2} = \zeta\sqrt{\frac{2k}{3}} \tag{3.63}$$

In the DRWM, the fluctuating velocity components are discrete piecewise constant functions of time. Their random value is kept constant over an interval of time calculated from the characteristic lifetime of eddies, τ_e. The lifetime scale is defined as equation (3.64):

$$\tau_e = 2T_L \tag{3.64}$$

For small particles that move with the fluid, the particle integral time becomes the fluid Lagrangian integral time, T_L. This time scale can be approximated as an equation based on k-ε model (3.65):

$$T_L = C_L \frac{k}{\varepsilon} \tag{3.65}$$

Where C_L is the time scale constant and is the only parameter to be determined by this model k is the turbulent kinetic energy; ε is the turbulent dissipation rate. For the k-ω models, substitute $\omega=\varepsilon/k$ into equation (3.65).

Another option for eddy lifetime is given by a log-normal variation:

$$\tau_e = -T_L \log(R) \tag{3.66}$$

Where R is a uniform random number between 0 and 1.

The eddy length scale is given as:

$$L_e = 0.15\frac{k^{3/2}}{\varepsilon} \tag{3.67}$$

The particle eddy crossing time, t_{cross} , is defined as:

$$t_{cross} = -\tau \ln\left[1-\left(\frac{L_e}{\tau|u-u_p|}\right)\right] \tag{3.68}$$

Where $|u\text{-}u_p|$ is the magnitude of the relative velocity; τ is the particle relaxation time defined as:

$$\tau = \frac{\rho_p d^2}{18\mu} \tag{3.69}$$

During the interaction process, the fluctuating velocities are kept as constant interaction time. The interaction time is either eddy lifetime or the crossing time, whichever is lower. When this time is reached, a new set of values for instantaneous velocities are obtained from a new random value of ζ.

Particle dispersion prediction makes use of the concept of the integral time scale, T, defined in equation. (3.63), which describes the time spent in turbulent motion along the particle path, d_s:

$$T = \int_0^\infty \frac{\overline{u'(t)u'(t+s)}}{\overline{u'^2}} ds \tag{3.70}$$

3.4.3.4 DPM boundary condition

The basic principles of particle trajectory are set out in the previous section. In order to implement a simulation such as flow simulation, some specific boundary conditions are required.

f. Initial condition of particles

Before injecting the particles into a flow domain, the particles' properties must be defined. The primary inputs required for the discrete phase calculations in Ansys Fluent are the initial conditions that define the starting position, velocity, density, size and other parameters for each particle stream, as well as the physical effects acting on the particle streams. The initial conditions for a particle stream are defined by creating an *injection* and assigning properties to it. Usually, the sediment is defined as an *inert* particle.

The initial conditions required depend on the injection type, while the physical effects are selected by choosing an appropriate particle type. Particle size distribution of sediment was estimated in two ways: firstly using a mean diameter to represent all particle sizes; and secondly by employing the Rosin-Rammler distribution function, a new feature to describe the granulometry of sediment in inlet injection. Using this feature the whole range of particle sizes is divided into a number of discrete intervals. Each interval is represented by a mean diameter and tracked for the particle trajectory calculation. The Rosin-Rammler distribution is an empirical distribution to describe particle sizes, proposed by Rosin and Rammler (1933). The Rosin-Rammler distribution is expressed as:

$$Y_d = 100 \exp\left[-\left(d \diagup \bar{d} \right)^n \right] \tag{3.71}$$

where Y_d is cumulative mass in % retained on size d, $\bar{d}$ is the size parameter, n is distribution parameter.

Taking the logarithms two times to remove the exponent gives:

$$\log\left(\log\left(\frac{100}{Y_d} \right) \right) = n \log d - n \log \bar{d} + \log(\log e) \tag{3.72}$$

Where e is the nature constant. An example is shown in order to test the Rosin-Rammler model. A plot of log [log $(100/Y_d)$] versus log$d$ should give a straight line. The parameters of the Rosin-Rammler distribution, n and $\bar{d}$ are obtained from the slope of the straight line and the intercept at the horizontal line at Y_d = 36.79, respectively. An example is given as follows. Table 3-5 and Table 3-6 show the particle size distribution by mass weight and cumulative mass fraction by particle size, respectively. A plot of Y_d against diameter d is shown in Figure 3-21.

Table 3-5 Particle size distribution by mass fraction (Dufresne, 2008)

d_{min}	d_{10}	d_{20}	d_{30}	d_{40}	d_{50}	d_{60}	d_{70}	d_{80}	d_{90}	d_{100}
350	535	593	642	689	738	790	851	931	1056	1400

Table 3-6 Mass fractions Y_d with diameter larger than d %

Diameter range(μm)	Mass fraction Y_d with diameter larger than d %
350	100
535	90
593	80
642	70
689	60
738	50
790	40
851	30
931	20
1056	10
1400	0

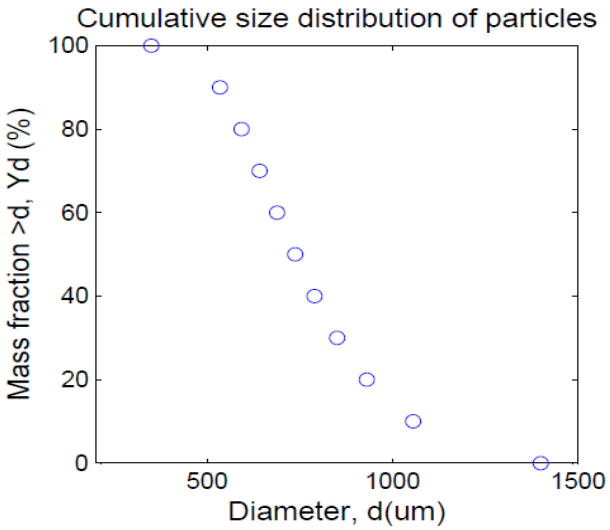

Figure 3-21 Cumulative size distributions of particles

According to the method above, in this example, the parameters found were: n=4 and $\bar{d}$ =810 μm. The Rosin-Rammler fit curve for particle size data is shown in Figure 3-22.

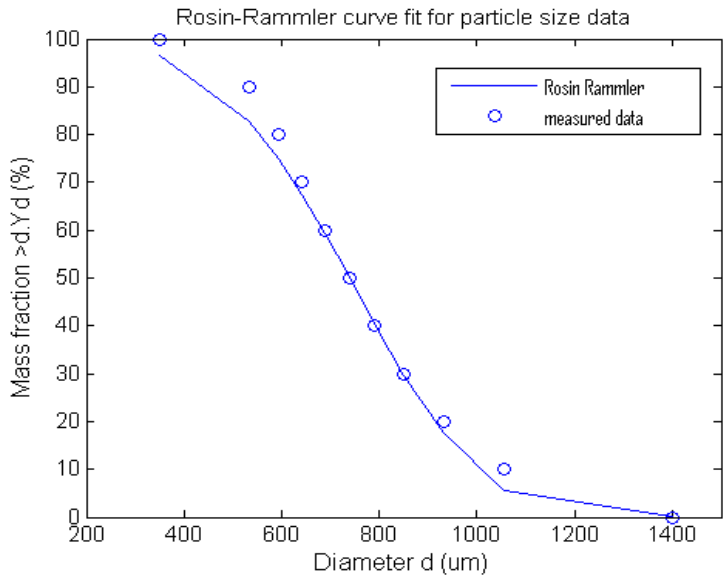

Figure 3-22 Rosin-Rammler curve fit for the cumulative size distribution of particles

g. Injection types

Before tracking the particles, the particles must be added into the flow domain. In Ansys Fluent, several different types of injection are available to meet different user needs in terms of injecting the particles into the flow domain. The most commonly used injection types are listed as follows (Ansys, 2011a):

- Single: one particle is injected
- Group: injection of a group of particles
- Cone (only in 3D): injection of a group of particles forming a cone
- Surface: injection of a group of particles across the entire surface
- File: specific injection defined by a file

In our case, it is assumed that the sediment is fully developed and homogenous across the whole surface. Hence we most frequently use surface injections.

h. DPM boundary condition at Inlet/Outlet

The particles are tracked through the flow domain. When a particle reaches a physical boundary (*e.g.*, bottom of detention basin) during the trajectory calculation, the interaction between the particle and physical boundary must be processed to represent particle motion and determine the fate of the trajectory. When a particle enters the flow domain at an inlet, the calculation of its trajectory starts. When a particle leaves the flow domain at an outlet, the calculation of its trajectory ends. In Ansys Fluent the boundary condition “escaped” is used at the inlet and outlet for this function.

i. DPM boundary condition for bed and side wall of the basin

For the boundary condition at the bottom of detention basin, previous CFD modelling research has shown that these boundary treatments are vital for accurate modelling of sediment transport, settling and erosion in stormwater detention basins (Stovin and Saul, 1994, 1996, 1998; Adamsson *et al.*, 2003; Dufresne, 2008; Vosswinkel *et al.*, 2012). Two kinds of boundary conditions available in Fluent are often used to deal with the particle trajectory fate when hitting the bottom: *trap* and *reflect.*

The *Trap* boundary condition

This boundary condition terminates the trajectory calculation at the physical boundary. In other words, particles settle out when they arrive at the bed of the basin. This boundary condition excludes the possibility of particle resuspension after hitting the bed and therefore often overestimates sediment removal efficiency in detention basins (Stovin and Saul, 1996).

The *Reflect* boundary condition

The particle rebounds off the boundary via an elastic or inelastic collision. The striking particle velocity breaks down into normal and tangential components with respect to the collision surface, v_{in} and u_{in}, respectively. It is assumed that these components are reduced after the collision. As shown in Figure 3-23, e and f indicate the restitution (or normal) and friction (or tangential) coefficients, respectively (Nino and Garacia, 1998). The normal coefficient of restitution defines the amount of momentum in the direction normal to the wall that is retained by the particle after the collision with the boundary. A normal or tangential coefficient of restitution equal to 1 implies that the particle retains all of its normal or tangential momentum (no energy lost) after the rebound (an elastic collision). A normal or tangential coefficient of restitution equal to 0 implies that the particle retains none of its normal or tangential momentum after the rebound (particle energy lost). In Fluent the normal or tangential coefficient of restitution is equal to 1 by default. The *reflect* boundary condition excludes the possibility of the particle settling out when it arrives at the bed. Therefore, when it is used as the boundary condition at the bed of basin, it often underestimates sediment removal efficiency in sediment transport modelling in a stormwater detention basin (Stovin and Saul, 1998; Adamsson *et al.*, 2003). In sediment transport modelling the *reflect* boundary condition is used at the vertical side wall.

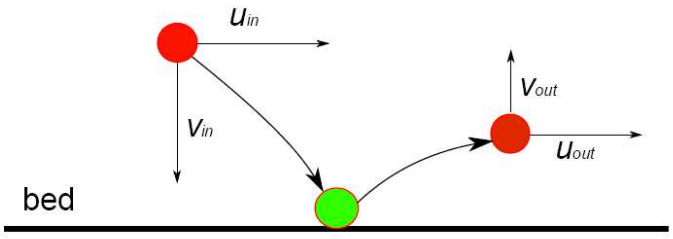

Figure 3-23 Diagram of the reflect boundary condition

$$e = \left| \frac{v_{out}}{v_{in}} \right| \tag{3.73}$$

$$f = \frac{u_{out}}{u_{in}} \tag{3.74}$$

Combination bed boundary condition with a fixed threshold

Previous research has shown that none of the available boundary conditions is particularly good at representing sediment settling and erosion process in detention basin modelling. Adamsson *et al.* (2003) developed a boundary condition for the bed of a basin by combining these two basic boundary conditions (*trap* and *reflect*) together with critical bed shear stress (BSS). They then implemented this boundary condition in Fluent as a user defined function (UDF). If the local bed shear stress is less than the critical value, the particle settles out as with *trap*, otherwise, the particle rebounds off the bed as with *reflect*. Dufresne (2008) used bed turbulent kinetic energy (BTKE) as the threshold in the same way to treat particle trajectory fate when it hits the bed of basin. Using this boundary condition when modelling sediment transport in the basin bed, removal efficiency was often overestimated (Dufresne, 2008). Another notable drawback with this method is that the simulated sediment distribution shows high levels of disagreement in full scale basins compared to observations. Furthermore, Adamsson *et al.* (2003) pointed out that this method was only valid for steady flow condition and the prediction was sensitive to the chosen threshold. Stovin and Saul (1998) argued that this critical value depends on both the characteristics of the basin (shape, roughness) and sediment properties (such as particle size, density, shape, etc.). This implies that it is vital that a suitable threshold is found when using this boundary condition for sediment transport modelling. This threshold is determined based on measurements or CFD simulation by comparing the BSS or BTKE distribution with the observation of sediment distribution at the experimental site.

Combination bed boundary condition with a varying threshold

According to the combination boundary condition with a fixed threshold, the state of the different particles on hitting the basin bed was determined under the same critical value. Obviously, different particles might settle out in different strengths of flow condition (*e.g.* bed shear stress strength). The results of observation (shown in chapter 4) of the Django Reinhardt detention basin support this general hypothesis. Given the large and heavy particles often settled out upstream near the basin inlet, it may suggest that when representing the non-uniform sediment characteristics, different critical values should be used for different particles. For noncohesive sediment, although there is an argument that bed shear stress may be the main factor driving particle resuspension, many researchers recognize the Shields relationship between dimensionless shear stress (or Shields parameter), τ_* (defined in equation (3.77)) and grain Reynolds number, R_*, as a more reliable predictor of entrainment. The curve known as the Shields Curve, which is shown in Figure 3-24, was proposed by Rouse (Vanoni, 1975). The Shields curve (Vanoni, 1975) can be expressed as equations (3.75)-(3.76), which are very convenient for computer programming.

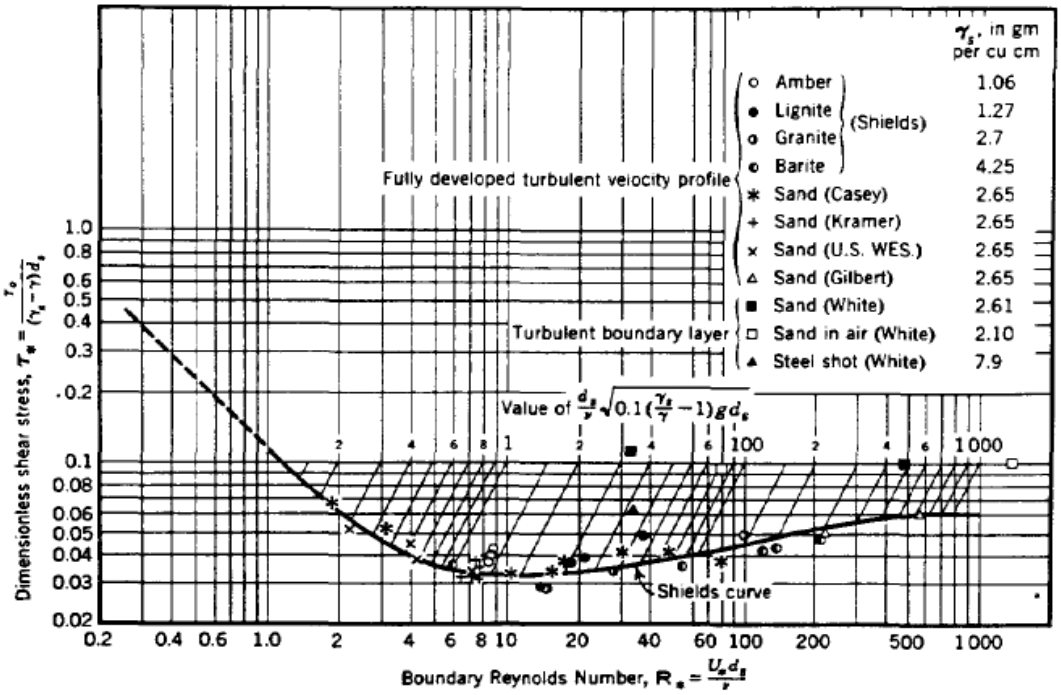

Figure 3-24 Shields curve (Vanoni, 1975)

$$\tau_{*_c} = 0.22\beta + 0.06\times 10^{-7.7\beta} \tag{3.75}$$

$$\beta = \left[\frac{\rho}{\mu}\sqrt{\frac{\rho_p - \rho}{\rho}gd^3}\right]^{-0.6} \tag{3.76}$$

$$\tau_* \equiv \frac{\tau_0}{(\gamma_s - \gamma)d} \tag{3.77}$$

$$R_* = \frac{u_* d}{\nu} \tag{3.78}$$

Where τ_0 is bed shear stress, γ_s is particle specific weight, γ is fluid specific weight, μ is dynamic viscosity of fluid, g is acceleration of gravity, d is particle diameter, u_* is shear velocity, ν is the kinematic viscosity of fluid.

The critical shear stress, τ_c, for a particle with a diameter, d, is then calculated using the following equation:

$$\tau_c = \tau_{*_c}(\gamma_s - \gamma)d \tag{3.79}$$

Dufresne (2008) used the BTKE (like the BSS) as the boundary condition threshold to determine whether particles settled out or not. If the local BTKE is larger than the threshold when the particle hits the bed, the particle rebounds, otherwise the particle is deposited. Although not explicitly stated, BTKE is considered to be a function of the bursting process since the bursting process is also associated with fluctuation velocity. ASCE (Vanoni, 1975) pointed out that turbulence is the most important impact factor in sediment suspension. Using the BTKE threshold to determine particle settling implies that the turbulence factor for sediment suspension may be characterised by the turbulent kinetic energy (TKE). It is easier for the particle to settle out under weak flow turbulence condition. The BTKE is calculated by equation (3.80) according to the turbulent kinetic energy, k, in the first cell near the bed (Dufresne, 2008).

$$\frac{\partial k}{\partial n} = 0 \tag{3.80}$$

The threshold used by Dufresne (2008) for the pilot basin is between 1.0e-4 m^2/s^2 and 3.0e-4 m^2/s^2. The BTKE threshold is determined by comparing the simulation results and the observed deposit zone. This method makes it difficult to determine the threshold for predicting sediment transport for the cases where no observations are available. The preliminary simulation results from the Django Reinhardt detention basin showed that the BTKE threshold is between 3e-5 m^2/s^2 and 5e-5 m^2/s^2 (Yan *et al.*, 2010). It differs from the threshold used by Dufresne (2008) in a small scale stormwater detention basin. Like the Shields curve for BSS, this may imply that the BTKE threshold for deposition depends on sediment characteristics. A formula has been proposed to provide a more convenient method for determining the BTKE threshold which takes the particle characteristics into account,. This formula is expressed as (Yan *et al.*, 2011, 2012):

$$k_c = \xi v_s^{\,2} \tag{3.81}$$

Where k_c is the BTKE threshold; v_s is the particle settling velocity; ξ is an adjustment coefficient that includes the unknown factors (*e.g.* concentration, particle shape, energy transferring rate, collision effects, etc.).

This formula is based on the following assumptions:

- Flow turbulence is an important factor for sediment suspension (Vanoni, 1975);
- Bed turbulent kinetic energy distribution can be used to estimate the deposition zone in the same way as bed shear stress (Dufresne, 2008);
- The turbulence factor for sediment suspension may be characterised by the turbulent kinetic energy with a threshold. For a given particle, if the local turbulent kinetic energy exceeds the threshold, the particle cannot settle out, otherwise the particle settles out;
- It is assumed that particle settling velocity can represent all other particle properties (such as density, size, shape, concentration, etc.) because settling velocity depends on all the other properties (Julien, 2010).

This formula considers not only the hydraulic condition, but also the properties of sediment. Thisformula makes it possible to estimate the BTKE threshold using sediment properties. The BTKE threshold does not need to be determined by comparing the simulated results with the observation sediment zone before performing the sediment transport simulation. It is therefore theoretically useful for sediment transport modelling under the unsteady flow conditions which often occur in real systems.

These combination boundary conditions were implemented using UDFs. The UDFs were coded with computer language C and compiled, then hooked into Fluent as bed boundary conditions for sediment transport modelling using a DPM model. An example of a UDF combination bed boundary condition is presented in appendix A.

Bed boundary conditions for dynamic sedimentation processes under unsteady flow condition

Previous research into the modelling of sediment transport in stormwater detention basins using the Euler-Lagrange approach have often been carried out in steady flow in an uncoupled way (also known as one-way coupling, as detailed in the next section). The modelling of particle trajectories makes sense when the flow condition and sediment discharge are stable. Furthermore, although not expressed explicitly, using the c*ombination of bed boundary condition with threshold BSS or BTKE* under steady state flow condition only makes it possible to represent whether particles settle out or not. It cannot represent the dynamic entrainment process (erosion) when the flow conditions change over time (*e.g.*, if the shear stress or turbulence increases, etc.). That is why with this method, the model prediction often overestimates removal efficiency even for high inflow rates in scale basins (Stovin and Saul, 1998; Dufresne, 2008). In order to accurately model the dynamic sedimentation and resuspension phenomena, a new approach which makes it possible to represent the dynamic settling and entrainment of deposit under unsteady flow conditions in two-way coupling with DPM is proposed. The the approach is shown in the diagram in Figure 3-25.

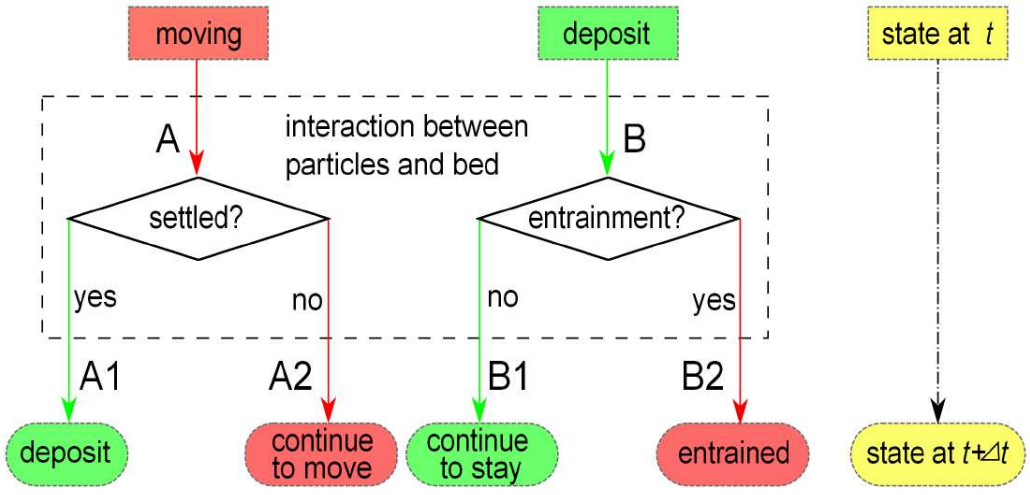

Figure 3-25 Diagram of dynamic sedimentation and bed load entrainment under unsteady flow conditions

The particles in contact with the bed during the particle tracking process under unsteady conditions are processed as follows. At the grain scale, two sediment states are clearly

distinguished at the moment *t*: it is either suspended away from the bed or it settles out as deposit. Depending on the state at the moment *t*, the states of particles at the moment $t+\Delta t$ may be different (suspension or deposit), as well as the treatment for the particle after hitting the bed. The treatment approach for particles shown in Figure 3-25 is described as follows:

Condition A: For those particles in motion at the moment *t*: there are two possible states at the moment $t+\Delta t$, either settled out as deposit (**condition A1** in Figure 3-25.) or continuing to move as suspended load or bed load after contact with the bottom (**condition A2** in Figure 3-25). In the present investigation, determining the state of the particle after contact with the bottom is either based on the widely acceptable parameter bed shear stress (BSS) or bed turbulent kinetic energy (BTKE). If local BSS or BTKE values are lower than the thresholds, the particle settles down as deposit, or else it continues to move. A threshold can be specified for all different particles (*e.g.*, BSS = 0.03 Pa or BTKE = 0.0002 m^2/s^2 for a scale basin according to Dufresne (2008) or different thresholds can also be specified for different particles, for example using Shields curves (dimensionless shear stress) to calculate a bed shear stress threshold according to the particle characteristics . Equations (3.75)-(3.76) show a set of fitted formula of the Shields curve.

BTKE threshold can also be calculated from equation (3.81). The settling velocity can be estimated using equations (3.82) and (3.83) (Julien, 2010):

$$v_s = \frac{8\nu}{d}\left[\left(1+0.0139D^{*3}\right)^{0.5}-1\right] \tag{3.82}$$

where v_s is particle settling velocity (m/s), ν is the kinematic viscosity of water (m^2/s) , D_* is the dimensionless particle diameter (-).

Condition A1: If the particle settles down from motion when it comes into contact with the bed, the available boundary condition '*trap*' should not be applied as it will end the particle trajectory calculation. Instead, the velocity and the forces associated with particle movement should be adjusted so it remains as deposit but the trajectory tracking calculation continues. In this way the deposit can be entrained if flow conditions change.

Condition A2: If the particle continues to move after comine into contact with the bed, a variant '*reflect*' boundary condition is applied (the particle rebounds with a certain velocity and returns to the flow as suspended load or bed load). This makes it possible to take into account energy losses due to friction at the bottom through the restitution normal coefficient *e* and tangential friction coefficients *f*. By default, both *e* and *f* are equal to 1. This implies that the resistance force is neglected. A value ranging from 0-1 should be used to account for friction resistance from the bed. An empirical model describing the restitution coefficient and tangential friction resistance coefficient has been proposed by Nino and Garcia (1998) as: $e = 0.84 - 4.84\tau_*$ and f = 0.73. In the present investigation, both the value of 1 and the empirical model are tested to determine rebound particle velocity. Since the particle is dragged by the near bed flow, it is assumed that the entrained particle follows the same longitudinal direction as the fluid flow.

Condition B: The particle settled at time *t* can be entrained as bed load or suspension at the moment $t+\Delta t$, flow conditions permitting. The local shear stress is compared to threshold

stress obtained from the Shields curve (equations (3.75)-(3.76)) according to the particle characteristics. If the local shear stress exceeds the threshold, the particle is entrained (**condition B2** in Figure 3-25); otherwise it remains in the same state (**condition B2** in Figure 3-25). Similarly, the BTKE is also used as the entrainment boundary condition. The BKTE threshold is estimated using the proposed formula (3.81).

Condition B1: The particle remains in the same location as deposit.

Condition B2: As for the entrained particle, it is necessary to specify its initial velocity (magnitude and direction) after entrainment in order to continue tracking its trajectory. Several studies were conducted to investigate the bed load movement of the individual particle (Bridge and Dominic, 1984; Van Rijn, 1984a; Nalpanis *et al*., 1993; Nino and Garcia, 1994; Hu and Hui, 1996; Lajeunesse *et al*., 2010). Saltation is the dominant mode of bed load movement. Several authors have characterised saltation height and the length of jump and the jump's initial velocity. In this study, the formulas proposed by Hu and Hui (1996) described by equations (3.83)-(3.85) were used to estimate the initial entrainment velocity:

$$u_d = 9.0u_* \quad \text{For smooth bed} \tag{3.83}$$

$$u_d = \begin{cases} (12.3 - 3.7\log\tau_*)u_*, \tau_* < 1.2 \\ 12.1u_*, \tau_* > 1.2 \end{cases} \quad \text{For rough bed} \tag{3.84}$$

$$v_d = \begin{cases} (3.2 - 4.5\log\tau_*)u_*, \tau_* < 1.2 \\ 3.1u_*, \tau_* > 1.2 \end{cases} \quad \text{For smooth and rough bed} \tag{3.85}$$

Where: u_d and v_d are the tangential and normal velocity components for the particle at the hitting surface respectively (m/s), $u_* = (\tau_0/\rho)^{0.5}$ is the shear velocity (m/s), τ_* is the dimensionless shear stress (-), τ_0 is the local shear stress.

Simple estimations of initial entrainment velocity component, as proposed by Van Rijn (1984a) were also tested:

$$u_d = 2u_* \tag{3.86}$$

$$v_d = 2u_* \tag{3.87}$$

Regarding the particle velocity direction, since the particle is dragged by the near bed flow, it is reasonable to assume that the entrained particle follows the same longitudinal direction as the fluid flow.

The proposed approach for dynamic sedimentation and resuspension was implemented using the UDF in C language. The UDF is compiled and hooked into Fluent as a bed boundary condition of basins under unsteady DPM modelling in two-way coupling. An example of a UDF for this proposed approach is presented in appendix B.

3.4.3.5 Solution strategies for the discrete phase

For the Euler-Lagrange approach, Fluent offers two ways of coupling the flow and discrete phase: uncoupled and coupled DPM modelling.

One-way coupling

With the uncoupled approach (also known as one-way coupling), the discrete phase patterns can be predicted based on a fixed continuous phase flow field, in which the effects of the discrete phase on the continuous phase are not taken into account. The scheme is shown in Figure 3-26.

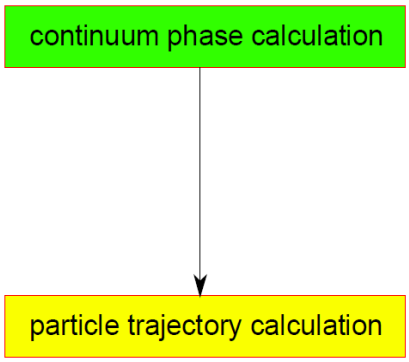

Figure 3-26 Scheme of uncoupled DPM

Two-way coupling

In the coupled approach (also known as two-way coupling), the continuous phase and discrete phase interact with each other. It means that influence of the discrete phase on the continuum phase is taken into consideration. The two-way coupling is accomplished by alternately solving the discrete and continuous phase equations until the solutions in both phases stop changing (see Figure 3-26). The interphase exchange of heat, mass, and momentum from the particle to the continuous phase is depicted qualitatively in Figure 3-27. The influence from discrete phase to continuum phase is performed by means of integrating the source terms in the continuous phase. The mass exchange from the discrete phase to the continuous phase is computed in Fluent simply as:

$$M_c = \frac{\Delta m_p}{m_{p,0}} \dot{m}_{p,0} \tag{3.88}$$

Where Δm is the mass lost in the control cell, $m_{p,0}$ is the initial mass of particle. $\dot{m}_{p,0}$ is the initial mass flow rate of injected particles.

The momentum transfer from the continuous phase to the discrete phase is computed in Fluent by the following equation when it passes through each control volume (Ansys, 2011b).

$$\Delta M = \sum \left(\frac{18\mu C_D \, \mathrm{Re}_p}{24\rho_p d} \left(u_p - u \right) + F_{other} \right) \dot{m}_p \Delta t \tag{3.89}$$

Where

μ= viscosity of the fluid

ρ_p = density of particle

d=diameter of the particle

Re_p= relative Reynolds number

u_p= velocity of the particle

u= velocity of the fluid

F_{ohter}=other interaction forces

C_D=drag force

Δt=time step

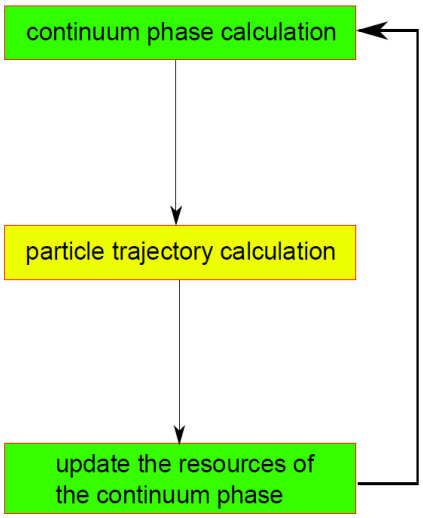

Figure 3-27 Diagram of the of two-way coupling DPM approach

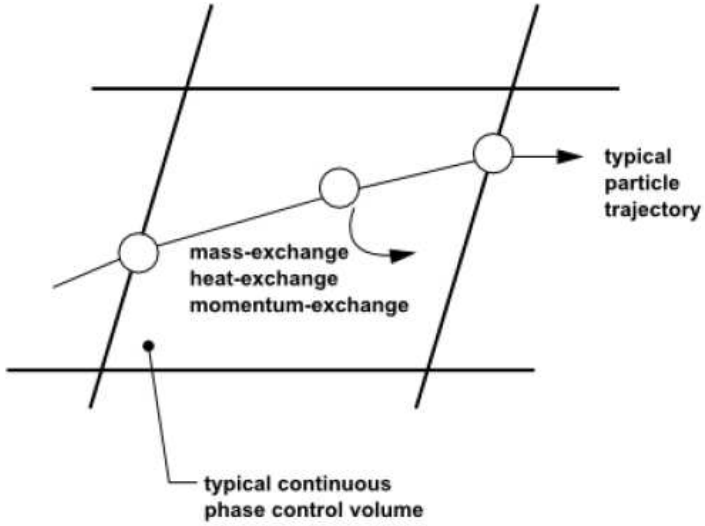

Figure 3-28 Heat, mass, and momentum transfer between the discrete and continuous phase (Fluent, 2011b)

3.5 Conclusion of Chapter 3

The objective of this chapter has been to introduce the materials and methods used in our investigation. The experimental site has been described briefly and experimental methods are also introduced. Another important part of this chapter is the numerical method used for fluid flow and sediment transport simulation in stormwater detention basins.

Regarding the solid phase modelling, after comparison between the Euler-Euler and Euler-Lagrange approach, it was decided to choose the Euler – Lagrange approach to model sediment transport in the stormwater basin.

One of the most important elements in sediment transport modelling using DPM is the boundary condition treatment for the basin bed. There is no general model available for this purpose and we have therefore had to develop the appropriate boundary condition. Both the bed shear stress (BSS) and bed turbulent kinetic energy (BTKE) for boundary condition were tested in this investigation. A new formula has been proposed to more easily estimate the BTKE threshold for different sediments.

In order to represent dynamic sediment transport, settling and entrainment in detention basins under unsteady flow conditions, a new method has been developed to deal with dynamic interactions, implemented using the UDF in Fluent for detention basins.

To account for the flow turbulence effect on the tracked particles, a stochastic method was used based on the discrete random walk model (DRWM). The influence of the parameters (Lagrangian constant time scale, C_L) of DRWM will be tested both in steady state conditions and unsteady state conditions.

Chapter 4 Sediment transport under steady state conditions

4.1 Introduction

This chapter aims to present i) the analysis of accumulated sediment in order to highlight the correlation between sediment characteristics and distribution and the hydrodynamic behaviour of the Django Reinhardt stormwater detention basin and ii) the simulated results for sediment transport and removal efficiency in both small-scale detention basins and full-scale detention basins under steady state conditions. The discussion will focus on the evaluation of the developed methods and models. This chapter is structured as follows:

- The presentation of the results related to accumulated sediment spatial distribution and physical characteristics in the full-scale basin,
- Highlighting the correlation between the spatial distribution of the sediment's physical characteristics (grain size, density, organic matter content) and the hydrodynamic behaviour of the full scale basin.
- The preliminary 3D modelling study of sediment transport with DPM in a full-scale detention basin in order to test the bed boundary conditions derived from literature, particularly fixed BSS (bed shear stress) and BTKE (bed turbulent kinetic energy) thresholds.
- The application of the new bed boundary conditions in order to represent the interaction between particles and the beds of both small and full-scale basins under steady flow conditions, using DPM.
- The application of the proposed methodology and CFD models in order to simulate dynamic sediment transport, deposition and erosion in the small- scale detention basin only, under unsteady flow conditions, using DPM .

4.2 Accumulated sediment analysis

Due to the lack of appropriate data (in term of velocity field, shear stress distribution, Residence Time Distribution, turbulence quantities, etc.) to validate both the hydrodynamic and solid transport models, the spatial distribution of sediment and its physical characteristics were analysed in order to highlight the correlation between the spatial distribution of the sediment and the hydrodynamic behaviour of the basin. Indeed, in the present study it was very difficult to obtain these types of hydrodynamic measurements due to the size of basin, the safety concerns during storm events, etc. Using this procedure (the use of sediment spatial distribution and characteristics to check hydrodynamic behaviour), the hydrodynamic modelling is assumed to be implicitly verified. This means sediment transport modelling can be done using verified hydrodynamic numerical options (turbulence models, boundary conditions, velocity field, shear stress distribution, etc.).

Large quantities of sediment have accumulated in the detention basin since its rehabilitation in 2004 (see Figure 4-1). The sediment had accumulated since the last clean in 2006 up until March 2013, and vegetation was growing above the sediment (see Figure 4-1 and Figure 4-4).

The sediment is spread over a large area in the basin. The accumulated sediment in the basin has been seen to affect particulate pollutant removal efficiency due to the effects of erosion or bed roughness. After the basin was cleaned in 2006, efficiency was high. Four measurements of the corresponding total suspended solids (TSS) mass loads taken in June to September 2006 showed efficiencies of 93%-94 %. However, as the basin was filled with sediment the efficiency decreased to a mean value of 57 % with usual values of between 33 % and 75 % (Torres, 2008; Gonzalez-Merchan, 2012). Hence a thorough understanding of the solids transport processes in the basin is important to improve design with respect to removal efficiency. Furthermore, data is also needed tovalidate the simulated sediment transport results. In order to better understand and explore the spatial characteristics of the accumulated sediment in Django Reinhardt detention basin, a field measurement of accumulated sediment was carried out on April 14 2011. The profile of the preferential sediment zone and discrete point sediment thickness were measured. The measurement points were located at a distance of 5m for the preferential sediment zone (left part of basin, Figure 4-2). The measurement points were closer together in the centre of the basin and further apart towards the basin inlet (see Figure 4-2). Meanwhile, for the physical sediment characterisation analysis, 11 reprentative samples of the accumulated sediment were collected, kept and measured in laboratory. The sediment samples were characterised in terms of particle size distribution, density, and organic matter content.

The sampling process and methods used for analysis were presented in chapter 3.

Figure 4-1 Accumulated sediment in the Django Reinhardt basin on 14/04/2011

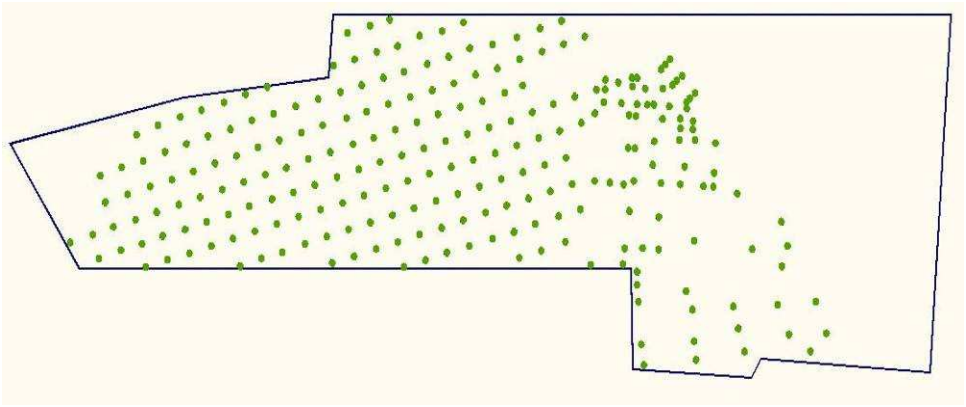

Figure 4-2 Layout of the sediment thickness spatial measurements carried out on 14/4/2011

4.2.1 Sediment depth spatial distribution

A general view of accumulated sediment in the Django Reinhardt basin can be seen in the Google map satellite photo shown in Figure 4-3. The preferential accumulated sediment depth distribution is shown in Figure 4-4, and ranged from 1 to 42 cm. The deepest sediment zone is located at the centre of the basin. The thinnest sediment zone is located downstream in the basin close to the overflow weir and near to orifice one. Another significant characteristic that can be observed in the photo and the contour of sediment depth is that there are two small thinner sediment zones near to the thickest part. These thinner zones are marked with a quadrilateral in Figure 4-3. The sediment has been accumulating since 2006 and the sediment volume is about 430±21 m^3 according to the measured thickness data. The dashed line zones labeled 1, 2 and 3 in Figure 4-4 present the temporary sediment zone meaning that sediment is sometimes found here, depending on the storm events and pollutant discharges.

Figure 4-3 Overhead view of the Django Reinhardt basin (from Google Earth in 2012) and the contour of sediment depths measured on 14 April 2011 - Up until the time at which the measurements were taken, the sediment had been accumulating since 2006

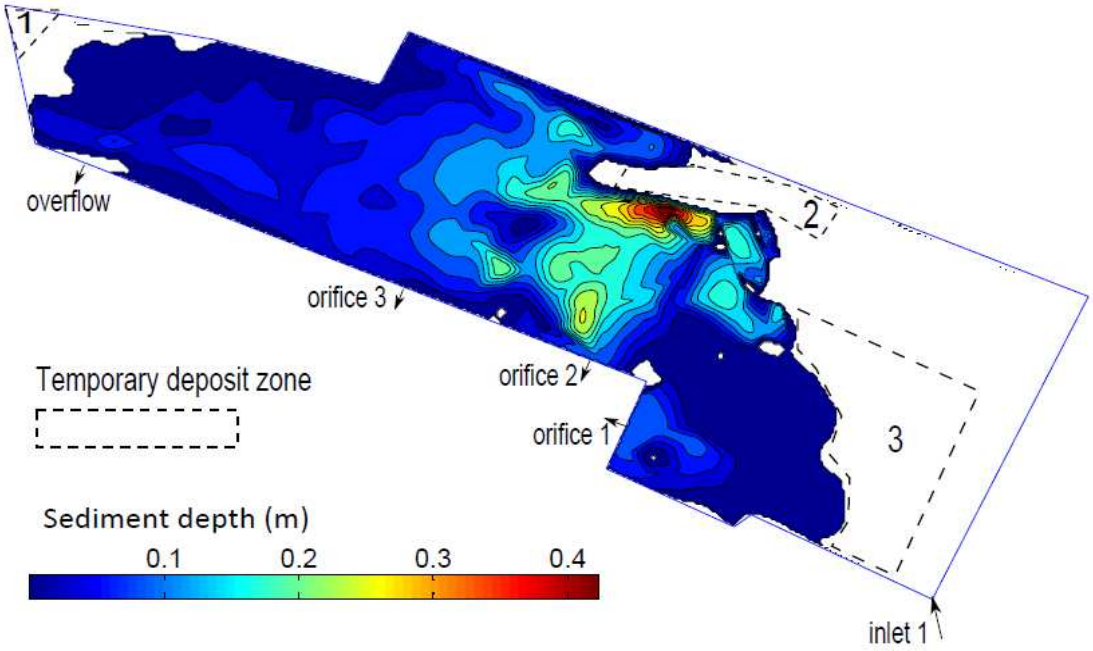

Figure 4-4 Contour of sediment distribution in the Django Reinhardt basin

4.2.2 Particle size distribution

Particle size was measured using wet sieving and a laser diffraction analyser (MALVERN MASTER SIZER 2000). The wet sieving method was used to determine the large fraction of sediment (larger than 80 µm) according to sediment mass. The laser diffraction analyser was used to determine the fractions of the samples smaller than 1600 µm according to sediment volume. The detailed method was described in chapter 3. In order to follow and understand the results of the analysis more clearly the layout of the 11 sampling locations is shown in Figure 4-5.

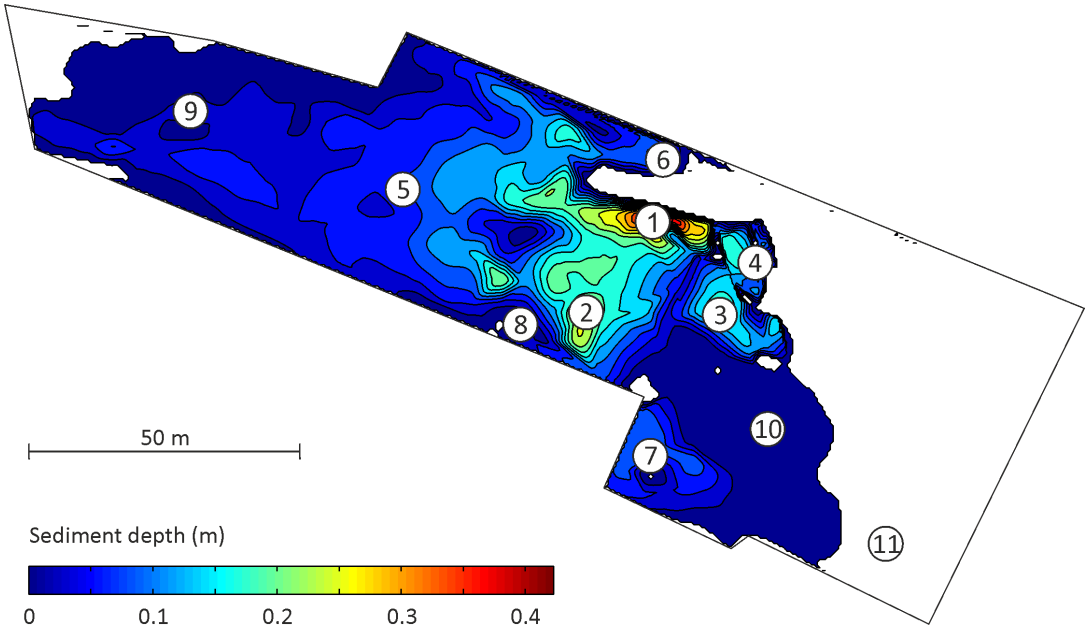

Figure 4-5 Layout of the sediment sampling locations in the basin, numbered according to sediment depth

Figure 4-6 Pictures of gravel-like sediment and of clayey/silty deposits accumulated in the Django Reinhardt basin. The picture of gravel sediment was taken in 2011 and the picture of clayey /silty deposits was taken in 2012.

Regarding the field observations, the particle size spatial distribution shows major variations between different parts of the basin, with gravel-like deposits close to the inlet (temporary sediment zone shown in Figure 4-4) and finer deposits observedin the centre of basin and near the outlet (see Figure 4-6).

Generally, the heavier and larger particles often settle out in the furthest upstream. Hence, the larger particles were observed near the basin inlet. The silty deposit was observed near the side of the dry channel (see Figure 4-6), maybe due to sediment transport during the dry period. More details are presented in Table 4-1, Figure 4-7 and Figure 4-8 .

Table 4-1 Particle size characteristics of the samples. The weight percentages of the fraction of sieving diameters less than 80 µm were obtained from the wet sieving analysis, and the d_{10}, d_{50} and d_{90} were obtained from the laser diffraction analysis of the fraction of sieving diameters less than 1600 µm. The values in brackets are from the measurements without ultrasound.

Number of samples	Sieving analysis	Laser diffraction analyser		
	Fraction <80µm (w/w %)	d_{10} (v/v %)	d_{50} (v/v %)	d_{90} (v/v %)
P01	66	4	37	295
P02	77	4 (5)	32 (45)	314 (467)
P03	59	4 (6)	49 (78)	518 (626)
P04	4	340	794	1435
P05	86	3	26	117
P06	63	5 (7)	39 (53)	392 (541)
P07	90	3 (4)	21 (33)	109 (290)
P08	93	3	22	95
P09	93	5 (18)	32 (185)	122 (828)
P10	17	20	507	1233
P11	<0.5	-	-	-

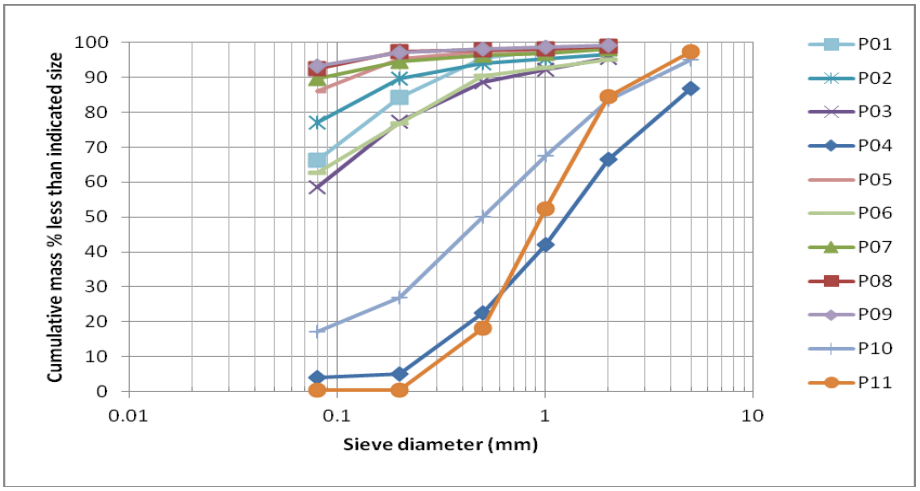

Figure 4-7 Accumulated particle size distributions of the samples from the sieving analysis. The sample names refer to the locations shown in Figure 4-5

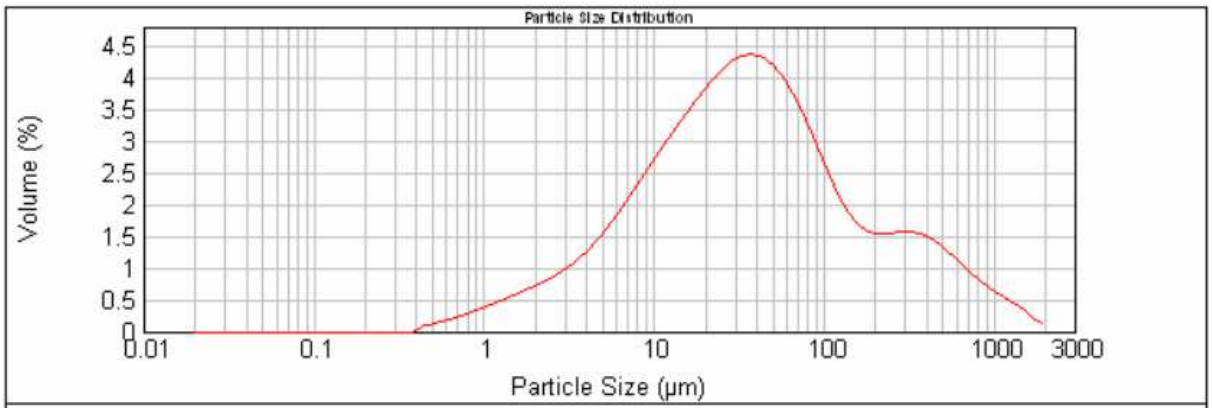

Figure 4-8 Particle size distributions of the sample P06 by Laser diffraction analysis

Figure 4-7 shows the accumulated particle size distribution curves for all samples from the sieving analysis. As an example, Figure 4-8 shows the particle size distribution of P06 by volume fraction, measured by laser diffraction analysis. As Figure 4-6clearly shows the particle sizes in samples P04, P10 and P11 were significantly coarser than the rest of the samples. In Table 4-1 the second column shows the weight fractions for all samples for sieving diameters of less than 80 µm. It was observed that the fractions in samples P04, P10 and P11 were much smaller than those from the rest of the samples (<0.5%-17% against 59% - 93%) and the particle sizes were significantly larger (sample point P11 was not measured by laser diffraction analysis due to its coarseness). According to the weight fraction of less than 80 µm, the particles can be categorised in three groups: the coarse group from samples P11, P04 and P10; the median group from samples P03, P06, P01 and P02; and the finer group from samples P05, P07, P08 and P09. The significant difference between the coarse group and the other groups is due to the location of these samples, close to the basin inlet (see Figure 4-5) and generally the coarse particles settle out faster due to the high settling velocity. The particle size characteristics of sample points P05, P08 and P09 were all finer than those of P01, which again was finer than those of P03, P04 and P10. In short, the deposited particles gradually became finer the further the distance from the detention basin inlet (Kayhanian *et al.*, 2012). According to this assumption, the finer mass fraction of sample P04 should be larger than that of P10. However, actually the opposite is true. The fraction of sample P04 (4%) is less than that of P10 (17%) according to the measurement. A similar result was also observed for P07, which is closer to the inlet than many other samples such as P05. Hence, hydrodynamic behaviour may explain those differences as demonstrated in the hydrodynamic simulations and the correlation between the hydrodynamics and the spatial distribution of the sediment's physical characteristics.

In Table 4-1 the particle size values (d_{10}, d_{50} and d_{90}) are the mean values of triple measurements of laser diffraction analysis (given as volume percentages). The values in brackets are from the measurements without ultrasound, in which the particle size values were slightly higher for all the measured samples, except for sample point P09. Here, the values were significantly higher (4-7 times the values with ultrasound). The sediment sample from sample point P09 was significantly drier than the other samples on which the particle size distribution was measured, either with and without ultrasound (around 20% water content compared to around 40%), suggesting that this had an effect on the measurements without ultrasound.

The results for the measurements with ultrasound generally varied little between the three measurements for the individual points with standard deviation on the particle size values of 5-10% on average. However, a few of the d_{90} measurements had standard deviations of 30%. Without ultrasound, the picture was the same except for sample point P09, which yielded standard deviations of 45% on the d_{50} and 21% on the d_{10} particle size value.

The results correspond well to the particle size distributions found in core sediment samples by Jacopin *et al.* (1999) in a grassed stormwater detention basin similar to the Django Reinhardt detention basin. In sediment core samples taken more than 175 m from the inlet, the fraction of particles less than 100 µm found was 73%-79% and the d_{10}, d_{50} and d_{90} were 4-5, 37-40 and 230-320µm, respectively. These values are similar to those obtained in this study, except for the "odd" measurement without ultrasound at sample point P09 and the three coarse samples (P04, P10 and P11).

However, particle size distribution is somewhat different from previous measurements taken in the basin. Torres (2008) measured particle size distribution using sediment traps, and Becouze-Lareure (2010) and Sebastian (2011) measured some particle characteristics using samples from the inlet. These experiments showed d_{10} values of 8-12µm (based on four different rain events) and d_{50} values of 49-117 µm (based on seven different rain events). This is in between the larger values of sampling points P04, P10 and P11 and the smaller values of the rest of the sample points found in this study (disregarding the measurement of sample point P09 without ultrasound). The difference in the measurement methods and sampling locations may be responsible for this difference. Indeed, previous measurements (Torres, 2008; Becouze-Lareure, 2010; Sebastian, 2011) were performed directly on the runoff water or water collected from sediment traps, adding it to the filtrated tap water. If this does not necessarily explain the differences, either the fractioning of the sediment within the basin or a change in the particle size distribution of the sediment should account forthe difference. However, one does not preclude the other.

4.2.3 Particle density and organic matter content

The density of each sieved fraction was measured for samples P03 and P04, and the results can be seen in Figure 4-9 It shows that for the fractions of sieving diameters larger than 0.08 mm, the density at sample point P04 was close to that of sand (around 2600 kg/m^3 (Kayhanian *et al.*, 2008)), while the density of the fraction of sieving diameters less than 0.08 mm was somewhat lower. This was also the trend in the measurements from the sample point P03, although it was not so pronounced. The results are based on one measurement, but the uncertainty of the method was very low with standard deviations of less than 0.2 % of the mean value based on the triple measurement of one sample.

For the rest of the samples, only the density of the fraction of sieving diameters of less than 0.08 mm was measured. These results can be seen in Figure 4-10 which also shows the organic matter content of the whole samples. As the figure shows, the density of the finest fraction was between around 2250 kg/m^3 and 2500 kg/m^3. In the three coarsest samples (P04, P10 and P11), the organic matter content was low compared to the rest of the samples, in which it was close to 15%. This value is almost identical to the organic matter content found in the core sediment samples in the previously mentioned study by Jacopin *et al.* (1999).

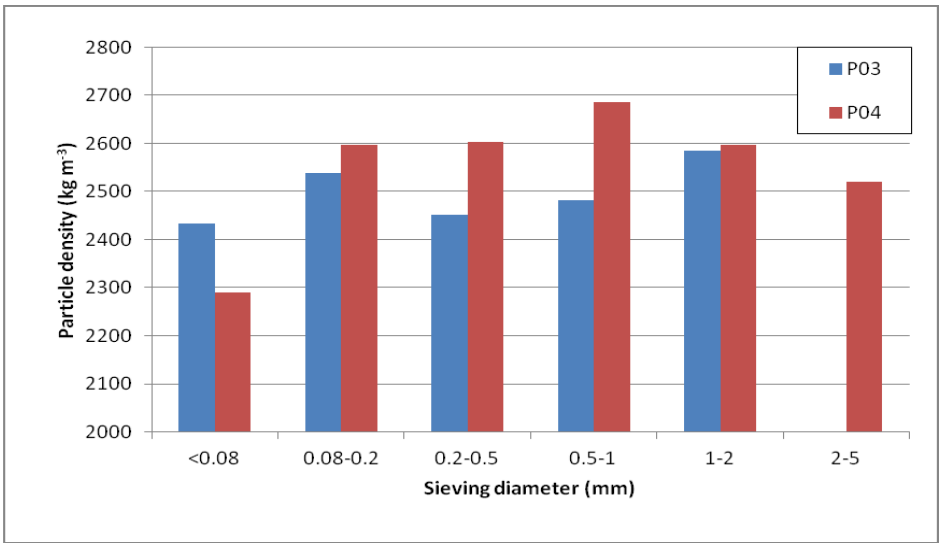

Figure 4-9 Density of each sieved fraction from sample points P03 and P04

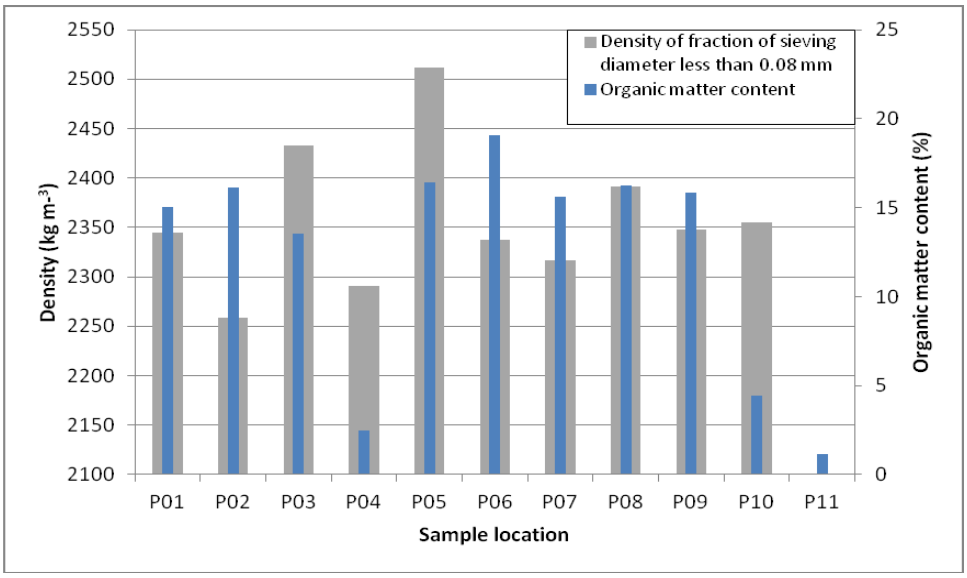

Figure 4-10 Density of the fractions of sieving diameters of less than 0.08 mm and the organic matter content of the whole samples.

In general, the measured densities of this study are higher compared to the results found in the literature (Jacobin *et al.*, 1999; Kayhanian *et al.*, 2012). Jacobin *et al.* (1999) measured densities of 2200-2300 kg/m^3 and Kayhanian *et al.* (2012) obtained values of 1750-2250 kg/m^3, both measured on sediment captured in sediment traps during storm events. This suggests that, since the sediment in the Django Reinhardt detention basin had accumulated since 2006, the organic matter content had transformed hence changing the sediment's characteristics. However, the nature of stormwater particles does vary from place to place, and the deposits in the Django Reinhardt detention basin may simply be naturally dense.

Since it has not been possible to obtain the actual particle density from the storm event, the data on physical sediment characteristics obtained from the experiments in this study and previous findings for the basin were used to input particle properties as realistically as

possible in the CFD model and to evaluate the simulated results. Hence, for the purposes of simplicity, just three different densities 1700, 2100 and 2400 kg/m^3 were tested for sediment transport modelling in this study.

4.3 Preliminary 3D modelling of the full-scale Django Reinhardt detention basin

Having selected the Euler-Lagrange approach (DPM), the first stage of the study tested previous research results from studies carried out on small-scale detention basins or similar research studies. In terms of sediment transport modelling using DPM in stormwater detention basins, the most important aspect is the boundary condition for processing the interaction between the particles and the bed of the basin during the sedimentation /erosion processes.

4.3.1 Modelling strategy

4.3.1.1 Geometry and meshing

As shown in Figure 4-11, the Django Reinhardt detention basin is divided into two parts by an inner detention wall since the 2004 retrofit. Long-term observations have shown that there is almost no deposit in part two adjacent to the outlet. It is therefore thought that the influence on sediment settling in part two can be disregarded. In order to reduce the mesh cells, the basin simulation geometry was simplified by removing part two since the investigation aims to model sediment transport. The simplified geometry is shown in Figure 4-12.

A preliminary meshing test was carried out by Lipeme Kouyi *et al.* (2010). The hexahedral elements cell was satisfactory in this case. Thus the hexahedral element cell is used. Three different scale meshes (650000, 850000, and 1000000) were established for the independent mesh test. Preliminary simulations revealed a convergence issue with the coarse mesh, and the median and fine meshes showed no great difference while comparing flow pattern and velocity field. The median mesh was selected for all simulations to balance computational time and accuracy. The mesh sizes are variable due to the complex geometry of the basin, balancing the cell numbers and numerical modelling requirements. The mesh had a height of around 2.5cm near to the bed, increasing to 10cm near the free surface. The max xy cell measurements were 0.4m x 0.4m. The geometry model and some of the meshing details are shown in Figure 4-12.

Figure 4-11 The geometric simplification of the Django Reinhardt detention basin

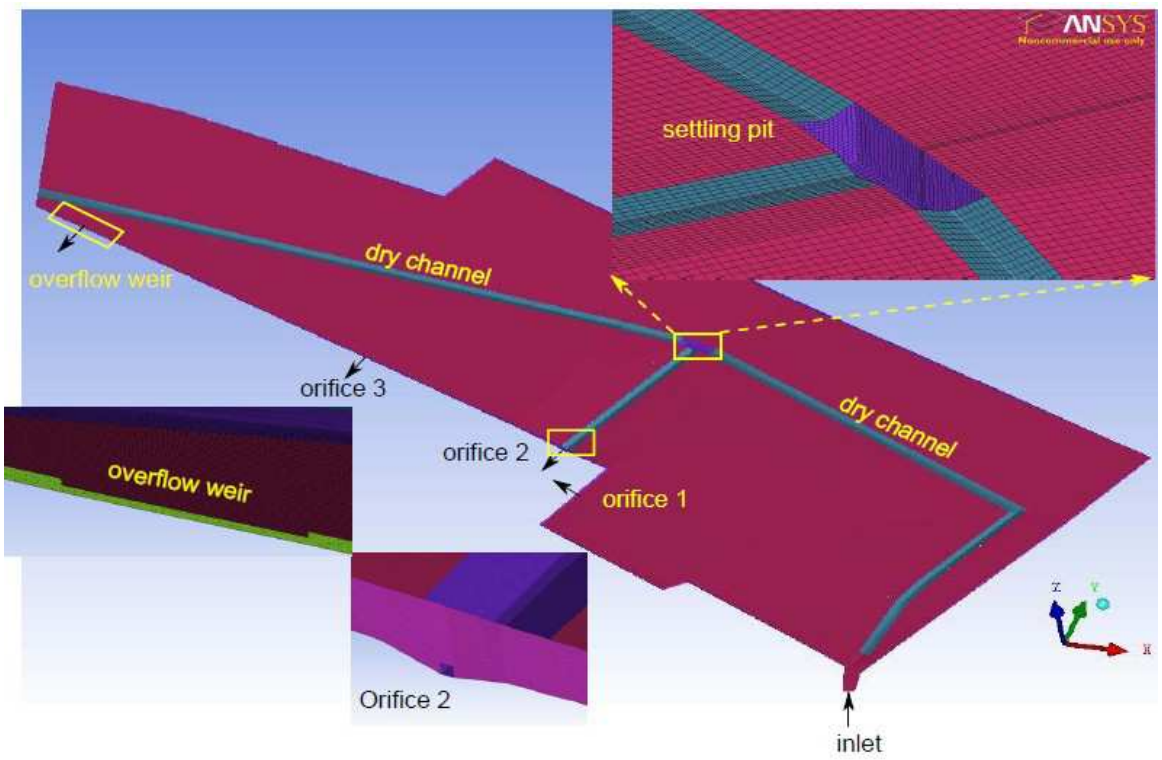

Figure 4-12 The simplified geometry of the Django Reinhardt basin and some of the mesh shown in detail

4.3.1.2 Flow condition selection

Preliminary simulation tests indicated that it is very difficult to simulate a complete storm event for hydrodynamics and sediment transport due to the complexity of the real basin and the limited computational hardware resources available in our laboratory. Therefore, steady condition simulations were performed for this basin. As described in the 'experimental site' section in chapter 3. Characterising flow pattern by water depth against inflow rate shows a transformed 'M'-shape curve for the storm events (Yan *et al.*, 2011) due to the retention by the inner detention wall and the limited maximum outflow rate controlled by a hydragate at the outlet (the outflow rate against the water depth h2 is shown in Figure 4-13). An example of a storm event occurred on 31/05/2007 and is shown in Figure 4-14. As Figure 4-14, the curve shows a back-and-forth disturbance (marked by a rectangle in Figure 4-14) around the inflow rate of 0.35 m^3/s (equal to the maximum outflow rate) with alsomt the same water depth at h1. It is speculated that the inflow rate of 0.35 m^3/s dominates the main flow pattern state in the basin, therefore the three inflow rates given in Table 4-2 were selected as the representative flow rates for steady flow simulation. It is thought that the free surface can be approximated as a plane wall. This reduces the computational time required because there is no need to capture the surface using VOF or other models.

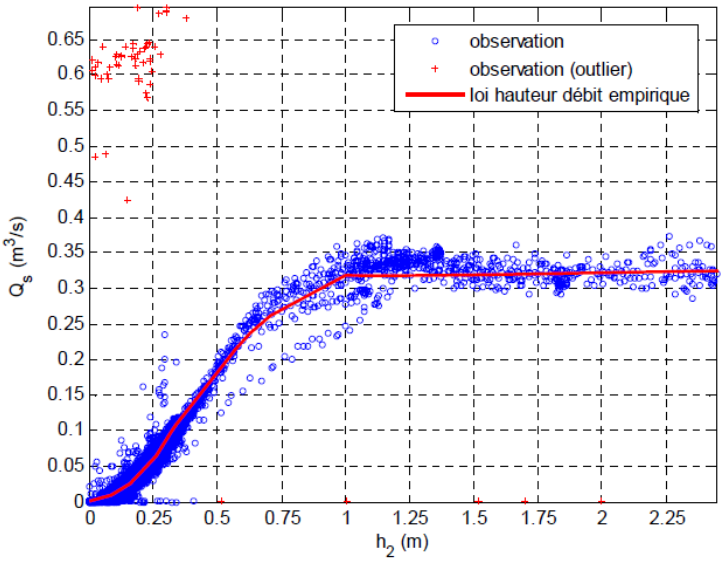

Figure 4-13 Changes in outflow rate against water depth h2 (adapted from Torres, 2008)

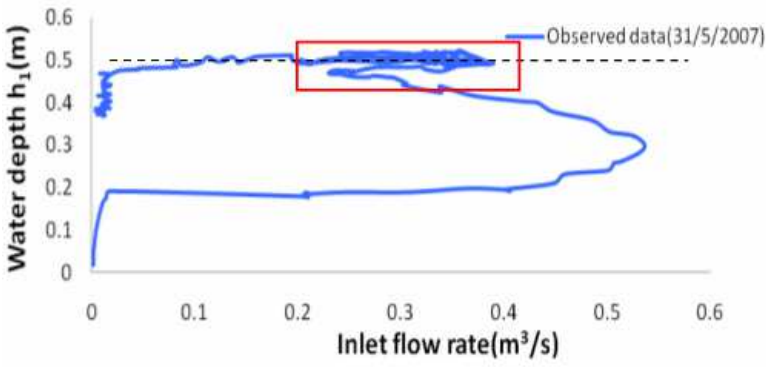

Figure 4-14 Inflow rate against the water depth h1 for the storm event 31/05/2007.

Table 4-2 Flow condition for representative steady simulation cases

Django Reinhardt Basin	DRB Case 1	DRB Case 2	DRB Case 3
Inflow rate (m^3/s)	0.25	0.35	0.45

4.3.1.3 Model setup

The renormalization group (RNG) *k-ε* model was employed to represent the turbulent phenomena. It is thought to be better than the standard *k-ε* model since it contains more refinement features. Whilst the standard *k-ε* model is a "high-Reynolds number model", the RNG *k-ε* model provides an analytically derived differential formula for effective viscosity that accounts for low-Reynolds number effects. These features make the RNG *k-ε* model more accurate and reliable for a wider class of flows than the standard k- ε model. Compared to the standard *k- ε* model and the RNG *k- ε* model, *RSM* (Reynolds Stress Model) is time consuming as it needs to solve more equations. Dufresne *et al.* (2009) and Mignot *et al.* (2011) tested the standard *k- ε* model, the RNG *k- ε* model and the *RSM* in various urban drainage structures (three combined sewer overflow chambers for solid separation and open channel junctions with low Reynolds number). They found that the *RSM* model did not offer any significant improvement on the results derived using the RNG *k- ε* model.

The inlet velocity is used for the inlet boundary condition. The three orifices and overflow weir are set as pressure outlet boundary. The free surface is treated as free-slip wall boundary without consideration of friction of air above the free surface.

4.3.2 Correlation between hydrodynamic behaviour and the spatial distribution of the sediment's physical characteristics

Three inflow rates were usedfor the fluid flow simulation. In terms of the full-scale detention basin, it is difficult to measure field flow parameters such velocity distribution due to the large domain of the basin, the high cost of the sensors and management difficulties. The hydraulic monitoring data available are the water depths in three locations inside the basin

(h1, h2 and h3, see Figure 3-4) and the inflow and outflow rates with a time step of two minutes. With a steady state simulation, the inflow rate and outflow rate are balanced after convergence, thus the flow rates cannot be used for validation. The free surface was treated as a free slip wall, i.e. the water depth is fixed and the monitoring water was used to determine the level of free surface. Therefore, the water depth data cannot be used for validation, either. In our research, the hydraulic performance was evaluated in relation to the spatial distribution of the sediment characteristics.

The analysis is based on the following assumptions:

- Sediment settles out in the low bed shear stress zones and low velocity zone, as found by numerous researchers (*e.g.* Stovin and Saul, 2008).
- When particles settle due to gravity, coarse particles generally settle faster than smaller ones (assuming that their density is identical and the influence of particle shape is disregarded) due to the higher settling velocity.

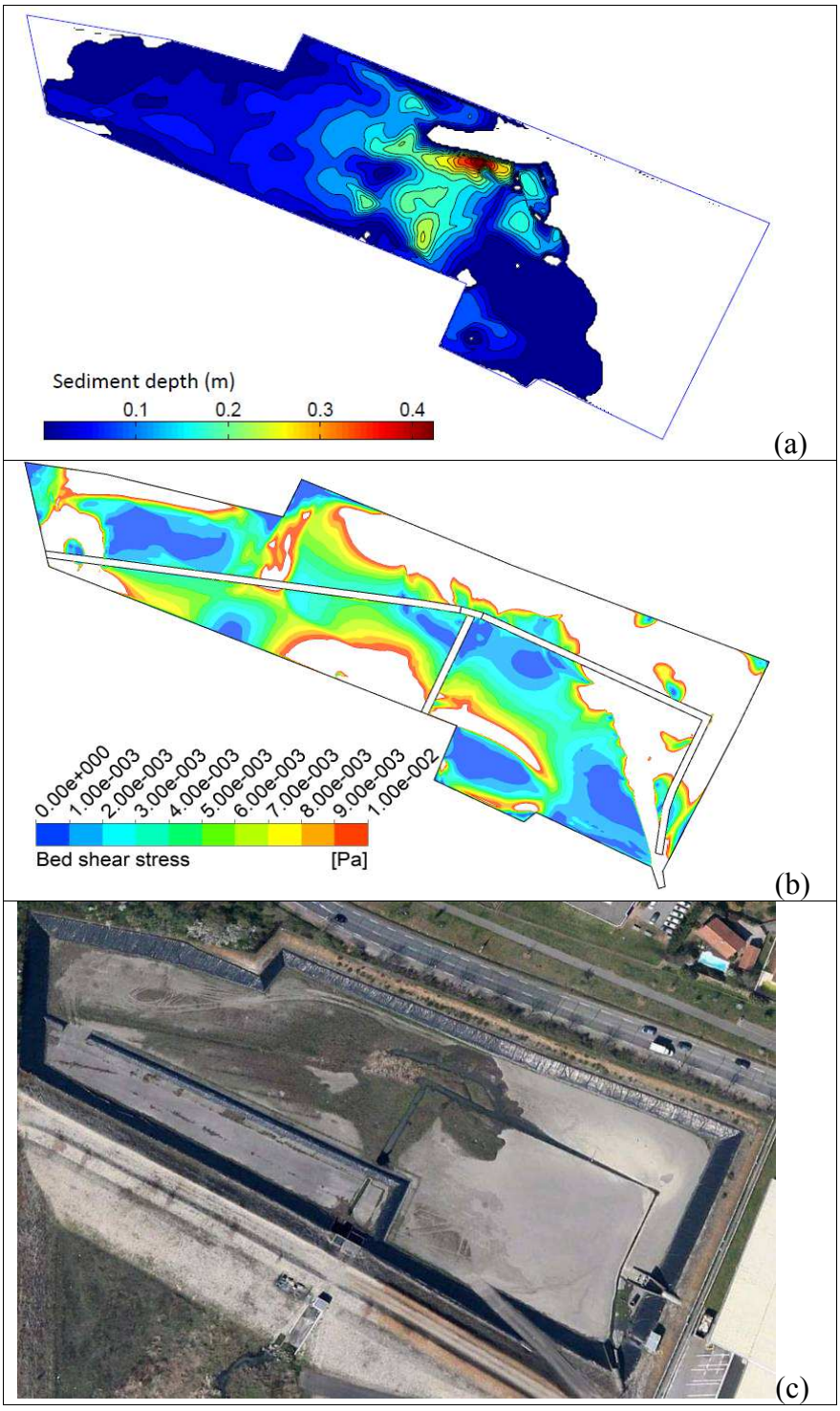

Figure 4-15 (a) Deposit spatial distribution, (b) BSS (<0.01 Pa) distribution and (c) Overhead view of sediment distribution of the basin (from Google maps, 2012)

Figure 4-15 shows that the BSS (<0.01 Pa) of DRB case two has a very similar profile to the spatial distribution of sediment in the basin and the photo from Google maps. Based on the assumption that there is a higher probability of sediment settling out in the lower BSS zone, and a comparison of BSS distribution and sediment depth distribution, the simulated BSS shows reasonable agreement in the central zone and the zone in front of orifice one

(see Figure 3-4), with lower BSS corresponding to higher accumulated sediment depth. In terms of the simulated results for the lower BSS zone close to the overflow weir (downstream), the deposit depth is thin. This is because the majority of sediment settles upstream. For another low BSS zone near the inlet (upstream), thin but coarse sediment was sometimes observed. This is because this low BSS zone is so close to the inlet flow jet that the sediment passes directly over this zone. There is is speculateation that just a small quantity of sediment settles in this zone. In fact, this zone is the downstream zoneaccording to the flow pattern analysis. This is one reason why so little sediment accumulates in this zone. For the higher BSS zone (>0.1 Pa, white zone in Figure 4-15b), there is almost no accumulated sediment. The sediment was flushed as soon as it settled.

Figure 4-16 shows that the low velocity (<0.04 m/s) zone near the basin bed and close to the free surface corresponds to deposit distribution in the basin. The analysis is similar to the low BSS distribution. In fact, BSS distribution shows a similar velocity distribution profile when comparing BSS distribution with the near bed velocity distribution.

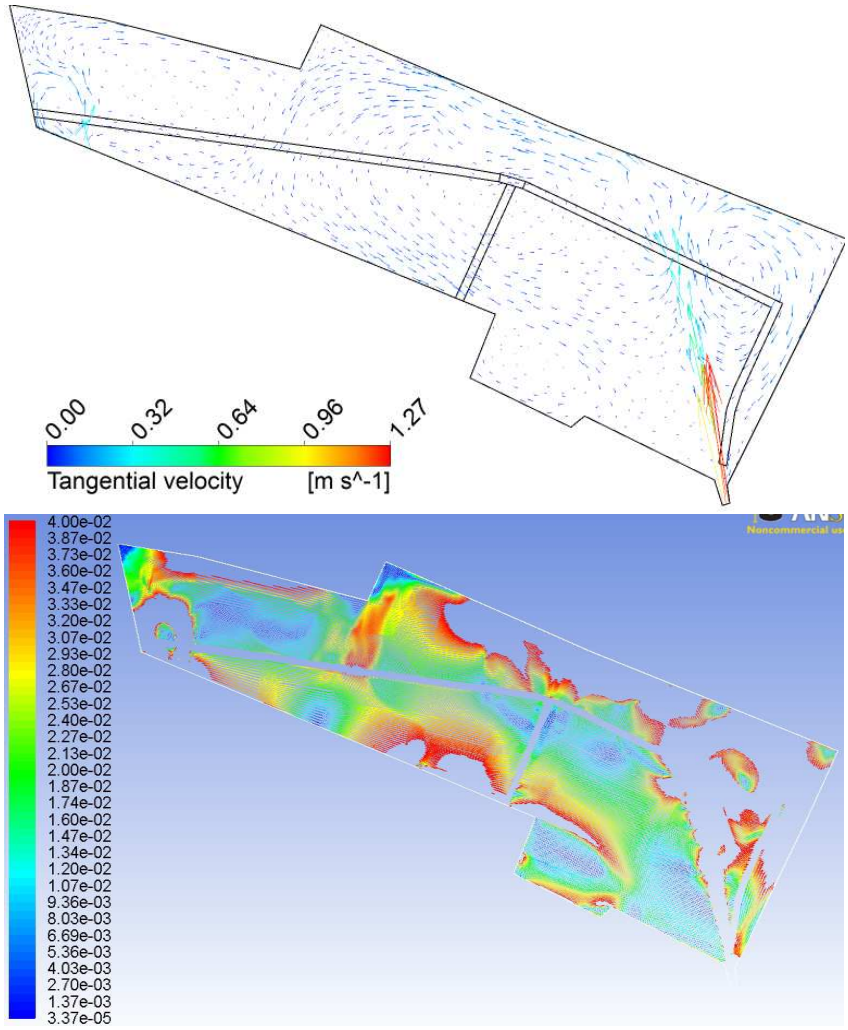

Figure 4-16 Velocity field of 5 cm under the free surface (top) and near bed low velocity field (<0.04 m/s) of Django Reinhardt basin (low)

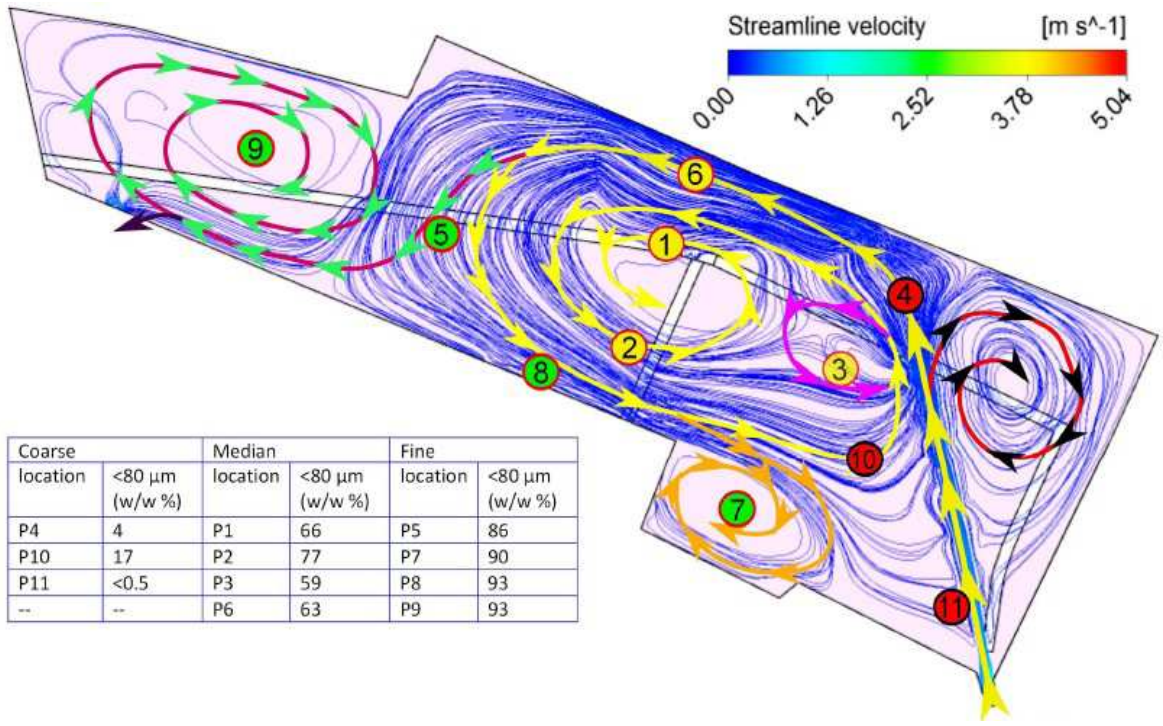

Coarse		Median		Fine	
location	<80 µm (w/w %)	location	<80 µm (w/w %)	location	<80 µm (w/w %)
P4	4	P1	66	P5	86
P10	17	P2	77	P7	90
P11	<0.5	P3	59	P8	93
--	--	P6	63	P9	93

Figure 4-17 Streamline of the fluid flow of DRB case two and the layout of the sample locations

The blue streamlines represent the flow pattern in the basin withinflow of under 0.35m^3/s. It describes the sediment transport path because the sediment was carried by the fluid flow. The thicker lines with arrows show the main flow patterns in the basin. The sample locations are also marked in Figure 4-17. As mentioned in the previous section, the results of the particle size measurement of the different samples show a quite different particle size distribution. The sieving analysis results were categorized under three groups: coarse, median and fine (with a fraction of less than 80 µm), shown in the table in the lower left-hand corner of Figure 4-17. The main flow pattern simulation accurately explains the particle size spatial distribution. Generally speaking, the coarse particles settle faster than the finer ones. Based on this hypothesis, it is easier to explain why the fine percentage in sample P10 is higher than sample P4. In Figure 4-17, the inlet flow jet can be seen to move along the locations P11and P4, location P10 is near to the middle zone of the flow jet between P11 and P04. It would therefore appear that the P04, P10 and P11 samples contain lower percentage of the fine fraction. It is logical that the percentage of fine fraction in sample P11 is less than in sample P4 because P11 is closer to the inlet. It is also logical that the percentage of fine fraction in sample P10 is higher than P4 because some of the deposit insample P10 comes from further downstream due to the recirculation although sample P10 is closer to the inlet than sample P04. Similarly, it is to be expected that sample P07 contains a high percentage of fine fraction due to the longer pathway for sediment transport. Although near to the inlet, it is actually in the downstream section of the flow pathway, and therefore only fine particles are carried along and settle down. This is the same case for samples P05, P08 and P09. The finest set of group samples' (numbers shown in green in Figure 4-17) is for the pure downstream group. For samples P01 and P02 near the end of the flow pathway, the percentage of the fine fraction is a little lower than samples P05, P07, P08 and P09 where are also at the end of the flow pathway because some of the sediment at P1and P2 comes from the upstream pathway, as for P6 and P03. Table 4-3 gives the measured accumulated sediment depth. It appears that the

sediment depth is inversally proportional to streamline density. As pointed out by Stovin and Saul (1994), the final pattern of sediment deposition depended not only on the velocity distribution, but also on the supply of sediment. Figure 4-18, shows that few streamlines arrive at locations P9 and P7, so few fine particles can arrive at these locations. This may explain why the deposit depth is thin at these locations. A lot of streamlines reach the centre of basin and are caught by the flow recirculation and therefore settle out in the region.

The flow pattern of transport obtained from the simulation result can be accurately displayed in the real basin above the accumulated sediment distribution (shown in Figure 4-18), and seem to be as expected.

Table 4-3 Sediment depth at the sampling locations

Locations	1	2	3	4	5	6	7	8	9	10	11
Sediment depth (cm)	42	30	27	9	10	12	6	3	3	3	1

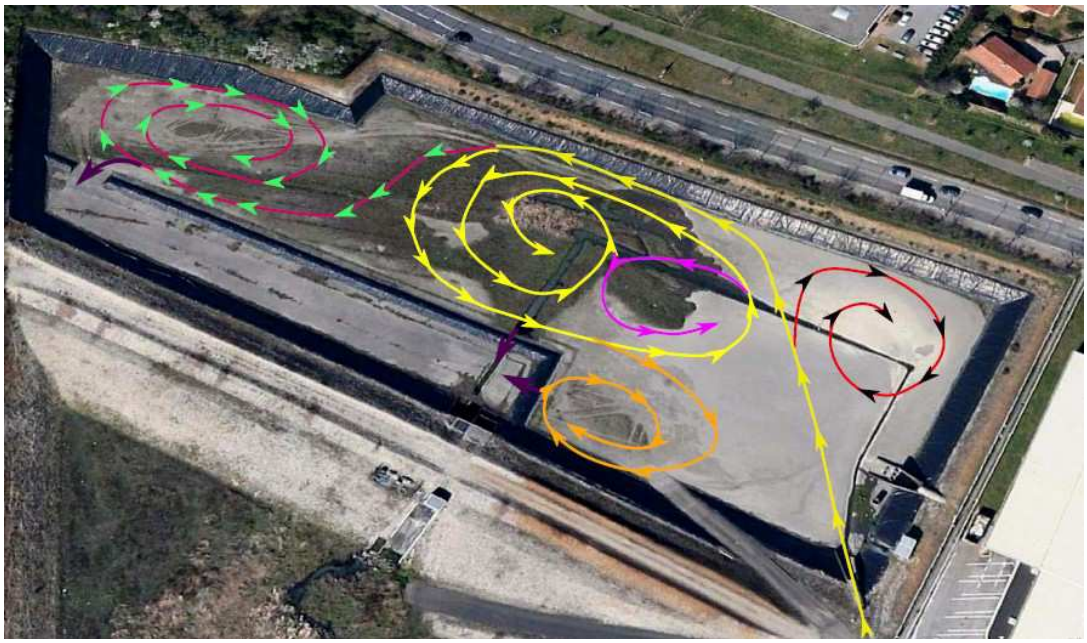

Figure 4-18 Deduction of simulated flow pattern on the real basin with the sediment spatial distribution

In comparison to the sediment accumulation distribution in years 2007 and 2012 (see Figure 4-19) which suggest the sediment had accumulated for about one year and six years respectively, it is speculated that there may be a main flow pattern in the basin due to the extremely similar sediment distribution in this basin. Based on the analysis above comparing observations, with the measurement of sediment characteristics (deposit zone, sediment depth spatial distribution, and particle size spatial distribution) and simulation results (especially, the BSS, velocity distribution and flow pattern), it could be hypothesised that the flow pattern for case two is the right main flow pattern for the basin. This would be logical because, as previously stated, the maximum outflow rate is limited to 0.35m^3/s by the hydraulic gate.

Figure 4-20 presents the bed turbulent kinetic energy (BTKE) distribution in the basin below the threshold of 4.5e-5 m^2/s^2. It shows a very similar distribution profile compared to the low BSS distribution. This may imply that the BTKE has a similar function to BSS as an indicator of deposition and deposition entrainment. In fact, Dufresne (2008) used the constant BTKE as the threshold for the bed boundary condition in a sediment transport simulation using the DPM approach. The threshold is determined by the comparing the observation sediment zone and the simulated BTKE result. However, the threshold is different, with 4.5e-5 m^2/s^2 in our case compared to the value of 1e-4-3e-4 m^2/s^2 observed by Dufresne (2008). It seems that the value is dependent on sediment characteristics.

Figure 4-19 Overhead view of sediment distribution on the bed of the Django Reinhardt basin from Google maps in 2007 and 2012.

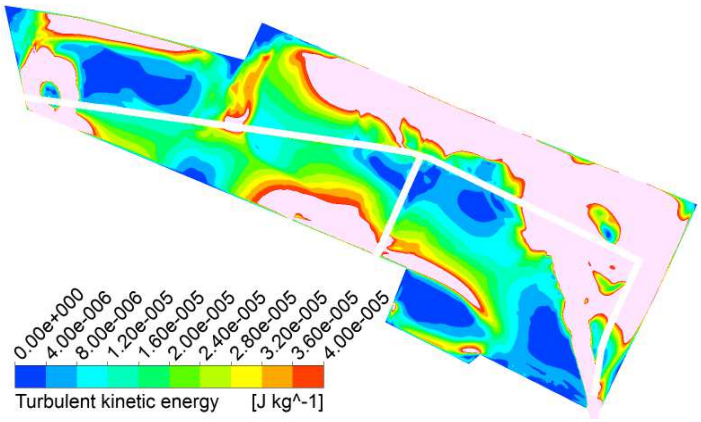

Figure 4-20 Low bed turbulent kinetic energy (<4.5e-5) distribution of DRB case two in the basin

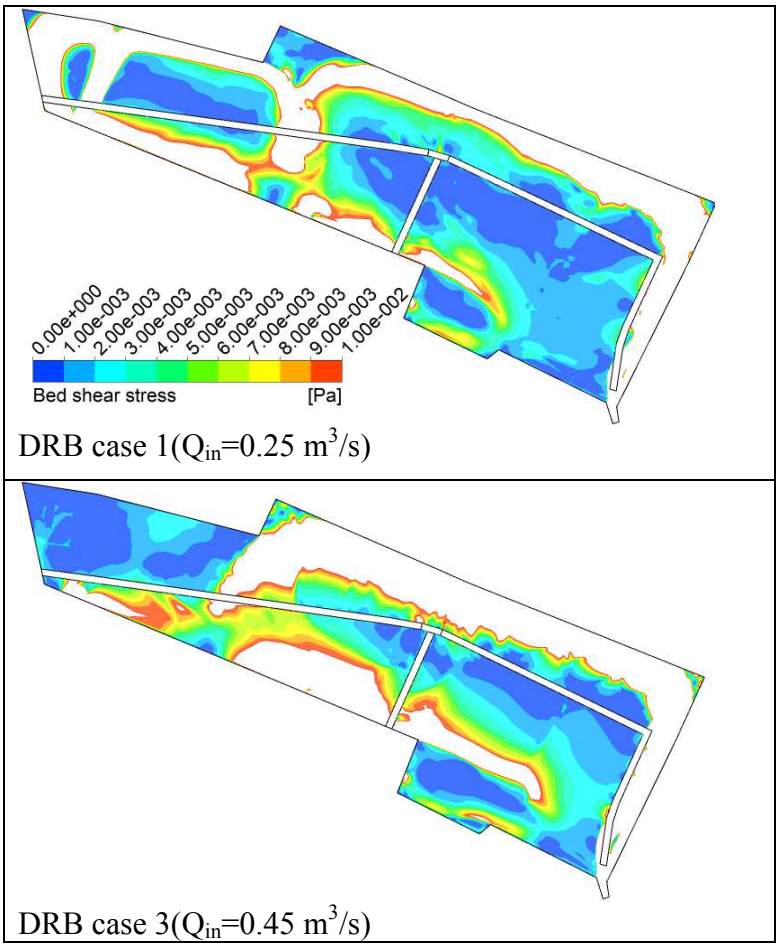

Figure 4-21 Bed shear stress in the Django Reinhardt basin in different inflow rates with an upper BSS limitation of 0.01Pa.

Figure 4-21 shows the low bed shear stress of the simulation results for DRB cases one and three. The profile distributions shown are quite different to the sediment spatial distribution, but still present the same lower BSS zone as in DRB case two in the zone close to the downstream overflow weir and the zone in front of orifice one for example (see Figure 4-15a).

DRB case 3 Qin=0.45 m3/s

Figure 4-22 present the streamline of these simulation cases with different inflow rates. Generally speaking, the flow streamlines indicate flow patterns in the basin. This means the streamline provides information on flow transport in the basin. Moreover, to a certain extent, streamline density roughly indicates the velocity of the flow field. This means that in a location with a high density of streamlines, flow velocity is high. Conversely, in locations with low streamline density, flow velocity is quite low. DRB case 3 Qin=0.45 m3/s

Figure 4-22, shows that all the cases have a similar large anti-clockwise recirculation around the centre of basin and a small clockwise recirculation in front of orifice 1 (labelled as o1 in Figure 4-22). Case 1 and 2 show a clockwise recirculation in the left part of basin near the overflow weir. Case 2 shows a different inflow jet direction from case 1 and 3. Moreover, case 2 shows a clockwise recirculation in the upper right corner of the basin. Overall, the simulated streamlines with different inflowsshow that the flow pattern in the basin depends on the inflow. The flow pattern leads to different hydraulic conditions which play a role in the sedimentation of particulate pollutants. Simulations were then performed to show the superposition of streamlines in order to gain insight into the flow conditions.

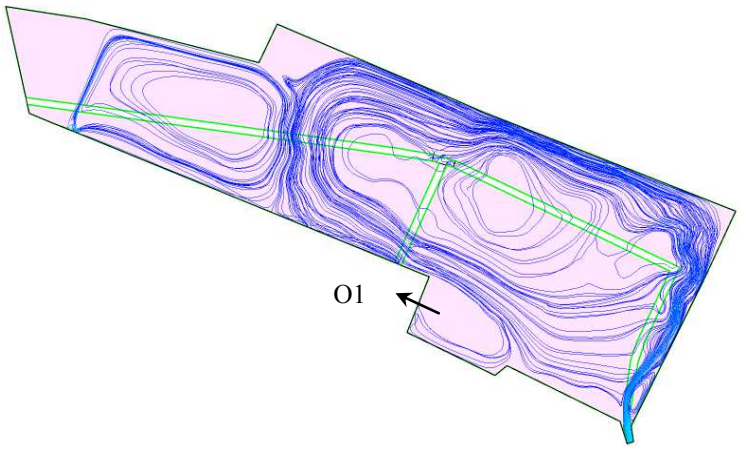

DRB case 1 Q_{in}=0.25 m^3/s

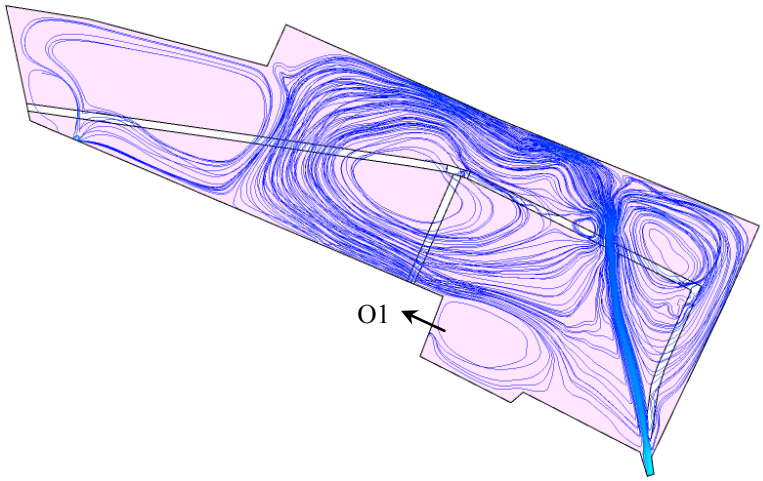

DRB case 2 Q_{in}=0.35 m^3/s

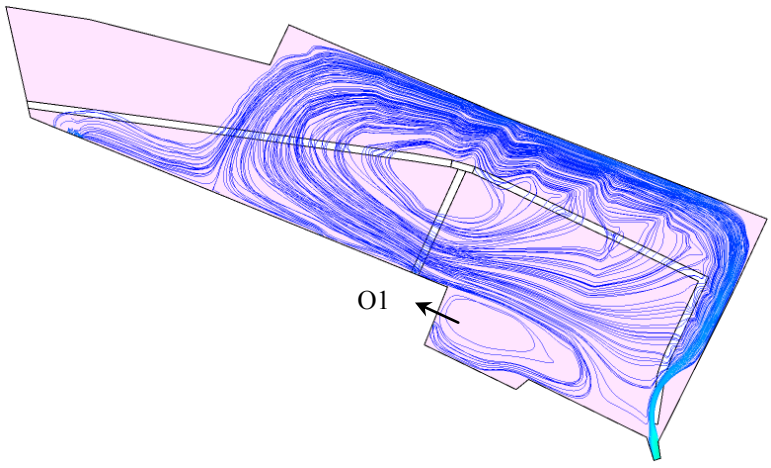

DRB case 3 Q_{in}=0.45 m^3/s

Figure 4-22 Streamline analysis of DRB case 1, 2 and 3.

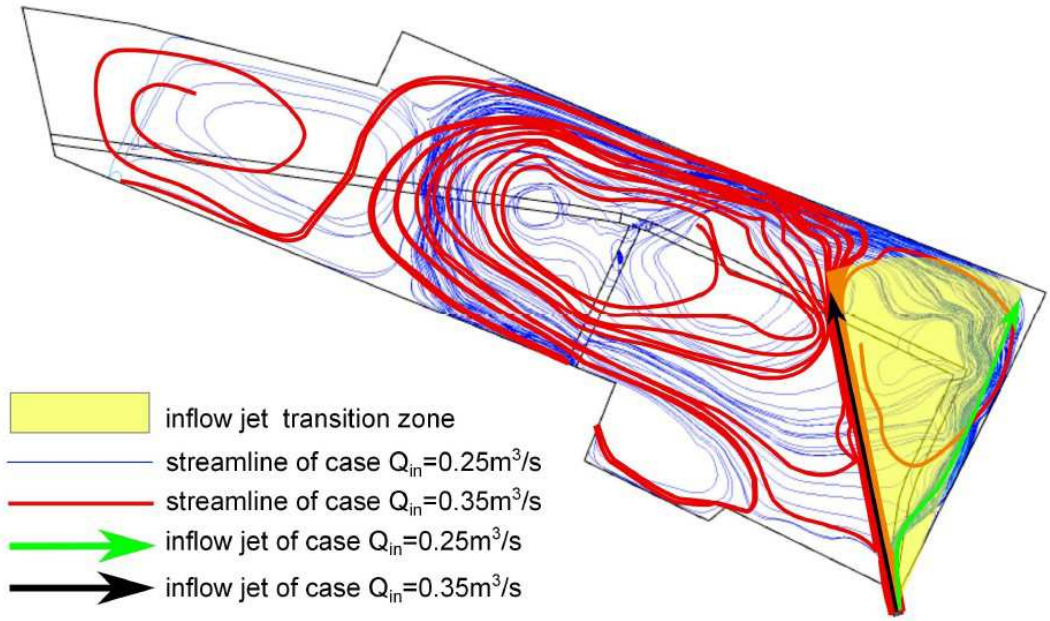

Figure 4-23 Superposition of streamlines of cases 1 and 2.

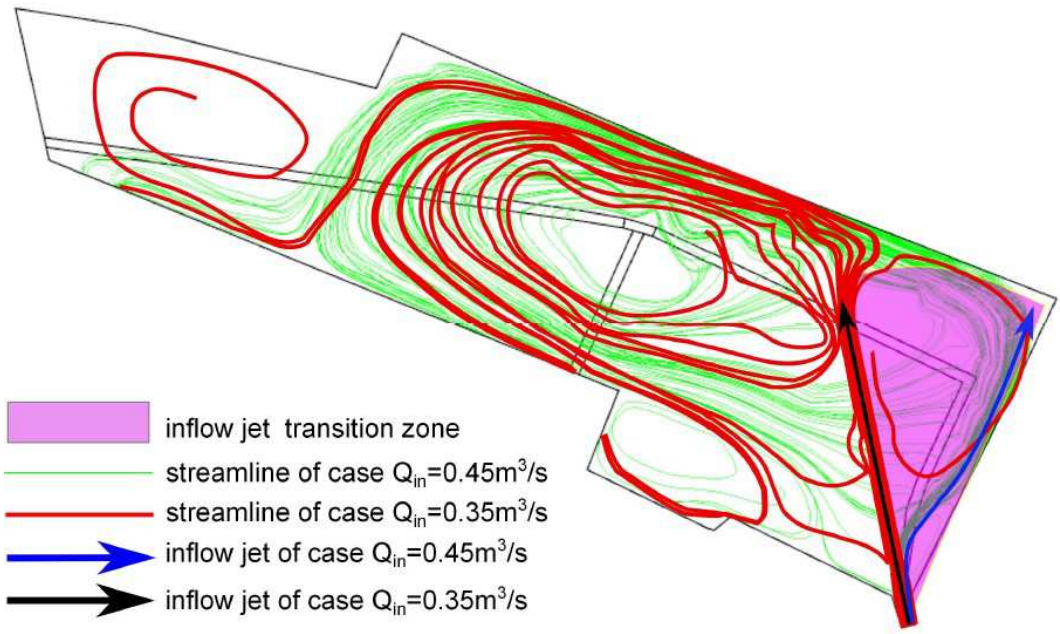

Figure 4-24 Superposition of streamlines of cases 2 and 3.

Figure 4-23 and Figure 4-24 show the superposition of streamlines for different simulated cases. Assuming that the rate of change of inflow is between 0.45 m^3/s to 0.25 m^3/s depending on the chosen flow condition for each case, Figure 4-24 shows that the inflow jet direction at the beginning and the end are almost the same. However, the inflow jet direction changes when the simulated results of case 1 are compared with those of case 2 or those of case 2 with those of case 3. It can be estimated from the simulated results, therefore, that if the inflow rate changes from 0.45 m^3/s to 0.35 m^3/s, the inflow jet (blue arrow line in Figure 4-24) changes

gradually within a sector zone to the direction of case 2 (black arrow line in Figure 4-24). Similarly, if the inflow rate changes from 0.35 m^3/s to 0.25 m^3/s, the inflow jet (black arrow line in Figure 4-23) changes gradually within the same sector zone to the direction of case 2 (green arrow line in Figure 4-23). Hence, it seems that the inflow jet changes in a small sector zone near the inlet according to variations in the inflow. Figure 4-22 shows that the inflow jet zone has dense streamlines; hence theoretically the sediment does not settle much in this zone. This analysis is consistent with observation and measurement. Almost no accumulated sediment can be observed in this sector zone near the inlet of the basin (see Figure 4-15a and Figure 4-15c).

Based on the analysis comparing observation, measurement and simulation, it was found that hydraulic simulations largely agree with the measured data. This may imply that the simplification of geometry and flow conditions (inflow rates, boundary conditions, etc.) is reasonable and acceptable. It also provides an alternative method for evaluating CFD modelling for full scale stormwater detention basins since it is difficult to obtain hydraulic measurement data. Case 2 was used to carry out the bed roughness influence test and sediment transport modelling, since it was most similar to the sediment spatial distribution and can therefore be considered as representing the main flow pattern in this basin.

4.3.3 Bed roughness influence on vertical bed turbulence kinetic energy profile

The effects of surface roughness on sediment distribution are of great importance as discussed by Papanicolaou *et al.*, (2001). The Django Reinhardt basin is covered with a concrete surface. Sediment has accumulated on the bed of basin, which results in bed surface roughness. BTKE boundary conditions were used for sediment transport modelling and therefore, it was important to evaluate the influence of roughness on the BTKE.

The equivalent grain roughness height was estimated by means of a relationship given by Hager (2010). The modified law of wall was used to model the roughness effects. The method used is described in detail in chapter 3. Table 4-4 gives the series of Strickler coefficients, K, and equivalent sand grain roughness height, k_s, for concrete (Graf and Altinakar, 2000).

***Table 4-4 Strickler roughness coefficient* K *and equivalent sand grain roughness height* k_s**

Roughness values	Ks1	Ks2	Ks3	Ks4
$K(m^{1/3}/s)$	75	65	55	50
k_s (m)	0.00040	0.00094	0.0026	0.0045

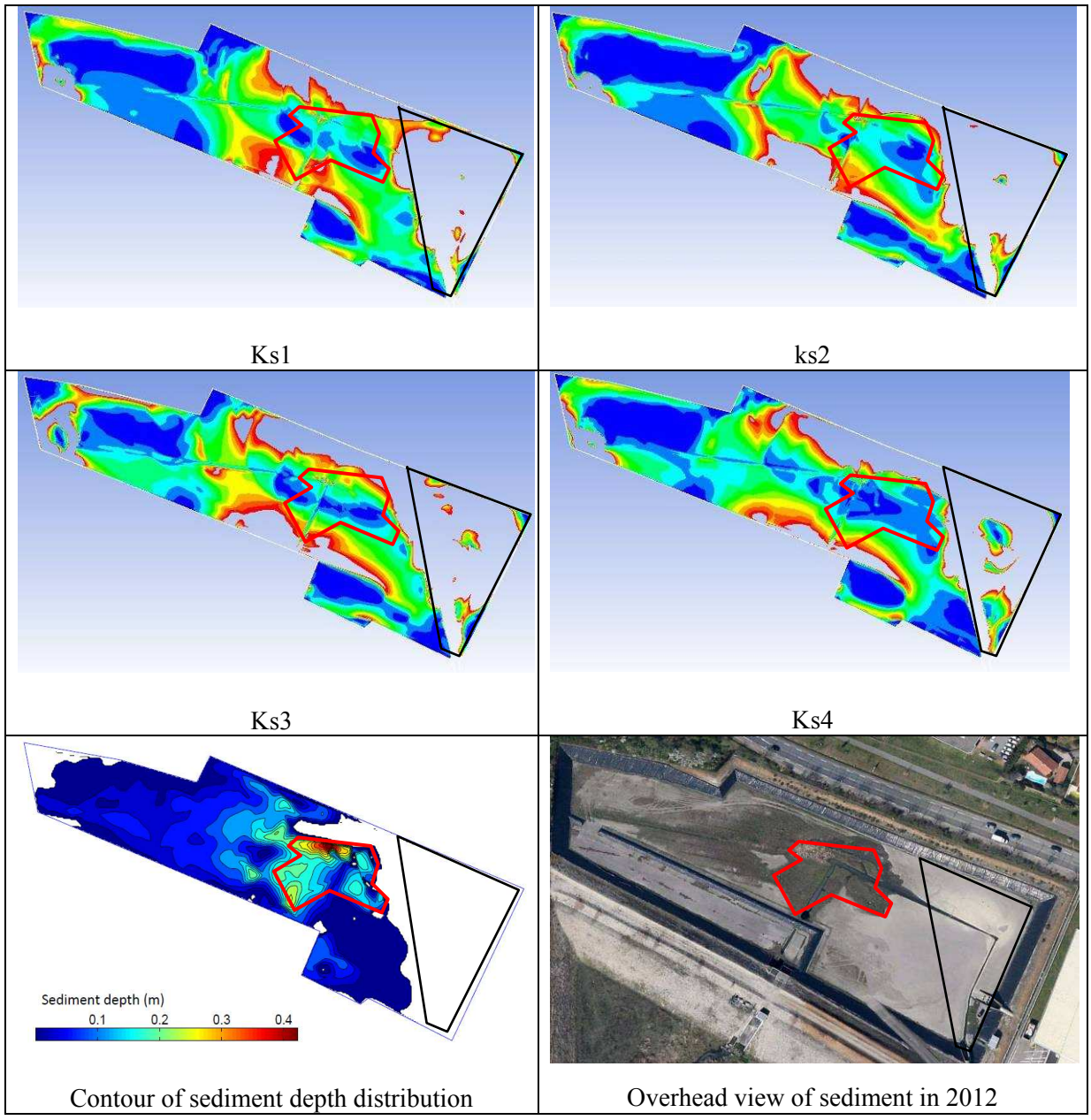

Figure 4-25 Similarity between observed deposition zones and simulated BTKE distribution (<4.4e-5= k_c) related to different surface roughnesses.

4 simulated cases for different bed roughness were performed with the same flow condition configurations of DRB case 2.

Dufresne (2008) showed that the distribution of bed turbulent kinetic energy (BTKE) below a critical value (1.0e-4 - 3.0e-4 m^2/s^2) corresponds well with the deposition zone in a pilot basin. Previous work in the Django Reinhardt basin (Yan *et al.*, 2011a) suggested that particle settling velocity (V_s measured with protocol VICAS – Torres, 2008) could be used to estimate the critical value to determine the particle state (*e.g.*, deposited or resuspended) based on the assumption that near bed turbulent kinetic energy has a significant influence on the motion of particle close to the bed. In that study, the V_{80} (=23.5m/h) settling velocity was used to estimate the critical value using the formula: $k_c=\xi v_s^2$, where k_c is the critical turbulent kinetic

energy and ξ is a coefficient that includes unknown factors (*e.g.* concentration, shape of particle, energy transferring rate, collision effect, etc.).

The simulated bed turbulent kinetic energy (BTKE) distributions with different bed surface roughness are shown in Figure 4-25Ks1, Ks2, Ks3 and Ks4 indicate the different surface roughness settings used in the simulation. Comparing the measured sediment spatial distribution found in 2011 and the overhead view observation of sediment made in 2007, all the simulations for BTKE distribution with a threshold showed similar outer contours for the preferential sediment zone except at the downstream corner near the over flow weir. This may be due to the fact tat the outer contour was slightly affected by surface roughness. It also shows that using the BTKE with an appropriate critical value makes it possible to identify the preferential sediment outer contour in the full scale detention basin. Out of all cases, Ks1 represents is most similar to observed results for the upstream blank part (shown in Figure 4-25 with trapezoid), while ks4 is most similar to observed results for the central thickness of sediment (shown in Figure 4-25 with a polygon). Assuming that a low BTKE corresponds to the thickest sediment layer, this might suggest that the sand grain roughness height for a sediment layer would be higher than that for bare concrete. There were clear differences in the outer contour zones, but the overall shape was similar. For example, all the cases showed almost the same low value BTKE zone in front of orifice 1 (see Figure 3-4 labeled with 'o1') which corresponds to observations made.

In order to further understand the effects of surface roughness on near bed turbulence, local vertical TKE distribution analysis was carried out at some specific locations. The positions of the local points are shown in Figure 4-26. Figure 4-27 (point 1, point 3 and point 4) shows that the near bed turbulent kinetic energy distribution is affected by surface roughness. In general, the vertical turbulent kinetic energy distribution shows a similar profile at almost all points and for all rough surfaces. The maximum beds turbulent kinetic energy was obtained close to the bed due to the influence of rough elements on the bed (see point 1, point 3 and point 4 in Figure 4-27). Figure 4-27 shows that a similar vertical profile was also obtained in an experimental investigation carried out by Dey *et al.* (2011). At point 2 vertical secondary currents were observed in the simulated results (see **Erreur ! Source du renvoi introuvable.**b). This might be the reason for the difference between the vertical TKE profile at point 2 and that at the other points. In fact, more vertical secondary currents above the gutter were observed when observing the gutter stream through the vertical plane. These were sensitive to the surface roughness.

The research results on the effect of roughness on BTKE suggest that modelling sediment transport in real storm water detention basin should take into account the bed surface roughness effects.

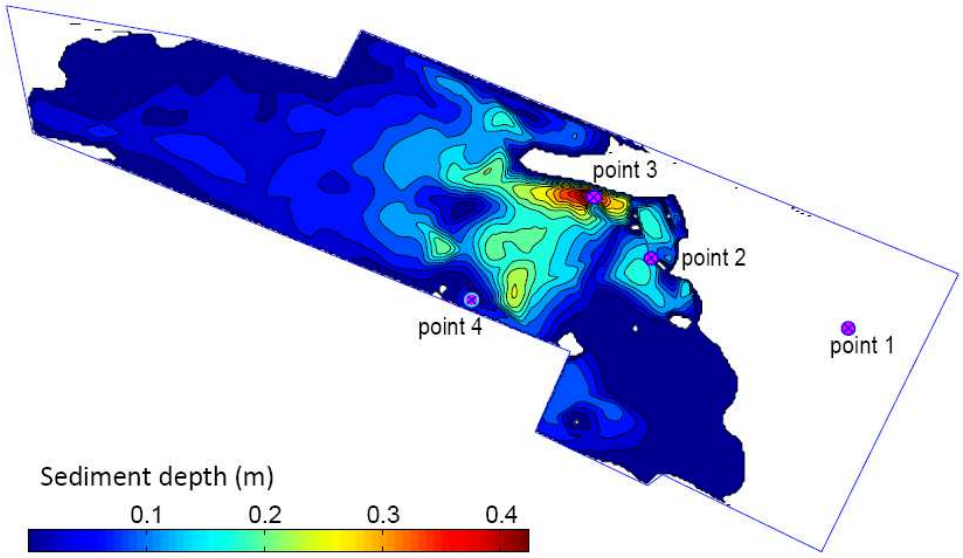

Figure 4-26 Vertical TKE distribution of points checked

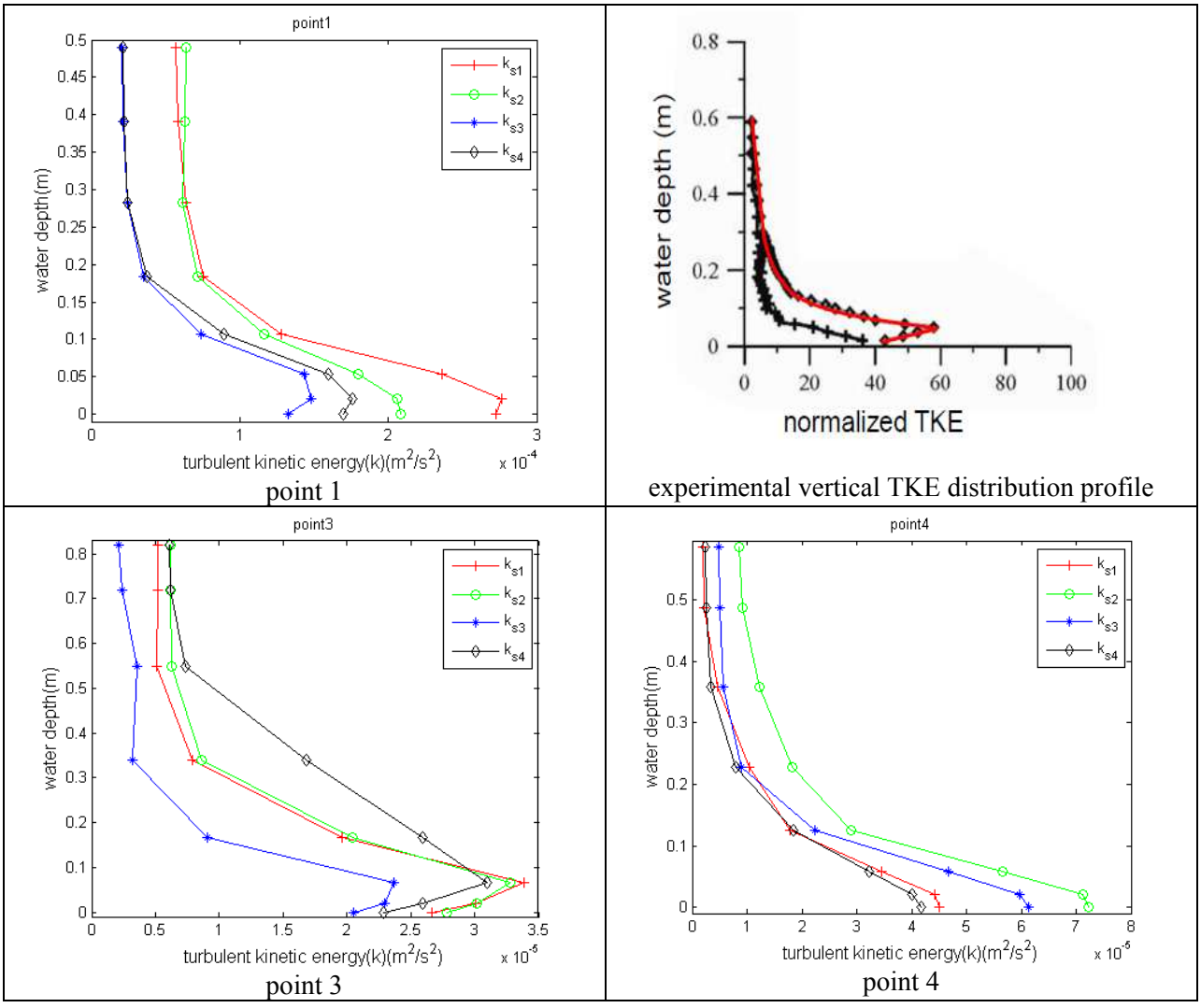

Figure 4-27 Experimental vertical TKE distribution profile adapted from Dey et al. (2011) and vertical TKE distribution for different roughness values (point 1, point 3 and point 4)

4.3.4 Sediment transport modelling with DPM

4.3.4.1 Particle tracking strategy

The aim of sediment transport modelling in detention basins is to predict the removal efficiency and sediment deposition zones in the basins. The removal efficiency predictions aim to find a way of improving pollutant abatement and of protecting receiving water bodies. The prediction of sediment deposition zones is done in order to create better strategies for basin management and maintenance, such as finding an appropriate frequency for deposit cleaning. This makes sense because the accumulated sediment affects removal efficiency: too much sediment accumulation reduces removal efficiency due to the effects of erosion.

As mentioned in chapter 2, in terms of sediment transport modelling for detention basins using DPM, the most important element is the bed boundary condition treatment for a particle arriving on the bed. Previous investigations have been carried out in small scale detention basins (Stovin, 1996; Stovin and Saul, 1998; Chebbo *et al.*, 1998; Adamsson *et al.*, 2003; Dufresne, 2008; Dufresne *et al.*, 2009; Zhang, 2009; Vosswinkel *et al.*, 2012). Chebbo *et al.* (1998) have used a stochastic approach, and other researchers have used one BSS threshold as the boundary condition in order to determine the particle settling state. For all kinds of particles, if the local BSS is larger than the given threshold, the particles rebound, otherwise, the particles settle. Stovin (1996), Adamsson *et al.* (2003) and Dufresne (2008) said that the threshold for a scale basin is in the range of 0.03-0.05Pa, while Vosswinkel *et al.* (2012) used Shields curve to estimate the BSS according to particle properties (density and diameter). Dufresne (2008) also used the BTKE as a boundary condition, and the critical value used for the scale basin was 1.0e-4 ~3.0e-4 m^2/s^2.

The final stage of the research would focus on the full scale basin, and the first step was to verify the suitability of available boundary conditions for the full scale basin.

Both the constant BSS and the constant BTKE were tested in the Django Reinhardt basin. A critical value of 0.03Pa for the BSS, as used by Adamsson *et al.* (2003) and Dufresne (2008), was applied into the full scale basin. A value of 0.01Pa was also tested by comparing obseved sediment distribution and the simulated BSS distribution (see Figure 4-15). For the BTKE, a value of 4.5e-5 m^2/s^2 was chosen after comparing the sediment distribution with the BTKE distribution in case 2. The BSS was estimated using the Shields curve and then tested. For the critical BSS and BTKE values, uniform particles sizes were used. These were based on the measurements taken by Torres (2008) and Becouze-Lareure (2010) using samples taken from the inlet and inside the basin with sediment traps during the storm events. There was some deviation between these measurements and the measurements performed for this study using samples from the accumulated deposits. The differences may be due to differences in sampling methods and the evolution of deposits in the basin. For this study, the campaign data used by Torres (2008) and Becouze-Lareure (2010) were used. The results from Torres (2008) and Becouze-Lareure (2010), were combined to give fine, median and coarse sizes (10 μm, 65 μm, 100 μm). These were chosen to perform simulations with critical BSS and BTKE, and a series of means particle distributions were chosen for the boundary conditions from the Shields curve. The particles sizes came from campaign measurement for a storm event (31/5/2007) collected using 15 sediment traps (Torres, 2008). The data are given in Table 4-5.

It should be noted that in Table 4-5, D_{10} here means the volume percentage, not the weight percentage.

Table 4-5 Mean particle sizes distribution (psd) of 15 trap samples from storm event 31/5/2007, adapted from Torres (2008).(D_{xx} = volume percentage)

v/v%	D_{10}	D_{20}	D_{30}	D_{40}	D_{50}	D_{60}	D_{70}	D_{80}	D_{90}	D_{100}
Diameter(μm)	15	26	38	50	65	82	106	146	241	923

Simulations were carried out for densities of 2400 kg/m^3 and 2100 kg/m^3 based on the deposit measurement and 1700 kg/m^3, from the literature (Ashley *et al.*, 2004) for density sensitivity test.

In order to account for turbulent dispersion effect, a stochastic model DRWM was used. The time scale factors C_L of 0.15 (by default in Fluent) and 2 (chosen by Dufresne (2008) that reflected the deposition zones in a scale basin better) were tested.

4.3.4.2 Removal efficiency and deposition zones

The simulated removal efficiencies of the basin are shown in Table 4-6 andTable 4-7, which show that when using a time scale factor of 0.15, all the tested boundary conditions captured all 100 μm particles and practically all 65 μm particles. For the 10 μm particles, the efficiencies were only slightly higher for 2400 kg /m^3 than for 1700 kg /m^3 particles. The efficiency of the BTKE boundary condition was in between the two critical BSS boundary conditions, for which a τ_c of 0.03 Pa gave the largest and 0.01 Pa the lowest efficiency. A density of 2100 kg /m^3 was used for simulation with the Shields boundary condition. And its simulated efficiency was 97.37% (with C_L=2).

These results, however, are not surprising, as the bed shear stress distribution and the bed turbulent kinetic energy distribution were very similar. The possible sedimentation zones with the BTKE boundary conditions were also larger than the critical BSS boundary conditions when using a τ_c of 0.01 Pa and smaller when using a τ_c of 0.03 Pa (data not shown here). In fact, the critical BTKE and critical BSS have a similar distribution (see Figure 4-15b and Figure 4-20), hence, the critical BTKE and the critical BSS boundary conditions are very similar, and the results depend on the BSS and BTKE thresholds.

Table 4-6 Simulated removal efficiencies with different bed boundary conditions (ρ=1700)

Particle properties		Simulated efficiency (%)			
Density (kg/m^3)	Diameter (μm)	BSS (τ_c=0.03Pa, C_L= 0.15)	BSS (τ_c=0.01Pa, C_L= 0.15)	BTKE (k_c=4.5e-5, C_L= 0.15)	BTKE (k_c=4.5e-5, C_L= 2)
1700	10	85.34	74.79	78.61	98.51
1700	65	99.99	99.99	99.98	99.74
1700	100	100	100	100	99.98
Means efficiency (%)		95.11	91.66	92.86	99.41

Table 4-7 Simulated removal efficiencies with different bed boundary conditions (ρ=2400)

Particle properties		Simulated efficiency (%)			
Density (kg/m^3)	Diameter (μm)	BSS (τ_c= 0.03 Pa, C_L= 0.15)	BSS (τ_c= 0.01 Pa, C_L= 0.15)	BTKE (k_c=0.000045, C_L= 0.15)	BTKE (k_c=0.000045, C_L= 2)
2400	10	87.42	77.80	81.05	96.66
2400	65	100	100	100	99.96
2400	100	100	100	100	100
Mean efficiency (%)		95.81	92.60	93.67	99.87

Changing the time scale factor from 0.15 to 2 significantly increased the efficiency of the basin for the 10 μm particles. This was probably due to the increased time spent in turbulent fluctuations, which made more particles travel away from the general flow direction. This also caused a small amount of 65 μm and 100 μm particles to escape the basin. It implies that the removal efficiency for small particles is more sensitive to the C_L than that of large particles. As mentioned in section 4.2, four storm events in June to September 2006 showed efficiencies of 93-94 % after sediment cleaning (Torres, 2008), and annual average of 57 % (2004-2010) gave normal values of between 33 % and 75 % (Gonzalez-Merchan, 2012). The lower annual average efficiency is caused by the erosion of accumulated deposits. When compared to the annual average efficiency, the modelled efficiency is much higher, but the mean modelled efficiency is close to single event efficiency measured after basin cleaning. This is reasonable because in the model, the basin is assumed to be empty and the effect of erosion is not included. However, it is not possible to determine the best simulation because the cases were modelled using steady conditions corresponding to conditions at one specific moment, while event efficiency or annual efficiency is calculated from one or many storm events.

In terms of settling zones, the boundary conditions also acted in very similar ways. From Figure 4-28 the settling zones when using BTKE boundary conditions are depicted, both for the results using a time scale factor of 0.15 and 2. The figures were ctreated by plotting the final location of each particle settled down. Only the results using particle diameters of 10 and 100 μm are shown, as the sedimentation zones of simulations done using particle sizes of 65 μm merely showed an intermediary stage between the two.

As can be seen from Figure 4-28, increasing the time scale factor increased the distribution of 100 μm particles, expanding the sediment zones. This result, however, was less significant for 10 μm particles, for which there was no deposit in the upper left corner of the basin when using the time scale factor of 2.

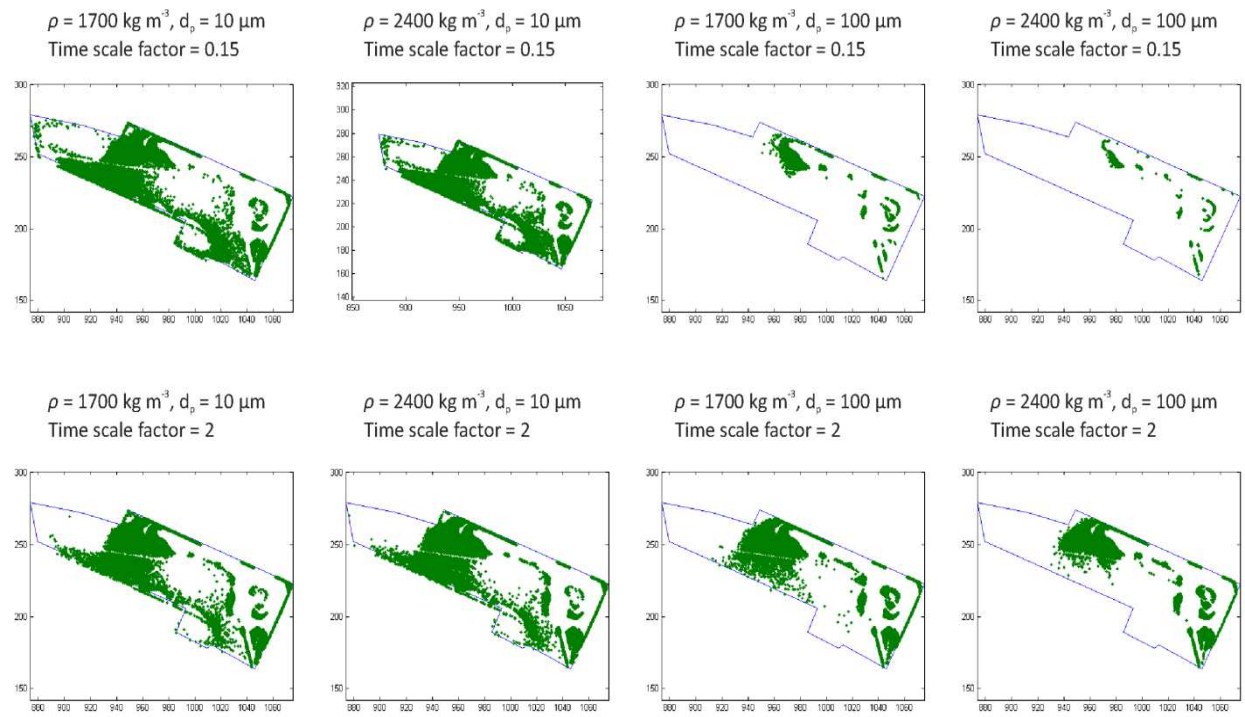

Figure 4-28 Simulated deposit zones using BTKE boundary conditions with different particle sizes and densities and using a time scale factor of C_L =0.15 and C_L = 2.

In the simulations, a significant amount of the particles settled in zones close to the inlet, which does not correspond to a significant deposit in the real basin.

The simulated zone created with Shields curve boundary conditions does not show model the deposit zone any better. As shown in Figure 4-29, the majority of particles settled in the location near the end of the inflow jet.

Figure 4-29 Simulated deposit zones using the Shield curve boundary condition with non-uniform particles sizes, the particle are shown as yellow dots

The discrepancy between the simulated deposit zones and observations may be caused by two reasons: the steady state configuration used in the simulation and limitations in the boundary conditions.

A real storm event is clearly an absolute example of unsteady conditions. The final deposition zones undergo a series of alternative processes of transport, settling and resuspension, so the deposit would probably be picked up after it had settled for the first time and and would move along the flow pathway acted on by the time-dependent effect. But in a simulation under steady conditions, this does not occur because the flow pattern is invariable and so the particle stays in the first location in which it settles. This suggests that more realistic simulations should be performed using unsteady conditions.

Furthermore, the critical BSS or BTKE boundary conditions used for all particles is overestimated in the case of small particles. It is thought that the small particles settled prematurely when transported along the flow pathway because of the use of a single value for BTKE or BSS as a settling boundary condition. Generally, this critical value derives from experimental measurements or simulations done by comparing the sediment zone with measurements or with a simulated BSS/BTKE. In actuality, this value is the upper limit for BSS or BTKE in the distribution zone. That is why in the simulated deposit zone, there is almost no particle settlement in the centre of the basin. All particles settle when they arrive at the edge of the BSS or BTKE zone, as is shown in Figure 4-15 and Figure 4-20, where particles are deposited the upstream in the flow pathway at the low BSS or BTKE zone.

As mentioned in Chapter 2, critical BSS for deposition τ_{cd} is often used in species models as a constant value for special cases. Sometimes due to the lack of measurement data, this value has been used as a calibration parameter. This works sometimes because in a species model, the sediment is treated as continuous phase fraction with a median particle size. This fraction

is termed concentration. Concentration combines the behaviours of a group of particles in motion. From the statistic point of view, τ_{cd} is a statistic mean value for special group of particles, balancing out the higher or lower values of different particles' deposition. This value depends on the characteristics of particles. This may be the reason why there is no a universal τ_{cd} that can be applied to all sediments. However, this critical value may not be true in the DPM approach. In the DPM approach, sediment is treated as an individual particle. Using a critical value for all the different particles seems to lead to overestimation or underestimation of deposition. The critical value is, in fact, the upper limit for the low BSS or BTKE distribution zone, and should correspond to the largest particles. In the previous experiments, this value was used for all particles (Adamsson *et al.*, 2003; Dufresne, 2008). This is why using the critical BSS or BTKE often leads to overestimation of removal efficiency. Thus, more precise values for different particles should be used.

Taking an estimated BSS from the Shields curve provides different values for different particles, and it works better than a constant BSS in small scale basin with non-cohesive sediment. However, it does not work well in full scale basin, such as in this case. The reason may be because the sediment in this case is more cohesive, and the Shields curve was developed based on experimental data with non-cohesive particles (Shields, 1936).

4.4 Improvement of boundary conditions for sedimentation modelling with DPM

4.4.1 Introduction

As discussed in the previous section, neither the fixed BSS/BTKE values nor the varying BSS calculated from the Shields curve work well in the full scale basin. This means that the main sediment zone in the centre of basin cannot be predicted accurately. It is thought that smaller particles settle prematurely when they arrive at the edge of sediment zone. In fact, this is also observed in a scale basin. It is, therefore, necessary to develop new more appropriate boundary conditions that overcome this drawback.

Turbulence plays an important role in settling and entrainment during the sedimentation processes. Particles settled when the local BTKE is less than a corresponding threshold that depends on the particle properties. This means that large and heavy particles need more turbulent energy to maintain them in a state of suspension. Based on this hypothesis, a new formula was devised to estimate this threshold for different particles according to their settling velocities, which is able to represent all the other properties such as density and size by taking their inner relationships into account. The formula was based on the theory that, since a small particle corresponds to a small BTKE threshold, its transport is likely to be longer and it would probably settle downstream in the flow pathway. In order to apply, this formula needs to be used for non-uniform particle size. This proposed formula was tested first as a boundary condition in a scale basin, then in a full scale basin.

4.4.2 Tests carried out in a small scale basin with a steady state DPM

The proposed formula was tested using the results from experiments carried out in a scale basin by Dufresne (2008), primarily for their simplicity and the availability of experimental data.

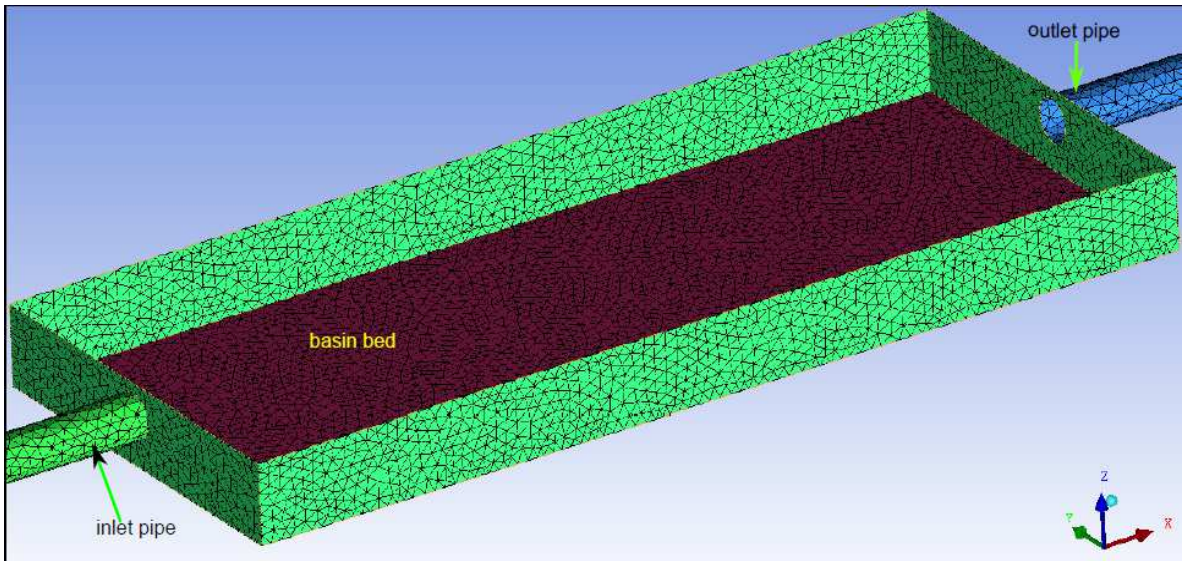

Figure 4-30 Computational tetrahedral mesh for small scale basin (Dufresne, 2008)

Steady conditions with an inflow rate of 3L/s were selected for the test. Dufresne (2008), showed that a tetrahedral cell mesh was better than hexahedral for this simulation, since it requires less computational cells as compared to the hexahedral cells. The tetrahedral cell elements were used. Three different scale meshes 10000, 50000 and 80000) were tested for mesh sensitivity. A 50000 tetrahedral cell mesh was then used for all the simulations, to provide the best balance between computational time and accuracy. The mesh is shown in Figure 4-30. The *k-ε* turbulent model was used for turbulence modelling, as suggested by Dufresne (2008), as it had already given satisfactory results. The other boundary condition configurations used for fluid flow simulation were as follows:

- Inlet: velocity inlet with a inflow rate of 3 L/s
- Outlet: pressure outlet
- Free surface: symmetrical boundary
- Side wall and bed: no-slip condition with standard wall function

The DPM modelling configurations were as follows:

- Injection: surface injection at the inlet boundary with a total of 7200 particles, this is enough to ensure numerial error is low due to the number of particles injected
- Particle density: 1034 kg/m^3
- Non-uniform particles: defined by the Rosin-Rammler equation, according to the data in Table 3-5, the calculated parameters are: n=4, d=810 μm, D_{min}=350 μm and D_{max}=1400 μm. The Rosin-Rammler curve is shown in Figure 4-31

- Max Number of steps: 50 000
- Stochastic modelling: discrete random walk model (DRWM), with CL=0.05, 0.15, 1, 2
- Inlet and outlet boundary condition: escaped
- Side wall boundary condition: reflected
- Bed boundary condition: BTKE estimated using the proposed formula according to the particle properties, carried out with UDF, a fixed BTKE boundary with a value of 2e-4 m2/s2 was also tested for the purpose of comparison.

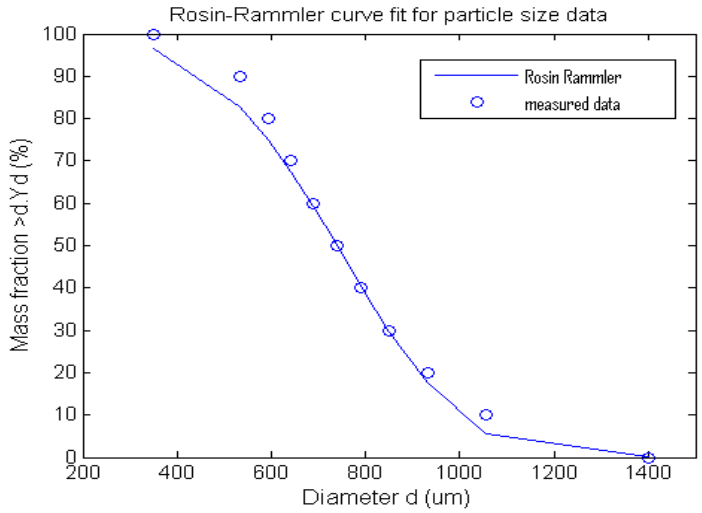

Figure 4-31 Rosin-Rammler curve fit showing the cumulative size distribution of particles

Figure 4-32 shows the velocity field of the basin on a horizontal plane at 9.5 cm from the bed. When compared with observed values, the simulation can predict the clockwise recirculation at the centre and the small anti-clockwise recirculation at the left upstream corner accurately.

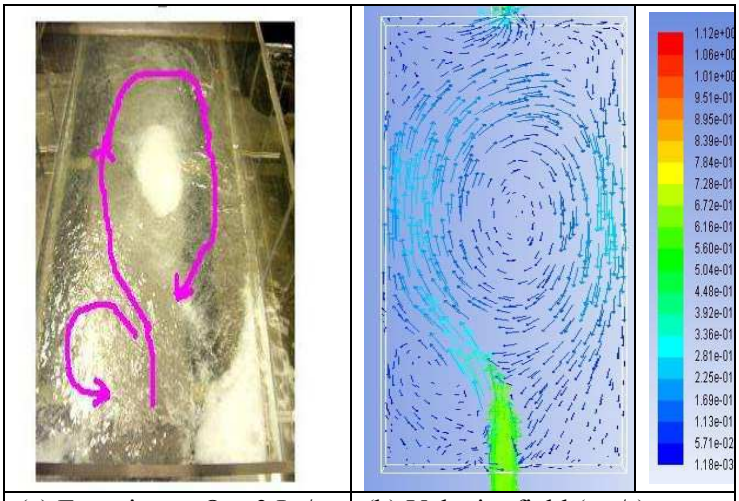

(a) Experiment Q_{in}=3 L·/s	(b) Velocity field (m·/s)

Figure 4-32 Comparison between (a) experimental sediment transport (Dufresne, 2008), and (b) simulated velocity field from* k-ε *model at the height of 9.5 cm from the bed with the inflow rate of 3L/s.

The simulated sediment zones are shown in Figure 4-33 . From the figure, we can see that the proposed BTKE boundary conditions predict a similar deposit zone to the fixed BTKE boundary condition. Both of them appear to have the same sensitivity to the time scale factor C_L: a larger C_L value lead to more widespread particle distribution. This appears to be logical, since a large C_L means a longer velocity fluctuation transport time which takes the particle away from the average velocity trajectory. It seems that the C_L value of 2 shows the best level of agreement with sediment zone prediction with the tested values, and a larger C_L value than 2 does not improve the prediction of sediment distribution in the central sediment zone.

Boundary cond.	Experimental deposits zone	Simulated deposits zone			
		C_L=0.05	C_L=0.15	C_L=1	C_L=2
Fixed BTKE		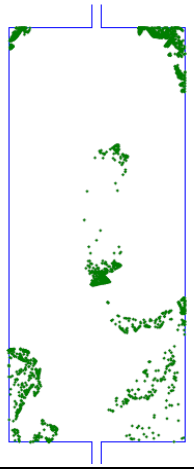	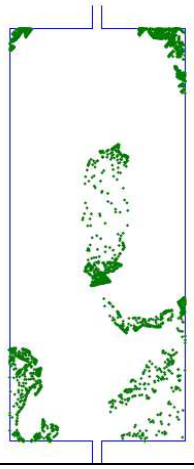		
Proposed BTKE		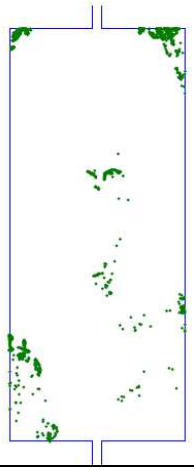	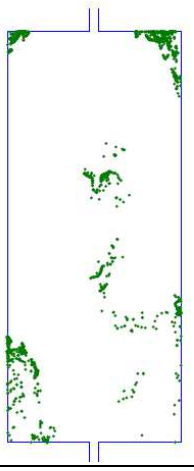	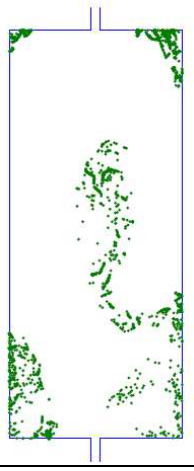	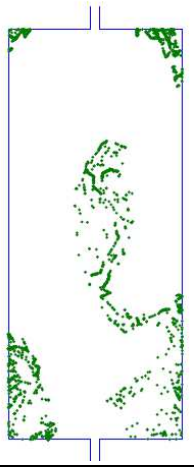

Figure 4-33 Comparison of sediment deposits zone between experimental observation and simulated deposit zones using bed boundary condition of fixed BTKE and using the proposed BTKE formula with different C_L values

Table 4-8 shows the experimental and simulated efficiencies. Compared to the experimental results, all the simulation cases overestimate the removal efficiency. The time scale factor C_L of DRWM appears to be a positive contribution to efficiency, the larger the C_L value, the higher the simulated efficiency. However, the simulated efficiency with the proposed BTKE bed boundary conditions predicts efficiency much better than that with the fixed BTKE, when compared to the experimental data. However, both of them overestimate the removal efficiency. Hence, the proposed BTKE is better than the fixed BTKE. Another advantage of

the proposed BTKE method is that it does not need to be compared with observation in order to determine a threshold for the BTKE as is required for fixed BTKE boundary conditions. This could be useful for predicting sediment transport where there is not experimental data or observed data for sediment zones to use as a reference.

Table 4-8 Comparison of experimental and simulated removal efficiency using bed boundary conditions of fixed BTKE and the proposed BTKE formula with different C_L values.

Boundary cond.	Experimental Efficiency (%)	Simulated Efficiency (%)			
		C_L=0.05	C_L=0.15	C_L= 1	C_L= 2
Fixed BTKE	33±5	67.61	62.88	71.52	74.19
Proposed BTKE	33±5	53.99	54.01	53.32	64.80

4.4.3 Tests in the full scale basin using a steady state DPM

Due to the scale effect and the more complex conditions in a real detention system, in general, it remains difficult to apply the results obtained from small scale basin to the full scale basin. The feasibility of the proposed BTKE boundary formula was therefore then tested in the Django Reinhardt basin based on the flow simulation results of DRB case 2.

The non-uniform particle size distribution is presented in Table 4-5, and it is the same as that used for the previous DPM modelling, i.e. it uses Shields curve boundary conditions. The density used was 2100 kg/m^3. For the purpose of comparison, the fixed BTKE (k_c=4.5e-5 m^2/s^2) boundary condition was also simulated with the same configuration. Due to the lack of an appropriate settling formula for estimating a settling velocity in accordance with the sediment properties in a selected sewer system, it was difficult to use a formula to estimate the settling velocity in the detention basin. Furthermore, the available values for settling velocity, as measured with the VICAS protocol, only give the relationship of maximum velocity for values below a certain fraction of mass (Chebbo *et al.*, 2003; Chebbo and Gromaire, 2009). A clear relationship between settling velocity and particle size has not yet been found. Therefore, an assumption had to be made in order to be able to use the proposed formula (equation (3.81) in Chapter 3) to estimate the BTKE corresponding to different sized particles. It was assumed that settling velocity increases with particle size over a certain density.

The measured results from the storm event on 31/05/2007 performed by Torres (2008) were chosen due to the complete nature of the data-set for measured particle sizes and settling velocity results across the 15 sediment trap samples. Within these samples, the particle sizes were measured by the Laser diffraction analysis and settling velocities were measured with the VICAS protocol in laboratory. The non-uniform particle sizes and the corresponding settling velocities are given in Table 4-9. Here V_{10} - V_{100} are the mean velocity of the 15 sediment samples. In order to estimate the BTKE with the proposed formula (equation (3.81) in Chapter 3), a settling velocity was used that corresponded to the particle sizes listed in Table 4-9, for example, particle size d_{10} corresponds to settling velocity V_{10}.

Table 4-9 Settling velocities measured in the storm event 31/5/2007 with 15 sediment trap samples, adapted from Torres (2008).

v/v%	V_{10}	V_{20}	V_{30}	V_{40}	V_{50}	V_{60}	V_{70}	V_{80}	V_{90}	V_{100}
Settling velocity (m/h)	0.88	1.85	3.06	4.57	6.55	9.23	13.27	21.64	35.23	57.46

The efficiency from the simulation calculated using fixed BTKE and the proposed calculated BTKE were 99.8% and 98.45%, respectively. It should be noted that in the simulations, some particles were always suspended (reported as *incomplete* in the simulation results). In the simulated domain, a maximum particle iteration steps of 6e+8 was set for particle tracking. These particles are captured by recirculation and remain in suspension, thus are ultimately considered to have settled as deposits by the programme. The simulated efficiencies were higher than the annual mean efficiency of 57% and the annual range of 33%-75% during 2004-2010 (Gonzalez-Merchan, 2012). However, it is close to the mean removal efficiencies of 93%-94% for single storm events after basin cleaning (Torres, 2008). It is thought that this simulation of sediment transport with steady DPM over-predicted efficiency because it did not take the time-dependent effect of erosion into consideration. An unsteady state DPM coupled with unsteady fluid flow simulation should, therefore, be performed.

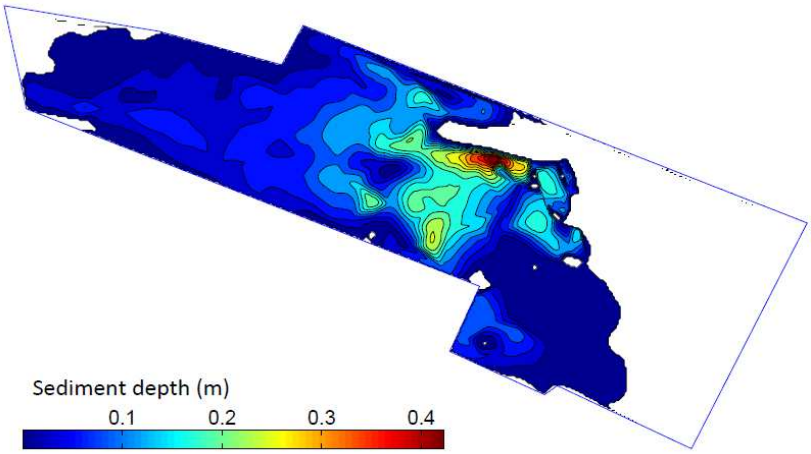

(a) measured sediment spatial distribution

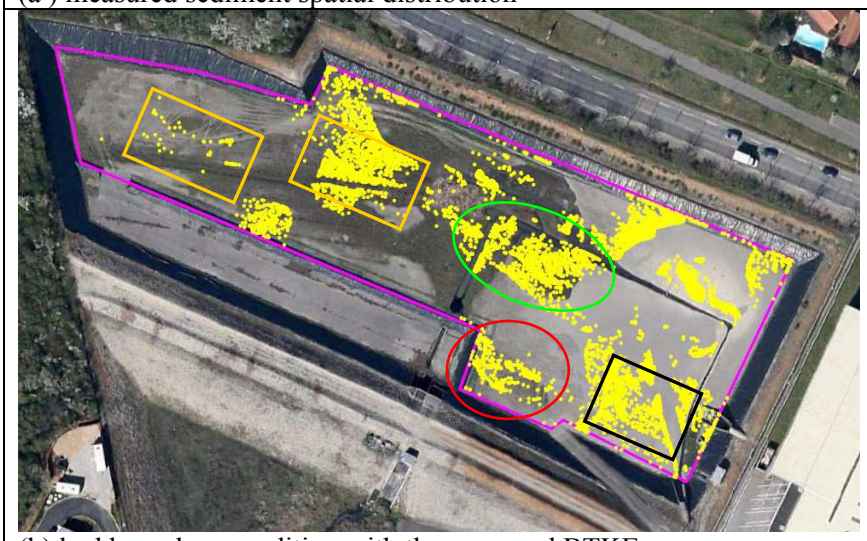

(b) bed boundary condition with the proposed BTKE

(c) bed boundary condition with fixed BTKE (4.5e-5 m^2/s^2)

Figure 4-34 Comparison between observed and simulated deposit zones using different boundary condition with non-uniform particles (shown in Table 4-10)

Figure 4-34 shows the simulated deposit zone with fixed BTKE and the proposed BTKE boundary conditions. Compared to the simulated results obtained with a fixed BTKE (shown in Figure 4-34c), the proposed BTKE boundary conditions were able to predict the main deposit zones in the centre of basin and in front of Orifice 1, as shown in Figure 4-34b with dashed line ellipses. The thin deposit zone near the outlet and the inlet were also predicted, as shown in Figure 4-34b and marked with the rectangules. From the point of view of sediment distribution prediction, the proposed BTKE formula is capable of identifying the most likely deposit zone in full scale basins.

4.5 Conclusions for chapter 4

A comparative analysis of the measured and simulated sediment characteristics spatial distribution and flow shows that there may be a main flow pattern in the Django Reinhardt detention basin. This main flow pattern has a representative inflow rate equal to 0.35 m^3/s which corresponds to the maximum outflow which is regulated by the hydro-regulator.

Where there is a lack of measured data to validate a flow simulation, the spatial distribution of sediment characteristics may provide an alternative way of checking the flow pattern.

The BTKE distribution has a similar function to BSS distribution in predicting the deposit zones in full scale detention basin. In general, in a zone with low BTKE there is a higher probability that sediment may settle. However, due to a lack of sediment transport information, the method proposed here is unable to describe the build-up of sediment. Sedimentation depends on both the flow conditions and the sediment transport characteristics. Near bed turbulence is influenced by the surface roughness.

It was not possible to predict sediment zones in the real Django Reinhardt basin using fixed BSS/BTKE boundary conditions because using a single threshold for all particle sizes allows small particles to settle too early. Fixed BSS/BTKE boundary conditions overestimate removal efficiency as they do not take the time – dependent effect of erosion into consideration. The Shields curve boundary does not work well in full scale basins in sewer systems either. This is because the Shields curve was calculated based on experiments carried out with non-cohesive particles, while particulate pollutants in sewer systems are predominantly made up of cohesive materials.

The proposed formula for calculating the BTKE boundary conditions is capable of identifying the preferred deposit zones in both small scale and full scale detention basins. This proposed method for estimating the BTKE threshold for different particles should be easier to use as it is not necessary to determine the BTKE by comparing it with observation, which is required when using a fixed BSS/BTKE. However, the proposed method for establishing BTKE boundary conditions overestimates predicted efficiency. Sediment transport modelling using a transient DPM clearly shows better simulated results than modelling done using a steady state DPM even when using the same boundary conditions.

Chapter 5 Sediment transport under unsteady conditions

The available bed boundary conditions have only been developed for uncoupled steady DPM modelling. Adamsson *et al.* (2003) concluded that these kinds of boundary conditions are suitable for steady flow conditions. These kinds of boundary conditions cannot account for dynamic settling and erosion due to the time–dependent effect (unsteady condition), found in real basin systems. The preliminary testing of full-scale detention basin modelling using DPM suggests that the time-dependent effect should be taken into account by combining unsteady flow simulation with an unsteady DPM approach. A method was therefore developed to represent the dynamic settling and erosion processes by coupling unsteady flow simulation with unsteady DPM. The method was first tested in a small-scale basin. This both reduced the computational time consumed and made it easier to validate the method using the available experimental data.

The method for dynamic sedimentation with DPM was described in chapter 3. Details about the method developed can found in that section.

In this section, the proposed method will be applied to two scale basins from Dufresne (2008) and Vosswinkel *et al.* (2012). A preliminary simulation was performed to evaluate the feasibility of using the method in a pilot basin (Dufresne, 2008), and further model parameters were examined in a transient flow condition (variable flow pattern and variable recirculation in the basin) basin because there is more experimental data available for validation (Vosswinkel *et al.*, 2012).

5.1 Preliminary test in a rectangular basin with permanent recirculation

5.1.1 Model setup

The experiment has already been described in section 4.2. The sediment transport modelling based on the flow simulation results is presented in section 4.4. Since the flow condition is a quasi-steady state, the steady flow condition was used instead of unsteady flow condition. Thus the simulation was configured forsteady flow simulation coupled with unsteady particle tracking. The particle size distribution was defined as Rosin Rammler distribution, as described in section 4.4. A total of 144360 particles, with 10 different sizes, were injected in one injection at the inlet section of the basin. The particle time step is 5 ms, and the maximum number of particle iteration steps was 50000 for each particle time steps. The bed boundary condition for particle dynamic settling and erosion was defined using the method proposed in chapter 3 and implemented using a UDF. Four different deposit conditions were tested, as shown in Table 5-1. It should be noted that as it is a preliminary test, this simulation does not model the complete experiment process which lasts for about 20 minutes, since the flow conditions are considered to be quasi-steady..

Table 5-1 Bed boundary condition test configuration

	A: settling condition	**B:** entrainment condition	Initial entrained velocity
Case 1: fixed BSS	BSS=0.03 Pa	Shields curve#	Hu and Hui's formula*
Case 2: varying BSS	BSS=Shields curve#	Shields curve#	Hu and Hui's formula*
Case 3: fixed BTKE	BTKE=0.0002 m^2/s^2	Shields curve#	Hu and Hui's formula*
Case 4: varying BTKE	BTKE: $k_c = \xi v_s^{\,2}$	Shields curve#	Hu and Hui's formula*

*: please refer to equations (3.84)-(3.85) in chapter 3;

#: please refer to equations (3.75)-(3.78) in chapter 3.

5.1.2 Deposition zone in the basin bed

Figure 5-1 shows the step-by-step evolution of sediment transport in the basin. The unsteady processes are accurately represented. Figure 5-2 shows the simulated deposition zones with particle tracking in steady flow conditions (b) and unsteady flow condition coupled with unsteady DPM (c). In the steady DPM, the particles in the centre of the basin are not accurately represented. Using the proposed method under unsteady DPM, the particles accumulated at the centre of the basin are accurately represented, mainly because the particle re-entrainment under unsteady conditions is taken into account by the proposed method.

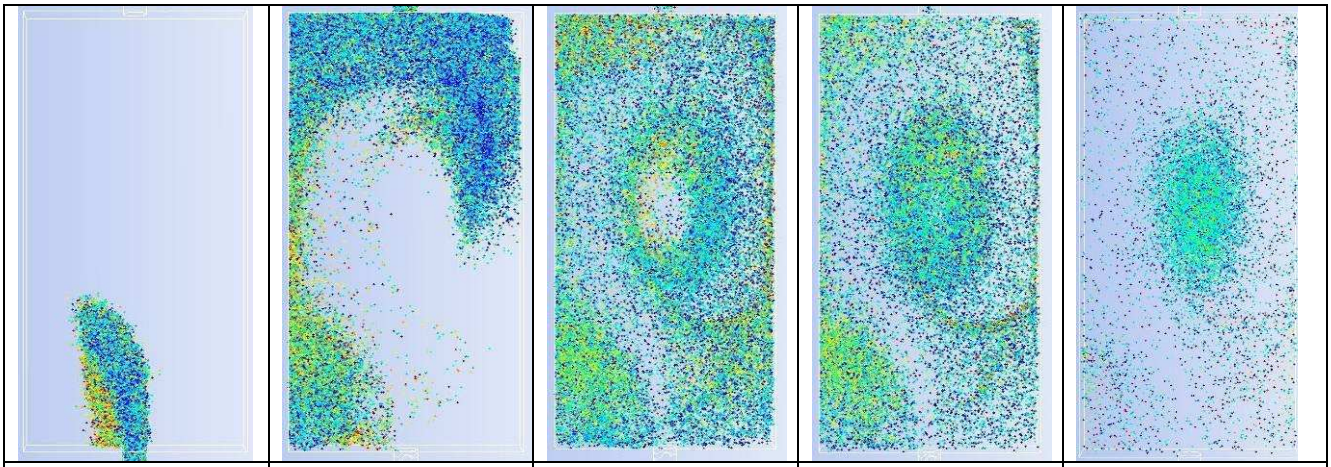

Particle discharge jet	t = 2s	t = 8 s	t = 40 s	Final deposition

Figure 5-1 Evolution of sediment transport with the varying BTKE boundary condition

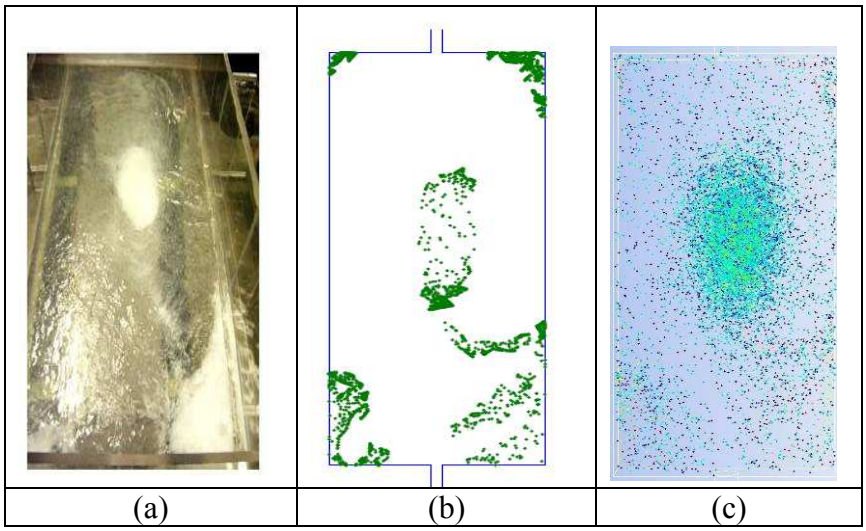

Figure 5-2 Comparison between (a) experimental deposition zone (Dufresne, 2008), and (b) deposition zone simulated using fixed BTKE boundary condition under steady flow conditions (C_L=0.15) and (c) deposition zone simulated using the proposed dynamic sedimentation method with the varying BTKE boundary condition.

Figure 5-3 shows the simulated deposition zones using the proposed dynamic sedimentation method with different boundary conditions. All conditions can identify i) the deposit zone at the basin centre similar to the experimental deposit zones except bed boundary condition 'trap', ii) the deposition zones in the left and right-hand upstream corners. The varying BSS and varying BTKE boundary conditions more accurately represent sediment spatial distribution than fixed BSS and fixed BTKE. Varying BSS and varying BTKE accurately represent the central deposit zone. However, the simulated deposit zone in the right-hand upstream corner does not appear to be dense enough compared to experimental observations. Figure 5-4 shows the spatial distribution of particle concentration on the basin cutting plane. This spatial concentration can then be used to estimate the thickness of sediment accumulated over the long term if a series of events are simulated over a long period of time.

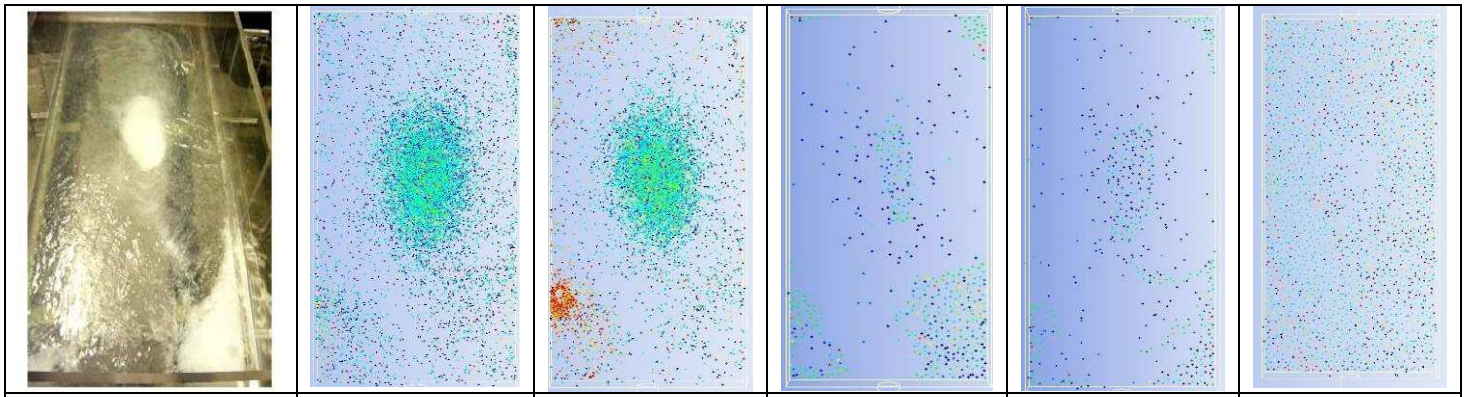

Figure 5-3 Comparison between (a) experimental deposit zones, (b) ~ (e) simulated deposit zones using the proposed dynamic sedimentation method with different boundary conditions, and (f) simulated deposit zones with the trap boundary condition

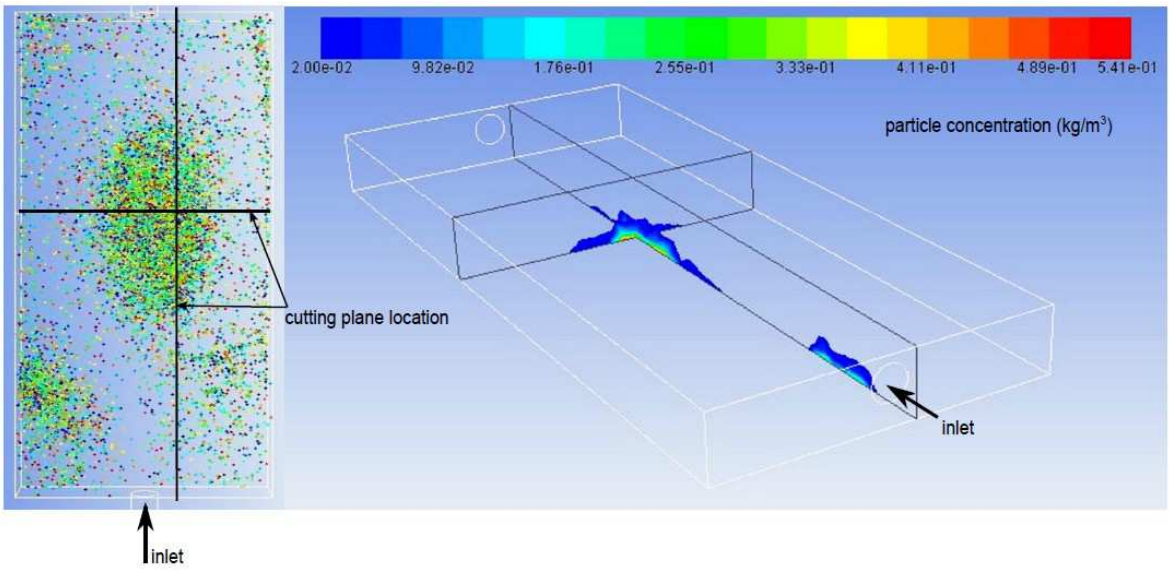

Figure 5-4 Particle spatial concentration distributions in the basin by vertical cutting plane

5.1.3 Removal efficiency

Removal efficiency η is defined by the equation (5.1), wherein m and M are the masses of particles settled out and injected at the inlet respectively.

$$\psi = \frac{m}{M} \tag{5.1}$$

Table 5-2 Experimental and simulated removal efficiency in the basin

	Experiment	Varying BTKE	Varying BSS	Fixed BSS	Fixed BTKE	Trap
Removal Efficiency (%)	33±5	28	22	47	46	88

The simulated efficiencies with different boundary conditions were shown in Table 5-2. Modelling with the bed boundary condition 'trap' largely overestimates the efficiency of sedimentation compared to the experimental data: 88% compared to 33%. Fixed BSS and fixed BTKE also overestimate removal efficiency. However, the overestimation is much lower than with the trap condition. The varying BTKE and varying BSS boundary conditions underestimate removal efficiency. However, varying BTKE most accurately predicts efficiency (close to the lower limit of the uncertainty interval) compared to the other conditions. Furthermore, it is possible to calibrate the coefficient ξ in equation (3.81) to obtain a better fit with the experiment data. Of the four boundary conditions (listed in Table 5-1), fixed BSS and BTKE need to be determined based on the comparison between the simulation results and the experimental observations. It is unfeasible to use this method in practice as observed data is unavailable. Varying BSS and varying BTKE are determined using formula, so they are easier to use if the sediment properties are available.

This simulation test demonstrated that the proposed dynamic sedimentation method is capable of representing sediment transport, settling and entrainment in unsteady flow conditions. It has showed potential capability for modelling sediment transport in detention basin over a complete storm event. The results for varying BTKE and BSS show satisfactory predictions of both deposit zones and removal efficiency. The sediment transport modelling results under unsteady DPM show that both removal efficiency and deposition zones are more accurately predicted than that under steady DPM conditions, as shown in the previous section. This may suggest that the unsteady sediment transport modelling should be used in order to accurately predict the removal efficiency and sediment zones in detention basins.

5.2 Preliminary test in a basin with variable inflow jet and recirculation zones

5.2.1 Numerical model setup

The model experiments showed strong turbulent behaviour in the flow field due to the time-dependent effect (Vosswinkel *et al.*, 2012). Vosswinkel *et al.* (2012) performed unsteady flow simulations and carried out uncoupled steady DPM with every time step flow simulation result, in order to evaluate the influence of unsteady flow on solids settling in stormwater tanks. Varying BSS calculated using the Shields curve was used as the bed boundary condition for DPM. However, this method cannot represent the erosion motion after settlement due to the unsteady flow condition.

Here, we will use the proposed method to represent the dynamic settling and entrainment processes, taking the time-dependent effect into account by coupling unsteady flow with unsteady particle tracking. The computational mesh was established by hexahedral element. The independent mesh was tested by Vosswinkel *et al.* (2012) with a 600000 cell mesh. The mesh is shown in Figure 5-5.

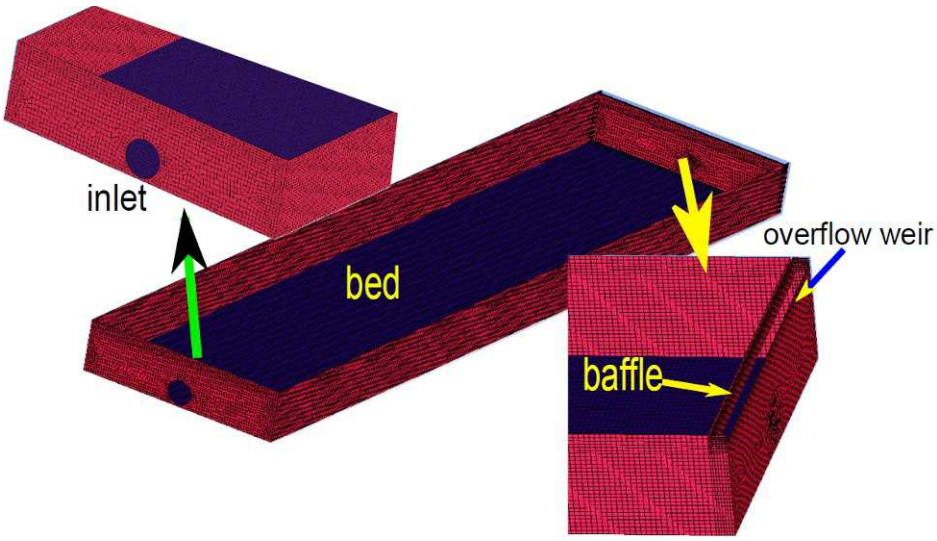

Figure 5-5 The computational mesh

The flow simulation setup uses the same configuration proposed by Vosswinkel *et al.* (2012). The basic configurations are as follows:

- **Inlet:** mass flow inlet, with a flow rate of 2.19 L/s;
- **Wall:** no-slip condition and enhanced wall treatment;
- **Free surface:** symmetry plan;
- **Outlet:** pressure outlet;
- **Turbulent model:** RNG k-ε model.
- **Unsteady Flow time step size** (s): 0.1
- **Iterations per flow time step**: 20
- **Wall function:** enhanced wall function

The basic DPM configurations excluding the bed boundary conditions are listed inTable 5-3. The bed boundary condition used was the proposed dynamic sedimentation method. Under this method, different treatment models were selected for processes A and B, different saltation frictional resistance models and two entrainment initial velocity models were tested. The turbulent dispersion effect defined by Discrete Random Walk model was also tested, in order to more accurately represent the sediment transport mechanism. As shown in Figure 3-25, different boundary conditions can be tested for process A (deposited) and process B (entrainment). Specific condition can be integrated to represent the sedimentation processes. The different bed boundary setups tested are set out in Table 5-4. The bed boundary conditions were implemented using the UDFs presented in chapter 3.

Table 5-3 Basic configurations for DPM model excluding bed boundary conditions

Basic parameter for DPM	Configuration	Remark
Particle time step size (s)	0.001	
Flow time step (s)	0.1	
Iterations per flow time step	20	
Max. number of steps	5e+6	
Coupling setup	Interact with fluid phase	
Particle treatment	Unsteady state	
Density (kg/m^3)	1020	
Particle size distribution (μm)	Defined using the Rosin - Rammler equation	Parameter: number of diameter=10, n=3.89, d_{min}=300μm, d_{mean}=565 μm,d_{max}=800 μm
Particle injection	at Inlet surface per flow time step	Initial velocity =2.8 m/s
Stochastic modelling	DRWM	Parameter:C_L=0.05, 0.15, 0.25, 0.5
Impulse sediment mass per time	0.1kg	

Table 5-4 DPM setup and different bed boundary conditions for the proposed method

Case No.	Process A: settling cond.	Process B: entrainment cond.	Total particle number	Rebound resistance coefficient e, f**	Initial entrained velocity (m/s)u_d,v_d	DRWM C_L
DPM 1	Varying BSS$^{\#}$	Varying BSS$^{\#}$	22400	e:1, f:1	Hu and Hui$^{*\#}$	0.15
DPM 2	Varying BSS$^{\#}$	Varying BSS$^{\#}$	44800	e:1, f: 1	Hu and Hui$^{*\#}$	0.05
DPM 3	Varying BSS$^{\#}$	Varying BSS$^{\#}$	44800	e:1, f:1	Hu and Hui$^{*\#}$	0.25
DPM 4	Varying BSS$^{\#}$	Varying BSS$^{\#}$	44800	e:1, f:1	Hu and Hui$^{*\#}$	0.5
DPM 5	Varying BSS$^{\#}$	Varying BSS$^{\#}$	44800	e:0.84-4.84τ_* f:0.73	Hu and Hui$^{*\#}$	0.05
DPM 6	Varying BSS$^{\#}$	Varying BSS$^{\#}$	67200	e:0.84-4.84τ_* f:0.73	u_d=2u_* v_d=2u_*	0.05
DPM 7	Varying BSS$^{\#}$	Varying BSS$^{\#}$	67200	e:0.84-4.84τ_* f:0.73	u_d=2u_* v_d=2u_*	No DRWM
DPM 8	BTKE 1	Varying BSS$^{\#}$	22400	e:1, f:1	u_d=2u_* v_d=2u_*	0.15
DPM 9	BTKE 2	BTKE 2	67200	e:0.84-4.84τ_* f:0.73	u_d=2u_* v_d=2u_*	0.05
DPM 10	BTKE 1	BTKE 1	67200	e:0.84-4.84τ_* f:0.73	u_d=2u_* v_d=2u_*	0.05
DPM 11	BTKE 2	Varying BSS$^{\#}$	67200	e:0.84-4.84τ_* f:0.73	u_d=2u_* v_d=2u_*	0.05
DPM 12	Fix BSS =0.03 Pa	BTKE 1	67200	e:0.84-4.84τ_* f:0.73	u_d=2u_* v_d=2u_*	0.05

$^{*\#}$: refer to equations (3.84)-(3.85) in chapter 3;

**: definition of e and f please refer to equations (3.73)-(3.74) in chapter 3.

e=0.84-4.84τ_* *f*=0.73 are from Nino and Garcia (1994): gravel saltation.

#: calculated according to Shields curve, please refer to equations (3.75)-(3.78) in chapter 3.

BTKE1: ξ=1 for equation (3.81) in chapter 3.

BTKE2: ξ=1.5 for equation (3.81) in chapter 3.

Note: process A and process B are shown in Figure 3-25.

5.2.2 Evolution of sediment transport and spatial distribution

In the physical tank, unsteady behaviour was observed even though the tank was fully symmetrical with constant inflow. Recirculation zones were observed with oscillations from the left to the right-hand side. The oscillation of the inflow stream were periodical with a wave length of about 100s. More details can be found in the paper by Vosswinkel *et al.* (2012). This unsteady behaviour was also confirmed by the unsteady simulation. Since the

flow pattern is periodical, thus only the first injection and transport process were simulated, due to the significant computational time and memory required.

Figure 5-6, Figure 5-7 and Figure 5-8, present the simulated representative pattern and characteristics of sediment transport experiments. Figure 5-6 shows the experimental and simulated evolution of sediment transport processes for the first injection with an interval of 5 seconds. The simulation results are given as volume concentrations. This figure accurately reproduces the morphology of particle jet by the water inflow jet.

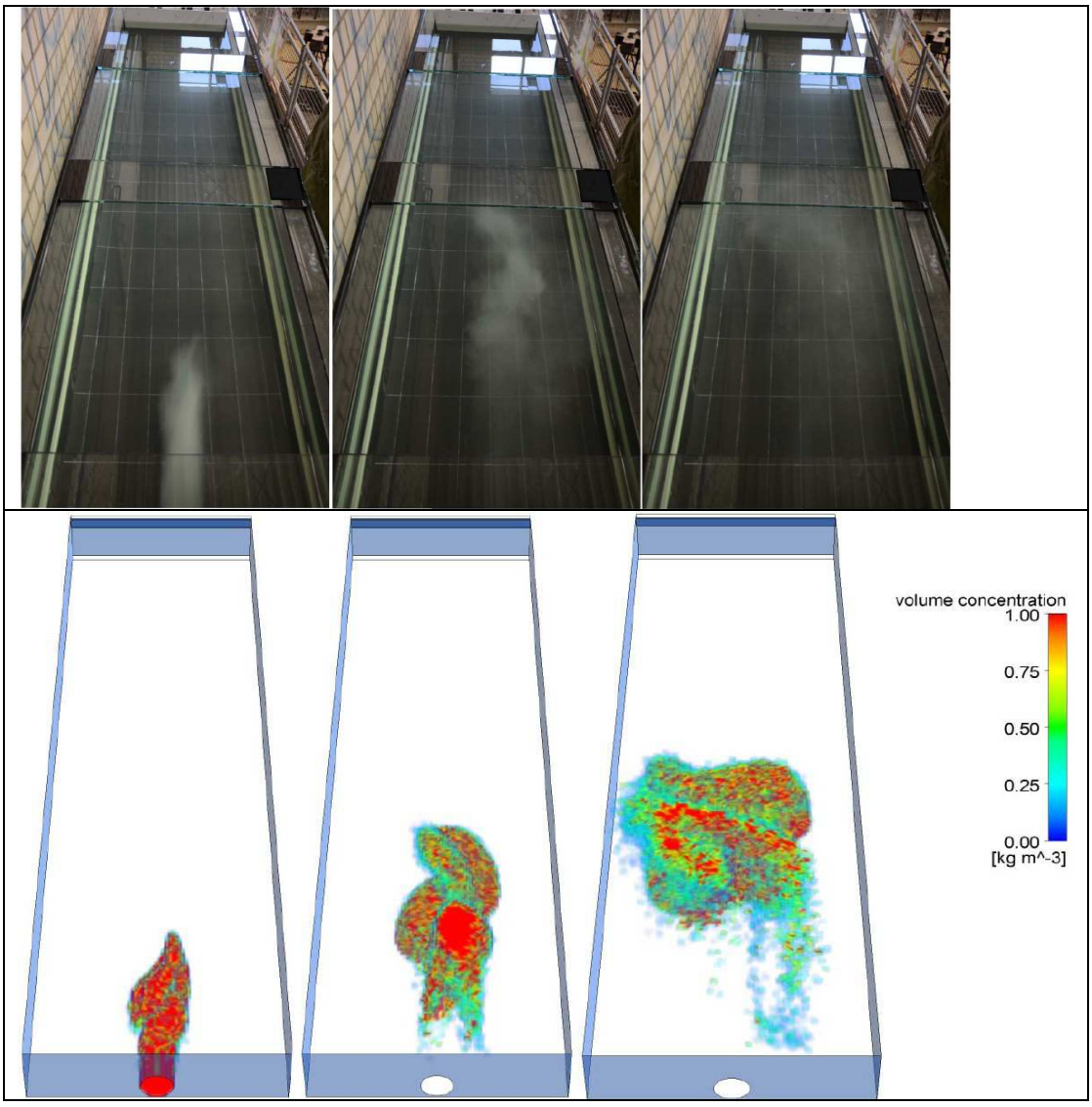

Figure 5-6 Comparison of the experimental (according to Vosswinkel et al., 2012) and simulated evolution of sediment transport after first injection at an interval of 5 seconds (results of case DPM 1, time 10s-15s-20s)

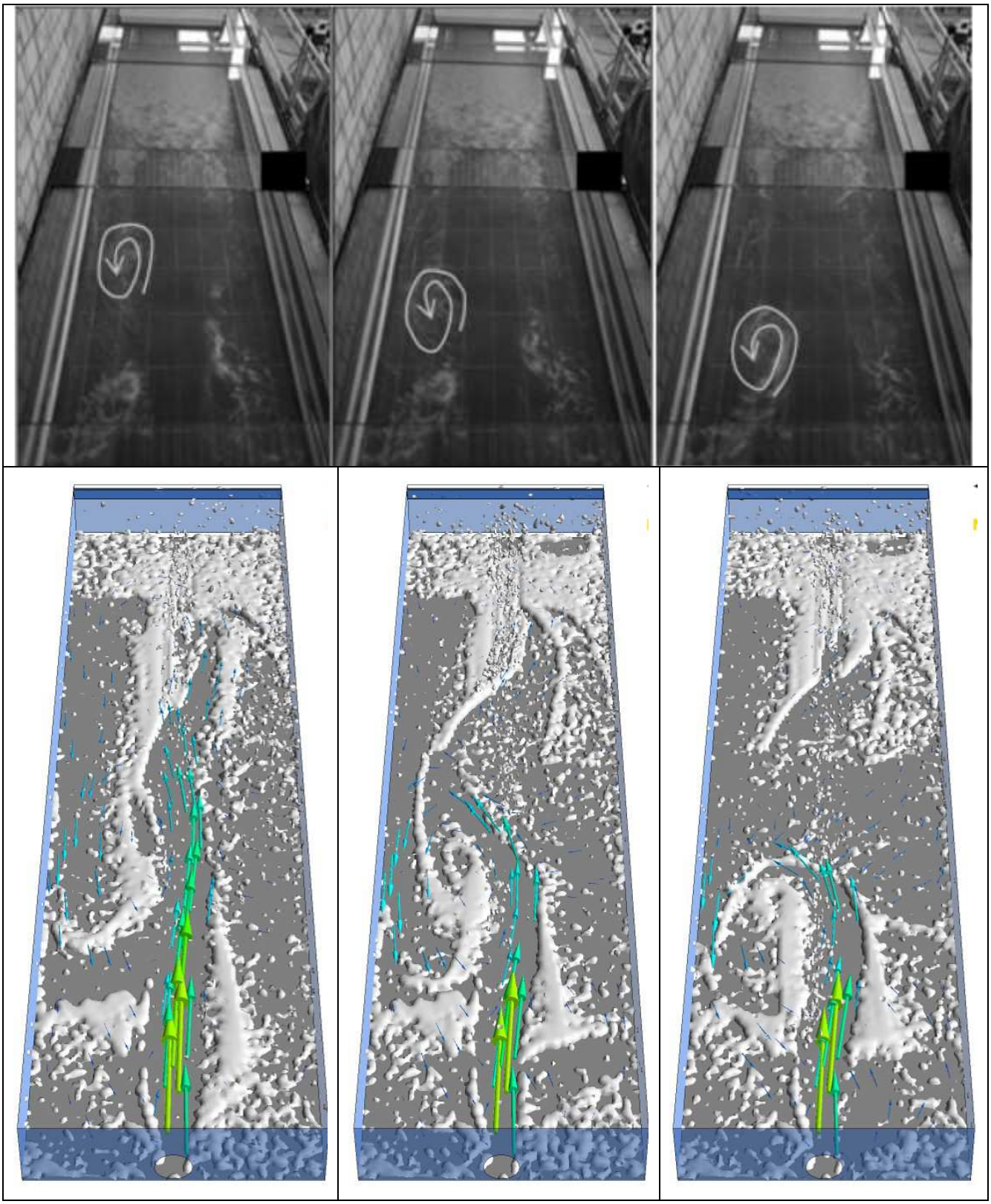

Figure 5-7 Evolution of experimental observations (according to Vosswinkel et al., 2012) and simulated recirculation at the left-hand side at a time interval of 15 s (results of case DPM 5, time-200s-215s-230s)

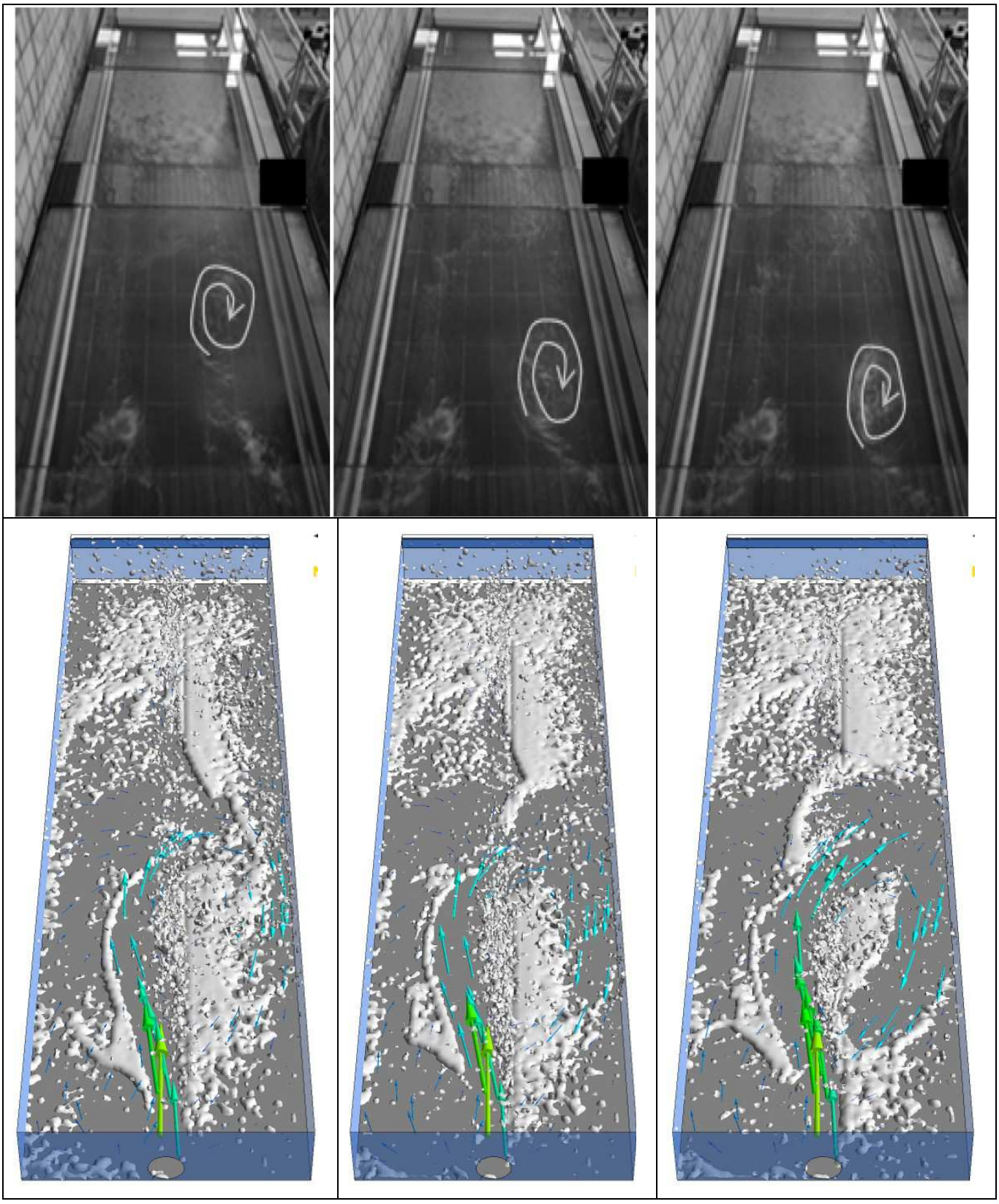

Figure 5-8 Evolution of experimental observations (according to Vosswinkel et al., 2012) and simulated recirculation at the right-hand side at a time interval of 15 s (results of case DPM 5, time-90s-105s-120s)

Figure 5-7 shows the evolution of the anti-clockwise recirculation at the upstream left-hand side. Figure 5-8 shows the evolution of the clockwise recirculation at the upstream right-hand side. The near bed sediment in the middle of the basin, at the end of the basin and at the left and right-hand upstream corners of the basin are accurately predicted as shown in Figure 5-7 Evolution of experimental observations (according to Vosswinkel et al., 2012) and simulated recirculation at the left-hand side at a time interval of 15 s (results of case DPM 5, time-200s-215s-230s) and Figure 5-8.

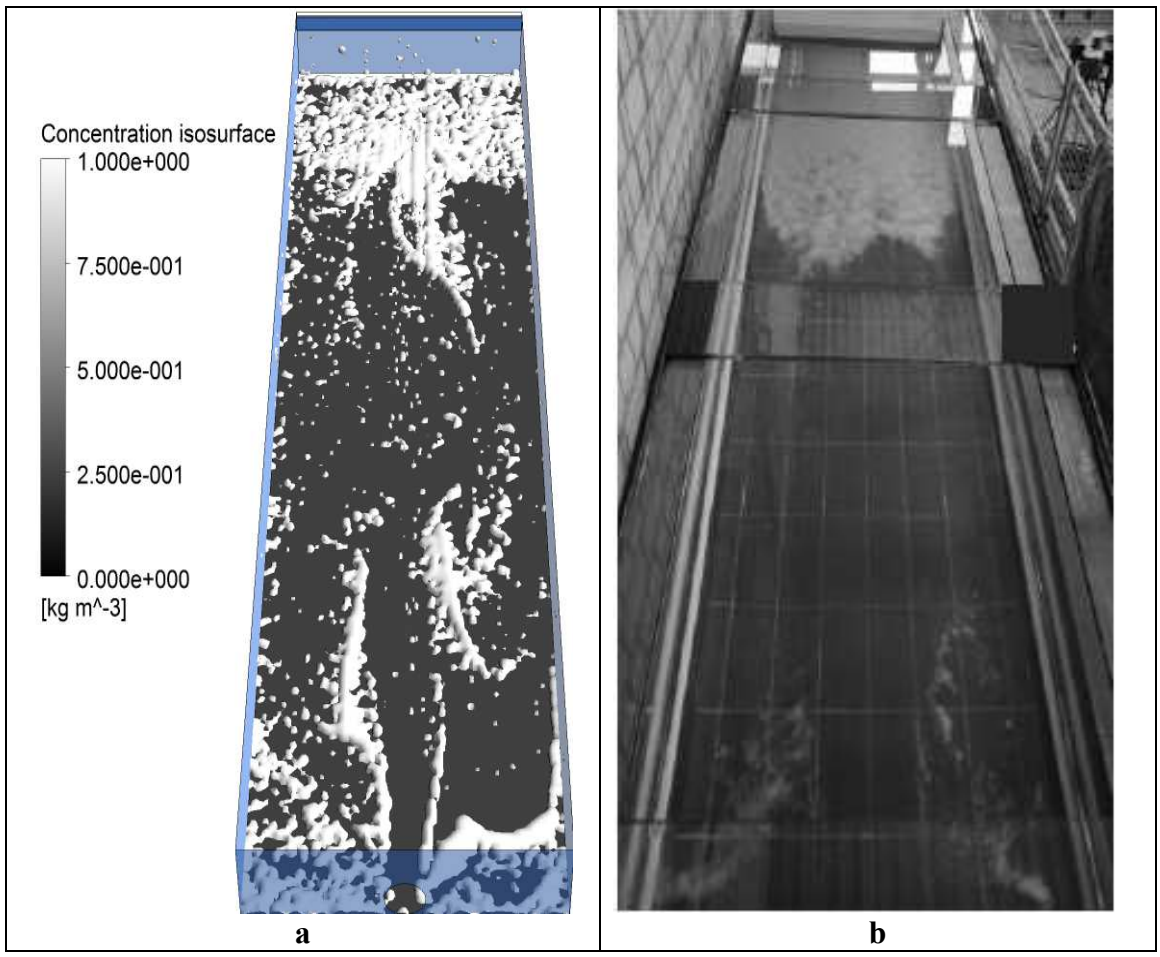

Figure 5-9 Comparison of (a) simulated deposit spatial distribution at the end ((results of case DPM 1)300s) and (b) experimental final deposit distribution (after Vosswinkel et al., 2012)

Figure 5-9a presents the final deposit zone from the simulated sediment transport results. As we can see from the figure, the simulated sediment distribution zone shows reasonable levels of agreement compared to the preferential experimental deposit zones, such as the deposits in the downstream section of the basin and in the left and right-hand upstream corners. The almost empty zone at the middle of basin is all accurately predicted.

Space constraints mean the results cannot be presented in their entirety. However, as shown in Figure 5-6, Figure 5-7, Figure 5-8 and Figure 5-9, the case tested can accurately capture the typical characteristics of the sediment transport process, notably the periodical vortex evolutions. In short, the newly proposed method has demonstrated its capability to simulate

unsteady sediment transport in stormwater detention basins. In the next section, we are going to explore the information from the simulated results.

Figure 5-10 shows the monitoring particle concentration at the outlet of basin. We can observe that the simulated result shows the instantaneous characteristics of sediment concentration. This result provides a more accurate way of obtaining the sediment concentrations. From the figure, it would seem that the particle concentration of outlet is periodical.

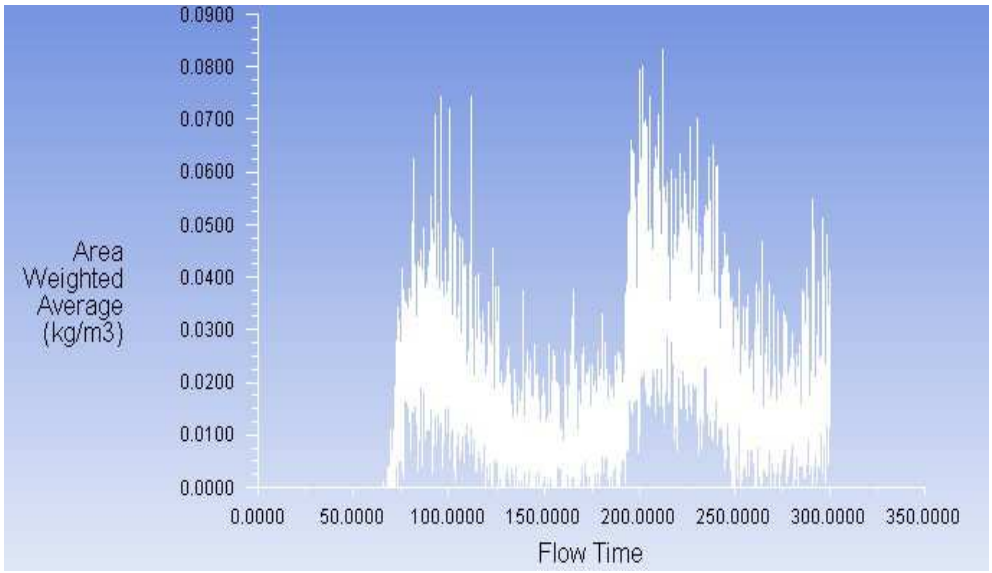

Figure 5-10 Monitoring sediment mass concentration at the basin outlet (simulation case DPM 11 from 0-300s)

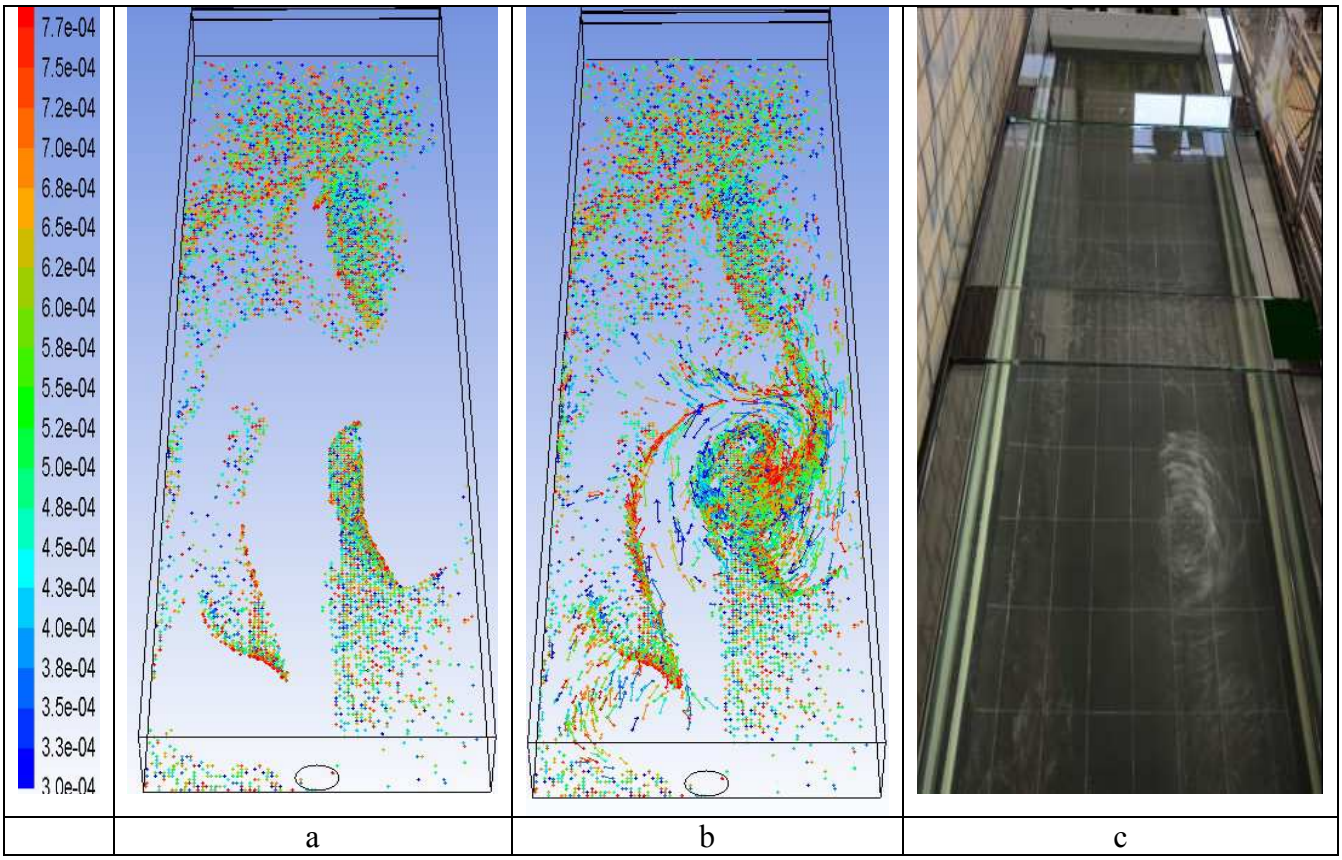

Figure 5-11 (a) Simulated deposits in the basin (case DPM 5 at 105s), (b) simulated deposits + moving bed load (<0.002m) (case DPM 5 at 105s) and (c) top view picture of experimental sediment spatial distribution (after Vosswinkel et al., 2012)

The simulated result makes it possible to access all the information about the sediment in the domain. Figure 5-11a shows the simulated deposits spatial distribution. These particles are marked as settled particles. In Figure 5-11a and Figure 5-11b, the different colours indicate the different particle sizes. This result provides more information than the species model or Eulerian model. Figure 5-11b demonstrates the deposited bed load and the near bed moving bed load, which is in the layer less than 0.002 m from the bed. The bed load motion can be observed in Figure 5-11b. It shows that the particles around the clockwise recirculation are entrained due to the strong flow motion. The trend in bed load movement is accurately represented, showing a reasonable level of agreement with the the experimental photographic observations. Similarly, the suspended particles can be represented in the same way.

In fact, by using a specific criteria flag, the simulation results can distinguish particles in different states. The particle mass or volume concentration spatial distribution can be accessed throughout the whole simulated field. Figure 5-12a shows the near bed mass concentration on the cutting planes. It is possible to predict the accumulated sediment thickness from the simulation results if the bulk density is known. This can provide useful information for drawing up the management and maintenance of basin strategy, such as deposit cleaning.

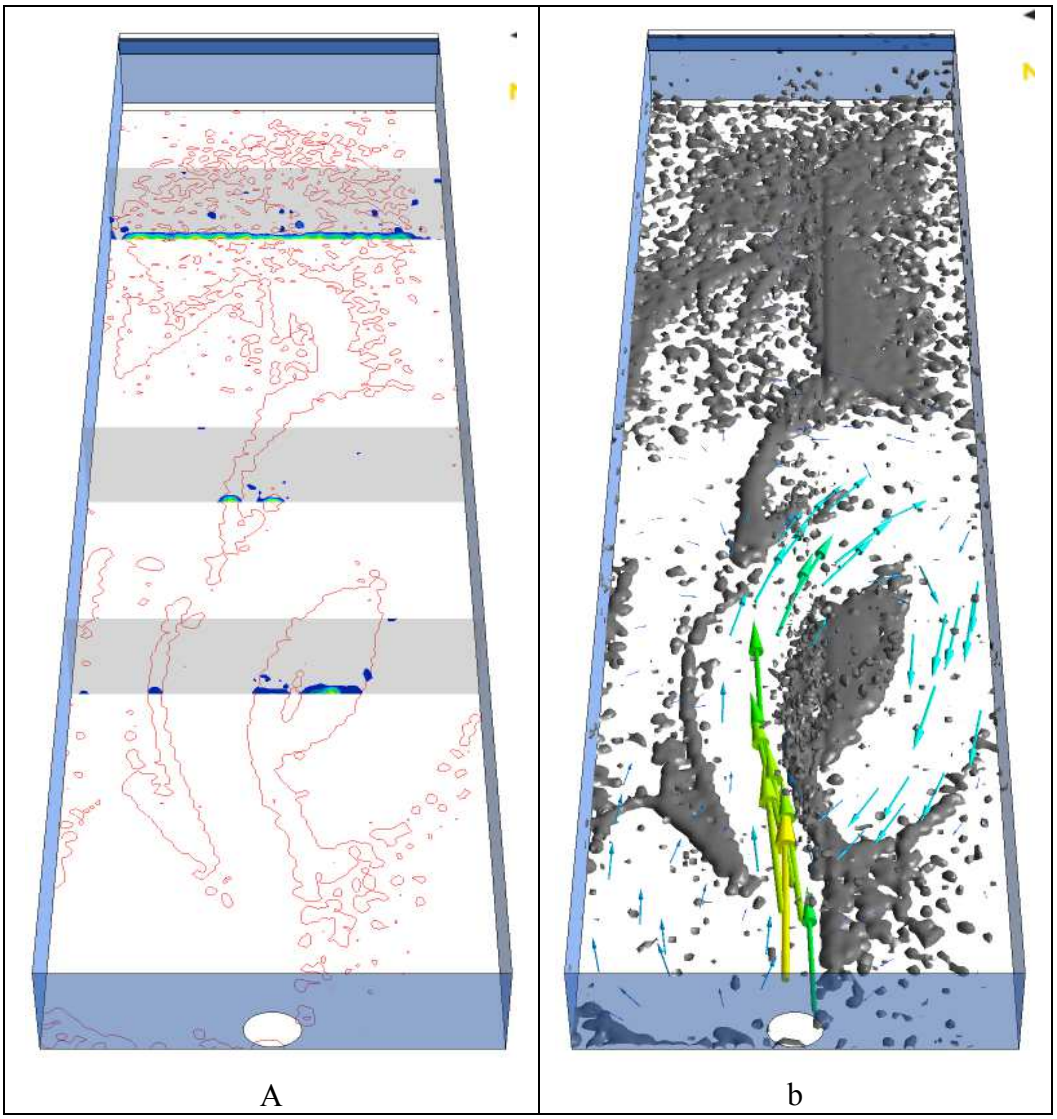

Figure 5-12 (a) Simulated near bed particle concentration distribution, the contour shows the deposition zone, and (b) the deposition zone distribution rendering with concentration isosurface.

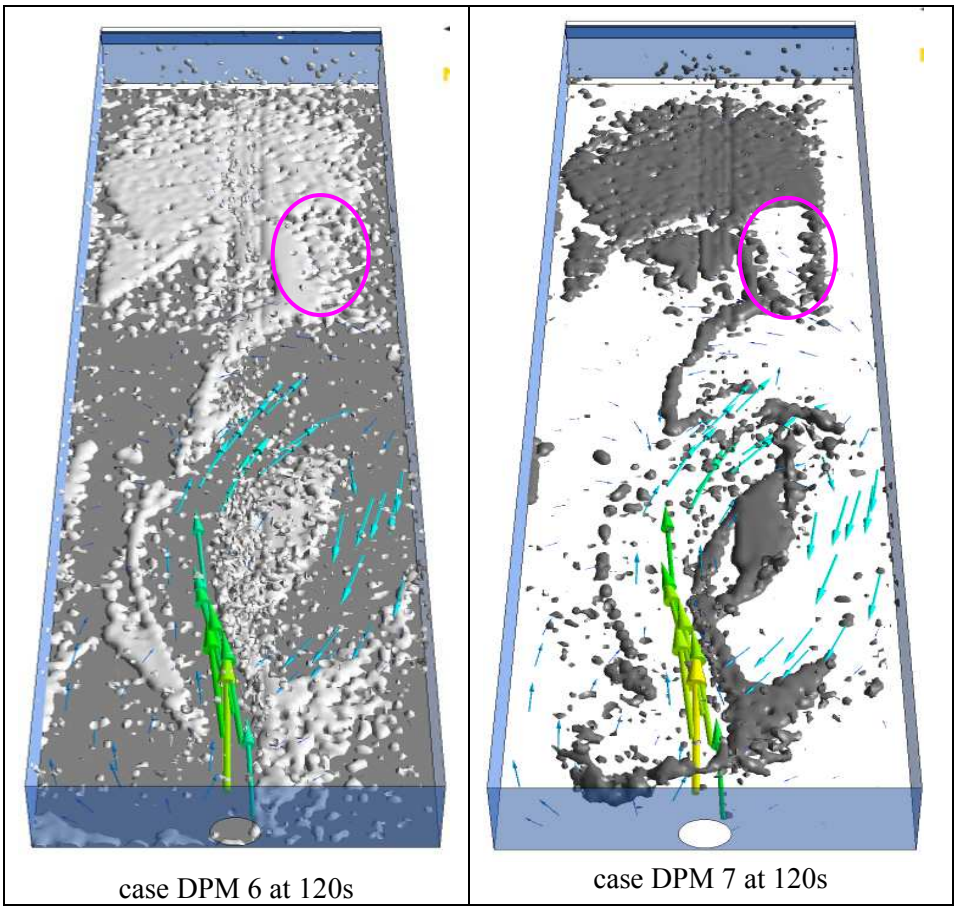

Figure 5-13 Comparison of simulation particle distribution with DRWM (C_L=0.05) and without DRWM

Figure 5-13 shows the different sediment spatial distributions with or without stochastic modelling (DRWM). Compared to the experimental observations shown in Figure 5-8, the simulation results with DRWM are better than the simulation results without stochastic modelling. For example, there is a missing zone shown as dashed ellipse in Figure 5-13 in the simulated results without DRWM modelling as well as the zones in the two upstream corners. Furthermore, the simulation results with DRWM showed more reasonable sediment spatial distribution across the basin. In terms of predicting the deposit zones, this may suggest that sediment transport using unsteady DPM in detention basins should take stochastic modelling into consideration in order to more accurately represent the turbulent dispersion effect.

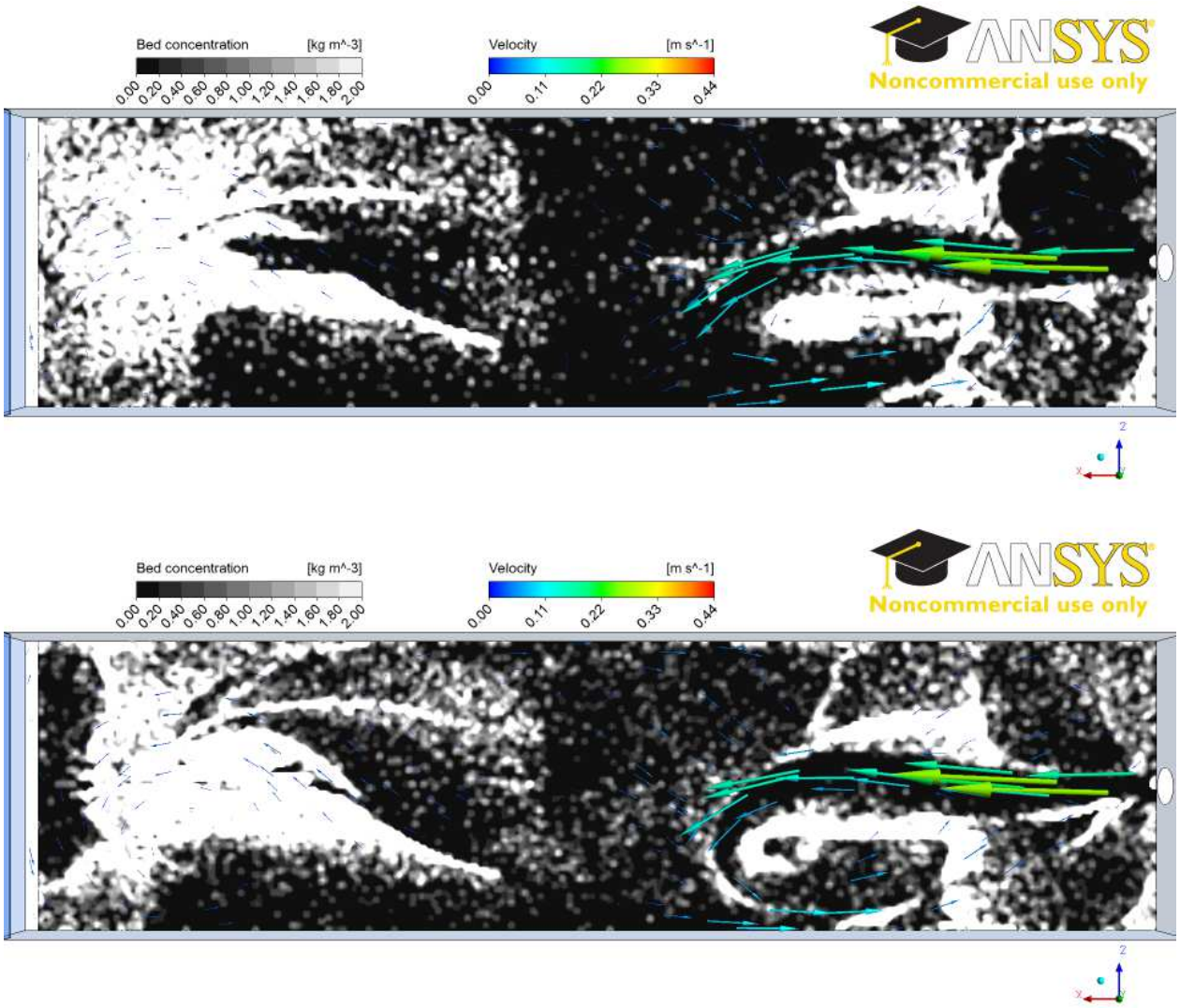

Figure 5-14 Comparison of simulated particle bed concentration with different C_L: case DPM 5 at 230s with C_L=0.05 (above) and case DPM 1 at 230s with C_L=0.15 (below)

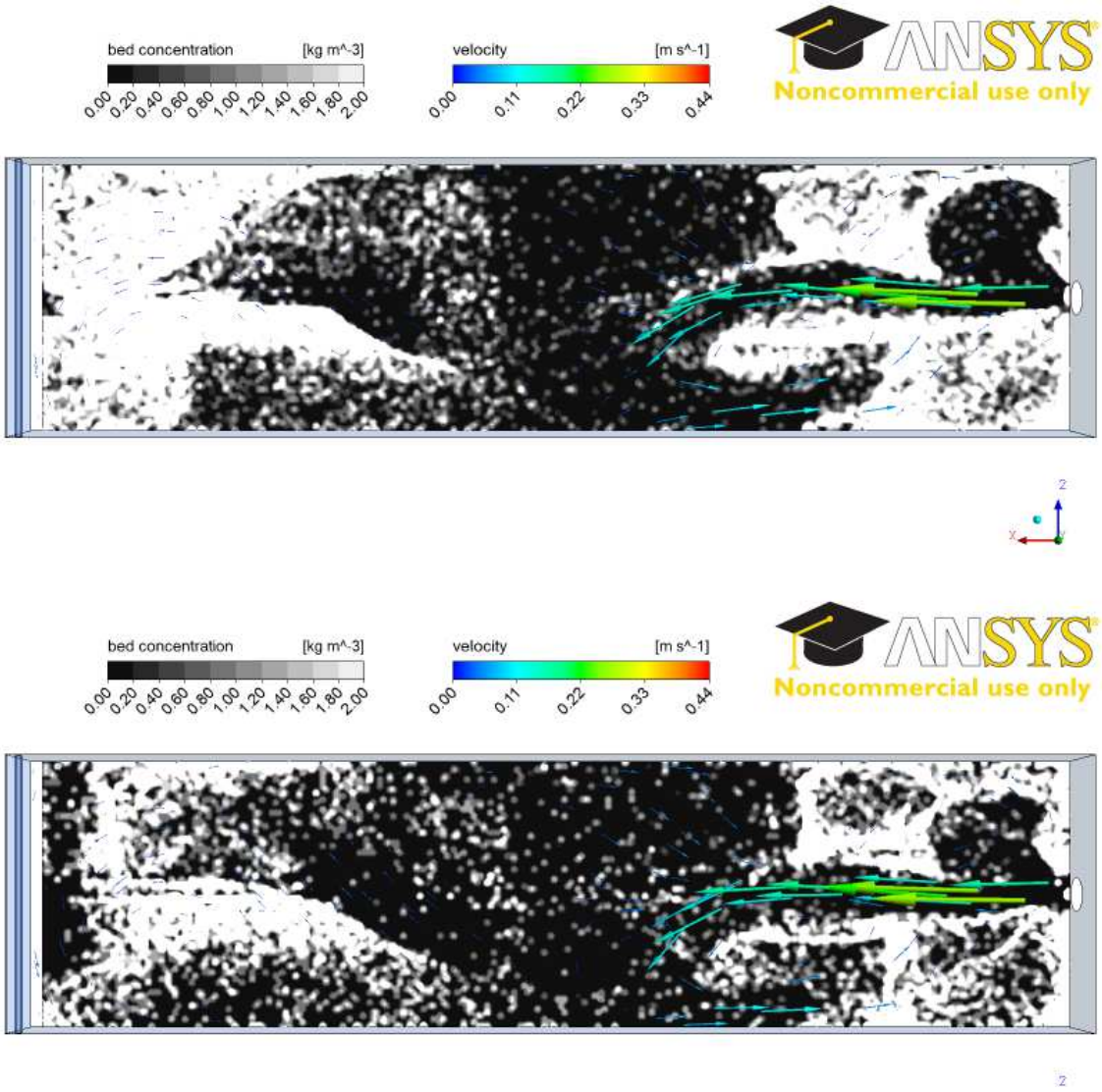

Figure 5-15 Comparison of simulated particle bed concentration with different C_L: case DPM 3 at 230s with C_L=0.25 (above) and case DPM 4 at 230s with C_L=0.5 (below)

Figure 5-14 and Figure 5-15 show the near bed particle concentration distribution with different DRWM modelling parameters C_L. Compared with the observations shown in Figure 5-7, the simulation results with C_L=0.05 seem to agree on near bed sediment distribution. Thus C_L=0.05 in DRWM was chosen for the subsequent tests.

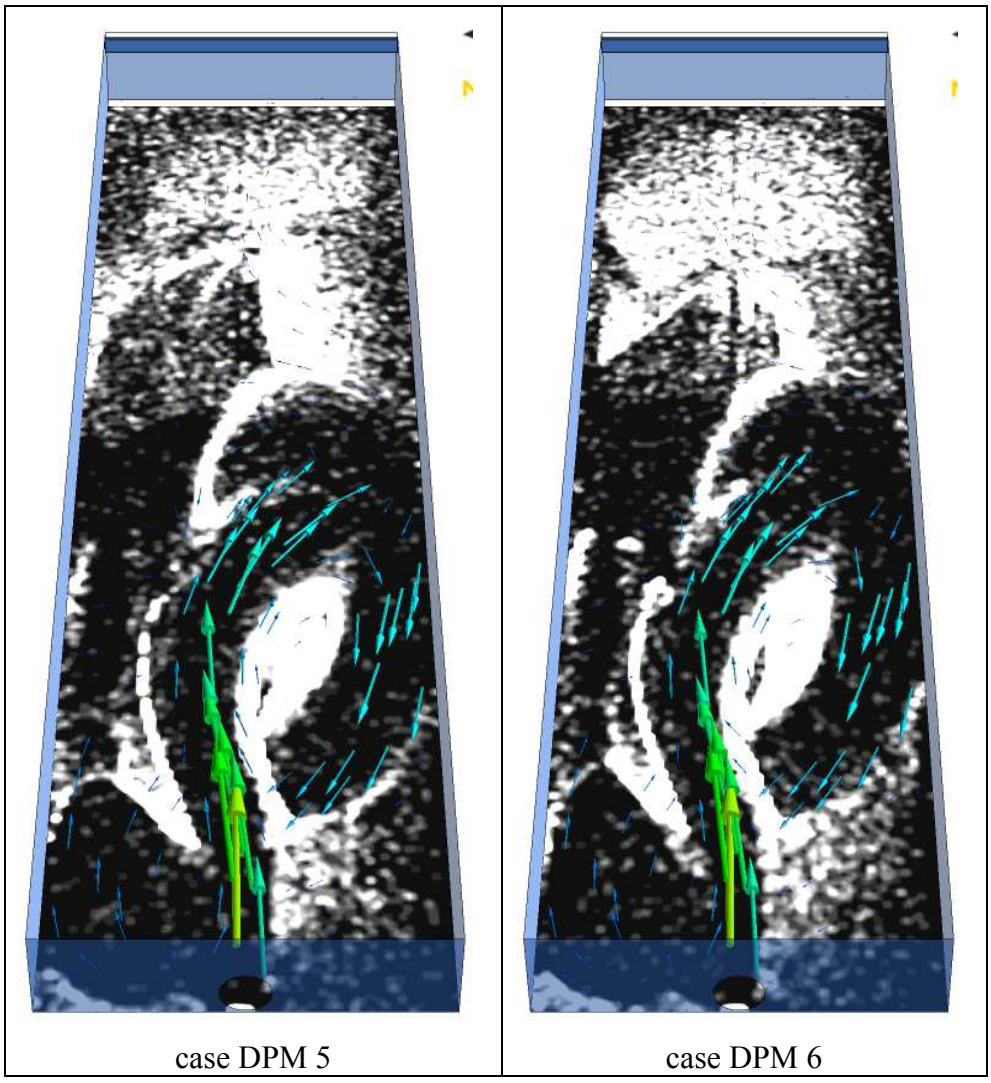

Figure 5-16 Comparison of simulated particle bed concentration with different initial pickup velocity: case DPM 5 at 120s with Hu and Hui formula (left) and case DPM 6 at 120s with formula van Rijn (right)

Figure 5-16 shows the near bed particle concentration distribution with different initial velocity models if the particle is entrained. Case DPM5 models the initial entrained velocity using the model proposed by Hu and Hui (1996), and case DPM 6 models the initial entrained velocity using the formula proposed by van Rijn (1984). Due to the lack of quantitive sediment spatial distribution data from experiments the simulation results can only be adjusted using the photos. In terms of the sediment spatial distribution, the difference is shown in the downstream section of the basin. The van Rijn model predicts greater spread with dense sediment accumulating in the downstream zone, which fits more closely with the observation. The van Rijn model was therefore used for subsequent tests in order to more accurately represent sediment spatial distribution.

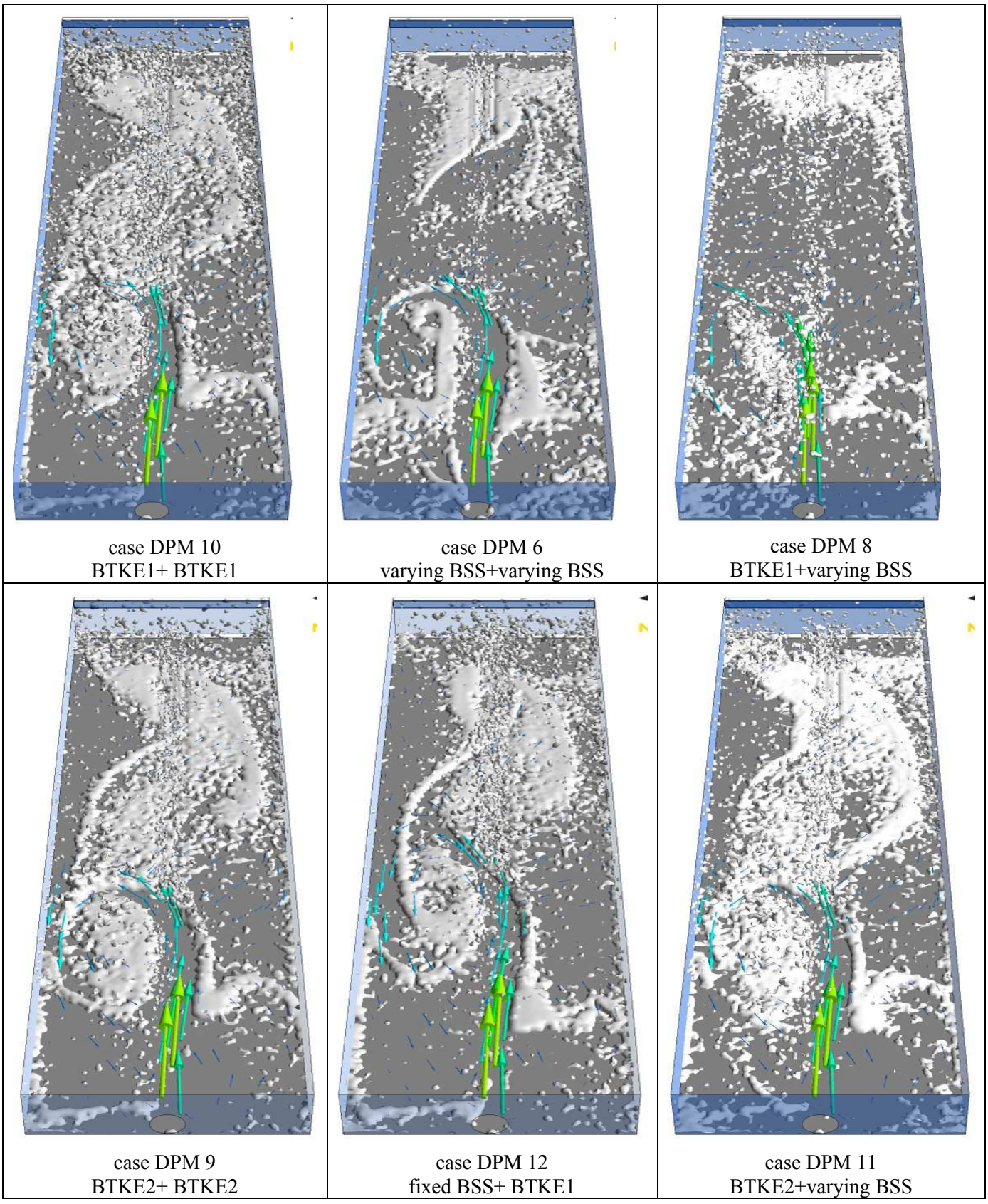

Figure 5-17 Comparison of particle spatial distribution with different settling and entrainment boundary conditions

Figure 5-17 shows particle spatial distribution with different boundary condition settings. Compared to the experimental observations, cases DPM 6 and DPM 11 appear to offer better levels of agreement for the recirculation zone, the upstream corner zone and the downstream zone. It seems that varying BSS is more accurate than BTKE as the entrainment condition. Cases DPM 9 and DPM 10 seem to over predict the sediment in the middle zone of basin. In cases DPM 9, 10, 11 and 12, the combination of BTKE with BSS is more accurate than BTKE and BTKE for sediment deposition zone prediction. The comparison of cases 9 and 11 shows no major differences for sediment zones across the basin. This may imply that for entrainment condition prediction, BTKE2 and varying BSS are almost the same if the settling condition is BTKE2. Case DPM 8 under predicts the sediment zone, perhaps because C_L value is higher than the other cases. Except for case DPM 6, all other cases shows high numbers of suspended particles, this may imply that the BTKE model has high levels of sediment pickup. In the proposed method varying BSS and BTKE have been shown to be adapted for us as both the settling and entrainment conditions. Out of all the boundary condition combinations tested, varying BSS+varying BSS and BTKE2+varying BSS show the best level of agreement compared to the experimental sediment zones.

5.2.3 Removal efficiency

Table 5-5 Simulated removal efficiency of different case setups

Case No.	DPM 1	DPM 2	DPM 3	DPM 4	DPM 5	DPM 6
Efficiency (%)	79.45	87.85	81.48	82.00	86.77	90.80
Case No.	DPM 7	DPM 8	DPM 9	DPM 10	DPM 11	DPM 12
Efficiency (%)	98.41	73.02	85.02	85.19	86.06	85.83

In terms of experimental removal efficiency, three tests were performed according to Vosswinkel *et al.* (2012) which found overall removal efficiencies of between 83% and 87%. Table 5-5 presents the simulated removal efficiency of sediment transport modelling using the proposed method. All the cases except for case DPM 7 without DRWM predicted reasonable removal efficiency. This suggests that turbulent dispersion effect should be taken into account in sediment transport using stochastic modelling such as DRWM. The simulated efficiency is affected by many factors. It seems that efficiency decreases as the C_L value for DRWM modelling increases. Out of the four test values, the smallest C_L value 0.05 seems to be show a higher level of agreement than the others. However, case3 has a larger C_L value but higher levels of efficiency than case 1 with a low C_L value. This difference is thought to be down to the impact factor of the number of particles injected. In our simulation 22400 particles were used, but this appeared to be insufficient. More particles were therefore injected for the subsequent simulations. From the simulation results available it would appear that between 44800 and 67200 particles are required for the present study. Cases 2 and 5 would appear to show that taking into consideration particle saltation friction resistance has a slight negative impact on the efficiency. Cases 5 and 6 show that van Rijn's initial entrainment velocity model has a positive impact on efficiency compared to Hu and Hui's (1996) model. In DPM cases 9, 10, 11, 12, with appropriate particle injection, and the appropriate rebound friction resistance model and initial velocity model, the BTKE and BSS boundary condition accurately predicts removal efficiency, showing 85.02%, 85.18%, 86.06% and 85.83% against the measured range of 83%-87%. However, it should be noted that, theoretically, the proposed method using DPM underestimates removal efficiency because the hiding effect and particle-

particle collisions are not taken into consideration in DPM. In the high concentration zones such as the near bed zone where the particles are in a dense state, the low layer particles might be hidden by the upper layer particles due to flow entrainment. Alternatively, the low layer entrained particle may be rejected due to inter-particle collision. However, in the proposed method, the probability of a particle being entrained is the same for all particles regardless of the accumulated layer structure. In the DPM approach, collisions are disregarded in order neglected to save calculation time. The sediment hiding effect should be taken into account to improve this method in future works.

There are a range of different parameters involved in the newly proposed method. Twelve different case studies were conducted to try to determine the optimal values or models for best predicting removal efficiency and sediment deposition zones in detention basin. However, no definitive conclusions could be drawn as the way in which these parameters combine is complex and how they interact is still unclear. More research is needed to further investigate these parameters.

5.3 Conclusion of chapter 5

The newly proposed dynamic sedimentation method was tested in two scale basins both under steady and unsteady flow conditions coupled with unsteady state DPM. With the proposed method coupled with the unsteady DPM, the simulated results under steady flow conditions demonstrated more accurate sediment zone prediction compared to steady DPM. Furthermore, the simulated results based on the proposed method under unsteady flow conditions coupled with unsteady DPM can accurately reproduce the evolution of the sediment transport processes in the scale basin. However, the different parameters involved in the proposed method influence the prediction of removal efficiency and sediment deposition zone. The optimal values still needed to be determined by carrying out more tests.

Overall, the proposed dynamic sedimentation method demonstrated its ability to represent the settling and entrainment dynamics under both steady and unsteady flow conditions. Base on the simulation cases and in light of the sediment zone and efficiency predictions obtained, the proposed BTKE boundary is suitable for use as the deposit boundary condition and Shields curve is suitable for use as the entrainment boundary condition in small-scale detention basins for non-cohesive sediment.

Chapter 6 Conclusions and perspectives

This research aims to provide a better understanding and method for the modelling of sediment transport processes in small scale and full scale detention basins. The general conclusions and perspectives are as follows.

6.1 General conclusions

Field measurement and observations

Field measurements were performed in order to obtain values for the accumulated spatial distribution and characteristics of sediment in the Django Reinhardt detention basin. 11 sediment samples were collected for and their physical properties analysed. Both Laser diffraction analyse and the wet sieving method were used for particle size distribution analysis. A pycnometer method was used to measure the density of particles.

The main sediment zone is located in the centre of the basin. The main sediment zones have remained similar from 2006 to 2012, but have increased in size and accumulated sediment depth. This implies that a main sediment deposit pattern exists in this basin. Both fine particles and gravel-like particles are present in the detention basin. Particle density was found to be between 2200 kg/m^3 and 2500 kg/m^3. From the simulated results available, a main flow pattern for the Django Reinhardt detention basin was assumed for further analysis of the comparison between the spatial distribution of measured sediment characteristics and the flow simulations. This main flow pattern had an inflow rate of 0.35 m^3/s, which corresponds to the maximum outflow rate regulated by the hydro-regulator. Hence, analysis of the spatial distribution and characteristics of sediment may help validate complex flow models.

Numerical Simulation

The simulated flow pattern with an inflow rate of 0.35 m^3/s showed a good level of agreement with the measured spatial distribution of particle size. Steady flow simulation with inflow rate of 0.35 m^3/s corresponded to the main flow pattern in the basin. Where there is a lack measured data for validating flow simulations, the spatial distribution of sediment characteristics might be an alternative way of providing a rough evaluation of flow simulation results.

BTKE distribution has a similar function to BSS distribution in predicting the deposit zone for a full scale detention basin. In general, the lower BTKE zones have a higher probability for sediment settlement. However, this distribution cannot describe the build-up of sediment due to the lack of the sediment transport information. Sedimentation depends upon both the flow conditions and the sediment transport characteristics.

Sediment transport simulations using a steady state DPM were carried out with different boundary conditions for sediment zones and efficiency predictions. The simulation results show that the boundary conditions for fixed BSS/BTKE were unable to predict the preferred sedimentation zones in the real Django Reinhardt basin due to the use of a single threshold for

different sized particles, which causes small particles to settle too early. The fixed BSS/BTKE boundary conditions result in an overestimation of predicted efficiency because they do not take the time-dependent effect of erosion into account. Shields curve boundary conditions do not work well full scale basins in sewer systems either. This is because the Shields curve was derived from experiments carried out with non-cohesive particles, while the cohesive materials predominate in particulate pollutants in sewer system.

Near bed turbulence is affected by surface roughness, so clearly surface roughness should be taken into account in flow simulations for full scale basins.

Turbulence plays a keyrole in determining sedimentation processes, and the BTKE can be used to predict the sediment zones in detention basins. Hence, a new formula has been proposed here for estimating the BTKE threshold for different particles according to their settling velocity. The settling velocity is thought to represent all other properties, such as density and size due to the inner relations. The formula (equation 3.81) is given in detail in chapter 3. The proposed formula was created with the aim of overcoming the notable drawbacks of the fixed BSS/BTKE values and the Shields curve, i.e. that they are unable to predict the preferential zone in full scale basin with DPM simulations. This proposed formula was tested initially within the boundary conditions for a scale basin, then in a full scale basin.

Sediment transport simulations based on the proposed BTKE method were performed both in small scale and full scale basins using a steady state DPM. The simulated results showed that the proposed formula for calculating BTKE boundary conditions is capable of identifying the preferred sedimentation deposit zones in both small scale and full scale detention basins. The proposed formula for estimating the BTKE threshold for different particles does not determine the BTKE using comparison with observed results, as required by fixed BSS/BTKE boundary conditions. However, the proposed BTKE boundary conditions overestimate predicted efficiency.

In order to take time-dependent effects for sediment transport into consideration when modelling with a DPM approach, a new method was devised for representing the dynamic sedimentation processes under unsteady flow conditions. This method is illustrated in Figure 6-1. This method was carried out using UDF in Fluent.

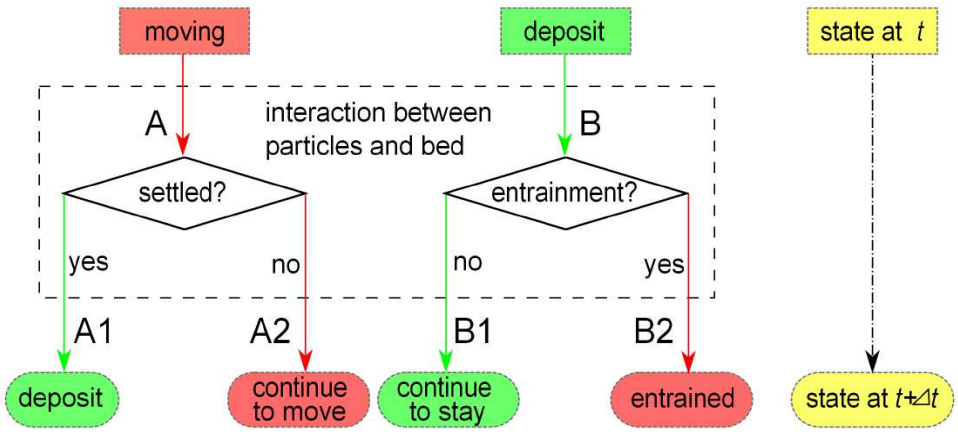

Figure 6-1 Sketch of dynamic sedimentation process treatment of interaction between particle and bed of basin under unsteady condition

12 sediment transport simulations were performed in a scale detention basin using the proposed method. The impact of different factors on efficiency and sediment zone prediction were tested. The proposed dynamic sedimentation method demonstrated a good overall ability for providing a representation of dynamic settling and entrainment under unsteady flow conditions.

The efficiency and the sediment zones predicted using DPM modelling under unsteady flow conditions based on the proposed method are sensitive to the quantity of the injected particles, the parameter of stochastic modelling, the rebound friction resistance model, the initial entrained velocity model, in particular, the settling and entrainment boundary conditions. A sufficient amount of particles are required in order to ensure statistical stability because a "particle" in DPM represents a parcel of physical particles. If the amounts of particles are too low, it leads to under-prediction of efficiency. Stochastic modelling is required for representing the turbulent dispersion effect of sediment transport. Out of the available test cases, a C_L value of 0.05 for DRWM shows the highest level of agreement compared to experimental observations for the scale basin in terms of predictions for efficiency and those for the sediment zones. The friction resistance model seems to have a small negative effect on the prediction of efficiency. The entrained initial velocity models have an impact on the sediment zone prediction. According to the experimental and simulated results available, the van Rijn model appears to predict wider spread but denser sediment accumulated in the downstream zone, which appears to show a higher level of agreement comapred to the observations. Taking both the prediction of the sediment zones and the prediction of efficiency into account, the proposed formula for calculating BTKE boundary conditions is suitable for use for deposit boundary conditions and the Shields curve is suitable for use for entrainment boundary conditions for non-cohesive sediment transport in a small scale detention basins.

6.2 Perspectives

Gravel-like particles had never been collected and analysed in previous research carried out for the Django Reinhardt detention basin. The sediment trap sampling method cannot collect coarse particles because coarse particles are often transported along the pathway within the bed load. This can lead to uncertainty when estimating removal efficiency. Within the framework of the CABRRES national project (http://www.graie.org/cabrres/index.php), new sediment traps are to be installed in the basin and at the inlet of the basin for sediment sampling in order to provide more complete information on the characteristics of sediment.

The BSS and the BTKE have similar capacities for predicting sediment zones and are both used as the bed boundary conditions in DPM modelling. However, neither of them works perfectly for predicting efficiency and sediment zones. It has been assumed that a possible combination of BSS and BTKE might be used when simulating full scale basin sedimentation processes.

The adjusted coefficient in the new formula has been assumed to be a constant. However, this value does not work well as entrained boundary conditions within unsteady DPM modelling with the dynamic sedimentation method. It is likely that the adjusted coefficient may be a

function that depends upon flow conditions and particle characteristics. This coefficient function can be obtained from a special experimental setup.

Up to now, there has been no appropriate formula for estimating the settling velocity for sewer solids. There does not appear to be a clear relationship between the measured settling velocity and particle properties. A relationship between the settling velocity and particle propterties is required by the proposed formula which allows estimating the threshold of BTKE as boundary condition in sediment transport modelling.

Unsteady sediment transport modelling coupled with unsteady flow conditions is recommended for predicting efficiency and sediment zones since sediment transport behaviours are highly affected by unsteady flow conditions. Unsteady sediment transport modelling is to be performed in the Django Reinhardt basin for complete storm events which last for a short period of time.

From a theoretical perspective it is likely that the proposed DPM method underestimates efficiency because the hiding effect and particle-particle collision are not taken into consideration. In high concentration zones, such as those areas the near bed zone, the particles are in a dense state. In these zones the lower particle layer may be hidden by upper particle layers from entrainment by the flow, or the low layer entrained particle might be rejected due to an inter-particle collision. However, in the proposed method, all particles have the same possibility of being entrained without taking the accumulated layer structure into account. In a DPM approach, collision is neglected in order to save calculation time. The hiding effect within the sediment should be taken into account in order to improve this method in future work. A possible solution might be to couple DPM and DEM to improve the method and to take into consideration the hiding effect.

Free surface measurement in Django Reinhardt basin with a camera is to be performed. The data taken from these measurements could be used to validate the numerical modelling results for the flow.

A probability method could also be introduced to the calculation of the bed boundary conditions in order to better represent the stochastic effect of the settling and entrainment processes.

References

A

Abad J.D., Buscaglia G.C., Garcia M.H. (2007). 2D stream hydrodynamic, sediment transport and bed morphology model for engineering applications. *Hydrological Processes*, **22**, 1443–1459.

Abbott J.E. and Francis J.R.D. (1977). Saltation and suspension trajectories of solid particles in a water stream. *Philosophical Transactions of the Royal Society,* London, U.K., **284**, 225-254.

Adler E. (1993). Aperçu des techniques de traitement des eaux pluviales. In: Tassin B. & Thevenot D., *Rejets urbains par temps de pluie: pollutions et muisances*, Actes des troisiémes journées du DEA STE. Paris: Presses de ENPC.

Adamsson Å., Stovin V.R, and Bergdahl L. (2003). Bed shear stress boundary condition for storage tank sedimentation. *Journal of Environmental Engineering*, **129**(7), 651-657.

Adamsson Å., Bergdahl L., and Lyngfelt S. (2005). Measurement and three dimensional simulation of flow in a rectangular detention tank. *Urban Water Journal,* **2**(4), 277-287.

Akan A.O. (1992). Storm runoff detention for pollutant removal. *Journal of Environmental Engineering*, **118**(3), 380-389.

Akan A.O. (2010). Design aid for water quality detention basins. *Journal of Hydrologic Engineering,* **15**(1), 39-48.

Akinlade O.G., Bergstorm D.J., Tachie M.F. and Castillo L. (2004). Outer flow scaling of smooth and rough wall turbulent boundary layers. *Experiments in Fluids*, **37**, 604-612.

Alderson A., Allison R., Chesterfield C., Lopreiato B., and Johnstone P. (1999). *Urban stormwater: Best practice environment management guidelines*. CSIRO Publishing, Australia.

Anderson R.S., and Hallet B. (1986). Sediment transport by wind. *Geological Society of America Bulletin*, **97**, 523-535.

ANSYS FLUENT (2011a). *Fluent 14.0 User's Guide*. ANSYS Inc.

ANSYS FLUENT (2011b). *Fluent 14.0 Theory Guide.* ANSYS Inc.

Apostolou K., Hrymak A.N. (2008). Discrete element simulation of liquid-particle flow. *Computers & Chemical Engineering*，**32**(4-5), 841-856.

Ashley R.M. and Crabtree R.W. (1992). Sediment origins, deposition and build-up in combined sewer systems. *Water Science and Technology*, **25**(8), 1-12.

Ashley R.M., Bertrand-Krajewski J.-L., Hvitved-Jacobsen T., and Verbanck M. (2004). *Solids in sewers: characteristics effects and control of sewer solids and associated pollutants*. London: IWA Publishing, U. K.

B

Bachoc A., Tahuchi J.P., Chebbo G., Philippe J.P. (1993). La pollution des rejets urbans par temps de pluie: flux, nature, origine et modélisation. *Colloque SHF La pluie : source de vie, choc de pollution*, Paris, France, 13-36.

Bagnold R.A. (1941).The physics of blown sand and desert dunes. London: Methuen

Bagnold R.A. (1966). An approach to the sediment transport problem from general physics. Prof. Paper 422-1, U. S. *Geological Survey.*

Bagnold R.A. (1973). The nature of saltation and bed load transport in water. *Proceedings of Royal Society of London, Series A*, London, U.K., **332**, 473-504.

Bakhtyar R., Yeganeh-bakhtiary A., Barry D.A. and Ghaheri A. (2009). Euler-Euler coupled two – phase flow modeling of sheet flow sediment motion in the near shore. *Journal Coastal Research, Special Issue*, **56**, 467-471.

Bartone D.M. and Uchrin C.G. (1999). Comparison of pollutant RE for two residential storm water basins. *Journal of Environmental Engineering*, **125**(7), 674-677.

Becouze-Lareure C.(2010). *Caractérisation et estimation des flux de substances prioritaires dans les rejets urbains par temps de pluie sur deux bassins versants expérimentaux*. Thèse de doctorat. INSA de Lyon. Lyon, France.

Bennett M.S., Mays L.W.(1985). Optimal design of detention and drainage channel systems. *Journal of Water Resources Planning and Management,* **111**(1), 99-112.

Bennett P. (2012). Identification of the hydraulic threshold in small diameter surcharged manholes. PhD Thesis, University of Sheffield, UK.

Bentzen T.R., Larsen T. and Rasmusssen M.R. (2008a). Wind effects on retention time in highway ponds. *Water Science and Technology*, **57**(11), 1713-1720.

Bentzen T.R., Larsen T. Bach C. and Raaberg I. (2008b). Numerical modeling of suspended transport and deposition of highway deposited sediment. *Technical report*. Series number 47, Department of Civil Engineering, Aalborg University.

Bentzen T.R., Larsen T., Bach C. and Raaberg I. (2008).Numerical modeling of suspended transport and deposition of highway deposited sediment. *Technical report*, Series number 47, Department of civil engineering, Aalborg University, Denmark.

Bentzen T.R. (2009). 3D numerical modeling of transport, deposition and resuspension of highway Deposited Sediment in Wet Detention Ponds. *Proceedings of the 8th UDM – Urban Drainage Modelling International Conference*, 7th - 12th September, Tokyo, Japan, 8 p.

Bertrand-Krajewski J.-L. (1993). Pollution des rejets urbains par temps de pluie. *Synthèse génerale. Rapport CIRSEE Lyonnaise des Eaux*, Le Pecq, November, 1993.137p.

Bertrand-Krajewski J. L. (2001). Détermination des vitesses de chute des polluants des rejets urbains par ajustement numérique de la courbe $M(t)$ pour le protocole VICTOR. *Research Rep.* Prepared for Institute National des Sciences Appliqués, INSA, Lyon, France.

Bertrand-Krajewski J.-L. (2004). TSS concentration in sewers estimated from turbidity measurements by means of linear regression accounting for uncertainties in both variables. *Water Science and Technology*, **50**(11), 81-88.

Bertrand-Krajewski J.-L. (2012). Short introduction to sediment transport. *Cours 4GCU Hydrologie Urbaine*. LGCIE (Eaux urbaines), INSA de Lyon, France.

Bertrand-Krajewski J.-L. (2012).Short introduction to sediment transport. *Lecture for Urban Hydrology.* LGCIE, INSA de Lyon, France.

Bertrand F., Leclaire L.-A. and Levecque G. (2005). DEM-based models for the mixing of granular materials. *Chemical Engineering Science*, **60**, 2517 – 2531.

Bogardi J. (1974). *Sediment Transport in Alluvial Streams*. Budapest: Akademiai Kiado.

Bogardi J.L. (1968). Incipient sediment motion in terms of the critical mean velocity. *Acta Tech. Acad. Sci. Hung,* **62**(1-2), 1-24.

Bonakdari H., 2006. Modélisation des écoulements en collecteurs d'assainissement-application à la conception de points de measures. Thèse de doctorat, Université de Caen, Basse Normandie, France.

Bradshaw P., Launder B.E., Lumley J.L. (1994). Collaborative testing of turbulence models, In Ghia K.N., Ghia U., Goldstein D. (Eds), *Advances in computational Fluid Mechanics*, ASME FED, 196ASMEm New York.

Bridge J.S. and Dominic D.F. (1984). Bed load grain velocities and sediment transport rates. *Water Resources Research,* **20**(4), 476-490.

Brown C.B. (1950). *Sediment transportation*. In Engineering Hydraulics, ed. H. Rouse. New York, Wiley. 769-857.

Brown C.B. (1943). Discussion of Sedimentation in reservoirs, by J. Witzig. *Proceedings of the American Society of Civil Engineers,* **69**, 493-1500.

Brown W.K. and Wohletz K.H. (1995). Derivation of the Weibull Distribution Based on Physical Principles and its Connection to the Rosin-Rammler and lognormal Distributions.

Journal of Applied Physics, **78**(4)2758-2763.

Broeker H.W. (1984). Impact of depositions on sewer operation. *Proceeding of 3rd Conference urban storm drainage*, Gothenburg.

Brown J.D. and Damery S.L. (2002) .Managing flood risk in the UK: towards an integration of social and technical perspectives. *Transactions of the Institute of British Geographers*, **27**(4), 412-426.

Brune G.M. (953). Trap efficiency of reservoirs. *Transactions of the American Geophysical Union,* **4**, 407-18.

C

Camp T.R. (1945). Sedimentation and the design of settling tanks. *Proceedings of the American Society of Civil Engineers*, **75**, 445-486.

Campbell C. S. (1990). Rapid Granular Flow. *Annual Review of Fluid Mechanics*, **22**, 57-92.

Cancino L. and Neves R. (1999). Hydrodynamic and sediment suspension modeling in estuarine systems, Part I: description of the numerical models. *Journal of Marine systems*, **22**, 105-116.

Cao Z., Wei L., and Xie J. (1995). Sediment-laden flow in open channels from two phase flow viewpoint. *Journal of Hydraulic Engineering,* **121**(10), 725-735.

Cao Z. (1997). Turbulent Bursting-Based Sediment Entrainment Function. *Journal of Hydraulic Engineering*, **123**(3), 233-236.

Cebeci T. And Bradshaw M.G. (1977). *Momentum Transfer in Boundary layers*. Hemisphere Publishing Corporation, New York.

Cemagref. (2004). *Logiciel Rubar 20. Notice d'emploi.* Lyon (France) : Cemagref, Département Gestion des Milieux Aquatiques, Unité de Recherches Hydrologie-Hydraulique, Mai 2004, 64 p.

Chancelier J. P., Chebbo G., and Lucas-Aiguier E. (1998). Estimation of settling velocities. *Water Research,* **32**(11), 3461–3471.

Chang H. H. (1982). Mathematical model for erodible channels. *J. Hydraul. Div., Am. Soc. Civ. Eng.*, **108**(5), 678–689.

Chanson H. (1999). *Hydraulics of open channel flow*: an introduction basic principles, sediment motion, hydraulic modelling, design of hydraulic structures. Aronld, London NW1 3BH, UK.1999.

Chanson H. (1999). *The Hydraulics of Open Channel Flow*. Arnold, 338 Euston Road, London NW1 3BH, UK.

Charru F., Larrieu E., Dupont J.B. and Zenit R. (2007). Motion of a particle near a rough wall in a viscous shear flow. *Journal of Fluid Mechanics*, **570**, 431-453.

Chen C. (1975). Design of sediment retention basins. *Proceedings, national symposium on urban hydrology and sediment control*, July, Lexington, KY: University of Kentucky, 285-298.

Cheng N.-S. and Chiew Y.-M. (1998). Pickup probability for sediment entrainment. *Journal of Hydraulic Engineering*, **124**(2), 232-235.

Chebbo G. (1992). *Solides des rejets pluviaux urbains caractérisation et traitabilite.* Thèse de doctorat, Ecole National des Ponts et Chaussées, Paris, France.

Chebbo G., and Bachoc A. (1993). Caractérisation physico-chimique des solides des rejets urbains par temps de pluie. *Techniques Sciences Méthodes*, **10**, 524-528.

Chebbo G.,Forgues N., Lucas-Augyuer E,m Berthebaud S.(1998). A stochastic approach to modeling solid transport in settling tanks. *Water Science and Technology*, **37**(1), 277-284.

Chebbo G., Gromaire M. C., and Lucas E. (2003). Vicas protocol: Measurement of TSS settling velocities in urban effluents. *TSM,* **12**, 39-49.

Chebbo G. and Gromaire M. C. (2009). VICAS-An Operating Protocol to Measure the Distributions of Suspended Solid Settling Velocities within Urban Drainage Samples. *Journal of Environmental Engineering*. **135**(9), 768-775.

Chien N. (1956). The present status of research on sediment transport. *Transactions*, ASCE, **121**, 833-868.

Chocat B. (1997). *Encyclopédie hydrologie urbaine et assainissement*. Technique et Documentation, 1136 p. ISBN 2-7430-0126-7. Paris, France.

Chocat B., Bertrand-Krajewski J.-L., Barraud S. (2007). Eaux pluviales urbaines et rejets urbains par temps de pluie. *Techniques d'Ingénieur,* W 6 800, 1-17.

Churchill M.A. (1948). Discussion of Analyses and use of reservoir sedimentation data by Gottschalk L.C. *Proceedings of the federal interagency sedimentation conference*, Denver, Colorado, Washington, DC: US Geological Survey, 139-140.

Clift R., Grace J. R., and Weber M. E. (1978). *Bubbles, drops, and particles,* Academic Press, London.

Comings K.J., Booth D.B., Horner R.R. (2000). Storm Water Pollutant Removal by Two Wet Ponds in Bellevue, Washington. *Journal of Environmental Engineering*, **126**(4), 321-330.

Corsi S.R., Greb S.R., Bannerman R.T. and Pitt R.E. (1999). Evaluation of the multi-chambered treatment train, a retrofit water-quality management device. *U.S. Geological Survey.*

Cundall P.A. and Strack O.D. (1979). A discrete numerical model for granular assembles. *Geotechnique*, **21**, 47-65.

D

Deletic A., Maksimovie C. and Ivetic M. (1997). Modeling of storm washoff of suspended solid from impervious surface. *Journal of Hydraulic Research*, **35**(1), 99-118.

Deletic A. (2001). Modeling of water and sediment transport over grassed areas. *Journal of Hydrology*, **248,** 168-182.

Dembélé A. (2010). *MES, DCO et polluants prioritaires des rejets urbains de temps de pluie : mesure et modélisation des flux événementiels*. Thèse de doctorat, INSA de Lyon, Lyon, France.

Department of Transport and Main Roads of Queensland Government. (2013). Road drainage manual. Queensland Department of Transport and Main Roads, Brisbane, Australia.

Deutsch J.-C., Bachoc A., Guichard M. A., Chebbo G., Flores- Rodriguez, Thévenot D.-R., Lebreton L. and Bussy A. L. (1990). Pour une nouvelle maîtrise des eaux pluviales. Actes du colloque (La Gestion de l'Eau). Paris: Presses de ENPC.

Dewals B.J., Kantoush S.A., Erpicum S., Pirotton M. and Schleiss A.J. (2008). Experimental and numerical analysis of flow instabilities in rectangular shallow basins. *Environmental Fluid Mechanics,* **8**, 31-54.

Dey S., Sarkar S., and Solari L. (2011). Near-Bed Turbulence Characteristics at the Entrainment Threshold of Sediment Beds. *Journal of Hydraulic Engineering,* **137**(9), 945-958.

Dore M.H.I. (2005). Climate change and changes in global precipitation patterns: What do we know? Environment international，**31** (2005), 1167-1181.

Dufresne M. (2008). *La modélisation 3D du transport solide dans les bassins en assainissement: du pilote expérimental à l'ouvrage réel*. Thèse de doctorat, Université Louis Pasteur, Strasbourg, France.

Dufresne M., Vazquez J., and Terfous A. (2009). Experimental investigation and CFD modeling of flow, sedimentation, and solids separation in a combined sewer detention tank. *Computers and Fluids*, **38**, 1042-1049.

Dufresne M., Vazquez J., Terfous A., Ghenaim A., and Poulet J.-B. (2009). CFD modelling of solid separation in three combined sewer overflow chamber. *Journal of Environmental Engineering*, **135**(9), 776-787.

Du Boys M.P. (1879). Études du régime du Rhône et de l'action exercée par les eaux sur un lit à fond de graviers indéfiniment affouillable. *Annales des Ponts et Chaussées*, **5**(18), 141-195.

Dyer K. R. (1986). *Coastal and estuarine sediment dynamics.* John Wiley & Sons, Inc., New York, N.Y.

E

Einstein, H.A. (1942). Formulas for the transportation of bed load. *Trans. ASCE*, **107**, 561-573.

Einstein H.A. (1944). Bedload transportation in Mountain Creek. Department of Agriculture, Washington, D.C.

Einstein H.A. (1950). The bed load function for sediment transportation in open channel flow. U.S. Dept. Agri. Tech. Bull. 1026.

El Ganaoui O., Schaaff E., Boyer P., Amielh M., Anselmet F. and Grenz C. (2004). The deposition and erosion of cohesive sediment determined by a multi-class model. *Estuarine Coastal and Shelf Science*, **60**, 457-475.

El Ganaoui O., Schaaff E., Boyer P., Amielh M., Anselmet F. and Grenz C. (2007). Erosion of the upper layer of cohesive sediment: characterization of some properties. *Journal of Hydraulic Engineering,* **133**(9), 1087-1091.

Elghobashi S.E. (1991). Particle laden turbulent flow: Direct simulation and closure models. Appl. Sci. Res., 48, 301-314.

Ellis J.B., Revitt D.M. (1982). Incidence of heavy metals in street surface sediment: solubility and grain size studies. Water, Air, and Soil Pollution, 17, 87-100.

Engelund F. (1965a) A criterion for the occurrence of suspended load. La Houille Blanche, 8, 802.

Engelund F. (1965b) Turbulent Energy and Suspended Load. Progress Report no. 10, 2-9. Coastal Engineering Laboratory, Hydraulic Laboratory, Technical University of Denmark, Lyngby, Denmark.

Engelund F. and Hansen E. (1967). A monograph on sediment transport in alluvial streams, Teknisk Forlag, Copenhagen.

Engineers Australia (2006). *Australian Runoff Quality: A Guide to Water Sensitive Urban Design.* Wong T. H. F. (Ed), ISBN 085825 852 8, April 2006.

F

Few R., Ahern M., Matthies F. and Kovats S. (2004). Floods, health and climate change: A strategic review. Tyndall Centre Working Paper 63, UK.

Ferrara R.A. and Witkowski P. (1983). Stormwater quality characteristics in detention basins. *Journal of Environmental engineering*, **109**(2), 428-447.

Ferziger J.H. and Peric M. (2002). *Computational methods for fluid dynamics*. Spring-veralg berlin Heidelberg, New York, U.S.

Francis J.R.D. (1973). Experiments on the motion of solitary particles along the bed of a water-stream. *Proc. Roy. Soc. London*, London, U.K., A332, 443-471.

Frey P., Champagne J.Y., Morel R., and Gay B. (1993). Hydrodynamics fields and solid particles transport in a settling tank. *Journal of Hydraulic Research*, **31**(6), 736-776.

Furumai H., Balmer H., and Boller M. (2002). Dynamic behaviour of suspended pollutants and particle size distribution in highway runoff. *Water Science and Technology*, **46**(11-12), 413-418.

G

Garde R.J., Ranga Raju K.G., Sujudi A.W.R. (1990). Design of settling basins. *Journal of Hydraulic Research,* **28**(1), 81-91.

Gardner W.D. and Southard J.B. (1975). Dynamics of boundary-layer deposition: A flume investigation. *Trans. Am. Geophys. Union,* **56**, 372 (Abstr).

Garcia M.H., Parker G. (1991). Entrainment of bed sediment into suspension. *Journal of Hydraulic Engineering*, **111**(4), 414–435.

Geiger W.F. (1986). Variation of combined runoff quality and resulting pollution retention strategies, urban storm water quality and effects upon receiving waters, TNO Committee on Hydrological Research. *Proceedings and Information 36, Int. Conf., Wageningen*, the Netherlands, 71–91.

German J., Jansons k., Svensson G., Karisson D. and gustafsson L.-G. (2005). Modelling of different measures for improving trap in a stormwater pond. *Water Science and Technology*, **52**(5), 105-112.

Gilbert G.K. (1914). The transport of debris by running water. *Geological Survey.* Professional Paper 86. Washington, D.C., U.S.

Gonzalez-Merchan G. (2012). *Amélioration des connaissances sur le colmatage des systèmes d'infiltration d'eaux pluviales.* Thèse de doctorat, INSA de Lyon, Lyon, France.

Gordon R., Carmichael J.B., and Isackson E.J. (1972). Saltation of plastic balls in 'one-dimensional' flume. *Water Resources Research*, **8**(2), 444-459.

Gourmelon M., Caprais M.P., Mieszkin S., Marti R., Wéry N., Jardé E., Derrien M., Jadas-Hécart A., Communal P.Y., Jaffrezic A., Pourcher A.M. (2010). Development of microbial and chemical MST tools to identify the origin of the faecal pollution in bathing and shellfish harvesting waters in France. *Water Research*, **44**(16), 4812-4824.

Graf W.H. and Altinakar M.S. (2000). *Hydraulique Fluviale: écoulement et phénomènes de transport dans les canaux à géométrie simple* (Fluvial Hydraulics: Flow and transport processes in channels with simple geometry). Traité de Génie Civil, Volume 16, L'école polytechnique fédérale de Lausanne, Publié sous la direction de René Walther, Presses polytechniques Romandes.

Grass A.J. (1982). The influence of boundary layer turbulence on the mechanics of sediment transport. *Proc. Euromech 156*: *Mech. of Sediment Transport*, Tech. Univ. of Istanbul, Istanbul.

Grizzard T.J., Randall C.W., Weand B.L., and Ellis K.L. (1986). The Effectiveness of Extended Detention Ponds for Urban Stormwater Pollution Management, Proceedings, EF/ASCE Conference on Urban Stormwater Quality, Impacts, and Enhancement Technology.

Guo Q., Agnoli N.W., Zhang N., and Hayes B.D. (2000). Hydraulic and water quality performance of urban storm water detention basin before and after outlet modification. *Conference on Water Resource Engineering and Water Resources Planning and Management*, Minneapolis, Minnesota, U.S., 30th July - 2nd August, 10 p.

Guo C.Y. (2009). Retrofitting detention basin with water quality control pool. *Journal of Irrigation and Drainage Engineering*, **135**(5), 671-675.

H

Haan C.T., Barfield B.J. and Hayes J.C. (1994).*Design hydrology and sedimentology for small catchments*. San Diego, CA: Academic Press.

Hager W.H. (2010). *Wastewater Hydraulics: theory and practice*. 2nd, Springer, Switzerland.

Hall M.J., Hockin and Ellis J.B. (1993). *Design of food storage reservations*. London: Butterworth Heinemann.

Han Q.W. (1980). A study on the non-equilibrium transportation of suspended load. *Proc., 1st Int. Symp. On River Sedimentation, IRTCES*, Beijing.

Hanjalić K. (1994).Advanced turbulence closure model: review of current status and future prospects. *Int. J. Heat Fluid Flow*.**15**, 178-203.

Hadzic I. (1999). *Second-moment closure modeling of transitional and unsteady turbulent flow*. PhD Thesis, Delft University of Technology.

Harwood R. and Saul A.J. (1996). CFD and novel technology in combined sewer overflow. Proceedings of the 7th Int. *Conf. on Urban Storm Drainage*, Hannover, Germany, 9th-13th September, 1025-1030.

Heinemann H.G. (1984). Reservoir trap efficiency. *Erosion and sediment yield: some methods of measurement and modelling,* Hadley, R.F. and Walling, D.E., ed., 201-218.

Hirt C.W. and Nichols B.D. (1981). Volume of Fluid (VOF) method for the dynamics of free boundaries. *Journal of Computational Physics*. **39**, 201-225.

Hjulström F. (1935). Studies of the morphological activity of rivers as illustrated by the river Fyris, University of Uppsala Geological Institute Bulletin, **25**, 221-557.

Holly F.M. and Rahuel J.L. (1990). New numerical/physical framework for mobile-bed modeling, Part I: Numerical and physical principles. *Journal of Hydraulic Research*, **28**(4), 401-416.

Holly F.M., Yang J.C., Schovarz P., Scheefer J., Hsu S.H., and Einhellig R. (1990). CHARIMA: Numerical simulation of unsteady water and sediment movements in multiply connected networks of mobile-bed channels. *Report No. 343*, Iowa Institute of Hydraulic Research, Univ. of Iowa, Iowa City, Iowa.

Hsu T. J., Jenkins J. T., and Liu P. L. F. (2001). Modeling of sediment transport a two-phase flow approach. *Coastal Dynamics '01,* Lund, Sweden.

Hsu T.-W., Chang H.-K., and Hsieh C.M. (2003). A two - phase flow model of wave-induced sheet flow. *Journal of Hydraulic Research*, **41**(3), 299-310.

Hu C. and Hui Y. (1996). Bed-load transport, I: Mechanical characteristics. *Journal of Hydraulic Engineering*. **122**, 245-254.

Hu C., Hui Y. and Xia Z. (1993). Analysis of saltation characteristics of bed load transport in flowing water. *Acta mechanica sinica*, **9**(2), 110-116.

Huber W.C. and Dickinson R.E. (1988). S*torm Water Management Model. User's Manual Ver. IV*, U.S. Environmental Protection Agency.

Hunze M. (2008). Investigation of clarification tanks using 3-dimensional simulation studies-part 1 circular clarification tanks. Hannover, Germany, Flow Concept GmbH.

Hu C. and Hui Y. (1996). Bed load Transport, part I: Mechanical Characteristics. *Journal of Hydraulic Engineering.* **122**(5), 245-254.

Huber, W. C., and Dickinson, R. E. (1988). Stormwater management model, version 4: User's manual, environmental research laboratory, U.S. Environmental Protection Agency, Athens, Ga.

Hvitved-Jacobsen T., Johansen N.B., and Yousef Y.A. (1994). Treatment systems for urban and highway runoff in Denmark. *The science of the Total Environment*, **146/147**, 499-506.

I

Ikeda S. and Asaeda T. (1983). Sediment suspension with rippled bed. *Journal of Hydraulic Engineering*, **109**(3), 409-423.

Ip N. (2009). *The role of mesh smoothness in the convergence of higher-order methods*. Thesis, Department of Mechanical and Industrial Engineering, University of Toronto.

Issa R.I. (1986). Solution of the implicitly discretized fluid flow equations by operator splitting. *Journal of Computational Physics,* **62**, 40-65.

J

Jackson R.G. (1976). Sedimentological and fluid-dynamic implications of the turbulent bursting phenomenon in geophysical flow. *J. Fluid Mech.*, **77**(3), 531-560.

Jarman D.S., Faram M.G., Butler D., Tabor g. Stovin V.R., Butt D., and Throp E. (2008). Computational fluid dynamics as a tool for urban drainage system analysis: A review of application and best practice. *Proceedings of the 11th International Conference on Urban drainage*, 31st August - 5th September, Edinburgh, Scotland, UK, 10 p.

Jayanti S., Narayanan S. (2004). Computational study of particle-eddy interaction in sedimentation tanks. *Journal of Environmental Engineering*, **130**(1), 37-49.

Jacopin C., Bertrand-Krajewski J.L. and Desbordes M. (1999). Characterization and Settling of Solids in an Open, Grassed, Stormwater Sewer Network Detention Basin. *Water Science and Technology*, **39** (2), 135-44.

Joshi A.S., Sun Y. (2009) Multiphase lattice Boltzmann method for particle suspensions. Physics Review, E 79, 066703.

Julien P.Y. (2010). *Erosion and sedimentation*. 2nd, Cambridge University Press, the Edinburgh Building, Cambridge CB2 8RU, UK.

K

Kadlec R.H. (1990). Overland flow in wetlands: vegetation resistance. *ASCE Journal of Hydraulic Engineering*, **116**(5), 691-705.

Kadlec R. H., and Knight R.L. (1996). *Treatment Wetlands.* Lewis Publishers, Chelsea, Michigan.

Kalinske A.A. (1942). Criteria for determining sand transport by surface creep and saltation. *Trans. AGU*, **23**, part 2, 639-43.

Kantoush S.A., Bollaert E., Boillat J.L., Schleiss A.J. (2006). Experimental study of suspended sediment transport and deposition in a rectangular shallow reservoir. Alves Ferreira, Cardoso Leal (Eds.), River flow 2006, 1623-1630.

Kantoush S., Dewals B., Erpicum S., Schleiss A., and Pirotton M. (2008a). Flow in shallow rectangular basins: experimental study and 2D numerical simulations. 8th International Conference on Hydro-science and Engineering (ICHE). 8th-12th September, Nagoya, Japan.

Kantoush S.A., Cesare G.D., Boillat J.L., Schleiss A.J. (2008b). Flow field investigation in a rectangular shallow reservoir using UVP, LSPIV and numerical modeling. Flow measurement and Instrumentation, **19**, 139-144.

Kantoush S.A., Bollaert E., Schleiss A.J. (2008c). Experimental and numerical modeling of sedimentation in a rectangular shallow basin. International Journal of sediment research. 23(3), 212-232.

Kantoush S.A., Schleiss A.J. and Nagy H. (2008d). Deposition of sediment mixture due to jet effluent into a rectangular shallow reservoir. *Alexandria Engineering Journal*, **47**(5), 451-462.

Kantoush S., Sumi T., Schleiss A. (2010).geometry effect on Flow and sediment deposition patterns in shallow basins. *Annual Journal of Hydraulic Engineering, JSCE*. **54**, 133-138.

Karim M. F. and Kennedy J. F. (1982). IALLUVIAL: A commuter based flow and sediment routing for alluvial streams and its application to the Missouri River. *Rep. No. 250*, Iowa Institute of Hydraulic Research, Univ. of Iowa, Iowa City, Iowa.

Kawanisi K., and Yokosi S. (1993). Measurements of turbulence and suspended sediment in tidal river. *Journal of Hydraulic Engineering,* **119**(6), 704-724.

Kayhanian M., McKenzie E.R., LeatherbarrowJ.E. and Young T.M. (2012). Characteristics of road sediment fractionated particles captured from paved surfaces, surface run-off and detention basins. *Science of the Total Environment,* **439**, 172-86.

Kayhanian M., Rasa E., Vichare A. and Leatherbarrow J.E. (2008). Utility of Suspended Solid Measurements for Storm-Water Runoff Treatment. *Journal of Environmental Engineering,* **134** (9), 712-21.

Keating M. (2011). Accelerating CFD solutions. *Ansys advantage*. **V** (1), 48-49, Ansys Inc.

Kloss C., Goniva C., Aichinger G. and Pipker S. (2009). Comprehensive DEM-DPM-CFD Simulation-model synthesis, experimental validation and scalability. *Seventh International Conference on CFD in the Minerals and Process Industries CSIRO,* 9th-11th December 2009, Melbourne, Australia

Knupp P.M. (2007). Remarks on Mesh Quality. Proceeding of 45th AIAA Aerospace Sciences Meeting and Exhibit, 7th-10th January, Reno, NV, US.

Kowalski R., Reuber J. and Köngeter J. (1999). Investigations into and optimization of the performance of sewage detention tanks during storm rainfall events. *Water Science and Technology*, **39**(2), 43-52.

Krištof P. Beneš B., Krivánek J. and Šťava O. (2009). Hydraulic erosion using smoothed particle hydrodynamics. *Computer Graphics Forum* (Proceedings of Eurographics 2009), **28**2), 219-228.

Krone R. B. (1962). Flume studies of the transport of sediment in estuarial shoaling processes. Final Rep., Hydraulic Engineering Laboratory and Sanitary Engineering Research Laboratory, Univ. of California at Berkeley, Berkeley, Calif.

L

Ladd A.J.C. and Verberg R. (2001). Lattice - Boltzmann simulation of particle- fluid suspensions. *Journal of Statistical Physics*, **104**(5/6), 1191-1251.

Lajeunesse E., Malverti L. and Charru F. (2010). Bed load transport in turbulent flow at the grain scale: experiments and modeling. *Journal of Geophysical Research*, **115**, F04001. 16 p.

Lafond J.-M. (1995). *Comparaison de modèles de transport en suspension application à des ouvrages de stockage dépollution*. Thèse de doctorat, université Claude Bernard, Lyon, France.

Larsen T., Broch K. and Andersen M.R. (1998). First flush effects in an urban catchment area in Aalborg. *Water Science and Technology*, **37**(1), 251-257.

Lau S.D., Stovin V.R. and Guymer I. (2007). The prediction of solute transport in surcharged manholes using CFD. *Water Science and Technology,* 55(4), 57-64.

Launder B.E. and Spalding D.B. (1974). The numerical computation of turbulent flow. *Computer Methods in Applied Mechanics and Engineering,* **3**, 269-289.

Launder B.E. (1990). Turbulence at the crossroads. *Lecture Notes in Physics*, **357**,439-485, springer, Berlin.

Launder B.E. and Spalding D.B. (1972). *Lectures in Mathematical Models of Turbulence*. Academic Press, London, England.

Lawrence A.I., Marsalek J., Ellis J.B. and Urbonas B. (1996). Stormwater detention & BMPs. *Journal of Hydraulic Research*, **34**(6), 799-813.

Laïly A.-G. (2012). Risque associé au transfert de polluants lors d'une inondation urbaine. Apporte de Projet EC2CO. LGCIE, INSA de Lyon.

Leclaire C. (1997). *Etude du fonctionnement d'un bassin de pollution en tête d'une station d'épuration, propositions de gestion*. Thèse de master, Ecole Nationale du Génie de l'Eau et de l'Environnement de Strasbourg, France.

Lee H.Y., and Hsu I.S. (1994). Investigation of saltating particle motions, *Journal of Hydraulic Engineering,* **120**(7), 831-845.

Lee H.Y., You J.Y. and Lin Y.T. (2002). Continuous saltating process of multiple sediment particles. *Journal of Hydraulic Engineering*, **128** (4), 443-450.

Lee B., Shimizu Y., Matsuda T., and Matsui S. (2005). Characterization of polycyclic aromatic hydrocarbons (PAHs) in different size fractions in deposited road particles (DRPs) from Lake Biwa area, Japan. *Environmental Science and Technology*, **39**, 7402-7409.

Letondu L. (1997). Suivi du bassin de dépollution des rejets urbains par temps de pluie de la commune de Sargé-Les-Le-Mans. Rapport de stage pour la Communauté Urbaine du Mans, France.

Ling C. (1995). Criteria for Incipient Motion of Spherical Sediment Particles. *Journal of Hydraulic Engineering*, **121**(6), 472-478.

Lipeme Kouyi G. (2004). *Expérimentations et modélisations tridimensionnelles de l'hydrodynamique et de la séparation particulaire dans les déversoirs d'orage.* Thèse de doctorat, Université Louis Pasteur, Strasbourg, France.

Lipeme Kouyi G., Vazquez J., Rollet D., Gallin Y., Sa dowski A-G. (2005). Use of 3D modelling and several ultrasound sensors to assess overflow rate. *Water Science and Technology*, **51**(2), 187-194.

Lipeme Kouyi G., Arias L., Barraud S., Bertrand-Krajewski J.-L. (2010). CFD modeling of flow in a large stormwater detention and settling basin. 7th International Conference on Sustainable Techniques and Strategies in Urban Water Management, Novatech, 27th June-1st July, Lyon, France. 10 p.

Loganathan G.V., Watkins E.W., and Kibler D.F. (1994). Sizing stormwater detention basins for pollutant removal. *Journal of Environmental Engineering.* **120** (6), 1380-1399.

Loch R.J. (2001). Settling velocity- a new approach to assessing soil and sediment properties. *Computers and electronics in agriculture*, **31**, 305-316.

Loganathan G.V., Watkins E.W., and Kibler D.F. (1994). Sizing storm-water detention basins for pollutant removal. *Journal of Environmental Engineering*, **120** (6), 1380-1399.

Lu N., Aderson M.T., Likos W.J., Mustoe G.W. (2008). A discrete element model for kaolinite aggregate formation during sedimentation. *International Journal for Numerical and Analytical Methods in Geomechanics,* **32**, 965-980.

Luque R. E., and Van Beek R. (1976). Erosion and transport of bed-load sediment. *Journal of Hydraulic Research*, **14**(2), 127-144.

Luyckx G., Vaes G. and Berlamont J. (1999). Comparison between the separating efficiency of an improved high-side weir overflow and a hydrodynamic Storm King (TM) separator. *Water Science and Technology,* **39**(9), 177-184.

M

Ma Department of Environmental Protection (MDEP) and MCZM (1997). *Stormwater Management: stormwater policy handbook*. Volume I, Massachusetts, U.S.

Maa J.P.-Y., Kwon J., Hwang K.-N., and Ha H.-K. (2008). Critical bed shear stress for cohesive sediment deposition under steady flow. *Journal of Hydraulic Engineering*, **134**(12), 1767-1771.

Mangelson K. and Watters G. (1972). Treatment efficiency of waste stabilization ponds. *Journal of the Sanitary Engineering Division,* SA2, 407-425.

Marcoon K.B. and Guo Q. (2004). Detention basin retrofit: optimization of water quality improvement and flood control. Critical Transitions in Water and Environmental Resources Management. 27th June - 1st July, 2004, Salt Lake City, Utah, U.S.

Marecos de Monte M.H.F., and Mara D.D. (1987). The hydraulic performance of waste stabilization ponds in Portugal. *Water Science and Technology,* **19**(12), 219-227.

Marsalek J., Krishnappan B.G., Watt W.E. and Anderson B.C. (1998). In Size distribution of suspended sediments in an on-stream stormwater management pond. 3th NOVATECH, 4-6 May 1998, Lyon, France.

Matuttis H.G., Luding S. and Herrmann H.J. (2000). Discrete element simulations of dense packings and heaps made of spherical and non-spherical particles. *Powder Technology*, **109**, 278-292.

Mantz P.A. (1980). Laboratory flume experiments on the transport of cohesionless silicon silts by water streams. Proc. Inst. Civ. Eng., (69), 977-994.

Mehta A. J. and Partheniades E. (1975).An investigation of the deposition properties of flocculated fine sediment. *Journal of Hydraulic Research*, **13**(4), 361–381.

Meyer-Peter E. and Muller R. (1948). Formulas for bed-load transport. *Proc. 2nd Meeting IAHR*, Stockholm, 39-64.

Mezhericher M., Brosh. T. and Levy A. (2011). Modeling of Particle Pneumatic Conveying Using DEM and DPM Methods, *Particulate Science and Technology: An International Journal*, (**29**)2, 197-208.

Mignot E., Bonakdari H., Knothe P., Lipeme Kouyi G., Bessette A., Rivière H. N., and Bertrand-Krajewski J.-L.(2012). Experiments and 3D simulations of flow structures in junctions and of their influence on location of flowmeters. *Water Science and Technology*, **66**(6), 1325-1332.

Momplot A., Bonakdari H., Mignot E., Lipeme Kouyi G., Riviere N., Bertrand-Krajewski J.-L.(2012). Effects of computational meshes on hydrodynamics of an open channel junctions flow using CFD technique. *Proceedings of the 9th Urban Drainage Modelling International Conference*, 3rd - 7th September, Belgrade, Serbia, 10p.

Morsi S.A. and Alexander A.J. (1972). An investigation of particle trajectories in two-phase flow systems. *Journal of Fluid Mechanics,* **55**(02), 193-208.

Moshiri G. A. (1993). *Constructed wetlands for water quality improvement.* Lewis Publishers, Chelsea, Michigan.

Murphy P.J., and Aguirre E.L. (1985). Bed load or suspended load. *Journal of Hydraulic Engineering*, **111**(1), 93-107.

N

Nalpanis P.; Hunt J.C.R. & Barrett C.F. (1993). Saltating particles over flat beds. *Journal of Fluid Mechanic,* **251**, 661-685.

Nascimento N.O., Ellis J.B., Baptista M.B. and Deutsch J.-C. (1999). Using detention basins: operational experience and lessons. *Urban water*, **1**, 113-124.

Nelson, J.M., Shreve R.L., Mclean S.R. and Drake T.G. (1995). Role of near bed turbulence structure in bed load transport and bed form mechanics. *Water Resources Research*, **31**(8), 2071-2086.

Nielsen P. (1992). Coastal Bottom Boundary Layers and Sediment Transport, *World Scientific,* U.S.

Nighman D., and Harbor J. (1997). Trap efficiency of a stormwater basin with and without baffles. *Proc. Int. Erosion Control Assn,* **28**, 469 - 483.

Niño Y., Lopez F. and Garcia M. (2003). Threshold for particle entrainment into suspension. *Sedimentology*, **50**, 247-263.

Niño Y., García M., and Ayala L. (1994a). Gravel saltation I: Experiments. *Water Resources Research*, **30**(6), 1907-1914.

Niño Y., García M., and Ayala L. (1994b). Gravel saltation II: Modeling. *Water Resources Research*, **30**(6), 1915-1924.

Niño Y. and García M. (1998a). Using Lagrangian saltation observations for bed load sediment transport modelling. *Hydrological Processes*, **12**, 1197-1218.

Niño Y., and García M. (1998). Experiments on saltation of fine sand in water. *Journal of Hydraulic Engineering*, **124**(10), 1014-1025.

Niño Y. & Garcia M. (1994). Gravel saltation-experiments. *Water Resources Research.* **30**(6), 1907-1914.

Nix S.J. (1985). Residence time in stormwater detention basin. *Journal of Environmental Engineering*. **111**(1), 95-100.

Nix S.J., and Heaney J.P. (1988). Optimization of storage release strategies. *Water Resources Research*, **24**(11), 1831-1838.

Nix S.J., Heaney J.P., and Huber W.C. (1988). Suspended solids removal in detention basins. *Journal of Environmental Engineering*, **114**(6), 1331-1341.

Novak P. and Nalluri C. (1972). A study into the correlation of sediment motion.in pipe and open channel flow. Proc. 2nd. Intern. Conf. on the Hydraulic Transport of Solids in Pipes, Hydrotransport 2, D4, 33-51.

Novak P., Nalluri C. (1975). Sediment transport in smooth fixed bed channels. Journal of the Hydraulics Division, 101(9), 1139-1154.

Novak P., Nalluri C. (1984). Incipient motion of sediment particles over fixed beds. Journal of Hydraulic Research, 22(3), 181-197.

O

Ormsbee L.E., Houck M.H. and Delleur J.M. (1987). Design of dual purpose detention systems using dynamic programming. *Journal of Water Resources Planning and Management*, **113**(4), 471-484.

Olsen N.R.B. (1999). Two-dimensional numerical modeling of flushing processes in water reservoirs. *Journal of Hydraulic Research*, **37**(1), 3-16.

P

Paintal A.S. (1971). A stochastic model of bed-load transport. *Journal of Hydraulic Research*, **9**(4), 527-554.

Papanicolaou A.N. (1997). *The role of turbulence on the initiation of sediment motion*. PhD thesis, Virginia Polytechnic Institute and State University. US.

Papanicolaou A.N. (2000). The role of near bed turbulence structure in the inception of particle motion. *International Journal of Fluid Dynamics,* 4, Article 2.

Papaniolaou A.N., Diplas P., Dancey C.L. and Balakrishnan M. (2001). Surface roughness effects in near-bed turbulence: implication to sediment entrainment. *Journal of Engineering Mechanics,* **127**(3), 211-219.

Papanicolaou A.N., Diplas P., Evaggelopoulos N., and Fotopoulos S. (2002). Stochastic incipient motion criterion for spheres under various bed packing conditions. *Journal of Hydraulic Engineering*, **128**(4), 369- 380.

Papanicolaou A.N., Elhakeem M., Krallis G., Orakash S., and Edinger J. (2008). Sediment transport modeling review- current and future developments. *Journal of Hydraulic Engineering*, **134**(1), 1-14.

Patankar S.V. and Spalding C.B. (1972). A calculation procedure for heat, mass and momentum transfer in three-dimensional parabolic flow. *International Journal of Heat and Mass Transfer,* **15**, 1787-1798.

Pathapati S., Dickenson J., Garofalo G., Sansalone J., Bolognese A., Maglionico M., Artini S. (2008). Calibration Testing and Modeling of a Hydrodynamic Separator for Urban Drainage Particulate Matter Separation and Scour. 11th International Conference on Urban Drainage, 31st August - 5th September, Edinburgh, Scotland, UK.

Pathapati S., and Sansalone G. (2009). CFD modeling of a storm-water hydrodynamic separator. *Journal of Environmental Engineering*, **135**(4), 191-202.

Pathapati S. and Sansalone G. (2009). Particle dynamics in a hydrodynamic separator subject to unsteady rainfall-runoff. *Water Resources Research*, **45**, W09408. 14 p.

Pearson L.G., Thornton R.C., Saul A.J. and Howard K. (1986). An introductory analysis of the factors affecting the concentration of pollutants in the first foul flush of a combined storm sewer system. *Proceeding s of international symposium on urban stormwater quality and effects upon receiving waters,* wageningen, the Netherlands, 93-102.

Persson J., Somes N.L.G., Wong T.H.F. (1999). Hydraulics efficiency of constructed wetlands and ponds. *Water Science and Technology*. **40**(3), 291-300.

Persson J. (2000). The hydraulic performance of ponds of various layouts. *Urban Water,* **2**, 243-250.

Pettersson T.J.R. (1997). FEM-modeling of open stormwater detention ponds. *Nordic Hydrology,* **28**(4-5), 339-350.

Pettersson T.J.R., German J., and Svensson G. (1998). Modelling of flow pattern and particle removal in an open stormwater detention pond. *HydraStorm'98,* Adelaide, Australia, 64-68.

Plate E.J. (2002). Flood risk and flood management. *Journal of Hydrology*, **267**(1-2), 2-11.

Prudhomme C., Jakob D. and Svensson C. (2003). Uncertainty and climate change impact on the flood regime of small UK catchments. *Journal of Hydrology*, **277**(1-2), 1-23.

Q

Quarini G., Innes H., Smith M., Wise D. (1996). Hydrodynamic modelling of sedimentation tanks. Proceedings of the Institution of Mechanical Engineers, Part E. *Journal of Process Mechanical Engineering*, **210**(2), 83-91.

R

Randall C.W., Ellis K., Grizzard T.J. and Knocke W.R. (1982). Urban Runoff Pollutant Trap by Sedimentation, *Proceedings, EF/ASCE Conference on Stormwater Detention Facilities - Planning, Design, Operation, and Maintenance*, Henniker, NH, 205-219.

Raudkivi, A.J. (1998). *Loose boundary hydraulics*, 4th Ed., Balkema, Rotterdam, The Netherlands.

Reizes J.A. (1978). Numerical study of continuous saltation. *J. Hydr. Div., ASCE,* **104**(9), 1305-1321.
Rosin P and Rammler E. (1933). The laws governing the fineness of powdered coal. *Journal of Institute of Fuel,* **7,** 29-36.

Rouse H. (1937). Modern conceptions of the mechanics of turbulence. *Transactions*, *ASCE*, **102**, 436-505.

Ryu J. and Butler D. (2008). Managing Sewer Flood Risk. *11th International Conference on Urban Drainage*, Edinburgh, UK.

S

Salim S.M. and Cheah S.C. (2009). Wall y+ strategy for dealing with wall-bounded turbulent flows. Proceedings of the International MultiConference of Engineers and Computer Scientists.Vol 2, March 18-20, Hong Kong.

Sansalone J.J. and Pathapati S.S. (2009). Particle dynamics in a hydrodynamic separator subject to transient rainfall-runoff. *Water resources Research*, **45**(9), W09408.

Saul A.J., Brownbill V.R., Skipworth P., Roulston M., Lafond J.M. (1992). Laboratory investigations of shaft-tank efficiency. *Proceedings of the 3rd International Conference NOVATECH.* 3th-5th November, Lyon, France.

Saul A.J. and Ellis D.R. (1992). Sediment deposition in storage tanks. *Water Science and Technology*, **25**(8), 189-198.

Schlichting H. (1979). *Boundary layer theory*. 7th ed. Mcgraw-Hill. New York.

Schmitt F., Milisic V. and Chebbo G. (2002). Storage settling basins design and management. Sewer Processes and Networks. France.

Sebastian C., Barraud S., Ribun S., Blaha D., Perrodin Y., Bazin C., Clozel B., Cournoyer B. (2011). Assessment of chemical and microbial hazards in a full-scale stormwater detention basin: Their characterization, toxicity and fate.*12th International Conference on Urban Drainage*, Porto Alegre, Brazil, 11th-16th September 2011, 8 p.

Sekine M., and Kikkawa H. (1992). Mechanics of saltating particles. *Journal of Hydraulic Engineering*, **118**(4), 536-558.

Self R.F.L., Nowell A.R.M. and Jumars P.A. (1986). Factors controlling critical shear for deposition and erosion of individual particles. *Marine Geology*, **86**, 181-199.

Shams M., Ahmadi G. and Smith D.H. (2002). Computational modeling of flow and sediment transport and deposition in meandering rivers. *Advances in Water Resources*, **25**, 689–699.

Shaw J. K. E., Watt W. E., Marsalek J., and Anderson B. C. (1997). Flow pattern characterization in an urban stormwater detention pond and implications for water quality. *Journal of Water Quality Research,* **32**(1), 53-71.

Shields A. (1936): Anwendung der Ähnlichkeitsmechanik und der Turbulenzforschung auf die Geschiebebewegung. Mitteilungen der Preußischen Versuchsanstalt für Wasserbau und Schiffsbau, Berlin, Heft 26. Translation: Application of similarity mechanics and turbulence research to bed load movement. Releases the Prussian Laboratory of Hydraulics and shipbuilding, Berlin, No. 26.

Shimizu Y., Yamaguchi H., and Itakura T. (1990). Three-dimensional computation of flow and bed deformation. *Journal of Hydraulic Engineering*, **116**(9), 235-253.

Smith J, and McLean S. (1977). Spatially averaged flow over a wavy surface. *Journal of Geophysical Research.* **83**, 1735-1746.

Southard J. (2006). Special Topics: An Introduction to Fluid Motions, Sediment Transport, and Current-generated Sedimentary Structures. *Lecture notes*. Massachusetts Institute of Technology. US.

Souders D.T. and Hirt C.W. (2002). Modeling Roughness Effects in Open Channel Flow. *Science Report FSI-02-TN60*, Flow Science Inc., Santa Fe, N.M.

Soulsby R. (1997). Marine Sands. Thomas Telford.

Spasojevic M. and Holly F.M. (1990). 2-D bed evolution in natural watercourses- New simulation approach. *J. Waterway, Port, Coastal, Ocean Eng.*, **116**(4), 425-443.

Stamou A.I. (2008). Improving the hydraulic efficiency of water process tanks using CFD models. *Chemical Engineering and Processing,* 47(2008).

Stovin V.R. and Saul A.J. (1994). Sedimentation in storage tank structures. *Water Science and Technology*, **29**(1-2), 363-372.

Stovin V.R. (1996). *The prediction of sediment deposition in storage chamber based on laboratory observations and numerical simulation*. PhD thesis, University of Sheffield, UK.

Stovin V.R. and Saul A.J. (1996). Efficiency prediction for storage chambers using computational fluid dynamics. *Water Science and Technology,* **33**(9), 163-170.

Stovin V.R. and Saul A.J. (1998). A computational fluid dynamics (CFD) particle tracking approach to efficiency prediction. *Water Science and Technology*, **37**(1), 285-293.

Stovin V.R. and Saul A.J., Drinkwater A., and Clifforde I. (1999). Field testing CFD-based predictions of storage chamber gross solids separation efficiency. *Water Science and Technology,* **39**(9), 161-168.

Stovin V.R. and Saul A.J. (2000). Computational fluid dynamics and the design of sewage storage chambers, *Water and Environmental Management*, **14**(2), 103-110.

Stovin V.R., Grimm J.P., Buxton A.P. and Tait S.J. (2002). Parametric studies on CFD models of sewerage structures. *9th International Conference on Urban Drainage*. American Society of Civil Engineering, Portland, OR, U.S.

Stovin V.R., Grimm J.P. and Saul A.J. (2002). Fine sediment retention in storage chambers: an assessment of time-dependent effects. *Water Science and Technology*, **45**(7), 123-131.

Stovin V.R., Grimm J.P., Lau S.-T.D. (2008).solute transport modeling for urban drainage structures. *Journal of Environmental Engineering*, **134**(8), 640-650.

Strickler A. (1923). Beitraege zur Frage der Geschwindigheitsformel und der Rauhikeitszahlen fuer Stroeme Kanaele und geschlossene Leitungen. Mitteilungen des Eidgenössischen Amtes für Wasserwirtschaft 16, Bern, Switzerland. Translated as "Contributions to the question of a velocity formula and roughness data for streams, channels

and closed pipelines." by T. Roesgan and W. R. Brownie, Translation T-10, W. M. Keck Lab of Hydraulics and Water Resources, Calif. Inst. Tech., Pasadena, Calif. January 1981.

Sun Z., and Donahue J. (2000). Statistically derived bed load formula for any fraction of non-uniform sediment. *Journal of Hydraulic Engineering,* **126**(2), 105-111.

Sundborg Å. (1956). The river Klarälven. A study of fluvial processes. *Geogr. Ann.*, **38**.

Sundborg Å. and Calles B. (2001). Water discharges determined from sediment distributions: a palaeohydrological method. *Geogr. Ann.*, **83** A.

Sumer B.M., and OguzB. (1978). Particle motions near the bottom in turbulent flow in an open channel. *Journal of Fluid Mechanics*, **86**(01), 109-127.

Sumer B.M., and Deigaard R. (1981). Particle motions near the bottom in turbulent flow in an open channel, part 2. *Journal of Fluid Mechanics*, **109**, 311-337.

Sutherland A.J. (1967). Proposed mechanism for sediment entrainment by turbulent flow. *Journal of Geophysical Research*, **72**, 6183-6194.

T

Ta C.T. and Brignal W.J. (1998). Application of computational fluid dynamics technique to storage reservoir studies. *Water Science and Technology,* **37**(2), 219-226.

Tachie M.F., Dergstorm D.J. and Balachandar R. (2004). Roughness effects on the mixing properties in open channel turbulent boundary layers. *Journal of Fluids Engineering*, **126**, 1025-1032.

Takamatsu M., Barrett M.E., and Charbeneau R.J. (2010). Hydraulic model for sedimentation in stormwater detention basins. *Journal of Environmental Engineering*, **136**(5), 527-534.

Takamatsu M., Barrett M.E., and Charbeneau R.J. (2012). Alternative approach to evaluation sedimentation performance of stormwater detention basins using a nondimensionlized time scale. *Journal of Environmental Engineering*, **138**(7), 809-814.

Tennekes H. and Lumley J. L. (1976). *A first course in turbulence*. MIT Press.

Thomas W.A. (1982). *Gravel-bed Rivers*. Hey R. D. *et al.*, ed., Wiley, New York.

Thomson, D.J. (1984). Random walk modelling of diffusion in inhomogeneous turbulence. *Quarterly Journal of the Royal Meteorological Society*, 110(466), 1107-1120.

Thomson D.J. (1987). Criteria for the Selection of Stochastic Models of Particle Trajectories in Turbulent Flows. *Journal of Fluid Mechanics*, **180**,529-556.

Thornton R.C. and Saul A.J. (1986). Some quality characteristics of combined sewer flow. *J. Inst. Public Health Engineers*, **14**(3), 35-39.

Torres A. and Bertrand-Krajewski J.L. (2008). Evaluation of uncertainties in settling velocities of particles in urban stormwater runoff. *Water Sciencea and Technology*, **57**(9), 1389-1396.

Torres A. (2008). *Décantation des eaux pluviales dans un ouvrage réel de grande taille : éléments de réflexion pour le suivi et la modélisation*. Thèse de doctorat, Institut National des Sciences Appliquées de Lyon, France.

Torres A., Lipeme Kouyi G., Bertrand-Krajewski J. L., Guilloux J., Barraud S. and Paquier A. (2008). Modeling of hydrodynamics and solid transport in a large stormwater detention and settling basin. *11th International Conference on Urban Drainage*, Edinburgh, Scotland. 31st August - 5th September, 10 p.

U

USEPA, Stormwater Management: http://www.epa.gov/oaintrnt/stormwater/index.htm

USEPA, (2011). http://www.epa.gov/greeningepa/glossary.htm#csos

V

Valiron F. (1985). *Gestion des Eaux: Alimentation en Eau*. Paris, Presses de ENPC.

Valiron F., and Tabuchi J.-P. (1992). Maitrise de la pollution urbaine par temps de pluie. Paris, Technique at Documentation-Lavoisier.

Van Doormaal J. P.and Raithby G. D. (1984). Enhancements of the SIMPLE method for predicting incompressible fluid flow. *Numerical Heat Transfer,* **7**(2), 147-163.

Van Rijn L.C. (1984a). Sediment transport, Part I: Bed load transport, *Journal of Hydraulic Engineering*, **110**(10), 1431-1456.

Van Rijn L.C. (1984b). Sediment transport, Part II: Suspended load transport, *Journal of Hydraulic Engineering*, **110**(11), 1613-1641.

Van Wachem B.G.M. and Almstedt A.E. (2003). Methods for multiphase computational fluid dynamics. *Chemical Engineering Journal*, **96**, 81-98.

Van Doormaal J. P. and Raithby G. D. (1984). Enhancements of the SIMPLE Method for Predicting Incompressible Fluid Flows. *Numerical Heat Transfer,* **7**, 147-163.

Vanoni V.A. and Brooks N.H. (1957). Laboratory studies of the roughness and suspended load of alluvial streams. Report E-68, Sedimentation laboratory, California Institute of technology, Pasadena, Calif.

Vanoni V.A. (1975). Sedimentation Engineering, Manuals and Reports on Engineering Practice No. 54, *American Society of Civil Engineers*, New York.

Vaze J., and Chiew F. H.S. (2004). Nutrient loads associated with different sediment sizes in urban stormwater and surface pollutants. *Journal of Environmental Engineering*, **130**(40), 391-396.

Verstraeten G., and Poesen J. (2000). Estimating trap efficiency of small reservoirs and ponds: methods and implications for the assessment of sediment yield. *Progress in Physical Geography*, **24** (2), 219-251.

Verstraeten G., and Poesen J. (2001). Modeling the long-term trap efficiency of small ponds. *Hydrologic processes*, 15, Wiley, Hoboken, N.J., 2797-2819.

Vega G.P., Pena M.R., Ramirez C. and Mara D.D. (2003). Application of CFD modeling to study the hydrodynamics of various anaerobic pond configurations. *Water Science and Technology,* **48**(2), 163-171.

Versteeg H.K., Malalasekera W. (2007). *An introduction to computational fluid dynamics- the finite volume method*. Essex.

Vetsch D. (2012). *Numerical Simulation of Sediment Transport with Meshfree Methods*. PhD. thesis, Technischen Hochschule Zürich.

Vosswinkel N., Lipeme Kouyi G., Ebbert S., Schnieders A., Maus C., Laily A.-G., Mohn R. and Uhl M.(2012). Influence of unsteady behaviour on the settling of solids in storm water tanks. *Proceedings of the 9th Urban Drainage Modelling International Conference*, 3rd - 7th September, Belgrade, Serbia, 14 p.

W

Walker D. (1998). Modeling residence time in stormwater ponds. *Ecological Engineering,* **10**, 247-262.

Wanker R, Gockler G, and Knoblauch H. (2001). Numerical modeling of sedimentation utilizing an Euler/Euler approach. *Computational Methods in Multiphase Flow,* **30**, 327- 336.

Ward A.D., Haan C.T., and Barfield B.J. (1977).The performance of sediment detention structures. *International symposium on Urban Hydrology, Hydraulics and Sediment Control*, University of Kentucky, Lexington, KY, 58-68.

Watters G.Z., Mangelson K.A. and George R.L. (1973). *The Hydraulics of Waste Stabilization Ponds.* Utah Water Research Laboratory - College of Engineering, Utah State University.

Werritty A., Black A., Duck R., Finlinson B., Thurston N., and Shackley S. and Crichton D. (2002). *Climate change: flooding occurrence review*. Report of Scottish Executive Central Research Unit, Scottish.

White B.R., and Shulz J.C. (1977). Magnus effect in saltation. *Journal of Fluid Mechanics*, **81**, Part 3, 497-512.

White F.M. (1986). *Fluid mechanics.* McGraw Hill, New York.

Wiberg P.L., and Smith J.D. (1985). A theoretical model for saltating particles in water. *J. Geophys. Res.*, **90**(4), 7341-7354.

Wilson B.N., and Barfield B.J. (1985). Modeling sediment detention ponds using reactor theory and advection-Diffusion concepts. *Water Recourses Research*, **21**(4), 523-532.

Wilcox D.C. (1988). Reassessment of the Scale-determining Equation for Advanced Turbulence Models. *AIAA J.,* **26**(11), 1299-1310.

Wilcox D.C. (1993a). Comparison of Two-equation Turbulence Models for Boundary Layers with Pressure Gradients, *AIAA J.*, **31**(8), 1414-1421.

Wilcox D.C. (1993b). *Turbulence Modelling for CFD*, DCW Industries Inc., La Canada, CA.

Wilcox D.C. (1994). Simulating Transition with a Two-equation Turbulence Model, *AIAA J.*, **32**, 247-255.

Wilkinson D., and Waldie B. (1994). CFD and experimental studies of fluid and particle flow in horizontal primary separators. *Chemical Engineering Research and Design*, **72**(A2), 189-196.

Wilson K. C. (1966). Bed-load transport at high shear stress. *Journal of the Hydraulics Division, ASCE*, **92**(6), 44-59.

Wilson B.N., and Barfield B.J. (1984). A sediment detention pond model using CSTRS mixing theory. *Trans. ASAE*, **27**(5), 1339- 1344.

Winterwerp J.C. (2006).On the sedimentation rate of cohesive sediment. Estuarine and coastal fine sediment dynamics-INTERCOH 2003, J.P.-Y. Maa, L.P. Sanford, and D.H. Schoellhamer, eds., Elsevier, Amsterdam, the Netherlands, 209-226.

Wong T.H.F., Fletcher T.D., Duncan H.P., Jenkins G.A. (2006). Modelling urban stormwater treatment - A unified approach. *Ecological Engineering*, **27** (1), 58-70.

Wood M.G., Howes T., Keller J., and Johns M. R. (1998). Two dimensional computational fluid dynamic models for waste stabilisation ponds. *Water Research,* **32**(3), 958-963.

Wu W., Rodi W., and Wenka T. (2000). 3D numerical modeling of flow and sediment transport in open channels. *Journal of Hydraulic Engineering*, **126**(1), 4-15.

Wu F.-C. and Lin Y.-C. (2002). Pickup probability of sediment under log-normal velocity distribution. *Journal of Hydraulic Engineering*, **128**(4), 438-442.

Wu W., and Vieira, D.A. (2002). One-dimensional channel network model CCHE1D 3.0-Technical manual. *Technical Rep. No. NCCHE-TR-2002-1*, National Center for Computational Hydroscience and Engineering, the Univ. of Mississippi, University, Miss.

Wu F.-C. and Chou Y.-J. (2003).Rolling and lifting probabilities for sediment entrainment. *Journal of Hydraulic Engineering*, **129**(2), 110-119.

Wu W. (2004). Depth – averaged two dimensional numerical modeling of unsteady flow and non-uniform sediment transport in open channels. *Journal of Hydraulic Engineering*, **130**(10), 1013-1024.

Y

Yakhot V. and Orszag S. (1986). Renormalization group analysis of turbulence I: Basic theory. *Journal of Scientific Computing*, **1**(1), 3-51.

Yakhot V., Orszag S. A., Thangam S., Gatski T. B. and Speziale C. G. (1992). Development of Turbulence Models for Shear Flow by a Double Expansion Technique, *Physics of Fluids A*, **4**(7), 1510-1520.

Yalin M.S. (1963). An expression for bed-load transportation. *Journal of the Hydraulics Division*, *ASCE*, **89**(3), 221-250.

Yan H., Lipeme Kouyi G., and Bertrand-Krajewski J.-L. (2011a). 3D modeling of flow, solid transport and settling processes in a large stormwater detention basin. *Proceedings of 12th International Conference on Urban Drainage*, 11th-16th September, Porto Alegre, Brazil, 8 p.

Yan H., Lipeme Kouyi G., Bertrand-Krajewski J.-L. (2011b). Modélisation numérique 3D des écoulements turbulents a surface libre charges en polluants particulaires dans un bassin de retenue - décantation des eaux pluviales. *La Houille Blanche*, **2011**(**5**), 40-44.

Z

Zanke U.C.E. (2003). On the influence of turbulence on the initiation of sediment motion. *International Journal of Sediment Research*, **18**(1), 17-31.

Zeng J. (2006). *Fully 3D non-hydrostatic model to compute flow, sediment transport and bed morphology changes for an alluvial open channel bend*. PhD thesis, Department of Civil and Environmental Engineering, University of Iowa, Iowa city, Iowa.

Zhang Z. and Chen Q. (2007). Comparison of the Eulerian and Lagrangian methods for predicting particle transport in enclosed spaces. *Atmospheric Environment*, **41**(25), 5236-5248.

Zhang L. (2009). *3D numerical modeling of hydrodynamic flow, sediment deposition and transport in stormwater ponds and alluvial channels*. PhD thesis, Old Dominion University, Virginia, U.S.

Zhao Z. and Fernando H.J.S. (2007). Numerical simulation of scour around pipelines using an Euler-Euler coupled two-phase model. *Environmental Fluid Mechanics*, **7**, 121- 142.

Zhou Y.C., Wright B.D., Yang R.Y., Xu B.H., Yu A.B. (1999). Rolling friction in the dynamic simulation of sandpile formation. *Physica A: Statistical Mechanics and its Applications*, **269**, 536- 553.

Appendix

Appendix A: combination bed boundary condition UDF using Shields curve

```
/************************************************************************
UDF for extending bed boundary condition processing of wall impacts
The function of this UDF is to determine the state of a particle when it
Hits on wall (bed) by Shields curve shear stress.
Author: Hexiang YAN email: hexiang.yan@insa-lyon.fr/yanhexiang@gmail.com
This UDF is coded in language C.

************************************************************************/
#include "udf.h"
#define G 9.81
FILE *pF;      /*handle of FILE*/

DEFINE_DPM_BC(settling_bss_Shields,p,t,f,f_normal,dim)
{
  int  IsTrap=0,
       idim=dim,
       i=0;
 real local_bed_shear_stress=0.0,
       local_bed_shear_force=0.0,
       critical_bed_shear_stress=0.03, /*ctritical value from default*/
       area=0.0,
       A[ND_ND],
       vnormal=0.0,
       tan_coeff=1.0,/* tangential coefficient of restitution  */
       nor_coeff=1.0;/* normal coefficient of restitution  */
       real phita_critical=0.0, /*dimensionless shear stress-Shields parameter*/
      dia=0.0, /*particle diameter*/
       rho_p; /*particle density*/
 real Rp=0.0;
 real beta=0.0;
```

```
 cphase_state_t *c;


  /*local bed shear stress calculation*/
 F_AREA(A,f,t); /*bed cell area in vector*/
 area=NV_MAG(A);/*bed cell area in scalar*/
 local_bed_shear_force=NV_MAG(F_STORAGE_R_N3V(f,t,SV_WALL_SHEAR));/*bed
shear force*/
 local_bed_shear_stress=local_bed_shear_force/area;


 /*critical bed shear stress calculation according to Shields curve(fit) */
 c=&(p->cphase);/*cell information of particle location*/
 dia=P_DIAM(p);
 rho_p=P_RHO(p);
 Rp=dia*sqrt(G*dia*(rho_p-c->rho)/c->rho);
 beta=pow((c->rho/c->mu*Rp),-0.6);
 phita_critical=0.22*beta+0.06*pow(10,(-7.7*beta));
  critical_bed_shear_stress=phita_critical*(rho_p-c->rho)*G*dia;


 if(local_bed_shear_stress<critical_bed_shear_stress)   /*particle condtion determination
determination*/
  {
       IsTrap=1;
  }


 /*treatment according to the determination */
 if (p->type==DPM_TYPE_INERT)
   {
     if (IsTrap)
       {
           pF=fopen("bss_shields.txt","a");
           fprintf(pF,"%10.6f  %10.6f  %10.6f %10.6f %10.6f
\n",P_POS(p)[0],P_POS(p)[1],P_POS(p)[2],P_DIAM(p),P_RHO(p));/* record the
informations of trap particle in a txt file*/
          fclose(pF);
               return PATH_ABORT;/* stop the calculation of particle trajectory */
```

```
            }
   else
   {
     for(i=0;i<idim;i++)/* computer the normal component of particle velocity  */
            {
                    vnormal+=P_VEL(p)[i]*f_normal[i];
            }

            for(i=0;i<idim;i++)/* subtract the normal velocity component  */
            {
                    P_VEL(p)[i]-=vnormal*f_normal[i];
            }
     for(i=0;i<idim;i++)/* Apply tangential coefficient of restitution  */
            {
                    P_VEL(p)[i]*=tan_coeff;
            }
            for(i=0;i<idim;i++)/* add reflected normal velocity  */
            {
                    P_VEL(p)[i]-=nor_coeff*vnormal*f_normal[i];
            }

            for(i=0;i<idim;i++)/* Store new velocity in P_VEL0 of partice  */
            {
                    P_VEL0(p)[i]=P_VEL(p)[i];/* the Macro can be found in the source header
file dpm_types.h  */
            }
            return PATH_ACTIVE;
   }
  }
 return PATH_ABORT;
}
```

Appendix B: UDF of dynamic sedimentation and resuspension processes approach

```
/**********************************************************************
UDF for extending bed boundary condition processing of wall impacts under unsteady flow
The function of this UDF is to determine the state of a particle when it hits on wall (bed) simply by bed shear stress calculatee from Shields curve.
Author: Hexiang YAN email: hexiang.yan@insa-lyon.fr/ yanhexiang@gmail.com
This UDF is coded in language C.
**********************************************************************/

/**********************************************************************
markers used to describe the state of particles
resting on the bed- 0
particle in motion- 1
all the particles injection are set as suspended when they are injected at the inlet
particle variables are used to record the states
P_USER_REAL(p,0) marks the current state
particle state change type:
1- from moving to moving
2- from moving to stay
3- from stay to stay
4- from stay to moving
when the current state of particle P_USER_REAL equal to 1, that is, the particle settled down, the drag force will be assigned to zero in order to make the particle stay until entrainment
**********************************************************************/
#include "udf.h"
#define G 9.81/*gravity acceleration*/
FILE  *pF;      /*handle of FILE*/
/* the macro DEFINE_DPM_BC is used to set the particle parameters such as velocity, etc.*/
DEFINE_DPM_BC(bss_shields_unsteady,p,t,f,f_normal,dim)
{
        int   state_change_type=0;  /*flag for state change type*/
        real local_bed_shear_stress=0.0,
```

```
            local_bed_shear_force=0.0,
            critical_bed_shear_stress=0.03,/* default ctritical bss value from  thesis of
Matthieu Dufresne(2008)*/
            area=0.0,
      A[ND_ND],
            tan_coeff=1.0,/* tangential coefficient of restitution  */


            nor_coeff=1.0;/* normal coefficient of restitution  */
         real critical_phita=0.0,local_phita=0.0,/*dimensionless shear stress*/
            local_friction_velocity=0.0,critical_friction_velocity=0.0;


         cphase_state_t *c;
         real Rp=0.0;
         real beta=0.0;
         real NV_VEC(vel),
              NV_VEC(vel_T),
              NV_VEC(vel_N),
              vel_normal=0.0,
             vel_tangent=0.0;/*vector for fluid velocity*/
         real NV_VEC(vel_p),
              NV_VEC(vel_p_T),
              NV_VEC(vel_p_N),
              vel_p_normal=0.0;/*vector for particle velocity*/
         real diameter=0.0,/*particle diameter*/
              rho_p=0.0;/*particle density*/
         diameter=P_DIAM(p);/*particle diameter*/
         rho_p=P_RHO(p);/*particle density*/
         c=&(p->cphase);/*cell information of particle location*/


         /*local bed shear stress calculation*/
         F_AREA(A,f,t); /*bed cell area in vector*/
         area=NV_MAG(A);/*bed cell area in scalar*/
         local_bed_shear_force=NV_MAG(F_STORAGE_R_N3V(f,t,SV_WALL_SHEAR));
/*bed shear force*/
```

```
        local_bed_shear_stress=local_bed_shear_force/area;
        /*critical bed shear stress calculation according to Shields curve(fit) */
        diameter=P_DIAM(p);/*particle diameter*/
        rho_p=P_RHO(p);/*particle density*/

        Rp=diameter*sqrt(G*diameter*(rho_p-c->rho)/c->rho);
        beta=pow((c->rho/c->mu*Rp),-0.6);
        critical_phita=0.22*beta+0.06*pow(10,(-7.7*beta));/*critical dimensionless shear
stress*/

        critical_bed_shear_stress=critical_phita*(rho_p-c->rho)*G*diameter;/*critical bed
shear stress*/
critical_friction_velocity=sqrt(critical_bed_shear_stress/c->rho);/*critical shear  velocity
U*c    */
        local_friction_velocity=sqrt(local_bed_shear_stress/c->rho); /*local shear  velocity
U*/
        local_phita=local_bed_shear_stress/((rho_p-c->rho)*G*diameter);/*local
dimensionless shear stress*/

  /*determination of boundary condition of particle impact with bed*/
if(0==P_USER_REAL(p,0))/* particle in motion*/
   {
        if(local_bed_shear_stress<critical_bed_shear_stress)
                {
                        state_change_type=2;/* mark the state change type--from moving to
stay*/
                        P_USER_REAL(p,0)=1;  /* update the current state after touch with
the bed--settled down*/
                }
        else
                {
                         state_change_type=1;/* mark the state change type--from moving to
moving*/
                }
    }
  else     /* particle already settled down --P_USER_REAL(p,0) equal to 1*/
```

```
  {
       if(local_bed_shear_stress>critical_bed_shear_stress)
         {
              state_change_type=4;/* mark the state change type--from stay to moving*/
              P_USER_REAL(p,0)=0; /* update the current state after touch with the bed--
entrainment*/
              }
              else
              {
                   state_change_type=3;/* mark the state change type--from stay to
stay*/
              }
    }

 /*treatment according to the determination */

 if(p->type==DPM_TYPE_INERT)
  {
       if(1==state_change_type)      /*from moving to moving*/
         {
              vel_p_normal=NV_DOT(P_VEL(p),f_normal);
              NV_D(vel_p_T,=,0,0,0);
              NV_D(vel_p_N,=,0,0,0);
              NV_VS(vel_p_N,=,f_normal,*,vel_p_normal);
 NV_VV(vel_p_T,=,P_VEL(p),-,vel_p_N);
              NV_VS(vel_p_N,=,vel_p_N,*,(-1*nor_coeff));
              NV_VS(vel_p_T,=,vel_p_T,*,tan_coeff);
              NV_VV(P_VEL(p),=,vel_p_T,+,vel_p_N);
              NV_V(P_VEL0(p),=,P_VEL(p));
              return PATH_ACTIVE;

         }
   if(2==state_change_type)/*from moving to stay*/
       {
```

```
                    NV_D(P_VEL(p),=,0,0,0);
                NV_D(P_VEL0(p),=,0,0,0);
                    return PATH_ACTIVE;
        }

      if(3==state_change_type)     /*from stay to stay*/
        {
            NV_D(P_VEL(p),=,0,0,0);
            NV_D(P_VEL0(p),=,0,0,0);
          return PATH_ACTIVE;
        }
      if(4==state_change_type)     /*from stay to moving--entrainment*/
        {
            real normal_v=0.0,tangent_u=0.0;/*normal and tangent particle velocity
component*/

            if(local_phita>1.20)
            {
                normal_v=3.1*local_friction_velocity; /* calcualation the normal
particle entrainment velocity*/
                tangent_u=12.1*local_friction_velocity; /* calcualation the tangent
particle entrainment velocity*/
            }
            else
            {
                normal_v=(3.2-4.5*log10(local_phita))*local_friction_velocity;
                tangent_u=(12.3-3.7*log10(local_phita))*local_friction_velocity;
            }
            /* calculate the tangent direct of flow, the particle tangent direct will follow
the same direct*/

            NV_D(vel,=,F_U(f,t),F_V(f,t),F_W(f,t));/*assign the value from the bed
face*/

  vel_normal=NV_DOT(f_normal,vel);/*magnitude of normal component of the water
```

```
velocity*/
                NV_D(vel_N,=,0,0,0);/* initialized magnitude of normal component of the
water velocity*/
                NV_V_VS(vel_N,=,vel_N,+,f_normal,*,vel_normal);/*normal component
of the water velocity*/
                NV_VV(vel_T,=,vel,-,vel_N);/*tangent component of the water velocity*/
                vel_tangent=NV_MAG(vel_T);
                NV_D(vel_p_T,=,0,0,0);/* initialized magnitude of tangent component of
particle velocity*/
        NV_D(vel_p_N,=,0,0,0);/* initialized magnitude of normal component of particle
velocity*/
                NV_D(vel_p,=,0,0,0);/* initialized magnitude of particle velocity*/
                NV_V_VS(vel_p_N,=,vel_p_N,+,f_normal,*,(-1*normal_v));/*normal
component of the particle velocity*/
        NV_V_VS(vel_p_T,=,vel_p_T,+,vel_T,*,(tangent_u/vel_tangent));/*tangent
component of the particle velocity*/
             NV_VV(vel_p,=,vel_p_N,+,vel_p_T);/*particle velocity*/
                NV_V(P_VEL(p),=,vel_p);/* Store new velocity in P_VEL0 of partice  */
                NV_V(P_VEL0(p),=,vel_p);/* Store new velocity in P_VEL0 of partice  */
             return PATH_ACTIVE;
           }

 }
}

/* the macro DEFINE_DPM_DRAG is used to change the drag force on the particle*/
DEFINE_DPM_DRAG(sphere_drag_force,Re,p)
 {
   real drag_force;

        if (1==P_USER_REAL(p,0)) /* particle marked as deposition--settled down*/
         {
                return 0.0;
         }
  else
```

```
    {
                drag_force =SphereDragCoeff(Re);  /* using spherical drag formula*/
       return (drag_force);
    }


 }


/*the macro DEFINE_DPM_BC is used to record the information of particle escaped from
the outlet*/
DEFINE_DPM_BC(outlet,p,t,f,f_normal,dim)
{
     if(p->type==DPM_TYPE_INERT)
          {
                pF=fopen("bssresusoutlet.txt","a");
                fprintf(pF,"%10.6f  %10.6f  %10.6f %10.6f %10.6f
%10.6f\n",P_POS(p)[0],P_POS(p)[1],P_POS(p)[2],P_DIAM(p),P_RHO(p),P_TIME(p));
                fclose(pF);
               return PATH_END;/* correspondent to condition escaped */
          }
}
```